DEVELOPMENT OF SURFACE ENHANCED RAMAN SCATTERING BASED DIAGNOSTIC PLATFORM FOR CANCER AND ALZHEIMER'S DISEASE

Thesis Submitted to Academy of Scientific and Innovative Research (AcSIR)
for the Award of the Degree of
DOCTOR OF PHILOSOPHY
in Biological Sciences

By

VARSHA KARUNAKARAN

Registration No: 10BB15A39024

Under the guidance of

Dr. KAUSTABH KUMAR MAITI

&

Dr. K.G. RAGHU

CSIR-NATIONAL INSTITUTE FOR INTERDISCIPLINARY
SCIENCE AND TECHNOLOGY (CSIR-NIIST)
THIRUVANANTHAPURAM-695019, KERALA, INDIA

July, 2020

Dedicated to

My Father

Declaration

I hereby declare that the matter embodied in the thesis entitled: "**Development of surface enhanced Raman scattering based diagnostic platform for Cancer and Alzheimer's Disease**" is the result of the investigations carried out by me at the Organic chemistry section, Chemical Sciences and Technology Division, CSIR-National Institute for Interdisciplinary Science and Technology (CSIR-NIIST), Trivandrum, under the supervision of Dr. Kaustabh Kumar Maiti and Dr. K.G. Raghu and the same has not been submitted elsewhere for any other degree.

In keeping with the general practice of reporting scientific observations, due acknowledgement has been made wherever the work described is based on the findings of other investigators.

24/07/2020

Varsha Karunakaran

National Institute for Interdisciplinary Science and Technology (NIIST)

Council of Scientific and Industrial Research (CSIR)
Industrial estate P.O., Thiruvananthapuram- 695019
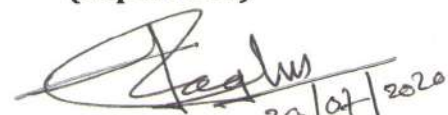**Kerala, India**

July, 2020

Certificate

This is to certify that the work incorporated in this Ph.D. thesis entitled **"Development of surface enhanced Raman scattering based diagnostic platform for Cancer and Alzheimer's Disease"** submitted by **Ms. Varsha Karunakaran** to Academy of Scientific and Innovative Research (AcSIR) in fulfillment of the requirements for the award of the **Degree of Doctor of Philosophy in Biological Sciences**, embodies original research work under our supervision/guidance. We further certify that this work has not been submitted to any other University or Institution in part or full for the award of any degree or diploma. Research material obtained from other sources has been duly acknowledged in the thesis. Any text, illustration, table etc., used in the thesis from other sources, have been duly cited and acknowledged. It is also certified that this work done by the student, under my supervision, is plagiarism free.

24/07/2020
Varsha Karunakaran

24/07/2020
Dr. Kaustabh Kumar Maiti
(Supervisor)

24/07/2020
Dr. K.G. Raghu
(Co-Supervisor)

Acknowledgements

CONTENTS

List of Schemes

microscope c) representative design for detection of biomarkers in cells/tissues by SERS-tags, d) SERS analysis in retrospective paraffin embedded breast tissue samples after antigen retrieval using a futuristic hand held Raman system.

List of Figures

dimensional LD score plot and loadings showing major discriminatory peaks.

Raman image, c) cluster map d) mean SERS spectra acquired and e) 3D Raman mapping (Scale bar =8 μm), laser power density 3-7 mW.

List of Tables

List of Abbreviations

a.u.	Arbitrary unit
aCSF	Artificial cerebrospinal fluid
AD	Alzheimer's disease
ADP3	Alzheimer's disease peptoid 3
APES	3-aminopropyltriethoxysilane
ATCC	American type culture collection
ATP	4-aminothiophenol
Au	Gold
AuNPs	Gold nanoparticles
AuNS	Gold nanostar
Aβ	Beta amyloid
BCB	Brilliant cresyl blue
BPE	1,2-bis (4-pyridyl)-ethylene
BSA	Bovine serum albumin
$CaCl_2$	Calcium chloride
CARS	Coherent anti-Stokes Raman spectroscopy
CCD	Charged coupled device
CD	Communicable disease
CD44, 47	Cluster of differentiation 44, 47
CEA	Carcinoembryonic antigen
CIN	Carcinoma in situ
cm	Centimeter
CNS	Central nervous system

CO_2	Carbon dioxide
CSCC	Cervical squamous cell carcinoma
CSF	Cerebrospinal fluid
CT	Computed tomography
CTAB	Cetyl trimethylammonium bromide
CV	Crystal violet
DAB	3,3'-diaminobenzidine
DLS	Dynamic light scattering
DMEM	Dulbecco's modified eagle's medium
DMSO	Dimethyl sulfoxide
DNA	Deoxyribonucleic acid
DOT	Diffuse optical tomography
DPX	Dibutylphthalate polystyrene xylene
DSM 5	Diagnostic and Statistical Manual of Mental Disorders, 5th Edition
DTNB	5,5'-dithiobis-(2-nitrobenzoic acid)
EA	Eosin azure
ECL	Enhanced chemiluminescence
EDC	3-(dimethylamino)-propyl)-N′-ethylcarbodiimide
EDX	Energy dispersive x-ray analysis
EGF	Epidermal growth factor
EGFR	Epidermal growth factor receptor
ER	Estrogen
Erbb2	Receptor tyrosine-protein kinase erbb-2
FBS	Fetal bovine serum

FDA	Food and Drug Administration
Fe@AuNS	Iron core- gold nanostar
Fe_3O_4	Iron oxide
FISH	Fluorescence in situ hybridization
FITC	Fluorescein isothiocyanate
fM	Femto molar
F-MR	Functional magnetic resonance
FNAC	Fine needle aspiration cytology
GLOBOCAN	Global cancer
GNP	AuNP@PMZ@PEG@A$\beta_{1\text{-}42}$ PAb
h	Hour
HCl	Hydrochloric acid
HEC	Human ethics committee
HER2	Human epidermal growth factor receptor2
HPLC	High performance liquid chromatogrphy
HPV	Human papilloma virus
HRP	Horse radish peroxidase
HR-TEM	High-resolution transmission electron microscopy
HSA	Human serum albumin
HSIL	High-grade squamous intraepithelial lesion
ICD-10	International Classification of Diseases
ICP-MS	Inductively coupled plasma mass spectrometry
IGF1R	Insulin-like growth factor 1 receptor
IONP	Fe@AuNS@PEG@A$\beta_{1\text{-}42}$ MAb

KCl	Potassium chloride
KH$_2$PO$_4$	Potassium dihydrogen phosphate
Knn	K-nearest neighbor
LBC	Liquid based cytology
LD	Linear discriminant
LDA	Linear discriminant analysis
LOD	Limit of detection
LSIL	Low-grade squamous intraepithelial lesion
LSL	Lipoic-squaraine-lipoic
LSPR	Localized surface plasmon resonance
M	Molar
MAb	Monoclonal antibody
MB	Methylene blue
MBA	Mercaptobenzoic acid
MCF7	Human breast cancer cell line
MDA-MB-231	Human breast cancer cell line
MEG	Methylene green
MG	Malachite green
mg	Milligram
MgSO$_4$	Magnesium sulphate
mi-DNA	DNA analogue of mi-RNA
min	Minutes
ml	Millilitre
mm	Millimeter

mM	Millimolar
MRI	Magnetic resonance imaging
MTT	3-(4, 5-dimethylthiazol-2-yl)-2, 5-diphenyltetrazolium bromide
NaCl	Sodium chloride
$NaHCO_3$	Sodium bicarbonate
nM	Nanomolar
NaOH	Sodium hydroxide
NCCS	National Centre for Cell Science
NCD	Non-communicable disease
NHS	N-hydroxysuccinimide
NIR	Near-infrared
NIRS	Near infrared spectroscopy
nm	Nanometer
NP	Nanoparticle
NR	Neutral red
NRML	Normal
NSE	Neuron specific enolase
OCT	Optical coherence tomography
OG	Orange G
OPA	O-phthalaldehyde
PA	Photoacoustic imaging
PAb	Polyclonal antibody
PALM	Photo activated localization microscopy
PBS	Phosphate buffered saline

PBST	Phosphate buffered saline with Tween 20
PCA	Principal component analysis
PCR	Polymerase chain reaction
PCTP	Pentachlorothiophenol
PEG	Poly(ethylene glycol)
PET	Positron emission tomography
pg	Picogram
pH	Hydrogen ion concentration at logarithmic scale
PLS-DA	Partial least square discriminant analysis
PMZ	Promethazine
PR	Progesterone
PSA	Prostate specific antigen
PVDF	Polyvinylidene difluoride
Pyk2	Proline rich tyrosine kinase 2
Qds	Quantum dots
R6G	Rhodamine 6G
RB	Rose bengal
RCC	Regional cancer centre
RIPA	Radioimmunoprecipitation assay
RNA	Ribonucleic acid
ROC	Receiver operating characteristic
rpm	Revolutions per minute
RR	Raman reporter
RRS	Resonance Raman spectroscopy

RT	Room temperature
S	Seconds
SDS-PAGE	Sodium dodecyl sulphate poly acrylamide gel electrophoresis
SERS	Surface enhanced Raman spectroscopy
SERRS	Surface enhanced resonance Raman spectroscopy
SH-SY5Y	Human neuroblastoma cell line
SiHa	Human cervical cancer cell line
SIM	Structure illumination microscopy
SK-BR-3	Human breast cancer cell line
SORS	Spatially offset Raman spectroscopy
SPECT	Single-photon emission computed tomography
SPIONS	Superparamagnetic iron oxide nanoparticles
SPR	Surface plasmon resonance
SRM	Super-resolution microscopy
SRS	Stimulated Raman spectroscopy
STED	Stimulated emission depletion
STORM	Stochastic optical reconstruction microscopy
STR	Short tandem repeat
SVM	Support vector machine
T	Temperature
TGFβRII	Transforming growth factor, beta receptor II
TBS	Tris buffered saline
TBST	Tris buffered saline with Tween 20
TE	Echo time

THz	Terahertz
TI	Inversion time
TMB	3,3',5,5'-Tetramethylbenzidine
TR	Repetition time
UFLC	Ultra-fast liquid chromatography
UV	Ultraviolet
Vis	Visible
WI-38	Human lung fibroblast cell line
WHO	World health organization
μg	Microgram
μm	Micrometer
μM	Micromolar
2D	2 dimensional
3D	3 dimensional

PREFACE

Early detection of the diseases is an essential criteria for improved treatment and thereby increased survival of patients. In the area of diagnostics, nanotechnology holds great promise for the development of rapid, highly sensitive, cost effective and easy to use nanodiagnostic platforms which resolves a variety of challenges associated with conventional detection strategies including time duration, high cost and invasiveness of the technique etc. Surface enhanced Raman spectroscopy (SERS), an improved version of Raman spectroscopy emerged as an outstanding technique which facilitates low analyte detection in an ultrasensitive manner in terms of increase in Raman signal intensity to several folds when the analyte molecule are in close proximity with the metallic nanoparticles. SERS enabled nanoparticle probes i.e. SERS-nanoprobes or SERS-tags has received huge scientific attention in the last decade for its extensive biomedical applications. A wide variety of nanomaterials of different shapes and sizes are available which can perform important functions in the molecular level for aiding SERS based diagnosis. In this regard, the design of versatile SERS nanoprobes holds exceptional interest among researchers in multidisciplinary areas to detect different non-communicable and communicable diseases. The present thesis describes two types of SERS based diagnostic techniques *viz.* label free and label based SERS for precise detection of disease etiology. Label free SERS provides direct inherent biomolecular signals which reveals subtle differences occurring due to a disease condition from biomolecules, cell, tissues etc. On the other hand, label based SERS analysis involves the interaction of biomolecules with a Raman labelled SERS substrate having a targeting moiety. The signals from the label indirectly correlates with the informations from the desired molecule recognition. In this regard, the present thesis defines the development of label free as well as label based SERS nanoprobes for the detection of non-communicable diseases like cervical cancer, breast cancer and Alzheimer's disease. Chapter 1 of the thesis provides an overview about the recent developments of surface enhanced Raman scattering based nano probes and its efficiency for diagnostic

applications. Moreover, specific objectives of the present thesis are briefly described at the end of this chapter. Although substantial efforts were made for the SERS based nanoprobe design and execution for diagnostic purpose, a thorough study in and around the topic is required to uplift the technique for the clinical diagnostic applications.

In Chapter 2, a label free detection technique for cervical cancer has been developed using SERS modality. Pap staining, the current golden standard for cervical cancer detection is less sensitive, highly subjective and time consuming. Ultrasensitive and cost effective screening techniques are therefore in high demand for implementation in low resource countries. A differential SERS spectral fingerprint pattern has been generated for the prediction of healthy, intermediate and squamous cell carcinoma from exfoliated cervical cell samples by three different approaches i.e. single-cell, cell-pellet and extracted DNA from pathologically confirmed clinical samples. Further the spectral data were subjected to chemometric analysis which yielded a diagnostic accuracy of 93, 74 and 92 % for the three different approaches respectively. The futuristic idea of a portable Raman system for SERS read-out with machine learning technique promises its utility as cervical cancer detection platform.[1, 2]

Chapter 3 deals with the fabrication of a label based SERS-nanoprobe for the detection of cervical cancer progression in single exfoliated cell analysis. The epithelial abnormalities arising in cervical cancer can be monitored along a long window period prior its progression to carcinoma stage. p16/ Ki-67 emerged as a potent dual biomarker recently for the detection of cervical cancer with improved sensitivity and specificity to replace the Pap test. In an attempt to address the subjective nature of cytology technique, a SERS based diagnostic assay has been designed for the simultaneous detection of p16/Ki-67 dual biomarker using dual antibody conjugated SERS nanoprobe during the progression of cervical cancer. The SERS based detection method was initially validated in cell line models and extended to different grades of cervical cancer which very well correlated with immunocytochemistry dual staining analysis.[3]

Chapter 4 deals with diagnosis of breast cancer which is the leading type of cancer among women worldwide. Evaluation of ER, PR and HER2 biomarker status in heterogeneous breast cancer subtypes is critical to design personalized treatment strategies. Immunohistochemistry analysis, the current golden standard is highly subjective and time consuming where multiplexing is not possible. FISH analysis is an alternative approach for HER2 analysis, but is very expensive. Thus, a SERS based ultrasensitive multiplexed detection strategy has been developed for ER, PR and HER2 biomarkers using respective antibody conjugated SERS nanotags. The proof of concept has been successfully executed in breast cancer cell lines having differential expression of ER, PR and HER2 and validated in paraffin embedded retrospective breast cancer tissue sample.[4, 5]

Chapter 5 describes the SERS label based analysis for the detection of biomarker relevant in Alzheimer's disease (AD), which is the most common form of dementia. Early diagnosis is crucial for improving the physical, emotional and financial effects of AD. An ultrasensitive SERS modality using targeting antibody conjugated gold nanoparticle and iron oxide nanoparticle forming a sandwich complex with $A\beta_{1-42}$ peptide, the AD biomarker, has been developed which turned out as an immunosensor platform with a limit of detection of 10 fM. The nanoprobe efficiently recognized $A\beta_{1-42}$ at cell line level by SERS and whose uptake was further confirmed by MRI analysis. This proof of concept study shows the potential to be extended in real patient samples.[6]

In summary, different strategies of SERS based nanoprobes towards disease biomarkers were explored which resembled a promising technique by tuning the type of ligand in order to achieve target specific binding towards desired disease biomarkers.

References

1. Kaustabh Kumar Maiti, K. Sujathan, **Varsha Karunakaran**; Screening Kit for Detection of Grades of Cervical Cancer and Process for the Preparation Thereof; **PCT Int. Appl. (2020), WO 2020021568 A1 20200130. Language: English, Database: CAPLUS, Date: 30th January, 2020**.

2. **Varsha Karunakaran**; Valliamma N. Saritha; Manu M. Joseph; Jyothi B Nair; Giridharan Saranya; Kozhiparambil G. Raghu; Kunjuraman Sujathan*; Krishnannair S. Kumar*; Kaustabh K. Maiti* Diagnostic Spectro-Cytology Revealing Differential Recognition of Cervical Cancer Lesions by Label-free Surface Enhanced Raman Fingerprints and Chemometrics.; **Nanomedicine: Nanotechnology, Biology, and Medicine**, 29(2020)102276.

3. **Varsha Karunakaran**; Deepika S, Valliamma N. Saritha.; Ramya A.N.; Vishnu Priya Murali.; P.T. Sujai; K.G. Raghu; K. Sujathan*; Kaustabh Kumar Maiti*; New Insight of Raman Image Guided Detection of Clinically Confirmed Grades of Cervical Exfoliated Cells by Dual Biomarker Appended SERS-Tag; *Manuscript under review.*

4. Maiti Kaustabh Kumar; Kunjuraman Sujathan; Murali Vishnu Priya; **Varsha Karunakaran**; S Deepika; M Madhukrishnan; Valliamma Neelakantapillai Saritha; Asha Lekshmi; A Diagnostic Screening Kit for Simultaneous Detection of Clinically Relevant Biomarkers from Breast Cancer Tissue Samples using Surface Enhanced Raman Scattering Platform and Process for the Preparation Thereof; **Indian Patent Application no. 202011034768, dated 11.08.2020.**

5. **Varsha Karunakaran;** Vishnu Priya Murali; Valliamma Neelakantapillai Saritha; Asha Lekshmi; Deepika S; Madhukrishnan M; Shamna K; Exploring the multiplexing SERS platform for the differential detection of clinically relevent breast cancer biomarkers using surface enhanced scattering nanoprobes; *Manuscript under preparation.*

6. **Varsha Karunakaran;** Saranya Giridharan; Manu M Joseph; Vishnu Priya Murali; Deepika S; Kaustabh Kumar Maiti*; An insight into a dual modal detection platform for the early diagnosis of Alzheimer's Disease biomarker $A\beta_{1-42}$ using SERS and MRI; *Manuscript under preparation*.

Chapter 1

Insights of Surface Enhanced Raman Scattering Based Diagnostic Platform:

The Future of Nanodiagnostics in Clinics
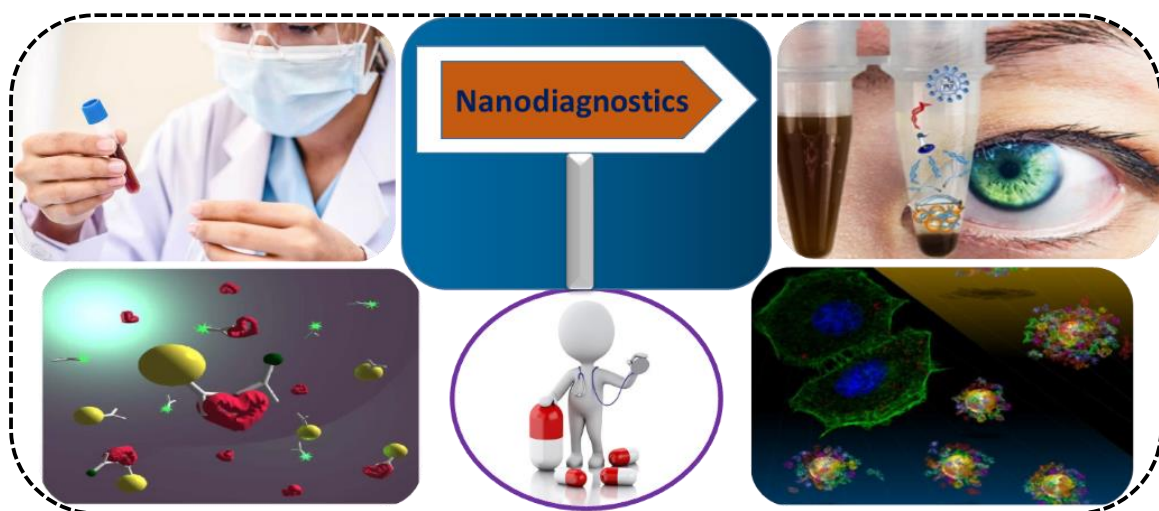
1.1 Abstract:

Unique fingerprints, ultrasensitive nature, highly specific analyte detection and excellent multiplexing properties has brought surface enhanced Raman spectroscopy (SERS) in the frontiers of sensing and imaging applications in biology and medicine. Diagnosis with minimized invasiveness and pain is desirable in clinical scenario for the comfort of patients. SERS renders a specific, non- invasive, spatially resolved and selective detection platform maintaining all these features including the advantages of conventional Raman spectroscopy. Employment of metallic nanoroughened SERS substrates aids as the hotspots for Raman active molecular enhancement to higher orders of magnitude which distinguishes it from conventional Raman spectroscopy. SERS modality has immense potential in identifying subtle differences in the biomolecular disease markers from complex biological samples in nanoscale for diagnostic and therapeutic applications along with improved clinical outcomes. A total

exploration of this technique covering all mechanistic and functional aspects along with safety and efficiency of SERS nanoparticles (NPs) are essential for its successful clinical translation. The present chapter gives an insight into SERS based diagnostic optical probe development for biomedical and related applications in disease diagnostics highlighting relevant clinical outcomes along with the aim and objectives of the thesis.

1.2 Nanotechnology in disease diagnostics

A disease is an abnormal medical condition which gradually disturbs the homeostasis maintained for the normal functioning of the body.[1] Diseases may be caused by infectious agents or by internal dysfunctions of the organs. Diseases can be classified as communicable diseases (CD) and non-communicable diseases (NCD) (**Figure 1.1**). An infectious disease that is contagious and that can be transmitted either directly or indirectly from one source to another by an infectious agent or its toxins can be regarded as CD and are generally caused by pathogenic agents including bacteria, fungus, viruses, protozoa etc. NCD is a noninfectious health condition which cannot be spread from person to person and normally lasts for a long period of time. Diseases including cancer, heart disease, respiratory disease, neurodegenerative disorder, autoimmune disease, genetic disease and many more can be added to this list.[2] According to World Health Organization (WHO) fact sheet published in 2018, NCD kills around 41 million people every year leading to 71% of deaths globally. About 15 million people die due to NCD between the 30 and 69 years i.e. over 85% of deaths happen in developing countries. Proper screening, detection methods and therapies are the key components for managing NCDs.

Existing diagnostic practices are not satisfactory for early detection and if so, are often expensive. Early identification of disease is the crucial factor for improving treatment strategies and thereby increasing patient survival.[3] Development of an ultrasensitive diagnostic platform may improve the difficulties existing in the currently available techniques. The capability to scrutinize nanomaterials at the molecular level has progressed the exploration for resources with exceptional features. One of the most sensational cutting edge innovation is the advance of nanomaterials for biomedical applications. The employment of nanomaterials has created a new research area named nano-biotechnology that plays

a key role in disease diagnostics and therapy. Nanobiotechnology renders countless applications for the challenges experienced in diagnosis and therapy of
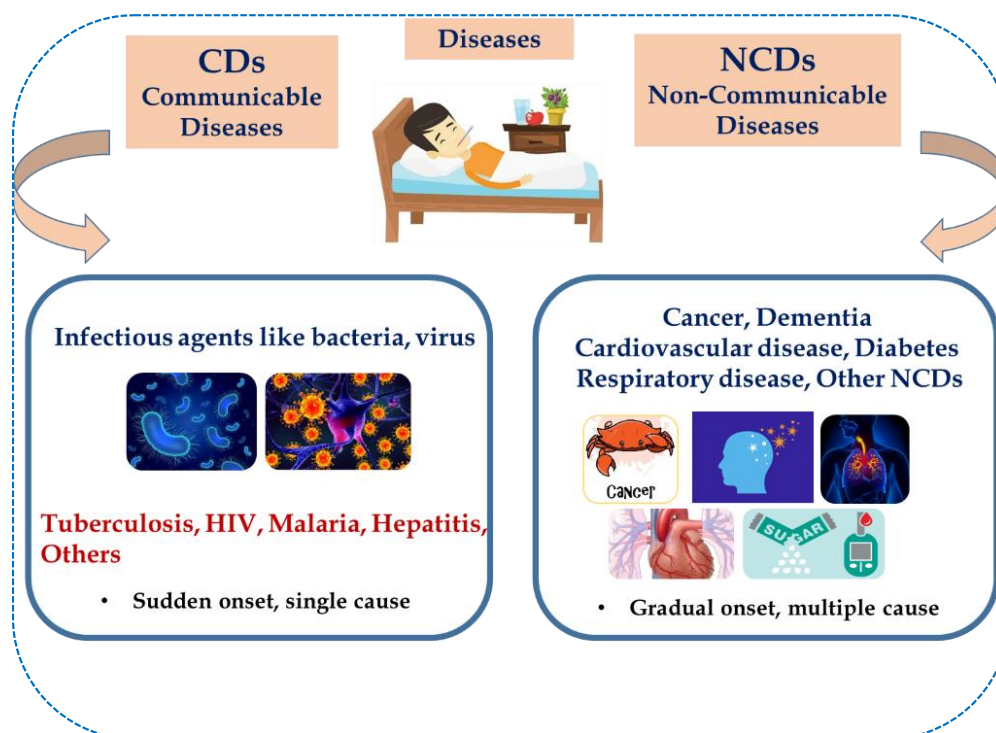
Figure 1.1: Classification of diseases as communicable and non-communicable diseases.

a diverse range of diseases.[4] Nano based technologies is the utilization of matter in atomic, molecular and supramolecular scale typically within 100 nm (**Figure 1.2**). NPs are prepared with monodispersity and reproducibility from different materials in different sizes and shapes by tunable controlled synthesis. NPs are constituted by organic or inorganic bulk materials which enable to tune its structural and functional features. Inorganic metal NPs are generally made using gold, silver, silica, iron oxide, titanium dioxide, copper etc. Organic nanomaterials includes dendrimers, liposomes, polymeric NPs, carbon NPs etc. Nanomaterials possess excellent physical, chemical, optical and electronic properties with high stability under ambient condition which evolved as a potential tool for diagnosis, treatment and proper control of the disease.[5] An assessment identified that more than 247 nano-based medical products got approved by the Food and Drug Administration (FDA) in 2013.[6] A recent update in 2019 shows the approval of new nanomaterials with diagnostic and therapeutic applications undergoing clinical trials.[7] In this regard, the present thesis describes the

design and development of nanomaterial based probes for two non-communicable diseases, viz. Cancer and neurodegenerative disorder, Dementia.
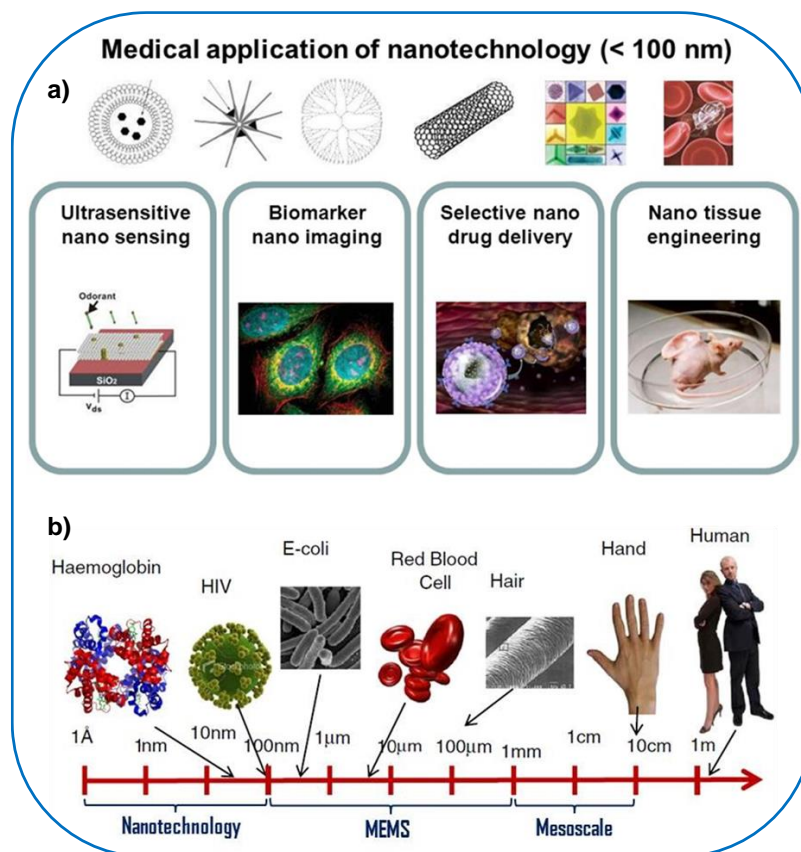
Figure 1.2: a) Biomedical applications of nanotechnology, b) representation of size scale towards nanotechnology.

1.2.1 Cancer

Cancer is a foremost public health problem around the world caused by the abnormal proliferation of cells with the potential to invade other parts of the body.[8,9] Cancer occurs when a progenitor single cell accumulates mutations and biochemical changes in the cell's genome. The signs and symptoms of cancer include a lump, cough, abnormal bleeding and change in bowel movements along with unexplained weight loss. [10] Global burden of cancer by WHO reports around 18 million cancer cases and 9.6 million cancer deaths as of 2020.[11] Cancer can occur anywhere in the human body and there are more than 100 types of cancers (**Figure 1.3**). The type of cancer is named according to the organs or tissues from which they form. The genetic change that leads to cancer is interplay of proto-oncogenes, DNA repair genes and tumor

suppressor genes. A cancer that has spread from a particular site where it started to another site in the body is called as the metastatic cancer. There are several types of cancer according to the specific types of cells including carcinoma (epithelial cells), sarcoma (soft tissues and bone), leukemia (blood forming tissue of bone marrow), lymphomas (T cells and B cells), multiple myeloma (plasma cells), melanoma (cells producing melanin), brain and spinal cord tumors, other tumors including germ cell, neuroendocrine, carcinoid etc.[12,13] Early diagnosis is the key factor for the proper treatment and survival in cancer. Staging of cancer also is a prerequisite to assess patient's prognosis and to develop strategies for the appropriate therapy. Staging and grading are the approaches taken as a diagnostic measure to evaluate how extend the cancer has progressed from initial stage.[14,15] Physical exams, laboratory tests, biopsy, imaging tests like X-ray, computed tomography (CT), MRI, positron emission tomography(PET), ultrasound imaging are employed in cancer detection.[16] The treatment of cancer includes surgery, chemotherapy, immunotherapy, hormone therapy, radiation therapy, targeted therapy, precision medicine, stem cell transplant etc.[17]
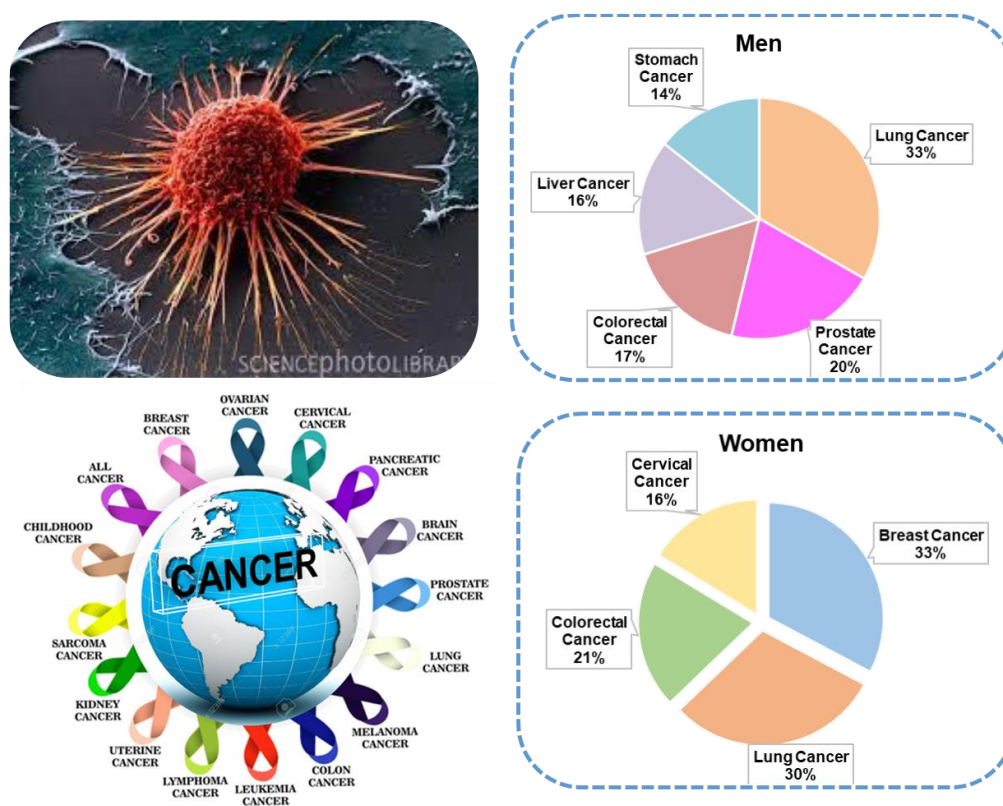
Figure 1.3: Cancer, its types and cancer related death statistics, WHO report, 2018.

Carcinoma is a class of type of cancers that is developed from epithelial cells. Several types of carcinoma includes squamous cell carcinoma, adenocarcinoma, adenosqaumous carcinoma, large cell carcinoma, anaplastic carcinoma, small cell carcinoma, carcinoma of unknown primary site etc. depending upon the lineage.[18] The eight distinctive hallmarks of cancer includes cell death resistance, nourishing avoiding growth suppressors, abnormal growth signaling, activating invasion supporting replicative immortality, angiogenesis induction and metastasis, cellular energetics deregulation and metabolism and preventing immune destruction.[19] Cervical cancer and breast cancer, two types of cancers commonly affecting the epithelial cells are included in the thesis.

1.2.2 Dementia

Dementia is a canopy term used to explain a neurodegenerative clinical syndrome consisting progressive cognitive declines which interferes with a person's ability for independent functioning.[20] The prevalence of dementia is nearly 50 million people worldwide, with around 10 million new cases annually.[21,22] The symptoms of dementia are persistent with a gradual progression.
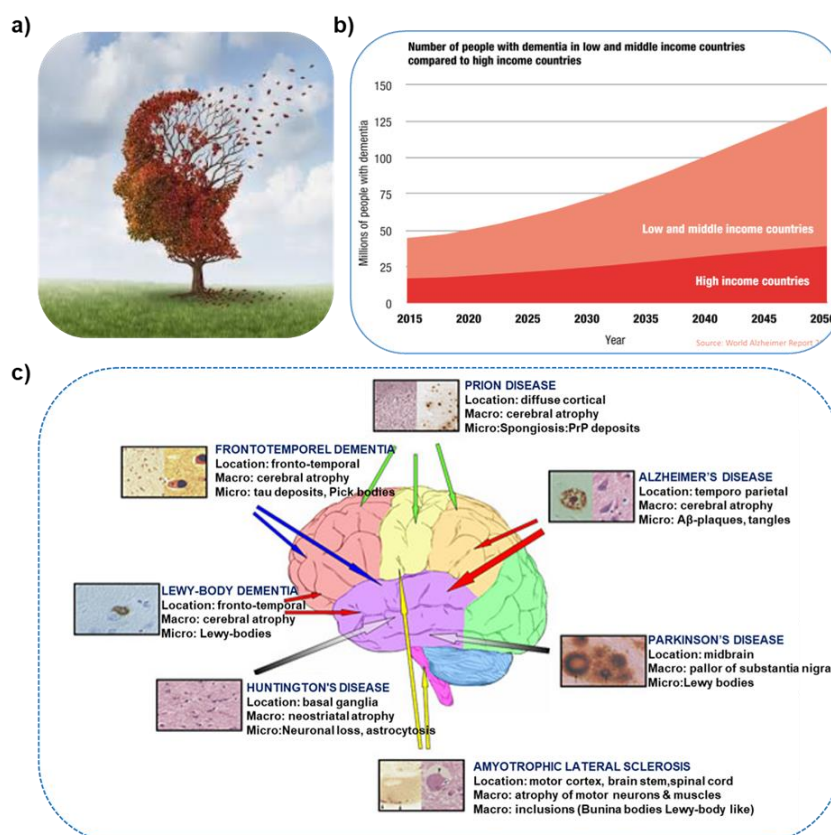
Figure 1.4: a) Representation of dementia, b) incidence of dementia in low, middle and high income countries c) different types of dementia and its histopathologic staining.

Dementia causes deterioration in memory, other cognitive domains, and behavior along with a physical, social, psychological and economic impact on the patients, their caregivers, families and society. The diagnosis of dementia within its subtypes can be challenging and no single test exists to diagnose it. Its subtypes include Alzheimer's Disease (AD), Lewy body dementia, vascular dementia and frontotemporal dementia which are classified according to the cause of dementia (**Figure 1.4**). Most of the subtypes interconnects in a heterogeneous group of disorders accumulating common pathologic proteins in the brain.[23] Current diagnosis of dementia is based on physical and neurological examination, lab tests, mental and neuropsychological testing using diagnostic criteria, e.g. Diagnostic and Statistical Manual of Mental Disorders (DSM-V) or International Classification of Diseases-10 (ICD-10),[24,25] based on the history etc. Brain imaging modalities like MRI, CT, PET and biomarkers in cerebrospinal fluid (CSF) etc are additional diagnostic measures.[26] AD, the most common category of dementia is included in the thesis.

1.3 Current diagnostic modalities and its disadvantages

Emergence of better diagnostic modality is essential for the early detection of diseases to design efficient treatment strategies. Biomedical imaging techniques are widely used in every phases of management of diseases. Imaging techniques like X-ray, CT, MRI, PET, SPECT, Ultrasound Imaging, Optical imaging etc are currently employed in clinics (**Figure 1.5**). The pros and cons of the current technique are depicted in **Figure 1.6**.

1.3.1 X-ray imaging

X-rays are the widely used diagnostic 2 dimensional (2D) imaging test which uses a form of radiation, to pass through the body or its parts which block the radiation looking white on the X-ray. The less dense tissues are difficult to see and appear gray in color. High-resolution non-invasive imaging of thick biological specimens is obtained using X-rays. High resolution images can be created because of its deep tissue penetration and low scattering coefficient relatively. Clinicians use X-rays for diagnosing infections, bone-fractures, tumors etc. The main disadvantage is that large X-ray doses can cause short term tissue damage increasing the risk of developing cancer. The specificity, sensitivity, resolution and acquisition rate should

be maximized with decreasing X-ray dose, contrast toxicity and concentration. Mammography is a process of employing low-energy X-rays to diagnosis and screening of breast cancer.[27,28]
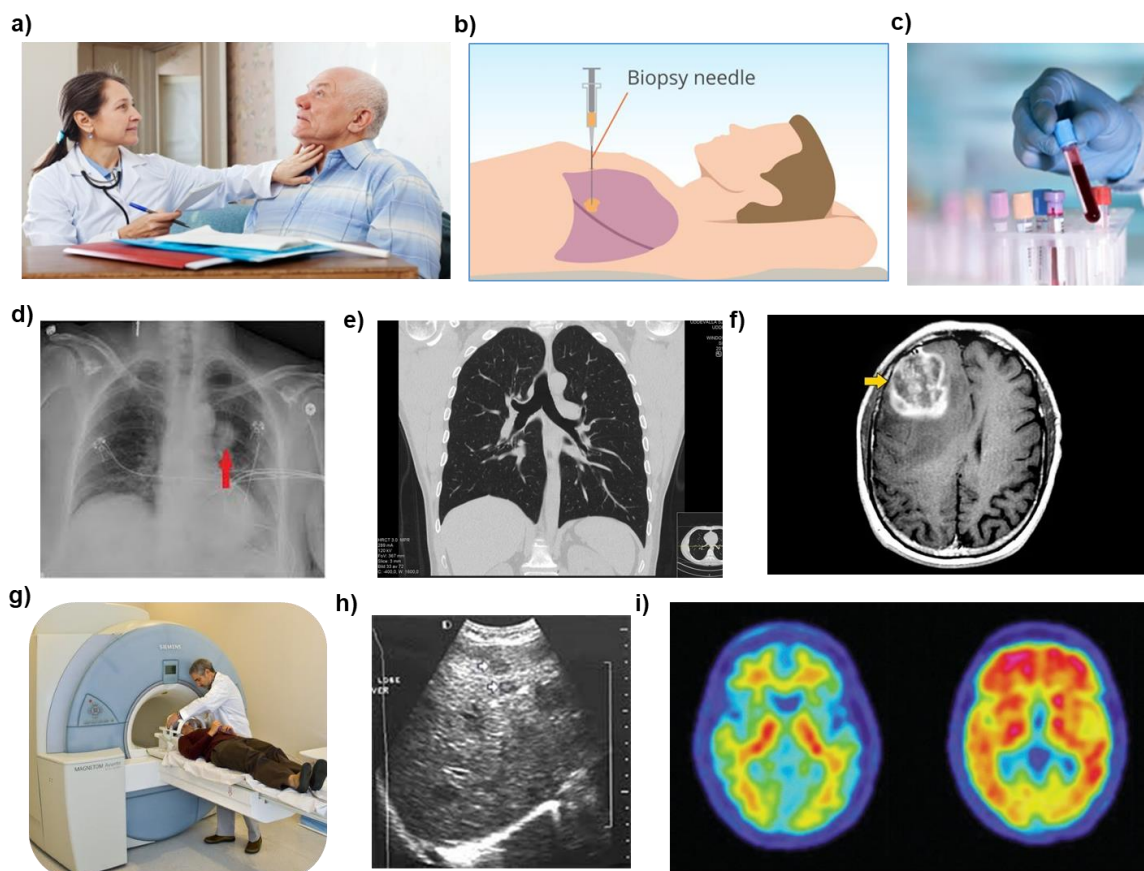
Figure 1.5: Current diagnostic modalities used in clinics, a) physical examination, b) biopsy, c) laboratory test, d) X-ray, e) PET, f) MRI, g) MRI scanning procedure, h) ultrasound, i) SPECT scan.

1.3.2 Computed tomography imaging

Computed Tomography based imaging is high quality detailed imaging of the body. A CT scan is a medical imaging technique that uses combinations of different X-ray measurements obtained from different angles to yield cross-sectional or tomographic images as slices from specific areas of a body, allowing to seeing inside the specimen without cutting. It is a more dominant and refined X-ray technique that takes a full image of the spine, bones, soft tissues, blood vessel and other internal organs etc. Sometimes a dye is also used for getting a contrast for the image. The CT scanning machine makes 3 dimensional images by rotating on an axis subsequently taking numerous 2D images of a subject's body from several angles. Using a computer, the cross sectional images will be combined together resulting in an image. CT scan is commonly used to help

diagnose medical conditions like cancer, neurodegenerative diseases, appendicitis, heart disease, infectious disease, trauma, muscle or skeletal disorders etc. The disadvantages include high radiation exposure and limitations in biocompatible contrast agents.[29,30]

1.3.3 Magnetic resonance Imaging

The growth of magnetic resonance imaging (MRI) in medical investigation has delivered a huge advancement in the field of diagnosis, which completely eliminates the exposure to possibly hazardous ionizing radiations. MRI is a medical imaging technique used commonly in radiology to image the anatomic and physiological processes in the body. The MRI scanners use strong magnetic fields with radio waves to generate images of the body. A computer is connected to function the magnetic components to create detailed images as slices. MRI has vast clinical applications like diagnosing joint and bone problems, monitoring treatment progress in cancer and neurological disorders etc. Even though MRI has advantages like spatial resolution and ability to collect lot of biological information, it is time consuming and expensive.[31]

1.3.4 Positron emission tomography imaging

Positron emission tomography is a technique which uses radioactive substances to image and analyze the metabolic processes in the body. A tracer containing glucose is swallowed, injected or inhaled into the body which reaches the desired location. Positrons emitted from the radiotracer will combine with nearby electrons to produce gamma rays which are detected by a detector. The location and energy of the gamma rays is recorded and a computer is used to reconstruct 3 dimensional (3D) images of tracer within the body. If there is high metabolic activity, the tracer will get accumulated more and show as bright spots. Generally, the dose of tracer is safe and clinicians used PET scanning for diagnosing problems related to cancer, heart and brain diseases.[32,33] Even though it has high penetration depth and high sensitivity, the technique is extremely expensive.

1.3.5 Single-photon emission computed tomography imaging

Single-photon emission computed tomography (SPECT) imaging is a technique which uses a gamma-emitting radioisotope through the blood stream into the patient. The tracers used in SPECT will emit gamma radiation which is measured directly

unlike PET. Moreover, SPECT scanning is less expensive than PET. Different radioactive isotopes labelling can be done at a time with high penetration depth. The application of SPECT imaging includes tumor, brain, heart imaging, identification of infections etc. Spatial resolution is limited in the case of SPECT scanning.[34,35]

1.3.6 Ultrasound imaging

Ultrasound imaging uses acoustic waves for the construction of image from the underlying body. It is based on reflection, frequency shift and scattering of sound waves. Ultra sound imaging can detect tissue elasticity in tumor cells as well as normal cells. It is a clinical friendly less expensive imaging technique having high temporal and spatial resolution. It is employed to generate an image of internal body structures such as blood vessels, muscles, tendons, joints and internal organs. The limitations of ultrasound imaging include its disability for bone and lung imaging. [36]
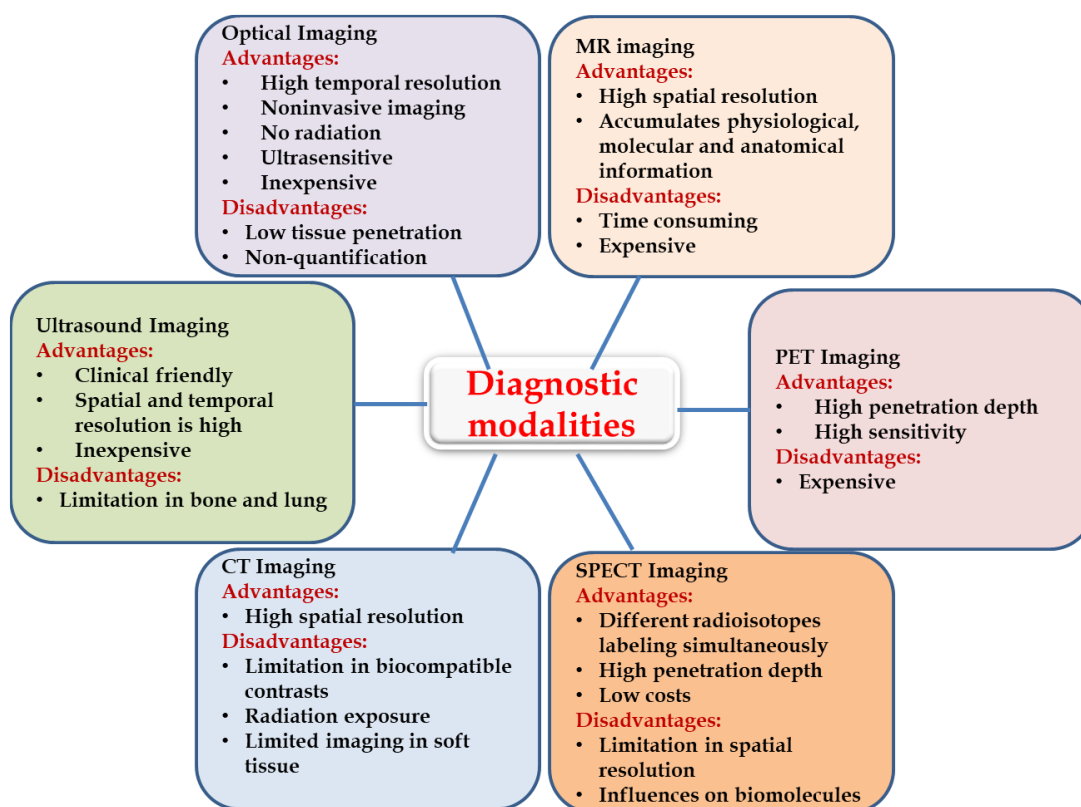
Figure 1.6: Advantages and disadvantages of currently used imaging techniques.

1.4 Optical imaging

Optical imaging involves the application of light as an imaging source for bio-medical applications. It generates images by exciting electrons using light to capture

reflection, scattering, absorption, emission, polarization, fluorescence and coherence of the electromagnetic spectrum (visible, ultraviolet, and infrared light) depending on the specimen properties. Optical imaging is highly efficient and safe due to the non-ionizing radiation. Hence, it has immense applications in diagnosis, and therapy processes. Another added advantage is its compactness, portability, and cost-effectiveness. The major types of optical imaging include endoscopy, photoacoustic imaging (PA), optical coherence tomography, diffuse optical tomography, super-resolution microscopy, terahertz tomography and Raman spectroscopy (**Figure 1.7**). Even though disadvantages in terms of low tissue penetration and non-quantification includes in optical imaging, the advantages like non-invasive imaging, high temporal resolution with no radiation exposure and minimal cost makes it a comparatively acceptable technique in the field of bio-imaging. Improvements in optical imaging can bring immense applications in biology and medicine.[37–39]
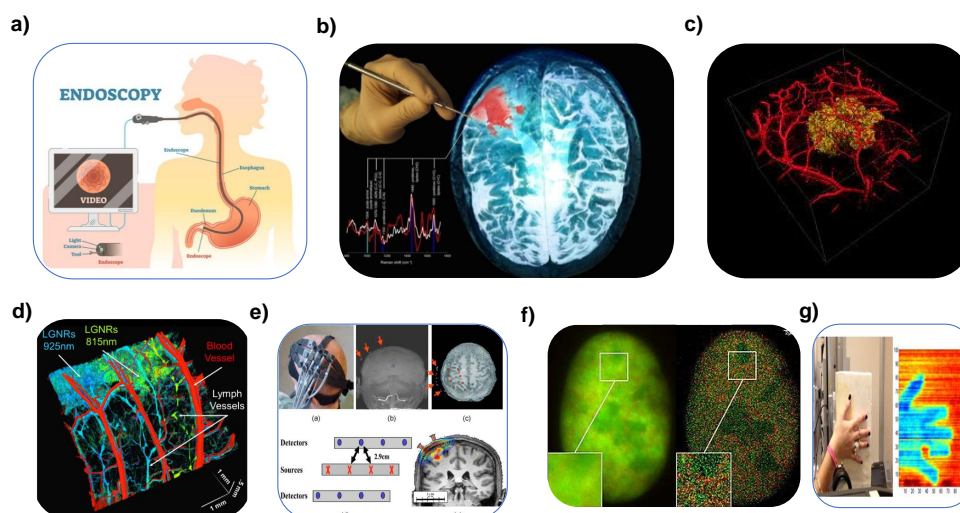
Figure 1.7: Optical imaging techniques having potential for clinical applications, a) Endoscopy, b) Raman spectroscopy, c) PA imaging, d) optical coherence tomography, e) diffuse optical tomography, f) super resolution microscopy, g) terahertz tomography.

1.4.1 Endoscopy

An endoscopy is an optical technique used to view inside the body. The procedure employs an endoscope which is capable of examining the interior of a hollow cavity of the body by directly inserting into the organ. It is used to investigate problems associated with the digestive system most commonly by a biopsy check for cancers, bleeding, infections associated with the digestive system. [40]

1.4.2 Photoacoustic imaging

PA imaging is a fusion technique which exposes the tissue using a laser and measures light induced ultrasound signals. Non-ionizing laser pulses are delivered into biological tissues to produce significant contrast making it visible to see the internal organs. The most astonishing factor of this technique is the capability to characterize tissue components like collagen, lipids, hemoglobin, melanin etc. Thus it possess immense application such as detection of breast, brain tumor and monitoring of hemodynamics.[41]

1.4.3 Optical coherence tomography

Optical coherence tomography (OCT) is a type of non-destructive biomedical imaging technique which uses low-coherence light for capturing 2D and 3D images from within a biological system. OCT imaging is used extensively for imaging applications in oncology, ophthalmology, cardiology, dermatology etc for analyzing and quantifying the morphological changes in various disease states.[42]

1.4.4 Diffuse optical tomography

Diffuse optical tomography (DOT), is one of the most refined optical imaging technique for 3D quantitative imaging of anatomical and functional aspects of biological tissues using near infrared spectroscopy (NIRS). It possess applications in brain, breast cancer, thyroid, muscle, joint, peripheral circulation, wound imaging etc.[43]

1.4.5 Super resolution microscopy

Super-resolution microscopy (SRM) allows images to be taken in a higher resolution than the diffraction limit which enables biologists to visualize individual molecules interacting dynamically. SRM can be grouped into two categories mainly explain ensemble and single molecule technique. In ensemble technique, fluorophores renders a nonlinear response upon excitation which enhances resolution. Such methods include Stimulated emission depletion (STED) microscopy, Structure illumination microscopy (SIM) etc. Single-molecule-based techniques uses the several molecular light sources making close by fluorophores emitting light at different times leading to resolution upon time. It includes photo activated localization microscopy (PALM), stochastic optical reconstruction microscopy (STORM), etc.[44]

1.4.6 Terahertz tomography

Terahertz tomography is a type of tomography where terahertz radiation performs sectional imaging which possess high signal to noise ratio because of its high frequency with short wavelength. It uses a frequency between 0.1 and 12 THz falling between radio waves and light waves on the electromagnetic spectrum. It shows applications in cancer cell detection, blood cell detection, identification of bacteria, biological tissue discrimination etc.[45]

1.4.7 Raman spectroscopy

Raman spectroscopy is a type of vibrational spectroscopy technique used to provide a structural fingerprint in which molecules can be identified non-invasively. Raman spectroscopy depends upon the inelastic scattering of light termed as Raman scattering. When photons in light interacts with molecules in a solid, liquid, or gas, majority of the photons get scattered or dispersed at the energy similar to the incident photons known as the Rayleigh scattering or elastic scattering.[46] A small proportion around 1 photon out of 10 million of these photons get scattered at a changed frequency than the incident photon called as the Raman effect or inelastic scattering. It is named after Sir C.V. Raman who received the Nobel Prize in Physics in 1930.[47] If the molecule relaxes to an energy level that is different than that of its incident radiation producing a photon of different energy is termed the Raman shift. If the later state has higher energy than the initial state, the scattered photons will be shifted to a lower energy called a Stokes shift. If the later state possesses lower energy, the scattered photons will be shifted to a higher energy known as an anti-Stokes shift. Raman spectroscopy allows to collect molecule's vibrational signature which provides the information about its structure and interaction with other molecules. Changes in the molecular polarizability are visualized using Raman spectroscopy. Raman spectroscopy set up includes a light source, typically a laser (532/633/785nm etc), filter for removing the Rayleigh scattering and a spectrograph based CCD detector. Raman spectroscopy offers benefits including use of less harmful Near Infra-Red (NIR) radiation high spatial resolution, less sample preparation, not influenced by water bands, use *in vivo/in situ* measurements etc. Raman spectroscopes has been
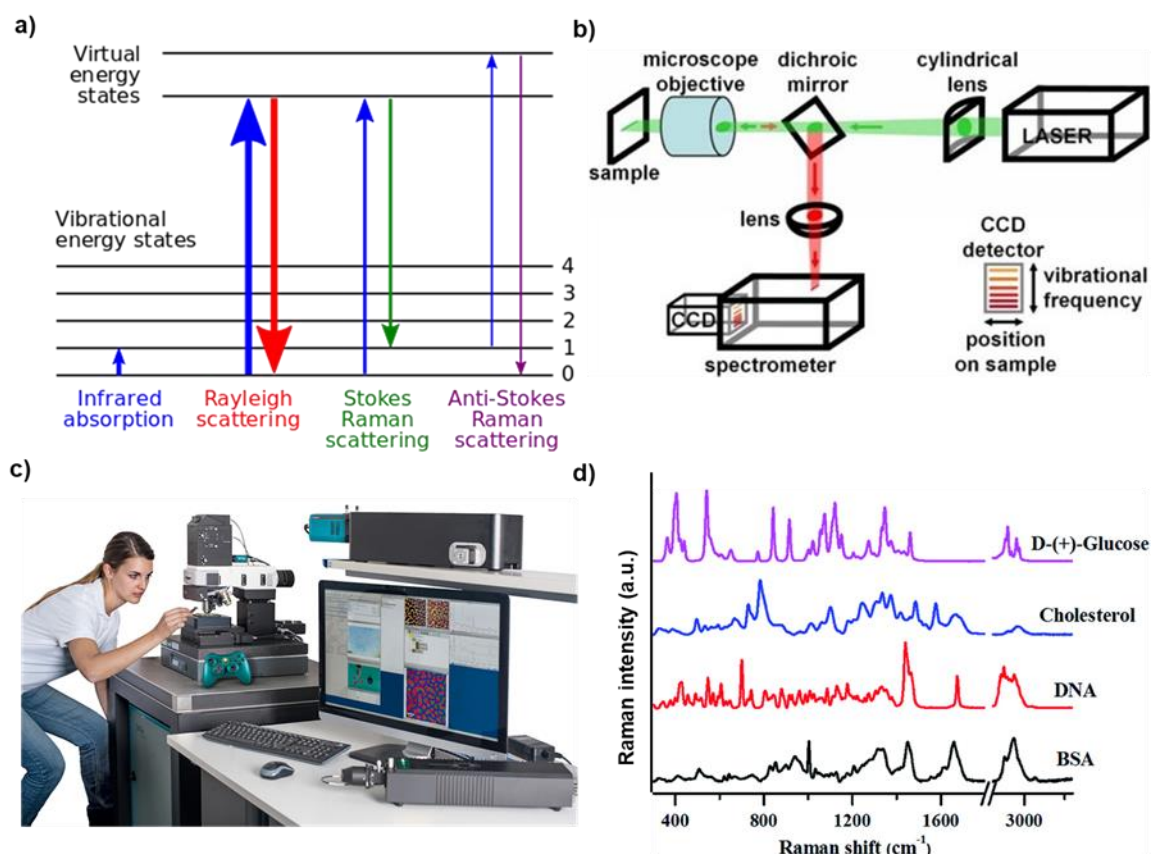
Figure 1.8: a) Principle of Raman spectroscopy, b) Raman microscopic set up, c) Raman instrument, d) Raman spectrum of biological molecules.

employed for a variety of applications since that time from material science, analysis of chemical and biochemical reaction to broad area of biomedical and diagnostics using chemometric analysis[48] (**Figure 1.8**).

1.5 Chemometric analysis

Chemometrics is the area in science which extracts information present in chemical systems by developing a mathematic or statistical algorithm. Chemometrics is an interdisciplinary method used in disciplines like mathematics, multivariate statistics and computer science in order to solve problems in chemistry, medicine, biology and engineering. The properties of a particular system are modeled to understand the structure and relationship of the system. It can also be used to predict new behaviors or properties which use datasets that are very large and hugely complex, involving thousands of variables, cases or observations. Raman spectroscopic studies of closely related species is usually accompanied by the employment of chemometric analysis for the efficient classification.[49] Principal

Component Analysis (PCA),[50] Linear Discriminant Analysis (LDA),[51] Support Vector machine (SVM),[52] Partial Least Square Discriminant Analysis (PLS-DA)[53] etc includes the list of multivariate analysis used for the discrimination between the groups. Several studies have been performed to investigate the biomedical uses of Raman spectroscopy in diagnosis of diseases including cancer and many more.

1.6 Diagnostics applications of Raman spectroscopy

A Raman spectroscopy based cervical has been carried out with four cervical cancer lines, C33A (HPV negative), HeLa (HPV-18 with 20-50 copies) SiHa (HPV-16 with 1-2 copies), CaSki (60-600 copies). The Raman spectroscopic analysis with PCA showed clear classification of the four groups. [54] Excisional breast biopsies are essential to classify the breast lesions like normal, fibrocystic change, infiltrating carcinoma, fibroadenoma etc. Raman spectroscopy along with logistic regression technique successfully classified the lesions with 94% sensitivity and 96% specificity which will be advantageous in reducing the excision rate.[55] Similarly a Raman spectroscopic study was carried out for the detection of pre-metastatic changes in mice lung microenvironment from primary breast tumors, using multivariate analysis of pattern variations in molecular expression. MDA-MB-231 cell having high and MCF-7 cells having low metastatic potential were grown as orthotopic xenografts in euthymic nude mice which provided objective identification of the premetastatic niche [56] (**Figure 1.9 a, b**). Oral cancer has improved survival rate if detected early. A Raman spectroscopy based study was successfully performed in tissues as well as cells showing the classification of cancer from the normal specimens along with PCA analysis.[57] Lung cancer possess poor patient survival even after diagnosis as the molecular changes are still unclear. Raman spectroscopy analysis together with K-nearest neighbor (kNN) and SVM successfully diagnosed lung cancer with an accuracy of 99 %.[58] A blood based Raman spectroscopy study was investigated to diagnose AD and dementia with lewy bodies in blood. Early stage, late stage, dementia with lewy body, and normal controls were used for the study. Good sensitivity and specificity were obtained for the four groups suggesting a cost effective analysis for neurodegneration in dementia (**Figure 1.9 c**).[59] For managing diabetes, self-monitoring is essential. A point of care Raman spectroscopy based system was developed for the detection of glucose in diabetes. The study showed a limit of
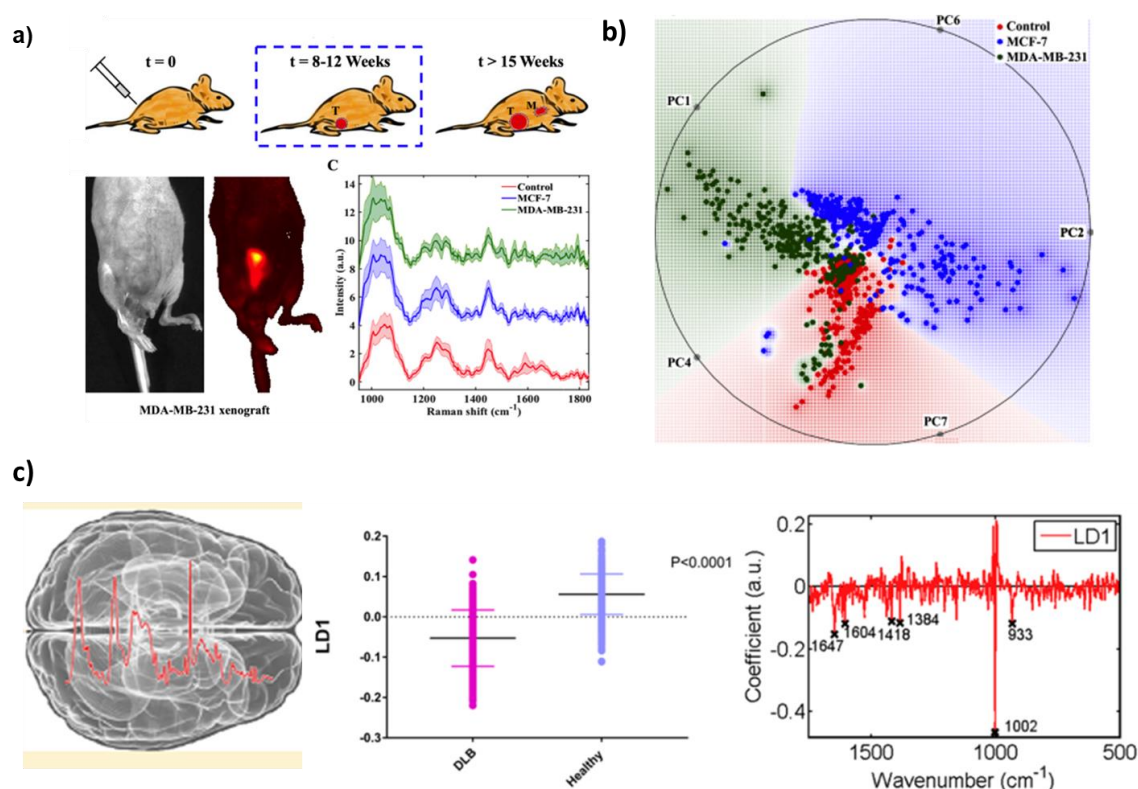
Figure 1.9: a) Raman signal profiling of mice pre-metastatic lungs from primary breast cancer, b) Radial visualization plot with three clusters for sacrificed mice's lung samples bearing MDA-MB-231 and MCF-7 breast cancer xenografts along with controls without xenografts,[56] c) Healthy versus Dementia with Lewy bodies, one dimensional LD score plot and loadings showing major discriminatory peaks.[59]

detection (LOD) of 0.9 mM displaying the potential of point of care monitoring of glucose.[60] Likewise infectious agents like bacteria and viral detection are also possible by Raman spectroscopy. A study for identification of single bacteria [61] and early detection of viral infection[62] in living human cells was demonstrated by Raman spectroscopy along with PCA analysis. All these studies show the universal diagnostic potential of Raman spectroscopy in various kinds of diseases.

1.7 Types of Raman spectroscopy

Raman effect is inherently weak which limited its applications at certain circumstances. Improvisation on the Raman spectroscopy has paved the way to the development of advanced techniques like surface enhanced Raman spectroscopy (SERS), tip enhanced Raman spectroscopy (TERS), stimulated Raman spectroscopy (SRS), coherent anti-Stokes Raman spectroscopy (CARS), resonance Raman

spectroscopy (RRS), hyper Raman spectroscopy, transmission Raman spectroscopy etc.[63]

1.7.1 Coherent anti-Stokes Raman spectroscopy

Coherent anti-Stokes Raman spectroscopy (CARS) is a type of Raman spectroscopy used in areas like physics, chemistry and related fields. It possesses sensitivity to the nuclear vibrations of chemical bonds of molecules as in Raman spectroscopy. The main difference of CARS from other Raman spectroscopy is the use of multiple photons for producing a coherent signal to represent the molecular vibrations resulting in orders of magnitude stronger than normal Raman. CARS also received immense attention in the scientific community and got several biomedical applications.[64]

1.7.2 Tip enhanced Raman spectroscopy

Tip-enhanced Raman spectroscopy (TERS) is an approach of Raman spectroscopy in which enhancement of the signal happens only at the point of a metallic sharp pin typically made of gold or silver. TERS is one the most capable analytical technique for investigating vibrational states within nanoscale resolution. It renders unique information regarding chemical interactions and structures. TERS possess several biomedical applications too.[65]

1.7.3 Resonance Raman spectroscopy

Resonance Raman spectroscopy is a type of Raman spectroscopy in which the incident energy of the photon possesses almost close or similar energy to an electron transition of a material or compound under investigation. The resonance or coincidence of the frequencies can lead to enhanced Raman signal intensity facilitating in studying low analyte concentrations. [66]

1.7.4 Stimulated Raman spectroscopy

SRS can take place when Stokes photons generated by spontaneous Raman scattering or deliberate injection of Stokes photons along with the original light. The Raman-scattering rate is increased much more than the spontaneous Raman scattering more effectively. Stimulated Raman scattering is an optical effect which is non-linear.[67]

1.7.5   Transmission Raman spectroscopy

TRS is a type of Raman spectroscopy favorable for probing bulk content samples like tableted or powdered in millimeter range. In pharmaceutical companies, characterization of bulk chemical materials is essential to characterize its constituency and purity in a non-invasive manner.[68]

1.7.6   Spatially offset Raman spectroscopy

Spatially offset Raman spectroscopy (SORS) is a kind of Raman spectroscopy allowing highly precise chemical analysis of objects under obscuring surfaces like tissue, bottles etc. Examples of uses include analysis of, bone under the skin, explosives inside containers, deep non-invasive diagnosis of breast tumors, tablets inside plastic bottles and packs.[69]

1.7.7   Surface enhanced Raman spectroscopy (SERS)

SERS received wide acceptance in research community due to its excellent enhancement (10^8 to 10^{14} folds) effect in the Raman spectrum of the molecules when it is in close proximity with the roughened metal NP surfaces like gold or silver.[70] The pioneering work by Fleischmann *et al* interestingly observed the enhancement of signal in the pyridine molecule Raman spectrum adsorbed over a roughened silver electrode.[71] Jeanmaire *et al* and Albrech tried to explain this surface effect partially. [72,73] Still, the actual reason behind the mechanism of enhancement in SERS is a matter of debate. Two primary mechanisms has been put forward, the electromagnetic enhancement[74] which proposes the localized surface plasmon excitation and chemical enhancement,[75] proposes the charge-transfer complex formation. A sensible maximum value for total enhancement was found to be about 10 orders of magnitude. SERS thus combines the advantages of bare Raman together with the benefits of metallic NPs which includes molecular identification, non-invasive nature, minimal sample preparation, un-influence of water bands, multiplexing capability due to narrow bands, portability and ultra-sensitivity for single molecule detection (**Figure 1.10**).

Figure 1.10. Applications of SERS in biology and medicine.[70]

1.8   SERS substrates

SERS renders the most important amplification technique for the enhancement of Raman signal using hotspots generated by plasmonic surfaces. The enhancement fallouts localized surface plasmon resonances (LSPR) excitation from amplification of the light. SERS substrates perform one of the most crucial role in the formation of hotspots for Raman signal amplification of the analyte molecules or reporter molecules. The presence of NPs makes SERS unique from bare Raman spectroscopy which commonly uses plasmonic surfaces include gold, silver, copper etc. The initially used substrates for SERS was metallic electrodes which were roughened electrochemically.[76] Metallic NPs were started to use shortly after the innovation of SERS effect and became the classic group of substrates. The LSPRs of the metal NPs span to NIR wavelength range from visible, making them suitable for Raman analysis. Gold and silver NPs are the most employed SERS substrates for the amplification of the Raman signatures from the analytes molecules which is faintly detected in conventional Raman owing to their less Raman cross-section. Design, optimization and tuning of new and existing plasmonic materials in different sizes and shapes are still going on for improving their enhancement efficiency. A wide range of SERS substrates were fabricated including gold and silver spherical NPs, bimetallic

composite NPs, nanostars, nanorods,   nanocubes, hollow gold NPs, nano rings, nanoflowers, nano pyramids, nanocages and many more[70] (**Figure 1.11**).
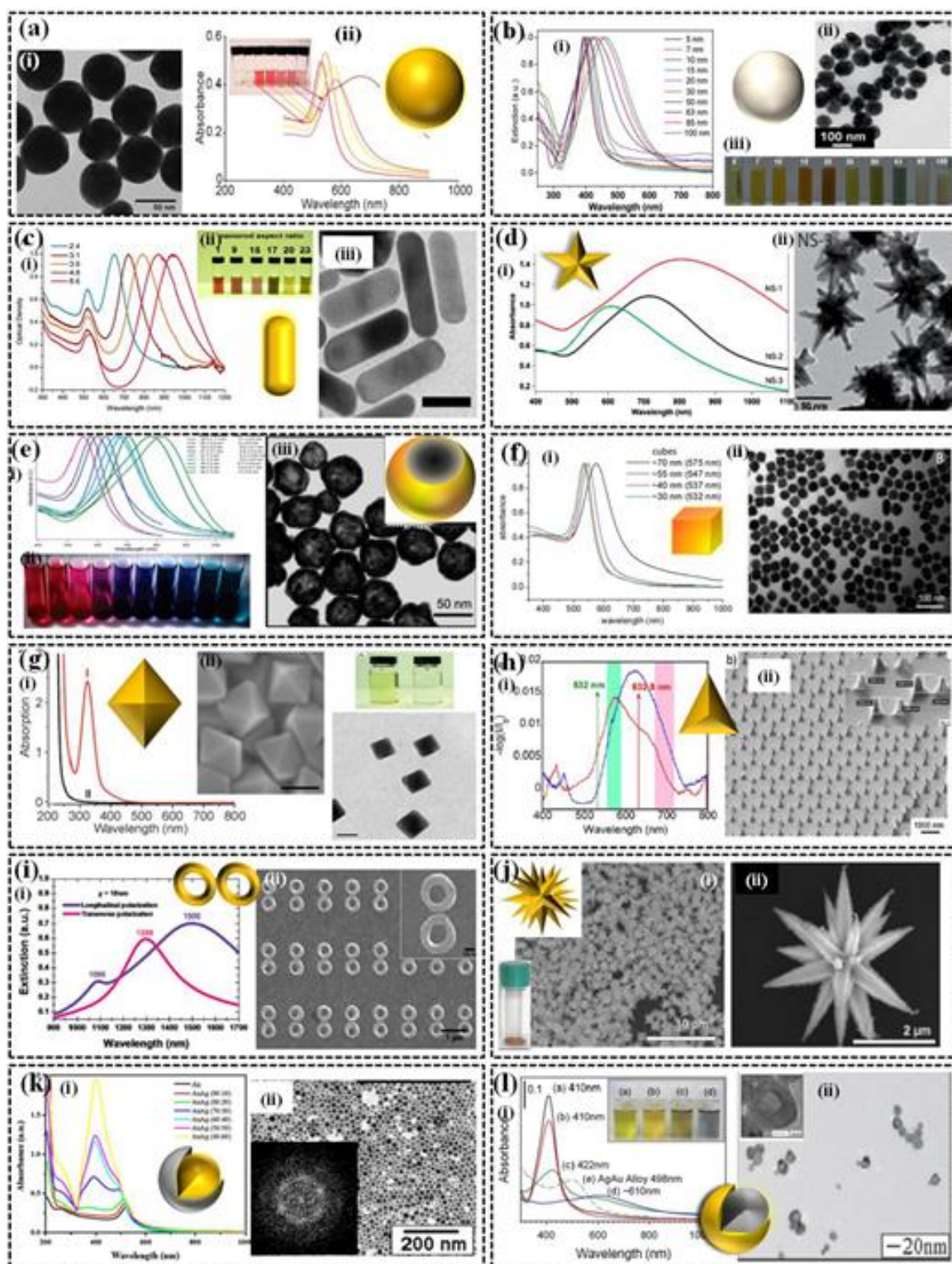
Figure 1.11: Different types of substrates used for SERS analysis. [70]

1.9 Types of SERS

SERS modality has been categorized into two types depending upon its use of Raman labels. SERS analysis based on SERS tags are called labelled SERS and which doesn't uses a Raman label is called label free SERS (**Figure 1.12**).
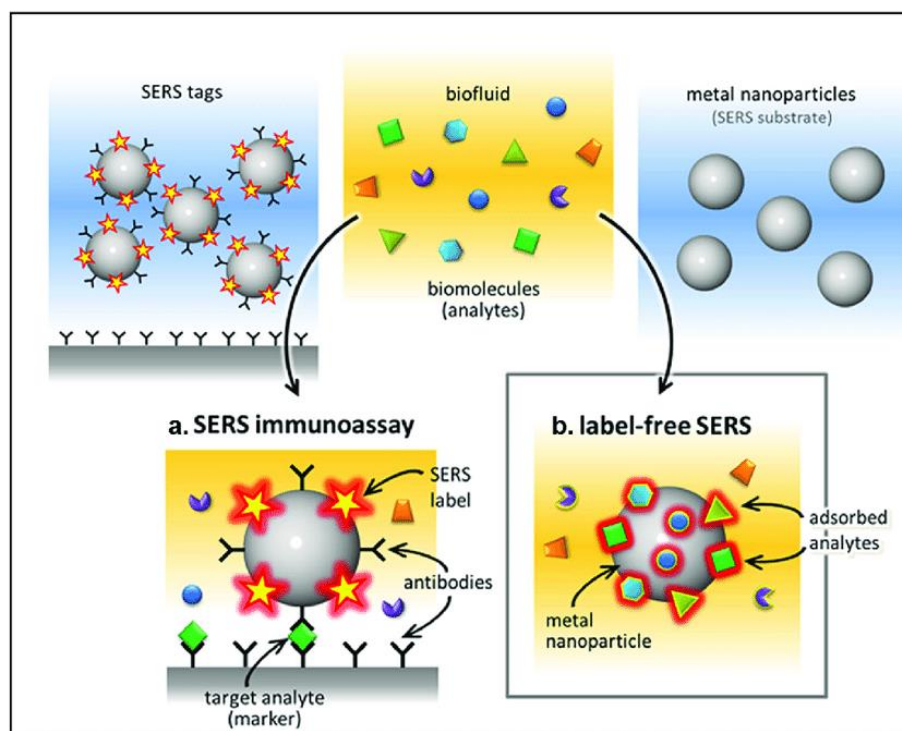
Figure 1.12: Types of SERS analysis, a) SERS immunoassay and b) label free SERS.

1.9.1 Label free SERS

Label-free techniques use physical factors like optical, electrical or sound signals instead of using any label or tag for detection purposes. Label free SERS analysis received immense scientific acceptance in biomedicine applications owing to its simplicity and sensitivity features. In label free analysis, the intrinsic signals will be obtained directly and specifically from the molecule under study providing insight into its detailed structural aspects which will be of significant importance in next generation screening methods. The narrow Raman spectral signals allows the multiplexed identification of complex biological mixtures including nucleic acids, proteins, lipids, sugars etc. providing vast information about its variations qualitatively as well as quantitatively. [77]

1.9.1.1   Applications of label free SERS in identification of biomolecules

Biomolecules are the essential constituents in a cell which includes mainly nucleic acids, proteins, lipids and carbohydrates. Any change happening to the biomolecules in terms of its structure or its expression level will result in a spectral change from its normal state reflecting variations its SERS fingerprint pattern (**Figure 1.13**.

1.9.1.1.a Proteins

Proteins constituted by the amino acids are one of the abundant biomolecules in biological system which is made up of amino acid peptide polymers. Any alterations in the protein level or its conformational changes lead to diseases. Several studies have been performed for the evaluation of protein molecules using SERS in a label free manner. A SERS modality has been developed for phenyl alanine, bovine serum albumin (BSA) and lysozyme detection using aggregation and plasmonic heating of gold nanorods at physiological pH.[78] Another study evaluated the label free detection of lysozyme, avidin, catalase and hemoglobin in aqueous solution which showed its practicability in protein detection in a high throughput manner[79]. In order to distinguish between two polypeptides having two different amino acids out of total nine amino acids, a SERS analysis was performed. Gold nanostars was used as the SERS substrate which was trapped in a gold nanohole to differentiate the polypeptides vasopressin and oxytocin.[80] Likewise the spectral fingerprint of hemoglobin,[81] insulin[82] etc also has been elucidated using SERS analysis.

1.9.1.1.b Nucleic acids

Detection of nucleic acids is highly advantageous and indispensable for screening of genome in the area of diagnostics, forensics etc. SERS has already shown its capability in identifying and detecting DNA samples with single base sensitivity.[83] Traditional DNA identification methods include polymerase chain reaction and gel electrophoresis which is usually time consuming and expensive. Spectral fingerprints of individual DNA bases like adenine, guanine, cytosine and thymine are elucidated by SERS analysis.[84] Likewise, DNA hybridization,[85] base mismatch identification[86] and homogenous nucleic acid detection[87] has been demonstrated using SERS. RNA detection was accomplished quantitatively using SERS by using single strands of polyadenosine, polyguanosine, polyuridine, polycytosine etc from non-hybridized

mixtures. Deconvolution of spectra was performed to identify the individual contribution of different strands. [88]A microfluidic associated SERS platform also showed the potential for RNA detection.[89]

1.9.1.1. c Lipids

Living cells are made up of lipid membranes which have functions like energy transfer, biosynthesis, immunological recognition etc. Thus it is vital to study the structural and dynamic property changes of lipid membranes for diagnosing certain kind of diseases. SERS analysis is capable of identifying signature peaks for lipid molecules. A SERS spectral model was generated using silicon substrate silver microprobe for sebaceous gland secretion and fatty acid generated by bacteria including fatty acids, triglycerides, hydrocarbons etc. having characteristic SERS fingerprint making them easily identified in mixtures. [90]A SERS analysis for studying the dynamic properties of the phospholipid has been carried out. Phospholipid coated gold NP has been used to study the phase state and the phase transition state of the lipids.[91] Microalgae accumulates neutral lipids as energy reserve in triacyl glycerol form. A SERS analysis has been performed in *Scenedesmus quadricada* and identified the unsaturated and saturated fatty acids under nitrogen starvation.

1.9.1.1.d Carbohydrates

Carbohydrates are one of the broad classes of organic biomolecule performing essential biological functions. Raman spectroscopy has been employed to differentiate between carbohydrate molecules when dissolved in aqueous medium. Seven structurally similar monosaccharide has been classified using spectral analysis along with mixture and disaccharide detection using colloidal silver NPs.[92] Likewise rapid glucose detection,[93] glycan-protein interaction[94] also has been investigated using SERS for the detection of carbohydrates.
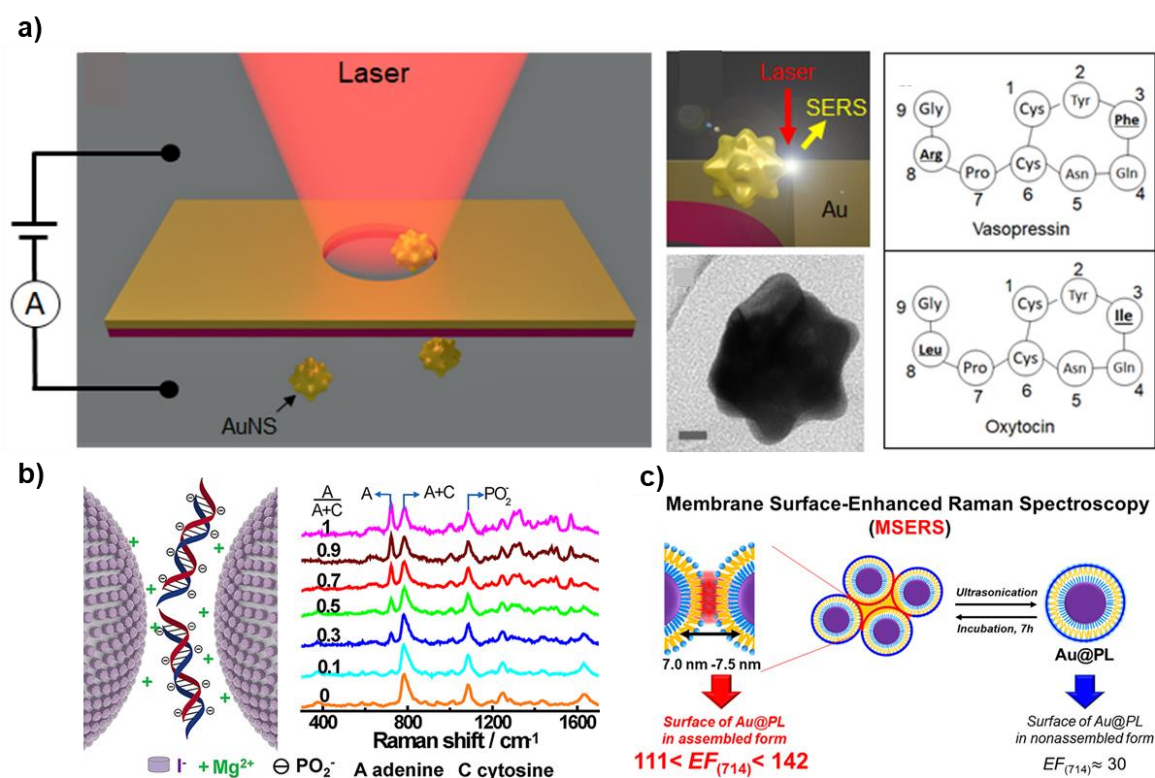
Figure 1.13: SERS label free detection of a) polypeptides,[80] b) nucleic acid base[83] and c) phospholipids.[91]

1.9.1.2 Diagnostic applications of label free SERS in communicable diseases

Communicable diseases are commonly caused by infectious pathogenic agents like virus, bacteria, fungi etc (**Figure 1.14**). Viruses are the abundant form of biological entities representing the most large and genetically diverse store of nucleic acid which can infect all types of life. Viruses are capable of evolving rapidly and turn out as a pandemic. A SERS based study has been investigated on influenza virus, non-influenza virus and model mutant strains showing its potential for clear discrimination of newly emerging viral samples.[95] Likewise SERS based studies on measles,[96] food and water borne viruses,[97] monitoring viral mutations[98] etc. has been established well. Pathogenic bacteria are a threat to human life and even low number of bacterial pathogens can induce serious fatal diseases. Ultrasensitive, rapid and accurate techniques are essential in such scenario. SERS has been already proved its potential for the detection of bacteria. A clinical study using blood sample identified *Staphylococcus aureus* and *Escherichia coli* with excellent sensitivity and specificity using gold NP coated SiO2 substrate.[99] Another study utilized silver dendrites for the detection and classification of *Salmonella enterica* and *E.coli*.[100] A highly enhanced

Raman signal has been generated by coating cell wall of bacteria than simply mixing bacteria and colloidal suspension.[101] Similarly detection of fungus,[102] mycoplasma,[103] protozoa[104] etc also has been investigated using SERS analysis.
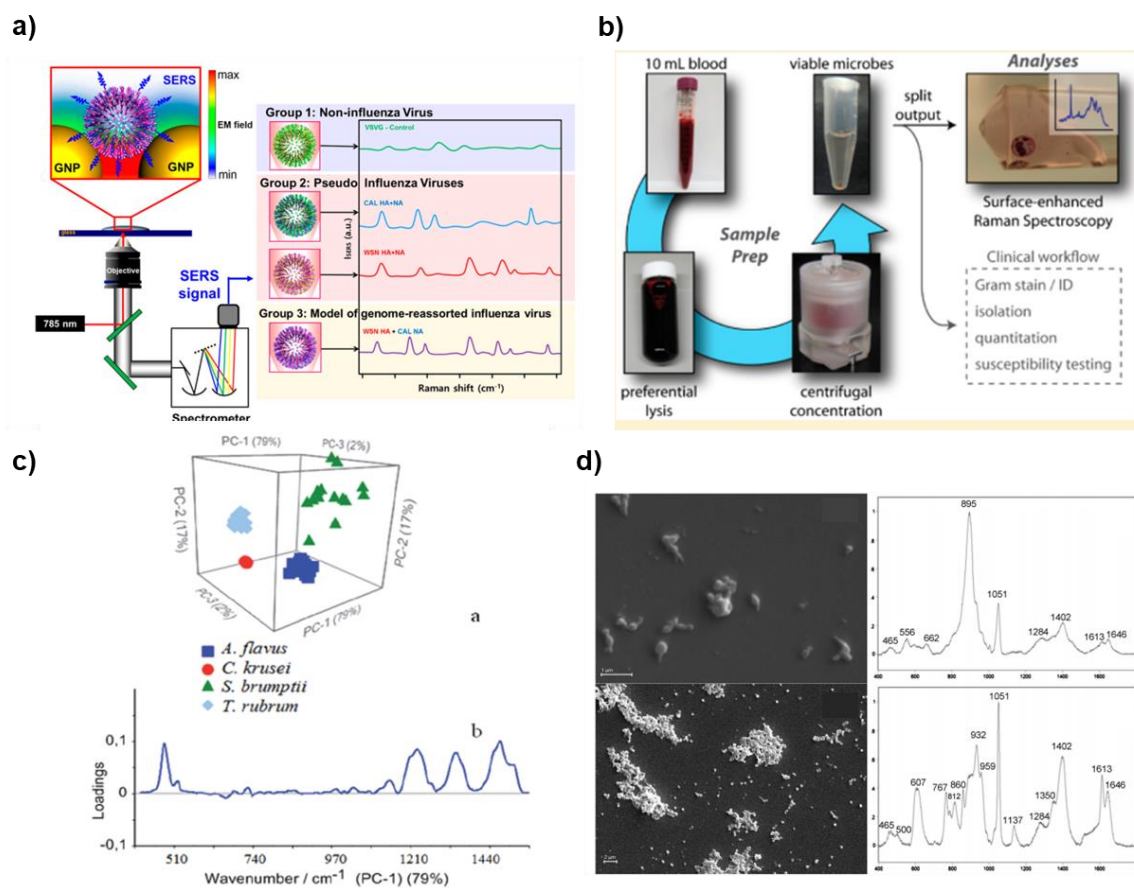
Figure 1.14: SERS label free detection of a) viruses,[95] b) bacteria,[99] c) fungus[102] and d) mycoplasma.[103]

1.9.1.3 Diagnostic applications of label free SERS in non-communicable diseases

Non-communicable diseases including cancer, diabetes, cardiovascular disease and neurodegenerative diseases are responsible for the 70% death worldwide according to WHO. Visualization of complex biochemical events like mitosis, apoptosis and many more has been made possible by surface enhanced Raman spectroscopy. Unraveling of complex processes involved in mitosis has been elucidated in healthy and cancer cells by the use of nuclear targeted gold nanocubes.[105] Apoptosis, the programmed cell death is a complex phenomenon which is an important biological process in aging, embryogenesis and various diseases. Proteolysis, protein denaturation and DNA fragmentation involved in apoptotic

cancer cells were identified using nuclear targeted gold nanospheres as the SERS substrates.[106]

Cancer, the deadly disease has been well explored by SERS technique. A blood plasma study based on SERS has been performed in a label free manner for the detection of cervical cancer. Colloidal silver NPs were used as the SERS substrate. The SERS analysis together with PCA-LDA classified the normal and cancerous samples with a diagnostic sensitivity and specificity of 96.7% and 92% respectively.[107] A similar kind of study has been performed for kidney tumor staging using tissue samples reaching about 100% sensitivity, specificity and accuracy.[108] A label free SERS analysis investigated for the detection of colorectal cancer and its lesions using blood plasma providing a diagnostic sensitivity and specificity of 86.4% and 80% respectively.[109] A breath analysis based SERS technique distinguished early as well as advanced gastric cancer from normal subjects using a graphene oxide-gold NP based sensor.[110] Likewise label free SERS analysis showed its potential in breast cancer,[111] parotid cancer, [112] bladder cancer[113] detection. The potential of SERS technique in diabetes detection also has been explored. A serum study for type II diabetes mellitus was investigated together with multivariate statistical analysis PCA using colloidal silver NPs.[114] Label free detection of oxyhemoglobin was able to discriminate the diabetes subjects from healthy samples. The blood based SERS analysis showed more than 90% diagnostic accuracies reflecting the structural changes like heme transformation and globin variations in diabetes. [115] Acute myocardial infarction is a serious disorder causing high morbidity and mortality. A label free SERS analysis has been investigated on blood plasma for acute myocardial infarction detection. Silver NPs were used which showed specific biomolecular peak variations based on protein, adenine, uric acid etc giving 87.5% sensitivity and 93.8% specificity.[116] Protein aggregation is a key feature of neurodegenerative disease like AD. These aggregated species have high affinity to cell membranes. A SERS technique was introduced to determine the conformation of membrane bound oligomer of beta amyloid 1-40.[117] Similarly a label free SERS analysis combined with nanofluidics has been performed to detect Aβ aggregates with a LOD of 10 fM which may help better understanding of conformational problems associated with neurodegenerative diseases [118] (**Figure 1.15**).
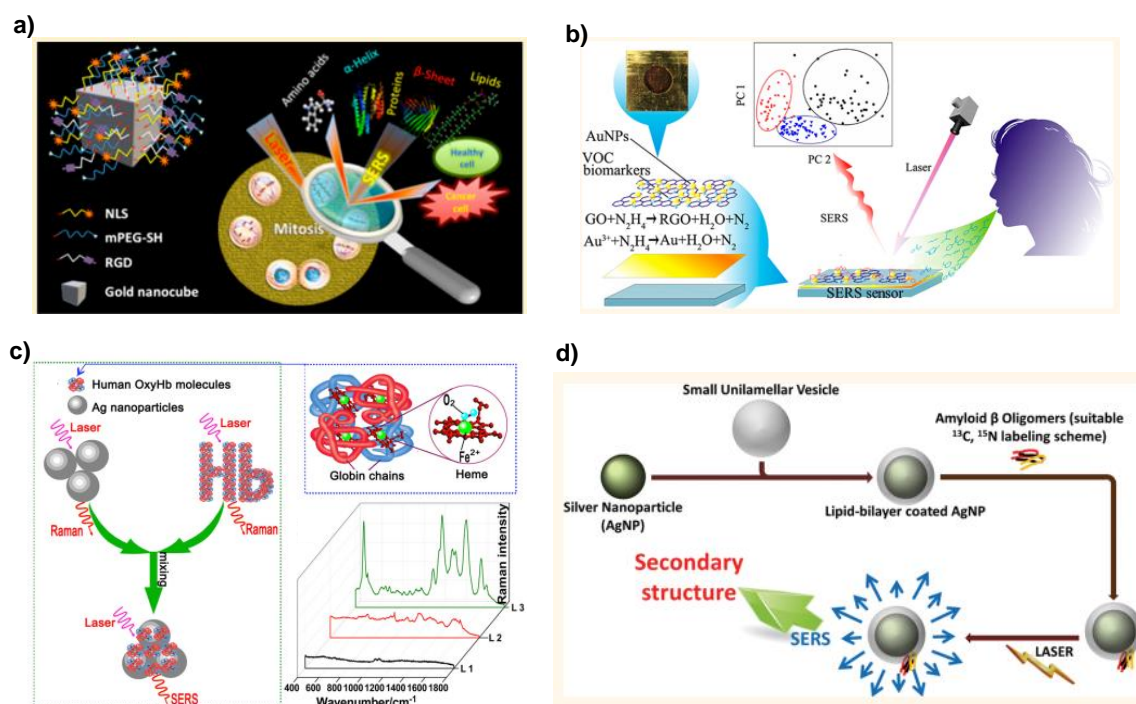
Figure 1.15: Label free SERS in identifying a) the steps in mitosis,[105] b) gastric cancer detection through breath analysis,[110] c) diabetes detection[115] and d) Aβ oligomer detection in AD.[117]

1.9.2 Labelled SERS

Label based SERS is one of the attractive strategy in the field of nano-biosensing which uses SERS labels for the identification of a particular overexpressed biomolecule like protein, nucleic acids, sugars or lipids. Label based SERS uses nanoconstruct made of a Raman reporter (RR), SERS substrate and a target molecule. RR or dye molecules has its own signature peak pattern which is attached to a SERS substrate providing signals as optical readout. The selection of a RR will be determined by its large Raman cross-section, presence of sulphur or nitrogen for its affinity towards SERS substrate for sufficient enhancement. For multiplexing applications, labels with non-overlapping peaks are of the utmost choice. SERS substrate is a plasmonically active metallic component like gold or silver NP generating hot spots to enhance the reporter Raman signal upon excitation with a suitable laser. The resultant construct is called as "SERS nanotag" which can be made biocompatible and targeted to a desired molecule by tethering antibodies, peptides of aptamers. A layer usually made of polyethylene glycol is coated to increase biocompatibility, reducing toxicity and minimizing non-specific binding. [119]

1.9.2.1   Raman reporters

SERS was found to be useful for increasing the capabilities of detection, imaging and biological sensing. A reporter molecule is used to bind to the surface of a NP, which renders the SERS signal as a label which in turn attached to a biomolecule using a targeting moiety like peptide, antibody or aptamers. This tactics has been shown its applications successfully in cell imaging, immunoassays and other biological applications. RR can be excited in the tissue window enabling *in vivo* detection and its imaging. A variety of organic RR such as malachite green, rhodamine B, methylene blue, crystal violet etc. are widely used in SERS based imaging because of its intense narrow as well as multiplexing signals (**Figure 1.16**). Multiplexing RR are organic molecules which have non-overlapping peaks which can be used for multiplexed detection of more than one analyte molecules. Thiolated molecules like 4-mercaptobenzoic acid, 4-methoxythiophenol etc are normally used because of their affinity to gold surfaces. [120]
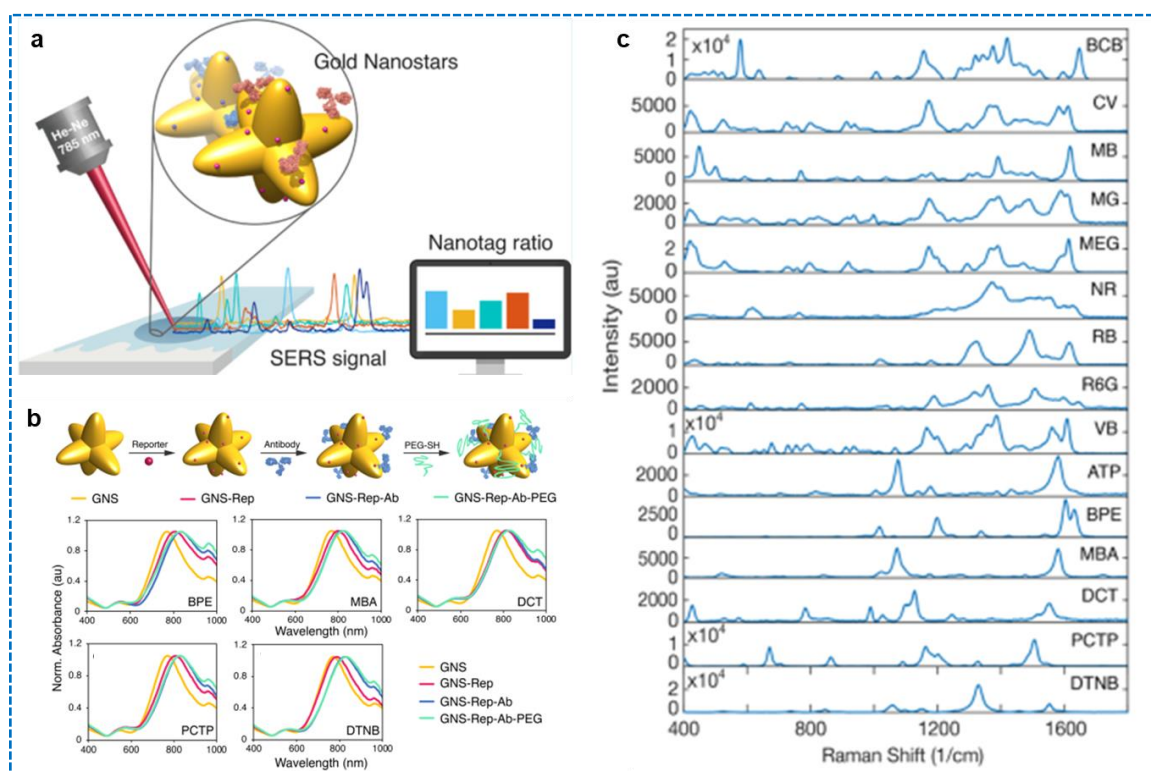
Figure 1.16: Different kinds of RRs used for SERS nanotag preparation viz. brilliant cresyl blue (BCB), methylene blue (MB), neutral red (NR), rose bengal (RB), rhodamine 6G (R6G), victoria blue (VB), BPE, MBA, 3,5-dichlorobenzenthiol (DCT), pentachlorothiophenol (PCTP), 4-aminothiophenol (ATP), crystal violet (CV), malachite green isocyanate (MG), methylene green (MEG) and 5,5′-dithiobis(2-nitrobenzoic acid) (DTNB).[120]

1.9.2.2   SERS nanotags

SERS technique has been employed to design nanoconstructs named "SERS nanotags" which consists of metallic NPs, specific RR molecules producing strong Raman signals to indirectly detect the desired molecules by SERS technique. SERS substrates commonly used include metallic NPs like gold and silver. SERS substrates of 40-50 nm are found to be the optimal size for obtaining the best SERS enhancement. A RR of suitable concentration is coated to the SERS substrate followed by a biocompatible layer usually made of polyethylene glycol (PEG) which also possess suitable functionalities for tethering the targeting moieties like antibodies, peptides or aptamers (**Figure 1.17**).
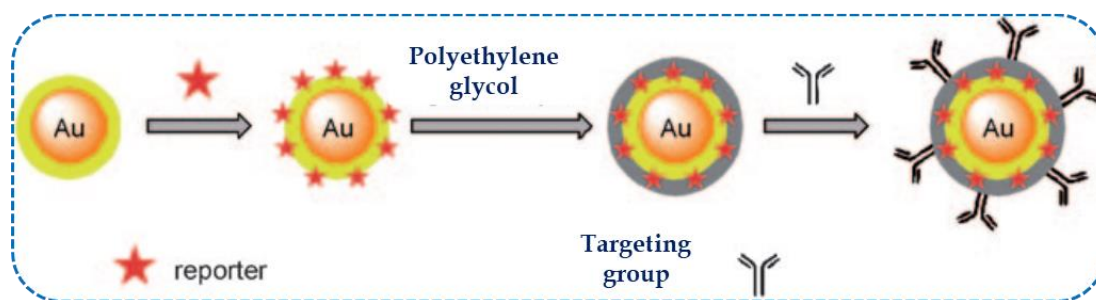
Figure 1.17: Steps towards preparation of SERS nanotags.

1.10 Approaches in nanodiagnostics using label based SERS

SERS nanotags have been widely used for the non-invasive detection of biomarkers in several diseases using SERS technique. Such SERS-active nanoconstructs produces strong characteristic Raman signature peaks which can be used for indirectly sensing the target molecules showing optical labeling activities. SERS probes possess ultra- sensitivity, multiplexing and quantitative abilities showing extraordinary features in bioanalysis. A nanocomplex made of in situ grown silver NP based silicon nanowires were used for the ultrasensitive detection of DNA. A DNA sensor was designed immobilizing DNA capture probe on the silver NP surface and a reporter probe with a dye for the target DNA detection. A LOD ~ 1 fM was achieved by this technique.[121] Similarly a sensitive detection of microRNAs in lung cancer has been established with a LOD of 0.5 fM using capture and SERS based reporter probe.[122] Likewise detection of proteins using SERS detection and capture probes are also

explored paving way for the real time detection of protein biomarkers in various diseases.[123] A sensitive SERS platform was developed for the detection of two pathogenic bacteria *Escherichia coli* and *Staphylococcus aureus*. Vancomycin modified Fe_3O_4 core-gold modified magnetic NPs and aptamers functionalized SERS nanotag were prepared for the bacterial detection.[124] SERS nanotag has also shown its potential for monitoring viral mutations. Gold nanostars were functionalized with DNA hairpins which are thiolated with a Raman active dye to identify RNA mutations in influenza virus.[98] A biocompatible SERS nanotag has been developed for the detection of EGFR and HER2 protein at *in vitro* as well as *in vivo* level.[125]
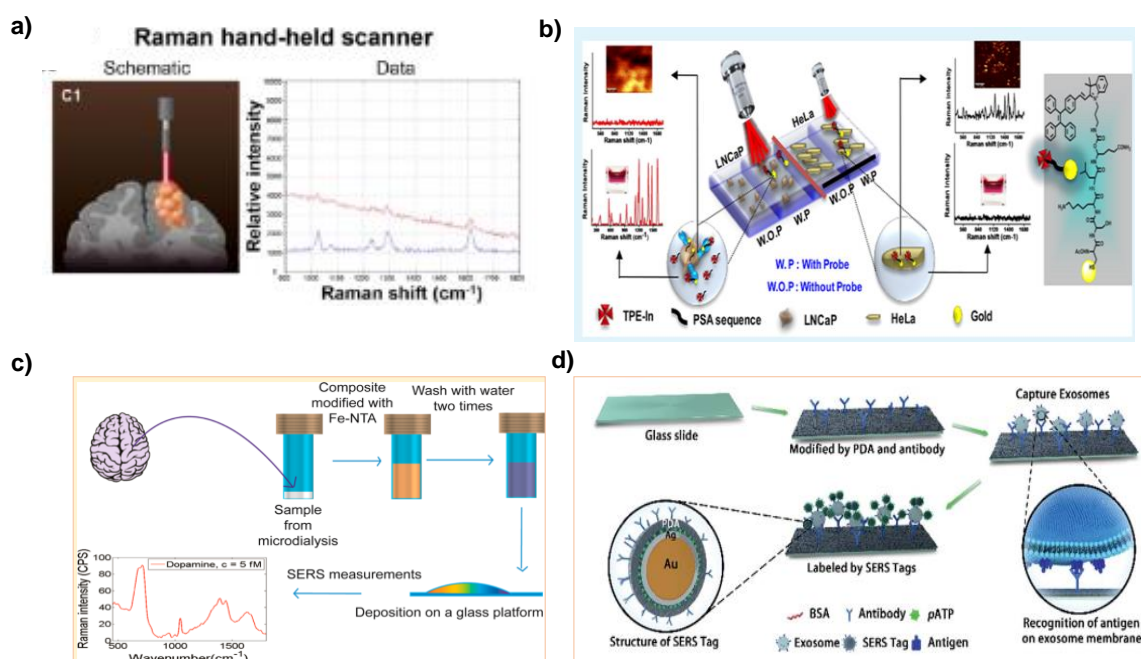
Figure 1.18: a) Brain tumor resection using SERS hand held Raman instrument, [128] b) PSA detection in prostate cancer, [130] c) dopamine detection using SERS,[133] d) exosomes based detection of pancreatic cancer using SERS nanotags.[131]

An application of immuno SERS imaging by wide field immunofluorescence for the detection of HER2 in breast tissue section has been established.[126] A SERS nanotag has been designed for the detection of gastrointestinal premalignant lesions like Surface enhanced resonance Raman spectroscopy (SERRS) endoscopy.[127] SERS nanotags and handheld scanner has also been used for the visualization of extent of malignant brain during tumor resection via surgery showing its strong potential for clinical translation. [128] SERS nanotags has been used for the SERS imaging of HER2 biomarker in breast cancer cells[129] and prostate specific antigen (PSA) in prostate

cancer.[130] For the classification of pancreatic cancer, and ultra-sensitive SERS immunoassay has been used for the exosomes based diagnosis. Polydopamine based SERS nanotags were used with and LOD of one exosome.[131] A squaraine based SERS nanotag was explored for the imaging of different types of cancer cells expressing EGFR and HER2.[132] Dopamine, a neurotransmitter has been detected in cerebrospinal fluid by a magnetic bead with silver NPs coated by RR molecules.[133] A SERS-fluorescence dual nanotag was also developed using aptamers conjugated gold silver nanorods for cervical cancer detection.[134] *In vivo* tumor targeting has been performed using single chain variable fragment antibody ligands in live animal and xenografts tumor models using SERS nanotags targeting EGFR biomarker[135] (**Figure 1.18).**

1.10.1 Multiplexed label based SERS approaches

SERS has already shown promising potential in multiplexing related applications with its narrow peak width and ultra-sensitivity allowing multiple analyte detection at the same time (**Figure 1.19**). Multiplexing analysis has been approached in different kinds of cancers with different biomarker levels. A multiplexing SERS method has been approached in bladder cancer detection which has the highest recurrence rate. To improve the resection and detection, a SERS nanoprobe made of gold core with silica shell along with endoscope system was designed to classify normal versus cancerous. Multiplexed imaging of carbonic anhydrase 9 and CD 47 tumor markers were evaluated *ex vivo*.[136] Three kinds of prostate related carcinoma genes mi-DNA-141, 21 and 7d were simultaneously detected by a multiplexing approach using gold-silver nano snowmen with high specificity and sensitivity employing three different Raman reporter having non-overlapping peaks.[137] Circulating biomarkers have shown its ability to act as non-invasive samples for cancer diagnosis. A SERS based immunoassay has been designed and executed for the multiplexed detection of breast cancer biomarkers, cancer antigen (27-29), cancer antigen (15-3) and cancer embryonic antigen (CEA) which may benefit the surveillance of treatment monitoring using a sample blood test. Gold nanostar with silica spacer was employed as the SERS substrate.[138] Likewise a specific and sensitive SERS based immunoassay has been investigated for the simultaneous detection of two lung cancer biomarkers including neuron specific enolase (NSE) and

carcinoembryonic antigen (CEA). An LOD of 1.48 pg/ml and 2.04 pg/ml was obtained for CEA and NSE respectively. Flower like gold NPs and magnetic NPs coated with gold
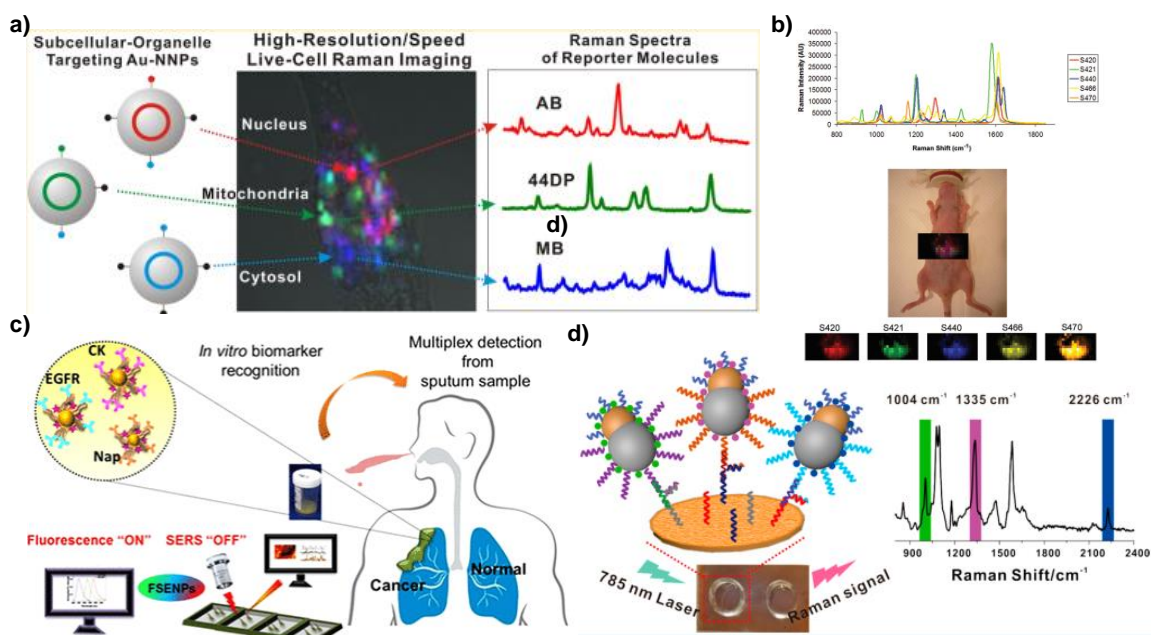
Figure 1.19: Multiplexing SERS detection of a) cell organelles,[141] b) *in vivo*[140] c) lung cancer biomarkers and d) disease related nucleic acids.[137]

were used as the SERS substrates.[139] Another study demonstrated use of 10 different types of SERS nanotags in a living mouse. The most intense 5 tags were injected simultaneously to image its liver accumulation. In addition to the spectral separation, linear correlation of the tags according to its concentration also has been established. Gold core with silica spacer was the SERS substrate along with different RR having different signature peaks.[140] A multiplexing SERS platform for the imaging of mitochondrial, nuclear and cytoplasmic targeted NPs were investigated which used three independent RR in gold NPs with highly narrow intragaps using 785 nm laser.[141] Another multiplexing study evaluated four biomarkers HER2, CD44, ER and EGFR in breast cancer using Raman encoded molecular imaging technique (REMI) with a sensitivity of 89.3% and specificity of 92.1% showing the potential to reduce the re-excision and recurrence rate.[142] Similarly the multiplexed detection of EGFR, CD44 and TGFβRII in breast cancer were studied *in vitro* and *in vivo* which shows the capability for tumor progression and therapy monitoring.[143]

1.11   Conclusion

Rapid, ultrasensitive, non-invasive and cost effective features have out looked in SERS as an excellent strategy for chemical as well as biological molecules signature fingerprinting in biomedical applications. Although approaches based on SERS exhibited an exponential growth during past and present decade, it should be reoriented for exploring its unseen applications in biomedicine. Label free SERS is a superior approach for diseases which do not have any significant biomarker giving the molecule's its own fingerprint features. Label based SERS using RR signals for indirect target detection is an alternative sensible approach which exploits specific targeting and affinity of the respective ligand attached in the SERS substrate. Solution state studies, *in vitro*, *in vivo* and *ex vivo* analysis were possible with this simple spectroscopic technique giving insights into several molecular events happening in the biological system. Proper and intelligent application of this technique can dramatically solve several problems associated with disease diagnosis.

1.12   Objectives of the present investigation

Inspired from the recent progress in the design of diagnostic nano-constructs based on SERS, the thesis is planned in such a way so as to sightsee the likelihood of developing and exploring their potential for clinical translation. Early diagnosis of diseases is the key factor for developing proper treatment strategies. It is well known from the literature that Raman spectroscopy combined with nanotechnology can render immense applications in diagnostic and broadly in the area of nano-biotechnology. Even though SERS has already shown its supremacy, its applicability in clinical scenario is still uncertain. Tracing and tracking molecular events with low analyte concentration makes diagnosis a puzzling process. An ultrasensitive, rapid diagnosis is essential for serious disorders for improved outcome in therapeutics. The high sensitivity, specificity, minimal sample preparation and integration of innovative chemometrics have improved the applications of SERS in a wide array of diseases. Diseases often occur resulting in a varied expression of biomolecules which can be traced using Raman spectroscopic analysis.

In this context, we have endeavored the development of SERS based diagnostic nanoprobes for the biomarker detection of two cancers, cervical and breast cancer together with neurodegenerative disorder, AD. Cancer can be treated and cured if detected at an early stage. Evaluating its stage wise or protein/gene expression wise spectral fingerprint or biomarker status is a forefront strategy for designing a diagnostic probe. Current techniques are highly subjective with low specificity, sensitivity, inter observer variability, false positive/negative results. A label free as well as label based approach has been designed and executed for cervical cancer. The biomolecular changes happening in the different grades of cervical cancer starting from normal to invasive carcinoma along with an intermediate stage has been evaluated and was successfully classified using chemometric analysis like PCA, LDA and SVM in **chapter 2.** Next a label based SERS approach has been demonstrated in cell line level and clinical samples for probing the overexpression of p16/Ki-67 protein in cervical cancer as the **3ʳᵈ chapter**. A multiplexing triple biomarker (ER/PR/HER2) detection has been achieved in the **4ᵗʰ chapter** using cell lines as well as paraffin embedded clinical breast tissue samples which show its capability to aid clinicians in developing proper treatment strategies. AD, the most common type of dementia is difficult to diagnose at the early stage. The objective of the **5ᵗʰ chapter** was to determine the biomarker expression of beta amyloid ($A\beta_{1-42}$) in AD using SERS based sandwiched nanoprobe. The present thesis is a systematic investigation on the development of potential diagnostic NP as SERS-tags or nanoprobes for the detection of Cancer and AD.

1.13   References

(1)   Scully, J. L. What Is a Disease? *Sci. Soc.* **2004**, *5* (7), 650–653.

(2)   Boutayeb, A. The Double Burden of Communicable and Non-Communicable Diseases in Developing Countries. *Trans. R. Soc. Trop. Med. Hyg.* **2006**, *100* (3), 191–199.

(3)   Rui Liu, Xiangdong Wang, Kazuyuki Aihara, and L. C. Early Diagnosis of Complex Diseases by Molecular Biomarkers, Network Biomarkers, and Dynamical Network Biomarkers. *Med. Res. Rev.* **2014**, *34* (3), 455–478.

(4)   Ramos, A. P.; Cruz, M. A. E.; Tovani, C. B.; Ciancaglini, P. Biomedical Applications of Nanotechnology. *Biophys. Rev.* **2017**, *9* (2), 79–89.

(5)   Mitragotri, S.; Anderson, D. G.; Chen, X.; Chow, E. K.; Ho, D.; Kabanov, A. V.; Karp, J. M.; Kataoka, K.; Mirkin, C. A.; Petrosko, S. H.; et al. Accelerating the Translation of Nanomaterials in Biomedicine. *ACS Nano* **2015**, *9* (7), 6644–6654.

(6)   Etheridge, M. L.; Campbell, S. A.; Erdman, A. G.; Haynes, C. L.; Wolf, S. M.; McCullough, J. The Big Picture on Nanomedicine: The State of Investigational and Approved Nanomedicine Products. *Nanomed-Nanotechnol. Biol. Med.* **2013**, *9* (1), 1–14.

(7)   Anselmo, A. C.; Mitragotri, S. Nanoparticles in the Clinic: An Update. *Bioeng. Transl. Med.* **2019**, *4* (3), e10143.

(8)   Fink, D. J. Cancer Overview. *Cancer Res.* **1979**, *39*, 2819–2821.

(9)   Sarkar, S.; Horn, G.; Moulton, K.; Oza, A.; Byler, S.; Kokolus, S.; Longacre, M. Cancer Development, Progression, and Therapy: An Epigenetic Overview. *Int. J. Mol. Sci.* **2013**, *14* (10), 21087–21113.

(10)   American Cancer Association. Estimated Number of New Cancer Cases, All EU Countries, **2018**.

(11)   World Health Organization. Global Cancer Profile 2020. **2020**, No. 2019, 2.

(12)   Bleyer, A.; Barr, R.; Hayes-Lattin, B.; Thomas, D.; Ellis, C.; Anderson, B. The Distinctive Biology of Cancer in Adolescents and Young Adults. *Nat. Rev. Cancer* **2008**, *8* (4), 288–298.

(13)   Institute, N. N. C. Cancer Facts & Figures 2020. *CA. Cancer J. Clin.* **2020**, 1–76.

(14)   Schiffman, J. D.; Fisher, P. G.; Gibbs, P. Early Detection of Cancer: Past, Present, and Future. *Am. Soc. Clin. Oncol. Educ. B.* **2015**, No. 35, 57–65.

(15)   Brierley, J.; Gospodarowicz, M.; O'Sulivan, B. The Principles of Cancer Staging. *Ecancermedicalscience* **2016**, *10*, 3–6.

(16)   Fass, L. Imaging and Cancer: A Review. *Mol. Oncol.* **2008**, *2* (2), 115–152.

(17)   Arruebo, M.; Vilaboa, N.; Sáez-gutierrez, B.; Lambea, J. Assessment of the Evolution of Cancer Treatment Therapies. *Cancers (Basel).* **2011**, *3*, 3279–3330.

(18)   Berman, J. J. Tumor Taxonomy for the Developmental Lineage Classification of Neoplasms. *BMC Cancer* **2004**, *4* (88), 1–6.

(19)   Hanahan, D.; Robert A, W. Biological Hallmarks of Cancer. *Holland-Frei cancer Med.* **2017**, *01*, 1–10.

(20)   Duong, S.; Patel, T.; Chang, F. Dementia: What Pharmacists Need to Know. *Can.*

Pharm. J. **2017**, *150* (2), 118–129.

(21)   International, A. D. *World Alzheimer Report 2019, Attitudes to Dementia*; 2019.

(22)   World Health Organization. Dementia a Public Health Priority. *Alzheimer's Dis. Int.* **2015**, 1–4.

(23)   Robinson, L.; Tang, E.; Taylor, J. P. Dementia: Timely Diagnosis and Early Intervention. *BMJ* **2015**, *350*, h3029.

(24)   Perminder S. Sachdev, MD, PhD, FRANZCP1, 2; , Adith Mohan, MBBS, Mrcp.; FRANZCP1, 2, Lauren Taylor, MBBS2, and Dilip V. Jeste, M. DSM-5 and Mental Disorders in Older Individuals: An Overview. *Harv Rev Psychiatry.* **2015**, *23* (5), 320–328.

(25)   Regier, D. A.; Kuhl, E. A.; Kupfer, D. J. The DSM-5: Classification and Criteria Changes. *World Psychiatry* **2013**, *12* (2), 92–98.

(26)   Keith A. Johnson1, Nick C. Fox2, Reisa A. Sperling3, and W. E. K. Brain Imaging in Alzheimer Disease. *Cold Spring Harb Perspect Med* **2012**, *2*, a006213.

(27)   Chen, H.; Rogalski, M. M.; Anker, J. N. Advances in Functional X-Ray Imaging Techniques and Contrast Agents. **2013**, *14* (39), 13469–13486.

(28)   Pauwels, E. K. J.; Foray, N.; Bourguignon, M. H. Breast Cancer Induced by X-Ray Mammography Screening? A Review Based on Recent Understanding of Low-Dose Radiobiology. *Med. Princ. Pract.* **2016**, *25* (2), 101–109.

(29)   Garvey, C. J.; Hanlon, R. Computed Tomography in Clinical Practice. *BMJ* **2002**, *324*, 1077–1080.

(30)   Peter B. Bach, MD, M.; James R. Jett, M.; Ugo Pastorino, M.; Melvyn S. Tockman, M.; Stephen J. Swensen, M.; Colin B. Begg, P. Computed Tomography Screening and Lung Cancer Outcomes. *JAMA* **2007**, *297* (9), 953–962.

(31)   Grover, V. P. B.; Tognarelli, J. M.; Crossey, M. M. E.; Cox, I. J.; Taylor-Robinson, S. D.; McPhail, M. J. W. Magnetic Resonance Imaging: Principles and Techniques: Lessons for Clinicians. *J. Clin. Exp. Hepatol.* **2015**, *5* (3), 246–255.

(32)   Rohren, E. M.; Turkington, T. G.; Coleman, R. E. Clinical Applications of PET in Oncology. *Radiology* **2004**, *231* (2), 305–332.

(33)   Kinahan, J. J. V. and P. Positron Emission Tomography: Current Challenges and Opportunities for Technological Advances in Clinical and Preclinical Imaging Systems. *Annu Rev Biomed Eng.* **2015**, *17*, 385–414.

(34) Mariani, G.; Bruselli, L.; Kuwert, T.; Kim, E. E.; Flotats, A.; Israel, O.; Dondi, M.; Watanabe, N. A Review on the Clinical Uses of SPECT/CT. *Eur. J. Nucl. Med. Mol. Imaging* **2010**, *37* (10), 1959–1985.

(35) Khalil, M. M.; Tremoleda, J. L.; Bayomy, T. B.; Gsell, W. Molecular SPECT Imaging: An Overview. *Int. J. Mol. Imaging* **2011**, *2011*, 1–15.

(36) Carovac, A.; Smajlovic, F.; Junuzovic, D. Application of Ultrasound in Medicine. *Acta Inform. Medica* **2011**, *19* (3), 168–171.

(37) Gayathri Acharya, Ashim K. Mitra, K. C. Nanosystems for Diagnostic Imaging, Biodetectors and Biosensors. *Emerging Nanotechnologies for Diagnostics, Drug Delivery and Medical Devices*; **2017**, 217–248.

(38) Luker, G. D.; Luker, K. E. Optical Imaging: Current Applications and Future Directions. *J. Nucl. Med.* **2008**, *49* (1), 1–4.

(39) Licha, K.; Olbrich, C. Optical Imaging in Drug Discovery and Diagnostic Applications. *Adv. Drug Deliv. Rev.* **2005**, *57* (8), 1087–1108.

(40) Lambert, R. Endoscopy in Screening for Digestive Cancer. *World J. Gastrointest. Endosc.* **2012**, *4* (12), 518–525.

(41) Valluru, K. S.; Willmann, J. K. Clinical Photoacoustic Imaging of Cancer. *Ultrasonography* **2016**, *35* (4), 267–280.

(42) Adhi, M.; Duker, J. S. Optical Coherence Tomography-Current and Future Applications. *Curr. Opin. Ophthalmol.* **2013**, *24* (3), 213–221.

(43) Hoshi, Y.; Yamada, Y. Overview of Diffuse Optical Tomography and Its Clinical Applications. *J. Biomed. Opt.* **2016**, *21* (9), 091312.

(44) Galbraith, C. G.; Galbraith, J. A. Super-Resolution Microscopy at a Glance. *J. Cell Sci.* **2011**, *124* (10), 1607–1611.

(45) Yu, L.; Hao, L.; Meiqiong, T.; Jiaoqi, H.; Wei, L.; Jinying, D.; Xueping, C.; Weiling, F.; Yang, Z. The Medical Application of Terahertz Technology in Non-Invasive Detection of Cells and Tissues: Opportunities and Challenges. *RSC Adv.* **2019**, *9* (17), 9354–9363.

(46) Kneipp, K.; Kneipp, H.; Itzkan, I.; Dasari, R. R.; Feld, M. S. Ultrasensitive Chemical Analysis by Raman Spectroscopy. *Chem. Rev.* **1999**, *99* (10), 2957–2975.

(47) Rao, A. R.; Hanchanale, V.; Javle, P.; Karim, O.; Motiwala, H. Spectroscopic View of Life and Work of the Nobel Laureate Sir C.V. Raman. *J. Endourol.* **2007**, *21* (1),

8–11.

(48) Tu, Q.; Chang, C. Diagnostic Applications of Raman Spectroscopy. *Nanomedicine Nanotechnology, Biol. Med.* **2012**, *8* (5), 545–558.

(49) Cooper, J. B. Chemometric Analysis of Raman Spectroscopic Data for Process Control Applications. *Chemom. Intell. Lab. Syst.* **1999**, *46* (2), 231–247.

(50) Sato-Berrú, R. Y.; Mejía-Uriarte, E. V.; Frausto-Reyes, C.; Villagrán-Muniz, M.; H.M., H. M.; Saniger, J. M. Application of Principal Component Analysis and Raman Spectroscopy in the Analysis of Polycrystalline BaTiO3 at High Pressure. *Spectrochim. Acta - Part A Mol. Biomol. Spectrosc.* **2007**, *66* (3), 557–560.

(51) Hutchings, J.; Kendall, C.; Shepherd, N.; Barr, H.; Stone, N. Evaluation of Linear Discriminant Analysis for Automated Raman Histological Mapping of Esophageal High-Grade Dysplasia. *J. Biomed. Opt.* **2010**, *15*, 066015.

(52) Sattlecker, M.; Bessant, C.; Smith, J.; Stone, N. Investigation of Support Vector Machines and Raman Spectroscopy for Lymph Node Diagnostics. *Analyst* **2010**, *135*, 895–901.

(53) Li, Y.; Jia, M.; Zeng, X.; Huang, K.; Bai, Z. Pattern Recognition Methods Combined with Raman Spectra Applied to Distinguish Serums from Lung Cancer Patients and Healthy People. *J. Biosci. Med.* **2017**, *05* (09), 95–105.

(54) Ostrowska, K. M.; Malkin, A.; Meade, A.; O'Leary, J.; Martin, C.; Spillane, C.; Byrne, H. J.; Lyng, F. M. Investigation of the Influence of High-Risk Human Papillomavirus on the Biochemical Composition of Cervical Cancer Cells Using Vibrational Spectroscopy. *Analyst* **2010**, *135* (12), 3087–3093.

(55) Haka, A. S.; Shafer-Peltier, K. E.; Fitzmaurice, M.; Crowe, J.; Dasari, R. R.; Feld, M. S. Diagnosing Breast Cancer by Using Raman Spectroscopy. *Proc. Natl. Acad. Sci. U. S. A.* **2005**, *102* (35), 12371–12376.

(56) Kumar, S.; Rizwan, A.; Zheng, C.; Cheng, M.; Glunde, K.; Barman, I. Label-Free Raman Spectroscopy Detects Stromal Adaptations in Premetastatic Lungs Primed by Breast Cancer. *Cancer Res.* **2017**, *77* (2), 247–256.

(57) Su, L.; Sun, Y. F.; Chen, Y.; Chen, P.; Shen, A. G.; Wang, X. H.; Jia, J.; Zhao, Y. F.; Zhou, X. D.; Hu, J. M. Raman Spectral Properties of Squamous Cell Carcinoma of Oral Tissues and Cells. *Laser Phys.* **2012**, *22* (1), 311–316.

(58) Zheng, Q.; Li, J.; Yang, L.; Zheng, B.; Wang, J.; Lv, N.; Luo, J.; Martin, F. L.; Liu, D.;

He, J. Raman Spectroscopy as a Potential Diagnostic Tool to Analyse Biochemical Alterations in Lung Cancer. *Analyst* **2020**, *145* (2), 385–392.

(59)   Paraskevaidi, M.; Morais, C. L. M.; Halliwell, D. E.; Mann, D. M. A.; Allsop, D.; Martin-Hirsch, P. L.; Martin, F. L. Raman Spectroscopy to Diagnose Alzheimer's Disease and Dementia with Lewy Bodies in Blood. *ACS Chem. Neurosci.* **2018**, *9* (11), 2786–2794.

(60)   Scholtes-Timmerman, M. J.; Bijlsma, S.; Fokkert, M. J.; Slingerland, R.; Van Veen, S. J. F. Raman Spectroscopy as a Promising Tool for Noninvasive Point-of-Care Glucose Monitoring. *J. Diabetes Sci. Technol.* **2014**, *8* (5), 974–979.

(61)   Strola, S. A.; Baritaux, J.-C.; Schultz, E.; Simon, A. C.; Allier, C.; Espagnon, I.; Jary, D.; Dinten, J.-M. Single Bacteria Identification by Raman Spectroscopy. *J. Biomed. Opt.* **2014**, *19* (11), 111610.

(62)   Moor, K.; Terada, Y.; Taketani, A.; Matsuyoshi, H.; Ohtani, K. Early Detection of Virus Infection in Live Human Cells Using Raman Spectroscopy. *J. Biomed. Opt.* **2018**, *23* (09), 097001–097006.

(63)   Jones, R. R.; Hooper, D. C.; Zhang, L.; Wolverson, D.; Valev, V. K. Raman Techniques: Fundamentals and Frontiers. *Nanoscale Res. Lett.* **2019**, *14* (1).

(64)   Chi Zhang, Delong Zhang, and J.-X. C. Coherent Raman Scattering Microscopy in Biology and Medicine. *Annu Rev Biomed Eng.* **2015**, *17*, 415–445.

(65)   Verma, P. Tip-Enhanced Raman Spectroscopy: Technique and Recent Advances. *Chem. Rev.* **2017**, *117* (9), 6447–6466.

(66)   G. Spiro, T.; C. Strekas, T. Resonance Raman Spectra of Hemoglobin and Cytochromec: Inverse Polarization and Vibronic Scattering. *Proc. Nat. Acad. Sci. USA* **1972**, *69* (9), 2622–2626.

(67)   Christian W. Freudiger,*, Wei Min,*, Brian G. Saar, Sijia Lu, Gary R. Holtom, C.; He, Jason C. Tsai, Jing X. Kang, and X. S. X. Label-Free Biomedical Imaging with High Sensitivity by Stimulated Raman Scattering Microscopy. *Science.* **2008**, *322* (5909), 1857–1861.

(68)   Buckley, K.; Matousek, P. Recent Advances in the Application of Transmission Raman Spectroscopy to Pharmaceutical Analysis. *J. Pharm. Biomed. Anal.* **2011**, *55* (4), 645–652.

(69)   Feng, G.; Ochoa, M.; Maher, J. R.; Awad, H. A.; Berger, A. J. Sensitivity of Spatially

Offset Raman Spectroscopy (SORS) to Subcortical Bone Tissue. *J. Biophotonics* **2017**, *10* (8), 990–996.

(70) Joseph, M. M.; Narayanan, N.; Nair, J. B.; Karunakaran, V.; Ramya, A. N.; Sujai, P. T.; Saranya, G.; Arya, J. S.; Vijayan, V. M.; Maiti, K. K. Exploring the Margins of SERS in Practical Domain: An Emerging Diagnostic Modality for Modern Biomedical Applications. *Biomaterials* **2018**, *181*, 140–181.

(71) Fleischmann, M.; Hendra, P. J.; McQuillan, A. J. Raman Spectra of Pyridine Adsorbed at a Silver Electrode. *Chem. Phys. Lett.* **1974**, *26* (2), 163–166.

(72) Jeanmaire, D. L.; Van Duyne, R. P. Surface Raman Spectroelectrochemistry. *J. Electroanal. Chem.* 1977, 84, 1–20.

(73) Albrecht, M. G.; Creighton, J. A. Anomalously Intense Raman Spectra of Pyridine at a Silver Electrode. *J. Am. Chem. Soc.* **1977**, *99* (15), 5215–5217.

(74) Ding, S. Y.; You, E. M.; Tian, Z. Q.; Moskovits, M. Electromagnetic Theories of Surface-Enhanced Raman Spectroscopy. *Chem. Soc. Rev.* **2017**, *46* (13), 4042–4076.

(75) Kim, J.; Jang, Y.; Kim, N. J.; Kim, H.; Yi, G. C.; Shin, Y.; Kim, M. H.; Yoon, S. Study of Chemical Enhancement Mechanism in Non-Plasmonic Surface Enhanced Raman Spectroscopy (SERS). *Front. Chem.* **2019**, *7*, 1–7.

(76) Mosier-Boss, P. A. Review of SERS Substrates for Chemical Sensing. *Nanomaterials* **2017**, *7* (6), 142.

(77) Bonifacio, A.; Cervo, S.; Sergo, V. Label-Free Surface-Enhanced Raman Spectroscopy of Biofluids: Fundamental Aspects and Diagnostic Applications. *Anal. Bioanal. Chem.* **2015**, *407* (27), 8265–8277.

(78) Fazio, B.; D'Andrea, C.; Foti, A.; Messina, E.; Irrera, A.; Donato, M. G.; Villari, V.; Micali, N.; Maragò, O. M.; Gucciardi, P. G. SERS Detection of Biomolecules at Physiological PH via Aggregation of Gold Nanorods Mediated by Optical Forces and Plasmonic Heating. *Sci. Rep.* **2016**, *6* (June), 1–13.

(79) Xiao X. Han,†,‡ Genin Gary Huang,‡ Bing Zhao,*, † and Yukihiro Ozaki*. Label-Free Highly Sensitive Detection of Proteins in Aqueous Solutions Using Surface-Enhanced Raman Scattering. *Anal. Chem.* **2009**, *81* (9), 3329–3333.

(80) Huang, J.-A.; Mousavi, M. Z.; Giovannini, G.; Zhao, Y.; Hubarevich, A.; Soler, M. A.; Rocchia, W.; Garoli, D.; De Angelis, F. Multiplex Discrimination of Single Amino

Acid Residues in Polypeptides by Single SERS Hot Spot. *Angew. Chemie* **2020**, *59* (28), 11423–11431.

(81) Kang, Y.; Si, M.; Liu, R.; Qiao, S. Surface-Enhanced Raman Scattering (SERS) Spectra of Hemoglobin on Nano Silver Film Prepared by Electrolysis Method. *J. Raman Spectrosc.* **2010**, *41* (6), 614–617.

(82) Drachev, V. P.; Thoreson, M. D.; Khaliullin, E. N.; Davisson, V. J.; Shalaev, V. M. Surface-Enhanced Raman Difference between Human Insulin and Insulin Lispro Detected with Adaptive Nanostructures. *J. Phys. Chem. B* **2004**, *108* (46), 18046–18052.

(83) Xu, L.-J.; Lei, Z.-C.; Li, J.; Zong, C.; Yang, C. J.; Ren, B. Label-Free Surface-Enhanced Raman Spectroscopy Detection of DNA with Single-Base Sensitivity. *J. Am. Chem. Soc.* **2015**, *137* (15), 5149–5154.

(84) Koglin, E.; Séquaris, J.-M.; Fritz, J.-C.; Valenta, P. Surface Enhanced Raman Scattering (SERS) of Nucleic Acid Bases Adsorbed on Silver Colloids. *J. Mol. Struct.* **1984**, *114*, 219–223.

(85) Barhoumi, A.; Halas, N. J. Label-Free Detection of DNA Hybridization Using Surface Enhanced Raman Spectroscopy. *J. Am. Chem. Soc.* **2010**, *132* (37), 12792–12793.

(86) Papadopoulou, E.; Bell, S. E. J. Label-Free Detection of Single-Base Mismatches in DNA by Surface-Enhanced Raman Spectroscopy. *Angew. Chemie - Int. Ed.* **2011**, *50* (39), 9058–9061.

(87) Wang, H.; Fales, A. M.; Vo-dinh, T. Plasmonics-Based SERS Nanobiosensor for Homogeneous Nucleic Acid Detection. *Nanomedicine Nanotechnology, Biol. Med.* **2015**, *11* (4), 811–814.

(88) Prado, E.; Daugey, N.; Plumet, S.; Servant, L.; Lecomte, S. Quantitative Label-Free RNA Detection Using Surface-Enhanced Raman Spectroscopy. *Chem. Commun.* **2011**, *47* (26), 7425–7427.

(89) Prado, E.; Colin, A.; Servant, L.; Lecomte, S. SERS Spectra of Oligonucleotides as Fingerprints to Detect Label- Free RNA in Micro Fluidic Devices. *J. Phys. Chem.* **2014**, *118*, 13965–13971.

(90) Weldon, M. K.; Zhelyaskov, V. R.; Morris, M. D. Surface-Enhanced Raman Spectroscopy of Lipids on Silver Microprobes. *Appl. Spectrosc.* **1998**, *52* (2),

(91) Suga, K.; Yoshida, T.; Ishii, H.; Okamoto, Y.; Nagao, D.; Konno, M.; Umakoshi, H. Membrane Surface-Enhanced Raman Spectroscopy for Sensitive Detection of Molecular Behavior of Lipid Assemblies. *Anal. Chem.* **2015**, 87 (9) 4772–4780.

(92) Mrozek, M. F.; Weaver, M. J. Detection and Identification of Aqueous Saccharides by Using Surface-Enhanced Raman Spectroscopy. **2002**, *74* (16), 4069–4075.

(93) Yang, L.; Du, C.; Luo, X. Rapid Glucose Detection by Surface Enhanced Raman Scattering Spectroscopy. *J. Nanosci. Nanotechnol.* **2009**, *9* (4), 2660–2663.

(94) Dr. Xiuru Li#[a], Dr. Sharon J. H. Martin#[b], Dr. Zoeisha S. Chinoy[a, b], Dr. Lin Liu[a], B.; Rittgers[b], Prof. Richard A. Dluhy*,[b, c], and Prof. Geert-Jan Boons*,[a, b, D. Label-Free Detection of Glycan–Protein Interactions for Array Development by Surface-Enhanced Raman Spectroscopy (SERS). *Chemistry (Easton).* **2016**, *22* (32), 11180–11185.

(95) Lim, J.; Nam, J.; Yang, S.; Shin, H.; Jang, Y.; Bae, G.-U.; Kang, T.; Lim, K.; Choi, Y. Identification of Newly Emerging Influenza Viruses by Surface-Enhanced Raman Spectroscopy. *Anal. Chem.* **2015**, *87* (23), 11652–11659.

(96) Hoang, V.; Tripp, R. a; Rota, P.; Dluhy, R. a. Identification of Individual Genotypes of Measles Virus Using Surface Enhanced Raman Spectroscopy. *Analyst* **2010**, 135, 3103–3109.

(97) Fan, C.; Hu, Z.; Riley, L. K.; Purdy, G. A.; Mustapha, A.; Lin, M. Detecting Food- and Waterborne Viruses by Surface-Enhanced Raman Spectroscopy. *J. Food Sci.* **2010**, *75* (5), 302–307.

(98) Dardir, K.; Wang, H.; Martin, B. E.; Atzampou, M.; Brooke, C. B.; Fabris, L. SERS Nanoprobe for Intracellular Monitoring of Viral Mutations. *J. Phys. Chem. C* **2020**, *124* (5), 3211–3217.

(99) Boardman, A. K.; Wong, W. S.; Premasiri, W. R.; Ziegler, L. D.; Lee, J. C.; Miljkovic, M.; Klapperich, C. M.; Sharon, A.; Sauer-Budge, A. F. Rapid Detection of Bacteria from Blood with Surface-Enhanced Raman Spectroscopy. *Anal. Chem.* **2016**, *88* (16), 8026–8035.

(100) Wang, P.; Pang, S.; Chen, J.; McLandsborough, L.; Nugen, S. R.; Fan, M.; He, L. Label-Free Mapping of Single Bacterial Cells Using Surface-Enhanced Raman Spectroscopy. *Analyst* **2016**, *141* (4), 1356–1362.

(101) Zhou, H.; Yang, D.; Ivleva, N. P.; Mircescu, N. E.; Niessner, R.; Haisch, C. SERS

Detection of Bacteria in Water by in Situ Coating with Ag Nanoparticles. *Anal. Chem.* **2014**, *86* (3), 1525–1533.

(102) Witkowska, E.; Jagielski, T.; Kamińska, A.; Kowalska, A.; Hryncewicz-Gwóźdź, A.; Waluk, J. Detection and Identification of Human Fungal Pathogens Using Surface-Enhanced Raman Spectroscopy and Principal Component Analysis. *Anal. Methods* **2016**, *8* (48), 8427–8434.

(103) Henderson, K. C.; Sheppard, E. S.; Rivera-Betancourt, O. E.; Choi, J.-Y.; Dluhy, R. A.; Thurman, K. A.; Winchell, J. M.; Krause, D. C. The Multivariate Detection Limit for Mycoplasma Pneumoniae as Determined by Nanorod Array-Surface Enhanced Raman Spectroscopy and Comparison with Limit of Detection by QPCR. *Analyst* **2014**, *139* (24), 6426–6434.

(104) Chen, K.; Yuen, C.; Aniweh, Y.; Preiser, P.; Liu, Q. Towards Ultrasensitive Malaria Diagnosis Using Surface Enhanced Raman Spectroscopy. *Sci. Rep.* **2016**, *6* (1), 20177.

(105) Panikkanvalappil, S. R.; Hira, S. M.; Mahmoud, M. A.; El-sayed, M. A. Unraveling the Biomolecular Snapshots of Mitosis in Healthy and Cancer Cells Using Plasmonically-Enhanced Raman Spectroscopy. *J. Am. Chem. Soc.* **2014**, 136 (45), 15961–15968.

(106) Kang, B.; Austin, L. a; El-Sayed, M. a. Observing Molecular Events in Real-Time of Apoptosis Dynamics in Living Cancer Cells Using Nuclear Targeted Plasmonically Enhanced Raman Nanoprobes. *ACS Nano* **2014**, *8* (5), 4883–4892.

(107) Feng, S.; Lin, D.; Lin, J.; Li, B.; Huang, Z.; Chen, G.; Zhang, W.; Wang, L.; Pan, J.; Chen, R.; et al. Blood Plasma Surface-Enhanced Raman Spectroscopy for Non-Invasive Optical Detection of Cervical Cancer. *Analyst* **2013**, *138* (14), 3967.

(108) Mert, S.; Özbek, E.; Ötünçtemur, A.; Çulha, M. Kidney Tumor Staging Using Surface-Enhanced Raman Scattering. *J. Biomed. Opt.* **2015**, *20* (4), 047002.

(109) Feng, S.; Wang, W.; Tai, I. T.; Chen, G.; Chen, R.; Zeng, H. Label-Free Surface-Enhanced Raman Spectroscopy for Detection of Colorectal Cancer and Precursor Lesions Using Blood Plasma. *Biomed. Opt. Express* **2015**, *6* (9), 3494–3502.

(110) Chen, Y.; Zhang, Y.; Pan, F.; Liu, J.; Wang, K.; Zhang, C.; Cheng, S.; Lu, L.; Zhang,

W.; Zhang, Z.; et al. Breath Analysis Based on Surface-Enhanced Raman Scattering Sensors Distinguishes Early and Advanced Gastric Cancer Patients from Healthy Persons. *ACS Nano* **2016**, *10* (9), 8169–8179.

(111) Gonzalez-Solis, J.; Luevano-Colmenero, G.; Vargas-Mancilla, J. Surface Enhanced Raman Spectroscopy in Breast Cancer Cells. *Laser Ther* **2013**, *22* (1), 37–42.

(112) Yan, B.; Li, B.; Wen, Z.; Luo, X.; Xue, L.; Li, L. Label-Free Blood Serum Detection by Using Surface-Enhanced Raman Spectroscopy and Support Vector Machine for the Preoperative Diagnosis of Parotid Gland Tumors. *BMC Cancer* **2015**, *15* (1), 650.

(113) Li, S.; Li, L.; Zeng, Q.; Zhang, Y.; Guo, Z.; Liu, Z.; Jin, M.; Su, C.; Lin, L.; Xu, J.; et al. Characterization and Noninvasive Diagnosis of Bladder Cancer with Serum Surface Enhanced Raman Spectroscopy and Genetic Algorithms. *Sci. Rep.* **2015**, 5:9582.

(114) Han, H. W.; Yan, X. L.; Dong, R. X.; Ban, G.; Li, K. Analysis of Serum from Type II Diabetes Mellitus and Diabetic Complication Using Surface-Enhanced Raman Spectra (SERS). *Appl. Phys. B Lasers Opt.* **2009**, *94* (4), 667–672.

(115) Lin, J.; Huang, Z.; Feng, S.; Lin, J.; Liu, N.; Wang, J.; Li, L.; Zeng, Y.; Li, B.; Zeng, H.; et al. Label-Free Optical Detection of Type II Diabetes Based on Surface-Enhanced Raman Spectroscopy and Multivariate Analysis. *J. Raman Spectrosc.* **2014**, *44*, 884–889.

(116) Chen, Y. X.; Chen, M. W.; Lin, J. Y.; Lai, W. Q.; Huang, W.; Chen, H. Y.; Weng, G. X. Label-Free Optical Detection of Acute Myocardial Infarction Based on Blood Plasma Surface-Enhanced Raman Spectroscopy. *J. Appl. Spectrosc.* **2016**, *83* (5), 798–804.

(117) Bhowmik, D.; Mote, K. R.; MacLaughlin, C. M.; Biswas, N.; Chandra, B.; Basu, J. K.; Walker, G. C.; Madhu, P. K.; Maiti, S. Cell-Membrane-Mimicking Lipid-Coated Nanoparticles Confer Raman Enhancement to Membrane Proteins and Reveal Membrane-Attached Amyloid-β Conformation. *ACS Nano* **2015**, *9* (9), 9070–9077.

(118) Choi, I.; Huh, Y. S.; Erickson, D. Ultra-Sensitive, Label-Free Probing of the Conformational Characteristics of Amyloid Beta Aggregates with a SERS Active Nanofluidic Device. *Microfluid. Nanofluidics* **2012**, *12* (1–4), 663–669.

(119) Narayanan, N.; Karunakaran, V.; Paul, W.; Venugopal, K.; Sujathan, K.; Kumar Maiti, K. Aggregation Induced Raman Scattering of Squaraine Dye: Implementation in Diagnosis of Cervical Cancer Dysplasia by SERS Imaging. *Biosens. Bioelectron.* **2015**, *70*, 145–172.

(120) Sánchez-Purrà, M.; Roig-Solvas, B.; Rodriguez-Quijada, C.; Leonardo, B. M.; Hamad-Schifferli, K. Reporter Selection for Nanotags in Multiplexed Surface Enhanced Raman Spectroscopy Assays. *ACS Omega* **2018**, *3* (9), 10733–10742.

(121) He, Y.; Su, S.; Xu, T.; Zhong, Y.; Zapien, J. A.; Li, J.; Fan, C.; Lee, S. T. Silicon Nanowires-Based Highly-Efficient SERS-Active Platform for Ultrasensitive DNA Detection. *Nano Today* **2011**, *6* (2), 122–130.

(122) Ye, L. P.; Hu, J.; Liang, L.; Zhang, C. Y. Surface-Enhanced Raman Spectroscopy for Simultaneous Sensitive Detection of Multiple MicroRNAs in Lung Cancer Cells. *Chem. Commun.* **2014**, *50* (80), 11883–11886.

(123) Liu, B.; Ni, H.; Zhang, D.; Wang, D.; Fu, D.; Chen, H.; Gu, Z.; Zhao, X. Ultrasensitive Detection of Protein with Wide Linear Dynamic Range Based on Core-Shell SERS Nanotags and Photonic Crystal Beads. *ACS Sensors* **2017**, *2* (7), 1035–1043.

(124) Zhang, C.; Wang, C.; Xiao, R.; Tang, L.; Huang, J.; Wu, D.; Liu, S.; Wang, Y.; Zhang, D.; Wang, S.; et al. Sensitive and Specific Detection of Clinical Bacteria: Via Vancomycin-Modified Fe3O4@Au Nanoparticles and Aptamer-Functionalized SERS Tags. *J. Mater. Chem. B* **2018**, *6* (22), 3751–3761.

(125) Maiti, K. K.; Dinish, U. S.; Fu, C. Y.; Lee, J. J.; Soh, K. S.; Yun, S. W.; Bhuvaneswari, R.; Olivo, M.; Chang, Y. T. Development of Biocompatible SERS Nanotag with Increased Stability by Chemisorption of Reporter Molecule for in Vivo Cancer Detection. *Biosens. Bioelectron.* **2010**, *26* (2), 398–403.

(126) Wang, X. P.; Zhang, Y.; König, M.; Papadopoulou, E.; Walkenfort, B.; Kasimir-Bauer, S.; Bankfalvi, A.; Schlücker, S. ISERS Microscopy Guided by Wide Field Immunofluorescence: Analysis of HER2 Expression on Normal and Breast Cancer FFPE Tissue Sections. *Analyst* **2016**, *141* (17), 5113–5119.

(127) Harmsen, S.; Rogalla, S.; Huang, R.; Spaliviero, M.; Neuschmelting, V.; Hayakawa, Y.; Lee, Y.; Tailor, Y.; Toledo-Crow, R.; Kang, J. W.; et al. Detection of Premalignant Gastrointestinal Lesions Using Surface-Enhanced Resonance

Raman Scattering-Nanoparticle Endoscopy. *ACS Nano* **2019**, *13* (2), 1354–1364.

(128) Karabeber, H.; Huang, R.; Iacono, X. P.; Samii, X. J. M.; Pitter, K.; Holland, E. C.; Kircher, M. F. Guiding Brain Tumor Resection Using Surface-Enhanced Raman Scattering Nanoparticles and a Hand-Held Raman Scanner. *ACS Nano* **2015**, *8* (10), 9755–9766.

(129) Lee, S.; Chon, H.; Lee, M.; Choo, J.; Shin, S. Y.; Lee, Y. H.; Rhyu, I. J.; Son, S. W.; Oh, C. H. Surface-Enhanced Raman Scattering Imaging of HER2 Cancer Markers Overexpressed in Single MCF7 Cells Using Antibody Conjugated Hollow Gold Nanospheres. *Biosens. Bioelectron.* **2009**, *24* (7), 2260–2263.

(130) Ramya, A. N.; Joseph, M. M.; Nair, J. B.; Karunakaran, V.; Narayanan, N.; Maiti, K. K. New Insight of Tetraphenylethylene-Based Raman Signatures for Targeted SERS Nanoprobe Construction Toward Prostate Cancer Cell Detection. *ACS Appl. Mater. Interfaces* **2016**, *8* (16), 10220–10225.

(131) Li, T. Da; Zhang, R.; Chen, H.; Huang, Z. P.; Ye, X.; Wang, H.; Deng, A. M.; Kong, J. L. An Ultrasensitive Polydopamine Bi-Functionalized SERS Immunoassay for Exosome-Based Diagnosis and Classification of Pancreatic Cancer. *Chem. Sci.* **2018**, *9* (24), 5372–5382.

(132) Ramya, A. N.; Samanta, A.; Nisha, N.; Chang, Y. T.; Maiti, K. K. New Insight of Squaraine-Based Biocompatible Surface-Enhanced Raman Scattering Nanotag for Cancer-Cell Imaging. *Nanomedicine* **2015**, *10* (4), 561–571.

(133) Ranc, V.; Markova, Z.; Hajduch, M.; Prucek, R.; Kvitek, L.; Kaslik, J.; Safarova, K.; Zboril, R. Magnetically Assisted Surface-Enhanced Raman Scattering Selective Determination of Dopamine in an Artificial Cerebrospinal Fluid and a Mouse Striatum Using Fe3O4/Ag Nanocomposite. *Anal. Chem.* **2014**, *86* (6), 2939–2946.

(134) Bamrungsap, S.; Treetong, A.; Apiwat, C.; Wuttikhun, T.; Dharakul, T. SERS-Fluorescence Dual Mode Nanotags for Cervical Cancer Detection Using Aptamers Conjugated to Gold-Silver Nanorods. *Microchim. Acta* **2016**, *183* (1), 249–256.

(135) Qian, X.; Peng, X.-H.; Ansari, D. O.; Yin-Goen, Q.; Chen, G. Z.; Shin, D. M.; Yang, L.; Young, A. N.; Wang, M. D.; Nie, S. In Vivo Tumor Targeting and Spectroscopic

Detection with Surface-Enhanced Raman Nanoparticle Tags. *Nat. Biotechnol.* **2007**, *26* (1), 83–90.

(136) Davis, R. M.; Kiss, B.; Trivedi, D. R.; Metzner, T. J.; Liao, J. C.; Gambhir, S. S. Surface-Enhanced Raman Scattering Nanoparticles for Multiplexed Imaging of Bladder Cancer Tissue Permeability and Molecular Phenotype. *ACS Nano* **2018**, *12*, 9669–9679.

(137) Guo, R.; Yin, F.; Sun, Y.; Mi, L.; Shi, L.; Tian, Z.; Li, T. Ultrasensitive Simultaneous Detection of Multiplex Disease-Related Nucleic Acids Using Double-Enhanced Surface-Enhanced Raman Scattering Nanosensors. *ACS Appl. Mater. Interfaces* **2018**, *10* (30), 25770–25778.

(138) Li, M.; Kang, J. W.; Sukumar, S.; Dasari, R. R.; Barman, I. Multiplexed Detection of Serological Cancer Markers with Plasmon-Enhanced Raman Spectro-Immunoassay. *Chem. Sci.* **2015**, *6* (7), 3906–3914.

(139) Song, C.; Yang, Y.; Yang, B.; Min, L.; Wang, L. Combination Assay of Lung Cancer Associated Serum Markers Using Surface-Enhanced Raman Spectroscopy. *J. Mater. Chem. B* **2016**, *4* (10), 1811–1817.

(140) Zavaleta, C. L.; Smith, B. R.; Walton, I.; Doering, W.; Davis, G.; Shojaei, B.; Natan, M. J.; Gambhir, S. S. Multiplexed Imaging of Surface Enhanced Raman Scattering Nanotags in Living Mice Using Noninvasive Raman Spectroscopy. *Proc. Natl. Acad. Sci. U. S. A.* **2009**, *106* (32), 13511–13516.

(141) Kang, J. W.; So, P. T. C.; Dasari, R. R.; Lim, D. K. High Resolution Live Cell Raman Imaging Using Subcellular Organelle-Targeting SERS-Sensitive Gold Nanoparticles with Highly Narrow Intra-Nanogap. *Nano Lett.* **2015**, *15* (3), 1766–1772.

(142) Wang, Y.; Reder, N. P.; Kang, S.; Glaser, A. K.; Yang, Q.; Wall, M. A.; Javid, S. H.; Dintzis, S. M.; Liu, J. T. C. Raman-Encoded Molecular Imaging with Topically Applied SERS Nanoparticles for Intraoperative Guidance of Lumpectomy. *Cancer Res.* **2017**, *77* (16), 4506–4516.

(143) Dinish, U. S.; Balasundaram, G.; Chang, Y.-T.; Olivo, M. Actively Targeted In Vivo Multiplex Detection of Intrinsic Cancer Biomarkers Using Biocompatible SERS Nanotags. *Sci. Rep.* **2014**, *4*, 4075.

Differential Recognition of Cervical Cancer Lesions by Label-free Surface Enhanced Raman Fingerprints and Chemometrics
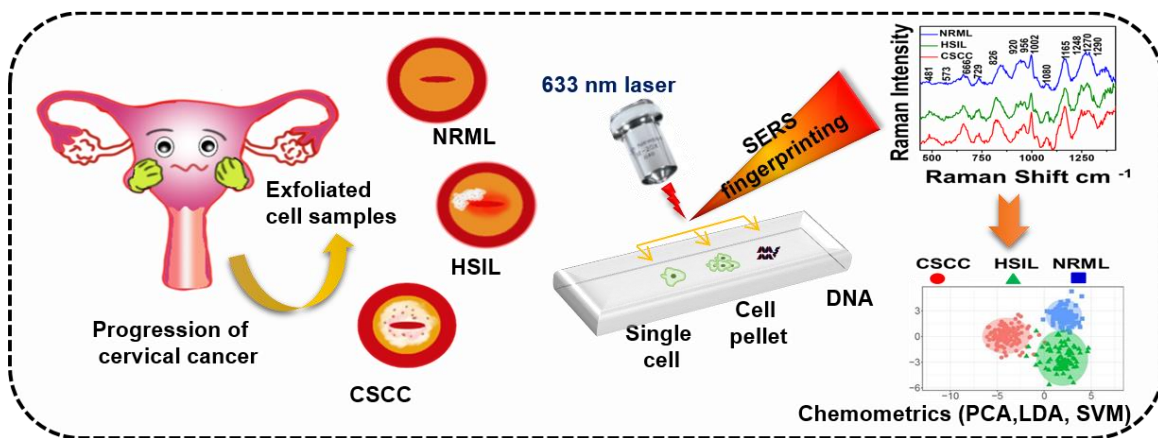
2.1 Abstract: *Cervical cancer stands among the most pervasive abnormal proliferations among women globally, can be treated and cured if diagnosed at an early stage. The current diagnostic practices including Pap test and Human Papilloma Virus (HPV) DNA identification suffer drawbacks like less sensitivity, subjective nature and is time consuming. Herein, a strategic spectroscopic modality have been successfully explored utilizing pathologically confirmed exfoliated cervical cell samples by label free surface enhanced Raman scattering (SERS) technique. A differential spectral fingerprint for the prediction of normal (NRML), high-grade intraepithelial lesion (HSIL) and cervical squamous cell carcinoma (CSCC) have been evaluated by comparing three different approaches i.e. single-cell, cell-pellet and extracted DNA. The tunable plasmonic properties of the gold nanoparticles as the SERS substrate favoured the increment of Raman intensity in minimal time in an ultrasensitive manner. The ratio of*

SERS signal intensities between 1270 /1370 cm^{-1} in single cell and 956 /1022 cm^{-1} in cell pellet exhibiting the signature identity for Amide III/nucleobases and carotenoid/glycogen respectively seemed proficient for establishing the empirical discrimination. The precise identification of DNA and amino acid specific Raman peaks were further confirmed by SERS spectral analysis from extracted DNA and Ultra-Fast Liquid Chromatography (UFLC). Moreover, all the spectral invention was subjected to chemometrics including Support Vector Machine (SVM) which furnished an average diagnostic accuracy of 94 %, 74 % and 92 % for single cell, cell pellet and extracted DNA respectively. The futuristic use of a handy Raman system united with SERS read-out and machine learning technique using cervical exfoliated cells in field trial promises its potential as a screening technique to reduce the incidence of this disease in low resource countries.

2.2 Introduction

Cervical cancer is the fourth most common cancer leading to malignancy related death in women worldwide[1]. According to 2018 GLOBOCAN report, 90 % of the death due to cervical cancer happened in low and middle income countries like Sub-Saharan Africa and South East Asia[2]. In India, the second most populous country in the world, cervical cancer accounts for 22.86 % of all cancers among women. The incidence of this disease has been reduced dramatically by the implementation of screening programmes in developed countries, which is not at all the case in low resource developing countries. The approach adopted in developed countries include a consolidated tactics inclusive of prevention, early detection, screening and proper treatment programmes. The most influencing factor for the cause of cervical cancer is the tenacious infection with high risk HPV[3]. Dr. George N Papanicolaou in 1926 introduced the Bethesda system for the nomenclature of different stages of cervical dysplasia detectible by a Pap smear test [4]. Pap smear test is a well-established multichromatic cytological staining technique practiced in clinics for morphologically testing the presence or absence of precancerous or cancerous lesions by gently scraping away the cells from the cervix. The reagents inside the staining formulation can specifically stain the nucleus, keratin, cytoplasm, nucleolus, glycogen etc. Three types of normal epithelial cells can also be visualized in a Pap smear. The superficial

cells stains orange to pink, and intermediate/parabasal cells shows light green to blue color. Dysplastic cells in its progressive order can be easily identified visually in the Pap smears. The chronological event of epithelial abnormalities leads to the development of invasive cancer starting from healthy to low grade squamous intraepithelial lesion (LSIL/ CINI/ mild dysplasia), then to high grade squamous intraepithelial lesion (HSIL/ CIN II & III / moderate) and finally to invasive squamous cell carcinoma (severe dysplasia/ in situ carcinoma) [5]. LSIL is a stage which has the possibility to resolve spontaneously back to normal within few years. In other way, LSIL can progress to HSIL stage wherein the treatment is still possible. So treatment management is being performed by a continuous follow up to check if it progresses or regresses. Thus such aberrations existing within a long window period can be subjected to proper diagnostic and therapeutic intervention before the transformation of mild abnormality into invasive cancer. Even though Pap staining is a well-established routine test, some recent reports suggest the limitations of the Pap smear owing to its low sensitivity, high false negative rates, and inter-observer variability. The sensitivity was found to be 51% only with around 98% specificity. The average false negative rate was identified as around 35.5% [6,7]. These limitations have led to the re-evaluation of the significance of cytology as a primary screening test. HPV DNA analysis has also been included in the cervical cancer detection strategy using polymerase chain reaction (PCR), an alternative diagnostic measure undertaken for this disease. Even though HPV DNA test has shown an increased sensitivity for the detection of cervical intra epithelial lesions in asymptomatic populations, many of the HPV infections are transient without causing any clinically significant lesions and gets cleared without any intervention, upon time. Hence the positive predictive value and specificity of HPV test for the identification of cervical intraepithelial lesions in a population is considerably low. A few prophylactic vaccines are also introduced against prominent high risk strains of HPV which can considerably decrease the incidence of cervical cancer. Therefore, developed countries adopt Pap smear test, HPV test and vaccination for the effective control of cervical cancer. Lack of enough trained personnels[8] to screen all worthy women in the community in a systematic manner is also an additional obstruction for implementing such population screening programmes. So there exists an urgent requirement for cheap, alternative techniques

which should preferably be rapid, objective and non-destructive to evolve as a population screening programme.

Study of cellular and biological processes in molecular scale are crucial for understanding the diagnosis of diseases together with therapy. There is a high demand for techniques which can impart ultra-sensitivity and specificity for detecting the role of the various cellular compositions in complex biological environment. The search for specific and precise cancer screening has led to the development of novel diagnostic strategies including spectroscopic techniques to distinguish early malignant lesions[9]. Optical spectroscopic methods, mostly Fourier-transform infrared spectroscopy [10], Raman [11] fluorescence [12] etc. has been well-studied and out of which Raman spectroscopy offers advantages over others. The inelastic scattering of monochromatic light in Raman spectroscopy possessing high spatial resolution can be performed in near-infrared (NIR) radiation with minimal influence of water bands and less sample preparation. Several groups explored the utility of Raman scattering like accurate database library for each characteristic peak frequencies for biological tissues,[13] classification of healthy, cancerous and benign samples for different cancers like, oral[14], cervical[15,16], colorectal[17], breast [18], gastric [19] and much more by employing different types of multivariate analysis.[20]Test samples including cells [21], tissues [22] body fluids [23] exosomes [24] extracellular vesicles [25] etc forms sources of analysis as it has the origin from normal or unhealthy system. The challenges associated with large data sets has been resolved extensively by applying various chemometric methods [26], such PCA[27], LDA[28], least-squares regression as well as cluster analysis, and machine learning techniques like SVM[29] which mostly intend to extract spectral features for the characterization of the sample. However, a major drawback of Raman scattering is its inherently weak signal which paved way to different type of improvisations over typical Raman spectroscopy including SERS,[30,31] CARS,[32] TERS[33], SRS[34] and many more. Among which SERS received huge acceptance which allows the ultrasensitive detection of low analyte concentration through the enhanced signals around 10^8-10^{14} folds by the excitation of surface plasmons from metallic nanoparticles. Two different methods were mostly adopted for SERS analysis, label-free and labeled SERS[35]. Label-free SERS is a direct method which involves the interaction of SERS substrates with the biomolecules, whereas labeled SERS uses a Raman reporter molecule together

with a targeting moiety [36] which indirectly fish out the target protein of interest within the heterogeneity of the sample. The potential of SERS analysis in single living cells has been demonstrated using colloidal gold nano particles (AuNPs) deposited inside cells which resulted in strong enhancement of Raman signals opening up exciting opportunities for biomedical studies[37]. Subsequently, several SERS based studies investigated this platform which includes some pioneer works like the precise tracking of the biomolecular changes in different stages of mitosis,[38] apoptosis,[39] classification of healthy and cancerous samples in breast cancer,[40] gastric cancer,[41] bladder cancer[42], kidney tumor staging,[43] colorectal cancer,[44] parotid cancer[45] and many more.

Raman spectroscopic investigation on cervical cancer has been well investigated including identification of pre-carcinogenic stages,[16] cervical exfoliated cells study of normal and abnormal samples[46], differentiation of normal and cancerous subjects using serum samples[47], *in vivo* cervical tissue analysis for differentiating normal and precancerous tissues,[48] distinguishing normal liquid based cytology cell types along with high grade dysplasia cells,[49] HSIL detection by analyzing morphologically normal appearing cells[50] etc. are a few among them. SERS studies on using blood plasma[51] and serum[52] samples has also been reported which involves invasive sample collection procedures. In addition, early stage detection using blood is not feasible as blood based biomolecular changes like leakage of circulating tumor proteins, cells, DNA and exosomes will be prevalent in the late metastatic stage only. Also such changes cannot be really attributed to a particular disease also. Employing SERS in exfoliated cervical cell samples for cervical cancer detection will assure direct insight into the origin of abnormality.

Considering the existing diagnostic modalities and fundamental issues, we report for the first time, a label free SERS based spectroscopic technique in exfoliated cells for generating a differential spectral pattern for the detection of squamous cell carcinoma and its precursor lesions during cervical cancer progression. The analysis has been performed for distinguishing three grades i.e. NRML, HSIL and CSCC using three different forms of analytes viz. single cell, cell-pellet, extracted DNA (**Scheme 2.1**).

Significant peak variations like shifts and spectral differences were evaluated within and between the groups using chemometric interpretation viz., PCA, LDA and SVM in order to obtain satisfactory prediction accuracy enabling its potential to emerge as a population screening method to monitor the progression of cervical cancer. Along with SERS based cytology as a new insight, comparative conventional cytological Pap staining and HPV PCR analysis were also carried out.
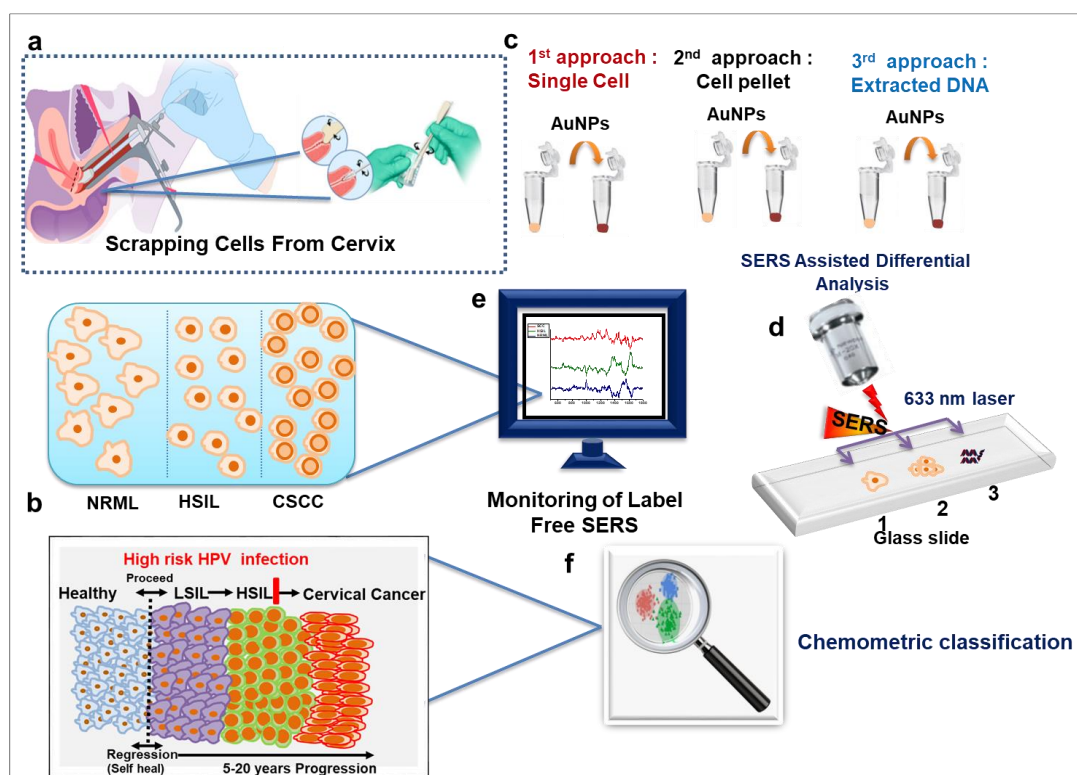
Scheme 2.1: Schematic illustration of experimental design for differentiating three grades viz. normal (NRML), high grade intraepithelial lesion (HSIL) and cervical squamous cell carcinoma (CSCC) using SERS., a) Scrapping cells from the cervix using cytobrush, b) progression pattern of cervical cancer c) Set 1: single cell, Set 2: cell pellet, Set 3: extracted DNA (mixed with AuNPs), d) independent SERS analysis of 1) single cell,2) cell pellet, 3) extracted DNA in glass slide, d) empirical signal monitoring of the three grades and f) chemometric analysis.

Another hallmark of cancer progression underlies the altered metabolism to satisfy the increasing need of energy and molecular building blocks like nucleic acids, amino acids, lipids etc. Intracellular concentration of amino acids is a diagnostic parameter for cancer as the abnormal proliferation requires more amino acids for protein synthesis. Therefore, amino acid profiling by UFLC technique[53] was attempted as an

alternative confirmatory approach for identifying the progression of cancer related amino acid metabolites along with SERS.

2.3 Results and Discussion

A thorough assimilation on SERS based minimally invasive spectro-cytology approach has been introduced when it culminated to generate molecular level differential spectra for chemometric prediction of major three grades of exfoliated cells from uterine cervix. As cervical cancer progress from normal to abnormal in a grade dependent way, the identification of precancerous lesions can be beneficial for the early stage diagnosis. Diagnosis of cancer always depends on the fact that the tumor cells will detach or desquamate from a surface or cellular lining in and around the area of its existence which can be collected for a simple, rapid, painless, minimally invasive analysis.

2.3.1 Fabrication of colloidal SERS substrate.

Colloidal spherical AuNPs have been utilized as well explored SERS substrate with tunable optical property and is chemically inert when mixed with a wide range of analytes or biomolecules providing characteristic Raman fingerprints. AuNPs (nearly 530 nm plasmon peak) were within a size range of 40-45 nm emphasizing its best SERS activity[54,55] reported so far. AuNPs were synthesized as per the standard method using citrate reduction method[56] with optimized size, shape and mono-dispersity confirmed by Ultraviolet–visible (UV-Vis) absorbance, Dynamic Light Scattering (DLS) and High Resolution Transmission Electron Microscopy (HR-TEM) (**Figure 2.1**).
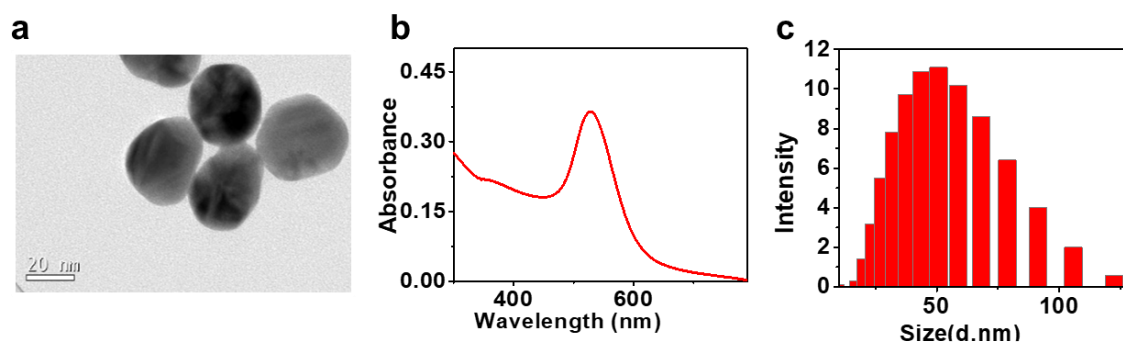
Figure 2.1: Characterization of SERS substrate**,** a) HR-TEM (scale bar: 20nm), b) UV–Vis absorption spectra and c) DLS of AuNPs 40-45 nm.

2.3.2 Biomolecular fingerprinting of cervical squamous cell carcinoma model

Label-free biomolecular SERS fingerprints were evaluated with SiHa, an epithelial type cell line, derived from grade II squamous cell carcinoma of the cervix which can be considered as the best *in vitro* model prior to the investigation in clinical samples. Squamous cell carcinoma was chosen for the study as 75-80 % of cervical cancers exist in this form and remaining prevailed as adenocarcinoma. The preliminary studies conducted in fixed SiHa cell showed fingerprint peaks corresponding to amino acids, nucleic acid bases, phosphate stretchings, carotenoids etc which formed a basis for the peak analysis in real patient samples. SERS analysis after incubation of AuNPs in SiHa cells showed the presence of a range of molecular fingerprints out of which Raman peaks at 481, 1330 and 1456 cm^{-1} corresponds to the -C-N-C-bending, -P=O-stretching vibration and -CH$_2$ vibration of DNA signal, 572 cm^{-1} designates the -O-C=O for tryptophan abundance, 621 and 1002 cm^{-1} relates to signals from -O-C=O and aromatic ring chain vibration in phenyl alanine, 643 and 1211 cm^{-1} represents -O-C=O bending and -C-C-N- vibration in tyrosine, 735 and 746 cm^{-1} represents -O-C=O bending vibration in adenine and thymine respectively (**Figure 2.2**). Raman peaks at 826 and 1085 cm^{-1}were observed corresponds to DNA phosphate backbone (-O-P-O-) stretching vibration, 957 and 1154 cm^{-1} indicated the presence of -C-C- aliphatic alicyclic chain vibration in carotenoids and peak at 1545 cm^{-1} resembled the presence of Amide II, nucleic acid and tryptophan, 1697 cm^{-1} corresponds to amide I (**Table 2.1**).[13]The distinct well resolved biomolecular fingerprints from SiHa cells provided a blue-print of the major molecular fingerprint viz., aromatic amino acids, DNA, amides (I & II), which are benchmarked as a model for clinical investigations.

2.3.3. SERS analysis in clinical samples

The analysis in clinical samples were approached by the modulation of three different sample sources, i.e. single cell, cell pellet and extracted DNA to arrive at a conclusion for adopting the most simplest and accurate results to uplift the technique as a diagnostic modality. Single cells were analyzed after morphologically identifying the

ratio of nucleus to cytoplasm features. Cell pellet analysis was performed in a blinded manner without any morphological evaluation of the cells which may be the most ideal option for conducting a screening study. Extracted DNA analysis was performed to confirm the identity of Raman fingerprints of nucleic acids. Liquid based cytology (LBC) fixation were performed which will render improved preservation of the cell sample eliminating artifacts and degenerative changes developed in the course of air-drying. Superior preservation of the cells allows precise assessments of the size of the nucleus, evaluating the ratio of nucleus to cytoplasm and the structure of chromatin which in turn will upsurge the accuracy for appropriately recognize and categorize cellular changes. In addition, LBC will reduce the background caused by blood contamination in the cervical scrape samples which usually interferes in the sample interpretation.[57] SERS substrate incubation in fixed cells and living cells are the two widely used methods to study single cells using SERS. Reports suggests that valuable information of real time cellular processes is obtained from live cells than fixed cells as fixation can lead to changes in the molecular vibrations leading to variations in the spectral pattern.[58]
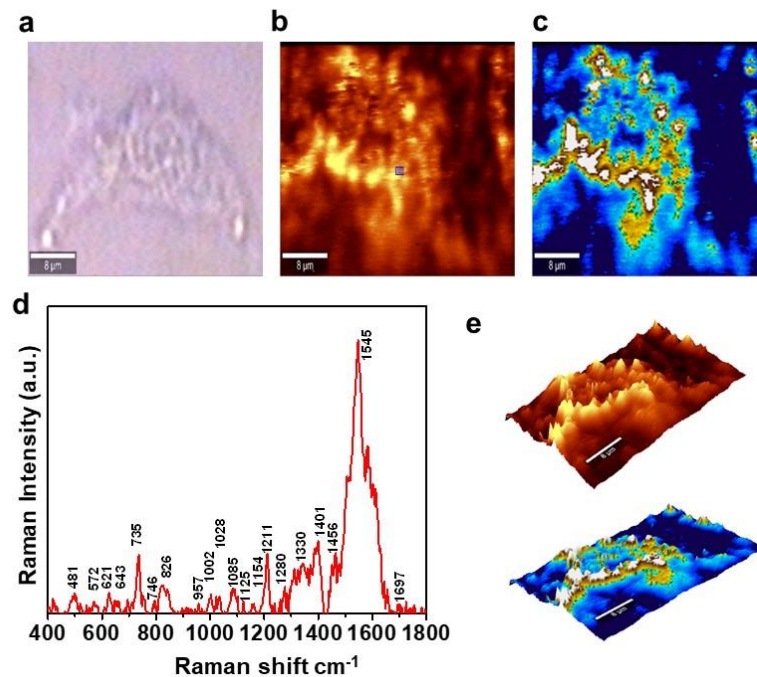
Figure 2.2: SERS analysis in SiHa cell line. a) Bright field image, b) Raman image, c) cluster map d) mean SERS spectra acquired and e) 3D Raman mapping (Scale bar =8 μm), laser power density 3-7 mW.

Table 2.1: Tentative SERS peak assignments from cervical squamous cell carcinoma model, SiHa

Wavenumber (cm⁻¹)	SERS peak assignment	Wavenumber (cm⁻¹)	SERS peak assignment
481, 1330	-C-N-C- bending, -P=O- stretching vibration of DNA	1028	-C-NH$_2$ in primary aliphatic amine in Phenyl alanine
572	-O-C=O bending vibration of Tryptophan/Cytosine, Guanine	1085	-O-P-O-stretching vibration in DNA
621	-O-C=O bending vibration in Phenyl alanine	1125	-C-N stretching vibration in protein
643	-O-C=O bending vibration in Tyrosine	1211	-C-C-N- bending vibration in Tyrosine, Phenyl alanine
735	-O-C=O bending vibration in Adenine	1280	Amide III in protein
746	-O-C=O bending vibration in Thymine	1401	-C-N- stretching vibration in Collagen
826	-O-P-O- stretching vibration in DNA	1456	-CH$_2$ vibration in deoxyribose
957, 1154	-C-C- aliphatic alicyclic chain vibration in Carotenoid	1545	Amide II in Tryptophan
1002	Aromatic ring chain vibration in Phenyl alanine	1697	Amide I

Recent report has already been demonstrated the accurate evaluation of surface charge of AuNPs for live cell uptake and deep tumor penetration by fabricating SERS nanotags made using positive, negative and neutral nanoparticles. SERS based tracing

analysis showed positive charged nanoparticles are the best for cellular internalization in 2D cell culture system and negatively charged AuNPs showed extended penetration and internalization into the tumor spheroid core. [59] In the present study, as the cervical scrape cells are already fixed during collection, the variations thus arising will be commonly to all the three groups, i.e. NRML, HSIL and CSCC spectra which can be nullified.

2.3.3.1 SERS aided grading with cervical exfoliated single cells

Pathologically confirmed cervical smears of major three grades i.e. NRML, HSIL and CSCC were collected and processed using liquid based cytology procedure. The details of patient samples is depicted in **Table 2.2**. A monolayer of diagnostically relevant cells upon incubation with AuNPs were evaluated for the single cell analysis. In a preliminary analysis, the SERS mapping of the single cell showed the variations in the morphology of three different types of cells, viz. NRML, HSIL and CSCC (**Figure 2.4a**). In single cells, 5 μm x 5 μm nuclear area was preferred for image scanning to avoid variability arising from the cytoplasmic area. Since the analysis involved addition of AuNPs, Pap stained slides were subjected to de-staining followed by SERS analysis to select the diagnostically relevant cells (**Figure 2.3**).

Table 2.2: Clinical details of the cervical exfoliated samples.

Groups	No: of patients	Total no. of spectra for single cell	Total no. of spectra for cell pellet	Total no. of spectra for extracted DNA	Mean age
NRML	47	1363	149	62	
HSIL	41	325	48	54	50
CSCC	36	850	127	65	
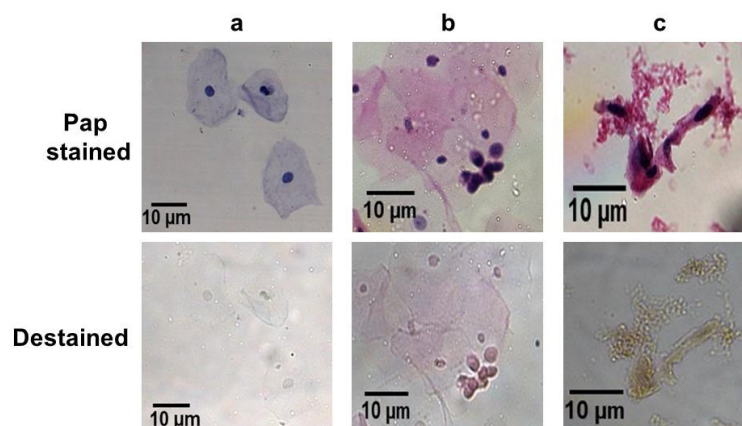
Figure 2.3: Bright field micrograph obtained after Pap staining and de-staining for Raman analysis a) CSCC, b) HSIL and c) NRML (Scale bar: 10 μm).

Initially, individual SERS fingerprint was evaluated empirically followed by chemometric statistical analysis to group the three classes. The mean spectra accumulated from the average of the collected spectrum excluding the outliers of each group were normalized to its highest peak (amide II at 1550 cm^{-1}) in which clear spectral variations were observed. The analysis in exfoliated single cell samples, NRML, HSIL and CSCC showed distinctive peaks correlating to the cell line signals. Distinct Raman peak at 481 cm^{-1} associated with -C-N-C bending vibration of DNA was found to be increased in HSIL and CSCC samples which showed an indication of high nuclear content. The -O-C=O- bending vibration of amino acid tryptophan corresponding to 573 cm^{-1} was prominent in HSIL and CSCC samples displaying the presence of high protein content which may be mostly from the histone protein and nuclear regulatory proteins inside the nucleus. The -O-C=O- bending vibration peak at 643 and 666 cm^{-1} are indicative to tyrosine, thymine and guanine ring vibrations present in all grades whereas adenine ring vibration at 729 cm^{-1} identified prominently in the abnormal grades i.e. HSIL and CSCC predicting the increase in nuclear elements. On the other hand, O-P-O stretching at 826 cm^{-1} and 1080 cm^{-1} favored the indirect existence of nucleic acid. The O-P-O stretching at 826 cm^{-1} showed the increased nuclear content in abnormal samples. Interestingly the peak at 826 cm^{-1} in HSIL and CSCC samples is identified as a shifted position in comparison to normal samples which showed a prominent peak at 850 cm^{-1}. Such a peak shift is visible in IR-FT Raman spectra in cancerous cervix comparing benign and normal [60] A -C-O-C- bending vibration peak at 920 cm^{-1} is slightly prominent in abnormal samples which correspond to the amino

acid, proline. Another distinguishing factor between the three groups were the presence of -C-O-C- stretching of the amino acid proline. It has been proven that proline rich tyrosine kinase 2 (Pyk2) plays an important role in tumor progression in various human cancers [61]. Pyk2 is a non-receptor tyrosine kinase which controls tumor survival, its proliferation, migration, invasion properties, metastasis and resistance to chemotherapy [62,63].
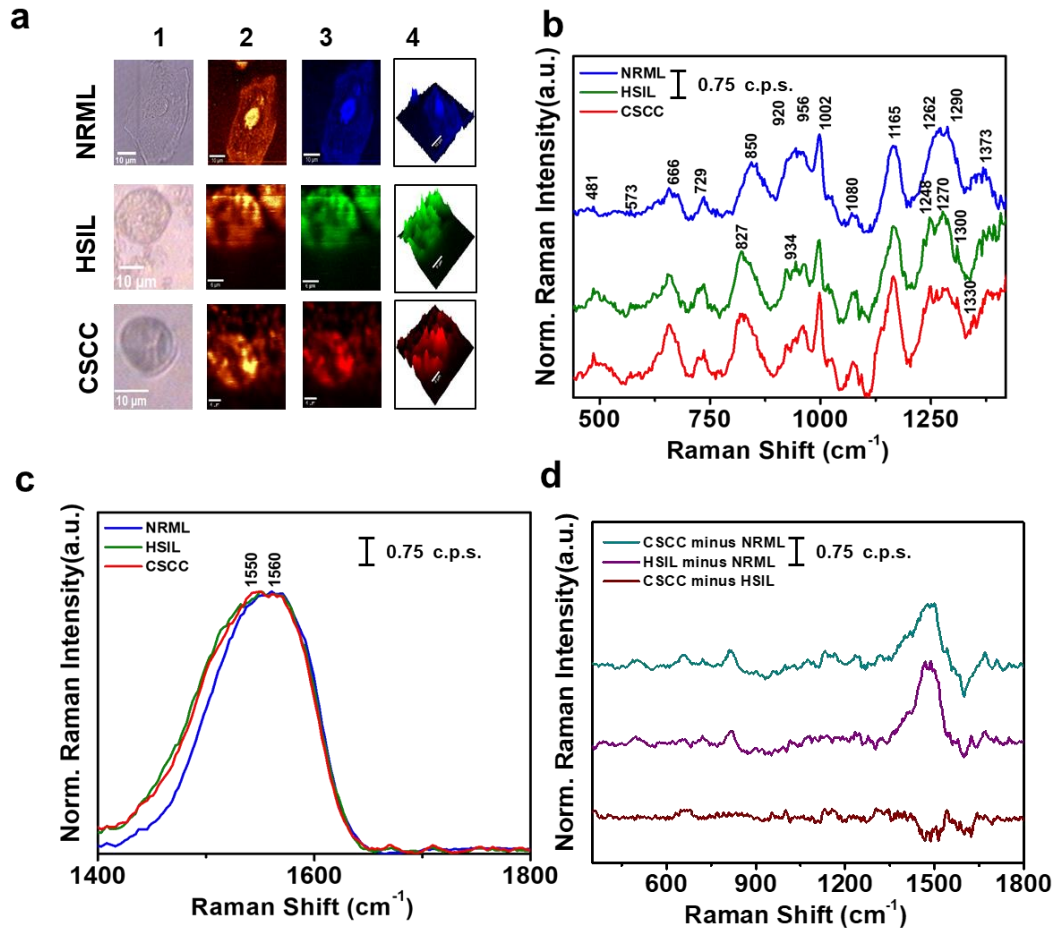
Figure 2.4: SERS analysis from exfoliated single cell samples. a) SERS imaging of single cell, 1) bright field, 2) Raman imaging, 3) cluster mapping and 4) 3D cluster mapping (Scale bar: 10 μm, laser power density 3-7 mW), b) mean SERS spectra acquired from cervical exfoliated single cell samples (region 400-1400 cm^{-1}), c) mean SERS spectra from range 1400-1800 cm^{-1}, d) difference SERS spectra for NRML, HSIL and CSCC samples.

In addition, there exists a correlation of a biomarker known as c-myc over expression distinct in cervical cancer which increases proline biosynthesis from glutamine and is a prognostic marker useful in guiding treatment decisions in cervical cancer. Yet

another study revealed that Pyk2 is essential for the intracellular trafficking of HPV 16 in human keratinocyte cells [64–66]. Thus the increase in proline may be indicative of tumor progression. C-C aliphatic, alicyclic peaks identified at 956 and 1165 cm^{-1} attributed to carotenoid showed higher intensity in CSCC compared with normal. The increase of carotenoid signal at 956 cm^{-1} and 1165 cm^{-1} in single cells might be due to the reason that cancer cells tends to accumulate carotenoids to resist damage [67]. Amide III signal from proteins at 1262 cm^{-1} in NRML is shifted in HSIL and CSCC samples to 1270 cm^{-1}. Similarly, amide II signal arising at 1560 cm^{-1} from the protein counterparts inside the nucleus showed a clear shift of around 10 nm between normal and abnormal samples (**Figure 2.4b, 2.4c**).[13] Interestingly, the ratio between 1270 and -O-C=O symmetric stretching at 1373 cm^{-1} were well resolved for the prediction of abnormality from the mean spectra. The ratio value was found to be 1.55, 1.2 and 1.02 for NRML, HSIL and CSCC respectively in single cells. The ratio is decreasing because the peak corresponding to 1373 cm^{-1} is increasing in the abnormal samples. The variations existing between the three groups were acquired by subtracting the mean spectra of NRML from CSCC, NRML from HSIL and HSIL from CSCC. The positive peaks in the difference spectra obtained showed the presence of bio-molecular activity and negative peaks showed the absence of the same (**Figure 2.4d**). The peak variations more prominent between normal and abnormal samples were visualized by box plot analysis performed in R software (**Figure 2.5**). All the peak assignments from the single cell analysis is depicted in **Table 2.3**.

2.3.3.2 SERS-aided grading with cervical exfoliated cell pellets

When coming to cell pellet, in positive patient sample it is said to be heterogenous, i.e., all the three types of cells; viz. NRML, HSIL and CSCC may be present. Even though all cell types are present, there occurs a presence of premalignant changes in the normal looking cells [50] of the positive smears. Pellet of the exfoliated cells, exhibited a prominent SERS peak representing -C-O-C bending vibration at 490 and 1022 cm^{-1} corresponding to the presence of glycogen prevalent in NRML cells compare to abnormal cells in cervical smears. The presence of glycogen is usually considered as a parameter for classifying normal and abnormal cells in cytological specimens of the cervix. [68,69] Identified -O-C=O Raman peaks at 667, 729

and 1373 cm^{-1} indicated the increase in the DNA material in HSIL, CSCC samples specific to thymine, guanine and adenine respectively. Again, sharp peak showing -C-C-N- at 1170 cm^{-1} corresponding to tyrosine was found in abnormal samples. Visible Raman peak shift was obtained at the amide II region in the CSCC samples when compared to NRML samples as specified a peak at around 1568 cm^{-1} in NRML shifted to 1547 cm^{-1} in CSCC specimen **(Figure 2.6 a, b**). We have evaluated the ratio between P-O-C anti symmetric stretch at 970 and 1022 cm^{-1} which is considered as a predictive indicator of abnormality from the mean spectra leading to the values of 0.61, 1.13 and 1.34 for NRML, HSIL and CSCC respectively. The pellet comprising cervical exfoliated cells was a mixture of normal and abnormal cells with its mean signature Raman spectra contained some common features.
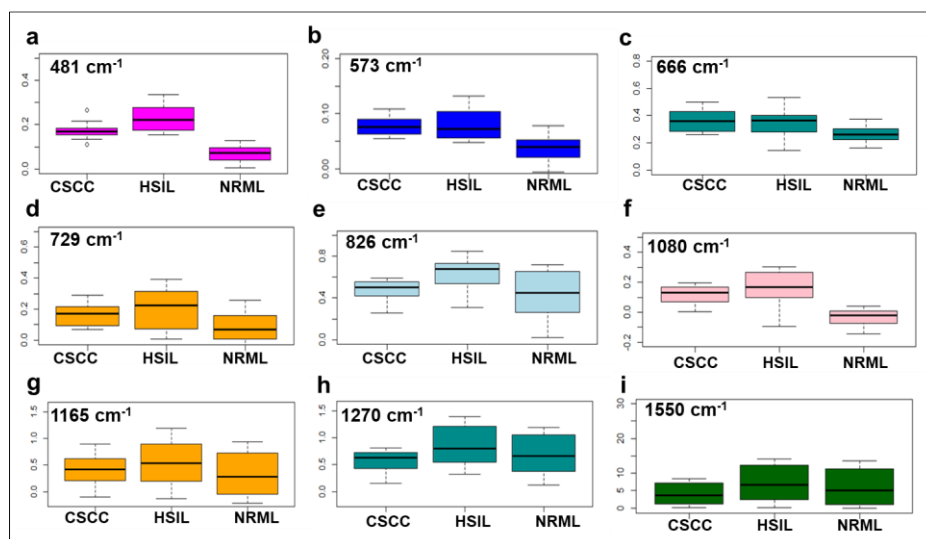
Figure 2.5: Boxplots of normalized scores of prominent peak variations evident in single cell analysis, specifically at a) 481, b) 573, c), 666, d) 729, e) 826, f) 1080, g) 1165, h) 1270 and i) 1550 cm^{-1}. Y-axis represents the quantity of total spectra used and its mean peak intensity (a.u.).

The variations existing between the three groups were attained by subtracting NRML from CSCC, NRML from HSIL and HSIL from CSCC mean spectra. The positive peaks in the difference spectra illustrated the presence of bio-molecular activity and negative peaks showed the absence of its fingerprints (**Figure 2.6c**). Standard deviation and mean spectra is shown in **Figure 2.6d**. The prominent peak differences between NRML, HSIL and CSCC samples were visualized in box plot analysis

performed in statistical R software (**Figure 2.7**). All the peak assignments from the cell pellet analysis is depicted in **Table 2.4**.

Table 2.3: Tentative SERS peak assignments from cervical clinical single cell samples; NRML, HSIL and CSCC.

Wavenumber (cm^{-1})	SERS peak assignment	Wavenumber (cm^{-1})	SERS peak assignment
481	-C-N-C- bending vibration of DNA	1002	Aromatic ring chain vibration in Phenyl alanine
573	-O-C=O- bending vibration in Tryptophan	826, 1088	-O-P-O stretching vibration in DNA
643, 1175	-O-C=O- bending, -C-C-N bending vibration in Tyrosine	1248	-C-N stretch in Cytosine, Guanine
666	-O-C=O bending vibration in Thymine, Guanine	1270	Amide III
729	-O-C=O bending vibration in Adenine	1290	-C-N stretching in Cytosine
920	-C-O-C- bending vibration in Proline	1373	-O-C=O symmetric stretch in Thymine, Adenine, Guanine
956, 1165	C-C aliphatic, alicyclic chain vibrations of Carotenoid	1550	Amide II

.
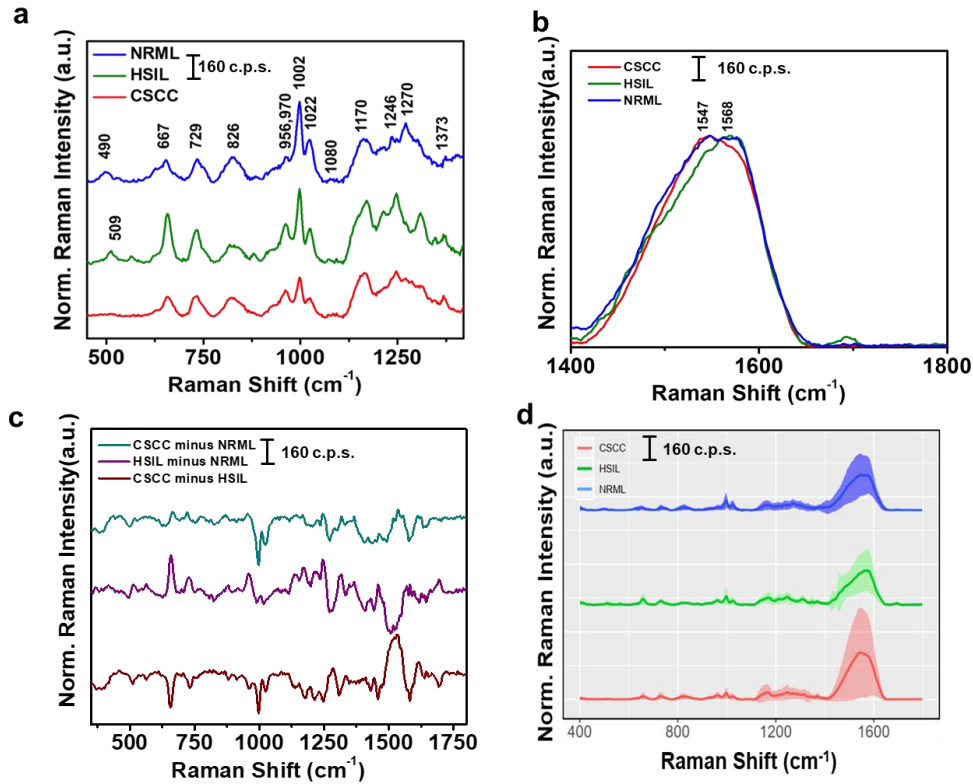
Figure 2.6: SERS analysis from exfoliated cell pellet samples. a) mean SERS spectra acquired from cervical exfoliated cell pellet (region 400-1400 cm⁻¹, laser power density 3-7 mW), b)mean SERS spectra of cell pellet from range 1400-1800 cm⁻¹, c) difference SERS spectra and d) tentative SERS peak assignments from cervical cell pellet samples; NRML, HSIL and CSCC.
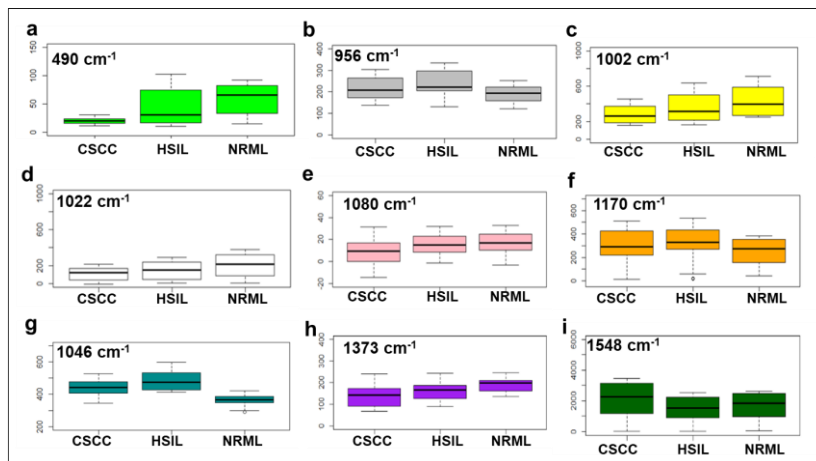
Figure 2.7: Boxplots of normalized scores of prominent peak variations evident in cell pellet analysis of CSCC, HSIL and NRML specifically at a) 490, b) 956, c) 1002, d) 1022, e) 1080, f)

1170, g) 1046, h) 1373 and i) 1548 cm^{-1}. Y-axis represents the quantity of total spectra used and its mean peak intensity (a.u.).

Table 2.4: Tentative SERS peak assignments from cervical clinical cell pellet samples; NRML, HSIL and CSCC.

Wavenumber (cm^{-1})	SERS peak assignment	Wavenumber (cm^{-1})	SERS peak assignment
490, 1022	-C-O-C bending vibration, ring breathing mode in Glycogen	970	P-O-C anti symmetric stretch in DNA
509	S-S disulfide stretching band of collagen	1002	Aromatic ring chain vibration in Phenyl alanine
667	-O-C=O bending vibration in Thymine, Guanine	1080	-O-P-O-stretching vibration in DNA
729	-O-C=O bending vibration in Adenine	1170	-C-C-N bending vibration in Tyrosine
826	-O-P-O- stretching vibration in DNA	1246, 1270	Amide III
956	C-C- aliphatic alicyclic chain vibration in Carotenoid	1373	-O-C=O symmetric stretch in Thymine, Adenine, Guanine

2.3.3.3 SERS-aided grading with cervical exfoliated cell DNA

In the progression of Raman fingerprinting obtained from single cell and cell pellet analysis for the differential diagnosis of cervical precancerous and cancerous lesions, cellular DNA was extracted to re-investigate nucleotide profiling. Increase in DNA content was evident between the groups when compared with normal counterparts. Majority of the SERS peaks obtained from extracted DNA correlated with the peaks obtained from the single cell and cell pellet. The specific peaks at 729

cm^{-1} corresponded to -O-C=O- adenine ring vibration, 826 and 1080 cm^{-1} related to the O-P-O stretching vibration in DNA, 1172 cm^{-1} attributed to -C-C-N- bending vibration in cytosine and guanine, 1421 and 1578 cm^{-1} were related to -C-N- stretching vibration and NH$_2$ deformation in amide II in adenine and guanine (**Figure 2.8a**). Difference spectra were assessed by subtracting NRML from CSCC, NRML from HSIL and HSIL from CSCC mean spectra from the DNA samples (**Figure 2.8b**). The mean spectra measured after averaging the collected spectra and standard deviation is shown in **Figure 2.8c**. All the peak assignments from the extracted DNA analysis is depicted in **Figure 2.8d**.

2.3.4 UFLC analysis of amino acid metabolites in cervical exfoliated cells

In the course of complementary validation, the presence of amino acids contributing to the differential spectra obtained from single cell and cell pellet analysis has been investigated by UFLC. Amino acids tend to be less sensitive chromophores whose correct quantification and visualization requires reactions with other chemicals to generate by derivatization easily detectable compounds. O-phthalaldehyde (OPA) can react with primary amino acids to produce a fluorescent derivative which excites at 338 nm and emits at fluorescence at 450 nm subsequently recorded by a detector. The peak variations significant between NRML, HSIL and CSCC DNA samples were measured in box plot analysis employing R software (**Figure 2.9**).

The analysis confirmed the results obtained in SERS analysis by signals obtained from amino acids, tryptophan, tyrosine, phenyl alanine and proline. A peak at retention time of 13.65 min in HSIL and CSCC samples were exactly correlating with the standard amino acid tryptophan. Similarly, the retention time of 15.45 min for tyrosine, 17.8 min for proline, and 18.6 min for phenyl alanine were identified in HSIL and CSCC with their respective standards. Interestingly, all the four amino acid peaks were negligible in normal samples **(Figure 2.10).**
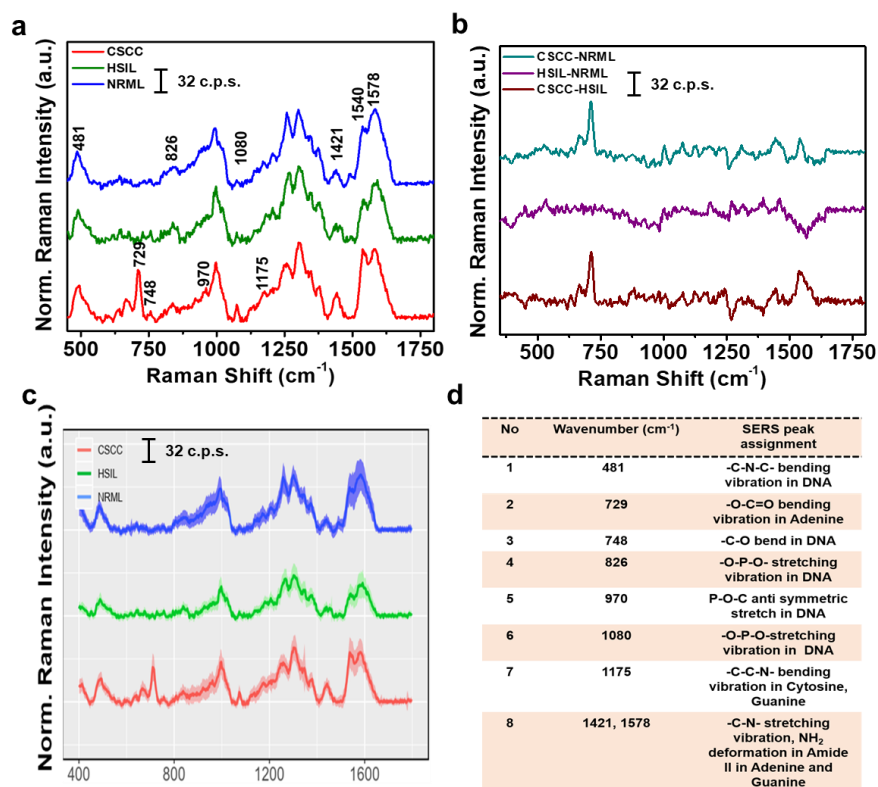
Figure 2.8: SERS analysis from extracted DNA samples from exfoliated cells. a) mean SERS spectra, laser power density 3-7 mW, b) the difference spectrum c) the standard deviation and d) tentative SERS peak assignments from cervical clinical DNA samples; NRML, HSIL and CSCC.
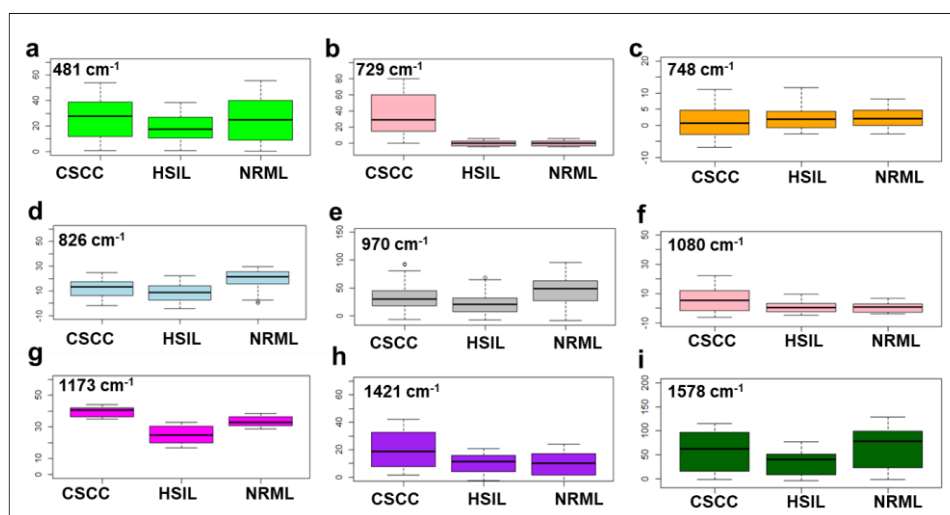
Figure 2.9: Boxplots of normalized scores of prominent peak variations evident in extracted DNA analysis of CSCC, HSIL and NRML specifically at a) 481, b) 729, c) 748, d) 826, e) 970, f) 1080, g) 1173, h) 1421 and i) 1578 cm^{-1}. Y-axis represents the quantity of total spectra used and its mean peak intensity (a.u.)
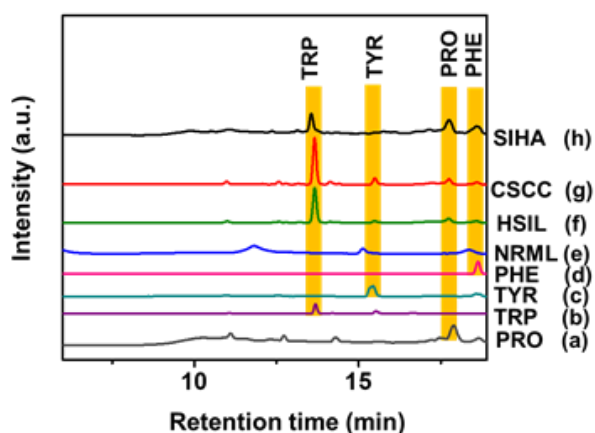
Figure 2.10: UFLC analysis of amino acids in cervical samples compared with amino acid standards. a) proline, b) tryptophan, c) tyrosine, d) phenyl alanine, e) NRML, f) HSIL, g), CSCC and h) SiHa.

The presence of tyrosine, phenyl alanine, tryptophan and proline reflected in the progression stage in HSIL and CSCC samples leading to the increased protein content. In addition to the real positive patient samples, SiHa cell also showed the presence of the above mentioned amino acids. As SiHa contains 1-2 copies [70] of HPV 16 and since Pyk2 is essential for the intracellular trafficking of HPV 16 in human keratinocyte cells, increase in proline may be the indicative for the tumor progression as mentioned earlier. Also it is evident that cancer cells require more metabolic requirements for uncontrolled prolif-eration when compared to normal cells which is assessed by the specific amino acids for the metabolic reprogramming resulting the deregulated replication.

2.3.5 Chemometric analysis

Since a huge spectral data set in all the three groups NRML, HSIL and CSCC has been accumulated, modelling and prediction of the same was very much essential to discriminate between them. Chemometry was thus utilized for the classification and prediction within the dataset employed for extracting informations comprising complex data set from a chemical or biological source based on multivariate, mathematical or computational models. It thus helps to find the relationship between two or more closely related entities, structural analysis etc. Initially, we adopted PCA

to classify them using MATLAB software. A predictive classification was obtained using PCA analysis in single cell, cell pellet and extracted DNA respectively (**Figure 2.11a, c and e**). It was observed that the increase of noise in Raman spectra using PCA. Subsequently, the intra-group variability was enhanced which reflected to the reduction of specificity in PCA. Therefore, to improve the specificity we adopted LDA analysis as the next trial. LDA is a stereotype of Fisher's linear discriminate used in statistics, machine learning and pattern recog-nition into linear combination of features that characterizes or separates two or more classes and attempts to amplify the difference between the classes of data which is difficult to get from PCA. We observed a clear demarcation between single cell, cell pellet and extracted DNA from LDA analysis (**Figure 2.11b, d, and f**). In the course of gradual improvement of prediction accuracy, SVM analysis was attempted by arbitrarily selecting 75 % of the spectra for the train set and remaining 25 % for the test set. The SVM analysis was repeated 500 times with different random samples and analysed the average prediction accuracy. The accuracy was found to be 93 % for single cell, 74 % for cell pellet and 92 % for extracted DNA with 0.73 %, 5.04 % and 3.84 % standard deviation respectively **(Figure 2.12a, b and c).** Thus based on the created reference spectral module an unknown sample can be predicted. The percentage of prediction accuracy was generated along with receiver operating characteristic (ROC) curve (**Figure 2.12d, e, and f**). ROC curve is a graphical plot which shows the classifier system's diagnostic ability by varying the discrimination threshold. At different threshold setting, the ROC curve is plotted by true positive rate against false positive rate. True positive is termed sensitivity and false negative is termed 1-specificity. The accuracy of the analysis depends on how good the test separates the group got tested into those with and without the disease. Accuracy is calculated by measuring the area under the curve. The ROC curve of single cell, cell pellet and extracted DNA showed that SVM is an incremental diagnostic model for classifying the groups (**Figure 2. 12g, h and i**). The sensitivity and prediction accuracy of the technique was calculated (**Table 2.5**). Out of the performed methods, SVM showed good classification between the classes. The main advantage of PCA technique enabled to reduce the huge dimension of data-set without losing much information. But as the specificity was less, LDA and SVM analysis was attempted which increased the classification much better.
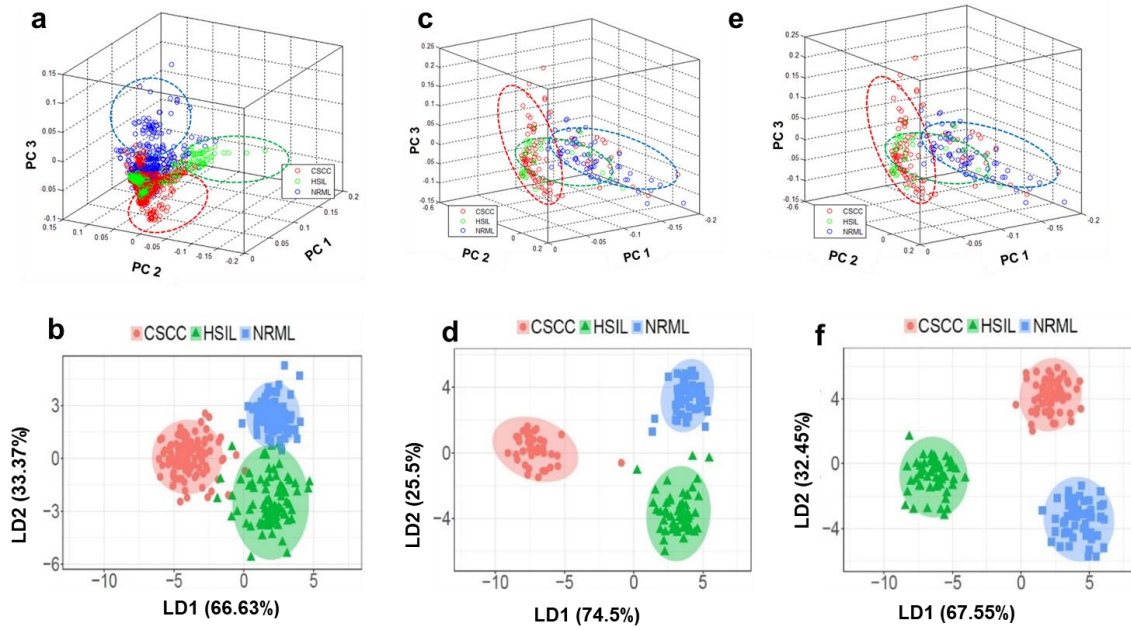
Figure 2.11: Chemometric discrimination between PCA and LDA scatter plots: (a, b) single cell, (c, d) pellet and (e, f) extracted DNA.
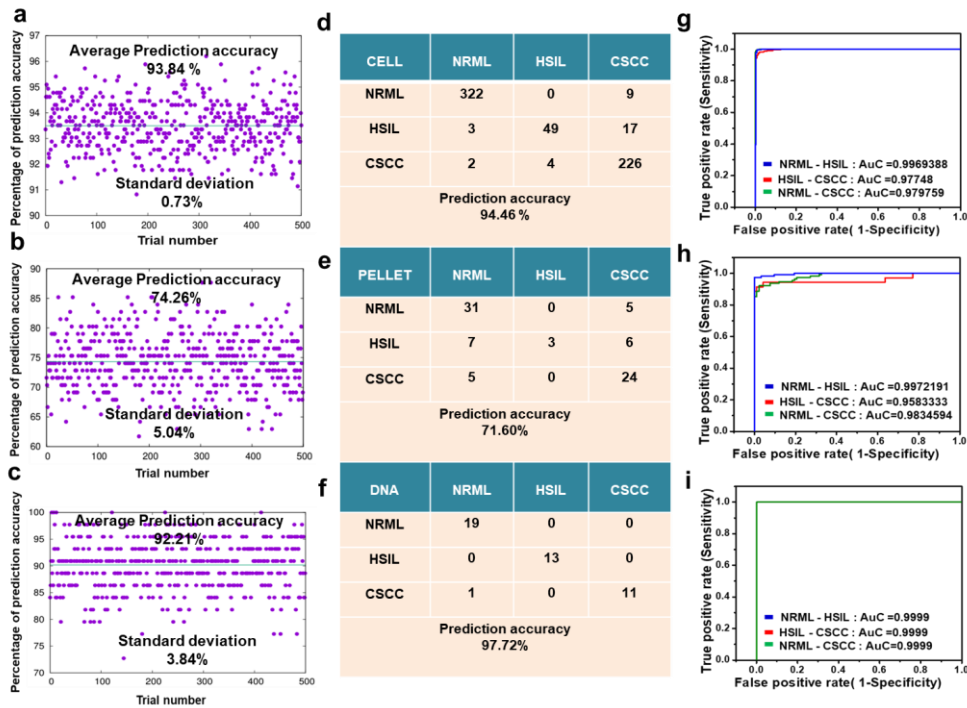
Figure 2.12: Percentage of average prediction accuracy chart in a) single cell. b) cell pellet and c) extracted DNA, Classification based on SVM analysis of d) single cell, e) cell pellet and f) extracted DNA, SVM ROC curve in g) cell, h) pellet and i) DNA.

Table 2.5: Sensitivity and prediction accuracy of SERS-based cervical precancerous lesions detection.

	Sample	Total	True prediction	False prediction	Prediction accuracy
Single cell	NRML	331	322/331	9/331	94.46%±0.73
	HSIL	69	49/69	20/69	
	CSCC	232	226/232	6/232	
Cell pellet	NRML	36	31/36	5/36	71.60%± 5.04
	HSIL	16	3/16	13/25	
	CSCC	29	24/29	5/29	
Extracted DNA	NRML	19	19/19	0/19	97.72%± 3.84
	HSIL	13	13/13	0/13	
	CSCC	12	11/12	1/12	

2.3.6 Cytopathological Pap staining analysis

Conventional analysis like Pap smear were performed to correctly identify the desired cells for SERS analysis. Normally, cervical cancer is diagnosed using cytopathology analysis commonly known as Pap smear test where single cells are tested. Since the sample source of interest was exfoliated cells, Pap staining was performed to identify the pathologically relevant cells. In order to get a clear discrimination between normal vs abnormal exfoliated cells, both bright field images from confocal Raman microscope and Pap staining of NRML, HSIL and CSCC were evaluated for morphological analysis (**Figure 2.13a and 2. 13b**). All the abnormal samples were further confirmed by colposcopic biopsy. In Pap staining, the superficial NRML cells

were stained pink with pyknotic nucleus, intermediate cells stained light blue to green colour where as in HSIL, the enlarged nucleus reflecting high DNA content with minimal cytoplasm showed purple colour nucleus. In CSCC, the cells started to show invasive nature with a slender shape formation to the nucleus. To correctly identify the desired classes of cells, initially the Pap staining was performed to mark the cell position and the same cells were subjected to SERS analysis. If only normal cells are present, the Pap tests predict as normal but in case of abnormal or atypical cells, it turned out as atypical squamous cells of undetermined significance (ASCUS), precancerous squamous intraepithelial lesion, squamous cell cancer or adenocarcinoma cells, atypical glandular cells etc. Primarily the emphasise to focus on the discrimination of NRML, HSIL and CSCC cells by SERS analysis after pathologically confirmed by Pap test.

2.3.7 Human Papillomavirus analysis:

HPV is identified as the primary etiologic factor comprising around 90 % causing the malignant transformation towards cervical cancer. As HPV specific DNA will be integrated in the infected patient samples, HPV PCR was employed for its amplification. But the disadvantage of HPV PCR technique is that as HPV infection can get cleared with the time and a few percentages of normal samples may be positive for HPV DNA, also the sensitivity from HPV PCR is considered significantly low. In order to evaluate and complement the Pap smear test, NRML, HSIL and CSCC samples were loaded after DNA isolation from the respective samples out of which HSIL and CSCC showed a band corresponding to HPV DNA. A PCR amplification product of size varying between 230-270 bp was obtained in 1.5 % agarose gel indicative of an infection with oncogenic HPV in HSIL and CSCC whereas no observable band was identified for NRML samples (**Figure 2.13c and 2.13d**). The PCR product obtained was indicative of oncogenic HPV types 16, 18, 31, 33, 35, 45, 52 and 58.
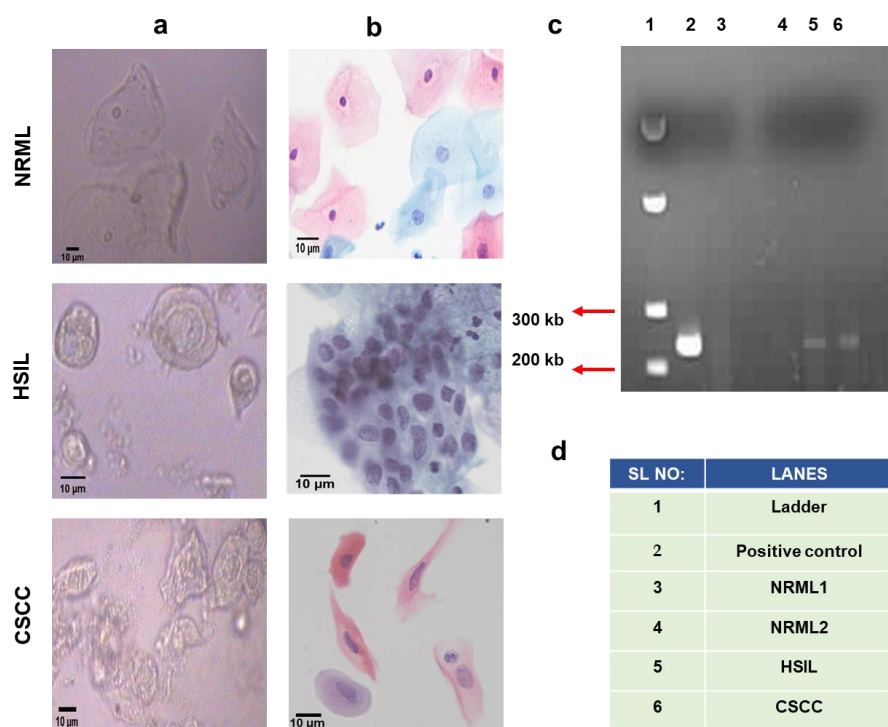
Figure 2.13: Conventional clinical cytopathological analysis of cervical exfoliated cells.a) bright field and b) Pap stained images of NRML, HSIL and CSCC exfoliated cells, scale bar corresponds to 10μm, c) HPV PCR of Clinical DNA samples, d) sample loading order of HPV PCR ladder (1), positive control (2), NRML1 (3), NRML2 (4), HSIL(5) and CSCC(6).

2.4 Materials and Methods

2.4.1 Chemicals and materials.

Gold (III) chloride hydrate, trisodium citrate dehydrate were procured from Sigma-Aldrich. Ethyl alcohol was obtained from Changshu Yangyuan Chemical, China.

2.4.2 SERS substrate preparation.

Gold nanoparticles (AuNPs, 40-45 nm) were synthesized by well-known citrate reduction method. For the synthesis, 50 ml ultrapure water was heated until boiling and 50 μl gold chloride solution of concentration 0.25 M was added. 125 μl of trisodium citrate solution of concentration 0.1 M was added after 10 min of boiling yielding a color change from dark purple to red which takes about 5 min. The solution was allowed to cool for 90 min with constant stirring. The synthesized nanoparticles were characterized using UV-Vis Spectroscopy, DLS and TEM. The as prepared

nanoparticles were enriched by centrifugation at 8000 rpm for 20 min for later use for SERS analysis.

2.4.3 Preparation of SiHa cells for SERS analysis

SiHa cells were seeded in a four welled chamber slide. After 24 h, two phosphate buffered saline (PBS) washes were done followed by fixing the cells in ethanol based fixative solution. Colloidal gold solution was added into the wells and following 15 min-30 min incubation, SERS spectra was generated using single spectral analysis as well as SERS mapping.

2.4.4 Collection and preparation of cervical exfoliated single cell, cell pellet and DNA samples

Age matched samples for the study was collected from women attending the department of Community Oncology, Regional Cancer Centre (RCC), Thiruvananthapuram, Kerala after getting approval from human ethical committee [HEC No.19/ 2014]. Informed consents were obtained from all the study subjects. A total of 36 CSCC samples and 41 HSIL samples were collected from patients with pathologically confirmed case of CSCC and HSIL respectively. Around 47 healthy female individuals were selected as the NRML group. The average age selected was 50 years. The cervical exfoliated cells were collected using sterile cytobrush and kept in ethanol based liquid based cytology preservative fluid till use. The cells were thus prefixed in ethanol containing LBC preservative solution immediately after collection. Density gradient centrifugation at 8000 rpm for 10 min is performed to concentrate or enrich the squamous epithelial cells from blood cells and other debrises. Cells collected after discarding the supernatant were re-dispersed in Tris buffered Saline (TBS) buffered deionized water and for further analysis was stored at -20 °C. About 500 µl of the diluted sample was cytocentrifuged in megafunnels onto 3-Aminopropyltriethoxysilane (APES) pre coated glass slides. After cytocentrifugation at 1000 rpm for one minute, the cells were found deposited as a monolayer on the coated area of the slide. The colloidal suspension is dropped over the monolayer of cells in the glass slide and after 15-30 min incubation, the SERS analysis has been carried out. Bright field images of cells from pathologically confirmed samples were

focused under the confocal Raman microscope 20X objective. Bright field images were acquired and by switching to Raman mode, spectral focusing was performed. For cell pellet analysis, the pellet obtained after density gradient centrifugation was sedimented with AuNPs. For DNA samples, DNA was extracted from the cell samples according to the protocol in HPV DNA analysis kit supplied by Bangalore GeNei (Cat no: 0670100011730) were utilized. For DNA extraction, centrifugation was done at 10,000 rpm for 10 min for 1 ml of the cell sample. The supernatant was decanted and 500 μl of wash buffer was added to the pellet. The mixture was again centrifuged at 10,000 rpm for 10 min. The supernatant was discarded and 500 μl of DNA extraction buffer was added to the remaining pellet. The pellet was mixed well, transferred into a 1.5 ml sterile vial, added 20 μl of proteinase K, incubated at 65 °C for 1 hour in a dry bath and then at 95 °C for 10 min in water bath. The whole content with vials were centrifuged at 10,000 rpm for 10 min and pipetted out the clear supernatant containing the DNA in to a fresh labeled vial and stored at -20 °C. Cell pellet analysis and DNA analysis were performed by mixing sample: AuNPs at 1:9 (v/v) ratio.

2.4.5 SERS analysis

Spectral analysis using confocal Raman analysis was performed with the aid of a confocal Raman microscope (WITec, Inc., Germany, alpha 300R) using a laser beam focused to the sample employing 20 X objective with a Peltier cooled CCD detector. Samples were excited with a laser excitation source of 633 nm with spectrograph grating 600 g/mm at 3-7 mW power. Raman spectra were accumulated in the range of 400–1800 cm^{-1} with 3 cm^{-1} resolution with 10 sec and 10 accumulations. integration time. Prior to every measurement, a calibration was perfomed with a silicon standard (Raman peak at 520 cm^{-1}). Single cell analysis was performed in SiHa cell line which is procured from National Centre for Cell Science (NCCS), Pune, India and is authenticated by STR profiling. The prepared cell samples were grouped and analyzed using SERS in three different methods, viz single cell, whole pellet and extracted DNA. For single cell analysis, the mapped area for image scan has been decided by visualizing the bright field image of the single cell, i.e. 5 micron x 5 micron nuclear area from which 150 x 150 points per line were scanned with 0.02 integration time. At least 15 high quality spectra were collected from image scan. We have used

the remaining cells of the cellular scrapes collected for the routine Pap smear examination. As the number of abnormal cells in a sample were limited, acquisition of as many number of good spectra were extracted from as many number of cells present in the sample for the image scan of the single cell analysis. Overall, 1363 spectra were collected from the single cell samples for CSCC; 325 spectra for the HSIL and 850 spectra for the NRML samples which were subsequently used for making the trained set in the statistical model. The average spectra were generated from this data set.

2.4.6 Data analysis

The raw spectral data were pre-processed by Project FOUR 4.0 (WITec, Germany) before the final statistical analysis to remove the noise and interferences, cosmic rays and oversaturated spectra. The background was removed by 4th polynomial function and smoothening of the SERS spectra was done by the Savitzky-Golay smoothing which in turn normalized in the region of 200–1800 cm^{-1}. Then the pre-processed data were put into the Origin Pro 8.0 software (Origin Lab, USA) to calculate and create the mean spectrum of each group. The comparison between the spectra of CSCC, HSIL and NRML groups were done by the subtraction of different mean spectra and different peak shift in the subtracted spectra were assigned to the biomolecular structures and components based on the literature reports.[13]

2.4.7 UFLC analysis

The extraction of amino acids from the cervical squamous cells was performed by methanol extraction. Three each samples of NRML, HSIL and CSCC were pooled and the cell pellet was re-suspended in 0.5 ml of methanol followed by freezing in liquid nitrogen with subsequent thawing in ice. The samples vial were then vortexed followed by centrifugation at 800 g for 10 min. The supernatant was stored and the pellet was re-suspended in 0.5 ml of 100 % methanol for a second freeze- thaw cycle. 0.5 ml ice cold sterile water was added was added to the collected supernatant for another freeze thaw cycle and centrifugation. The final supernatant was dried at 30 °C in a Speed Vac concentrator overnight. The amino acid analysis was performed on an High-performance liquid chromatography (HPLC) system with pre-column derivatization OPA employing a Shimadzu UFLC system along with Agilent Zorbax

Eclipse AAA, (4.6 X 150 mm, 5 µm) column from Agilent technologies, India. Amino acid standards, buffer components including sodium phosphate monobasic, sodium hydroxide and boric acid were procured from Sigma. The samples were diluted to the required concentrations after filtering through a 0.22 µm sized syringe filters. The reaction mixture constituted a total of 350 µl comprising 5 µl sample, 25 µl borate buffer pH 10.2 and 320 µl deionized water. A binary gradient elution program was used with 40 mM sodium phosphate buffer (pH 7.8) and 45:45:10 ratio of acetonitrile/ methanol/ water as the mobile phase. The flow rate was 2 ml per min with temperature of 40 °C. LC solution software was used for the analysis.

2.4.8 PCA analysis

PCA is a method of multivariate analysis generally used with multiple dimensions of datasets. It allows the reduction of variable numbers in a multidimensional dataset, by retaining most of the variations. The order of the principal components (PCs) represents their importance to the dataset. PC1 designates the highest amount of variation followed by PC2 and so on. Scores of first and second PCA component and first, second and third PCA components are plotted. In the plot PCA-1 versus PCA-2, class A corresponds to all scores having value less than zero for PCA-1 axis and greater than-8 for PCA-2 axis. Class B is created using all scores having both PCA-1 value and PCA-2 value greater than three. Class C consists all scores having PCA-1 value greater than zero and PCA-2 value less than -8. In the 3D representation, PCA-1, PCA-2 and PCA-3 components with same discrimination is used. However, while recording Raman data, the noise existing in the spectra can upturn the intra-group variability, reducing the PCA specificity. Typically the 10 first PCs may be taken into account for specific analysis. All the analysis were performed using the MATLAB 8.3 (MATLAB R2014a, MA) software.

2.4.9 LDA analysis

LDA has been performed in R software. Similar to PCA, LDA is also a linear transformation technique which is commonly used for dimensionality reduction. PCA ignores the class labels and try to find directions or axes which maximize the variance in a dataset and hence it can be considered as an "unsupervised" learning algorithm. In contrast to PCA, LDA considers the class labels and try to computes the directions

or linear discriminants which maximizes the separation between the classes. In this work, we employed LDA mainly to classify the dataset based on the classes labeled by NRML, HSIL and CSCC.

2.4.10 SVM analysis

SVM is supervised machine learning models used for data classification. An SVM is a binary classifier which is trained on a set of labelled patterns called training sets. The training of SVM will find a hyperplane which divides the samples into two sides so that all the points having same label will be on same side of the hyperplane. The programs were coded by using R software. Here 75 % of the sample were randomly selected for model building i.e. for the train set and remaining 25 % were used as the test set. When random sample used for train set changes prediction accuracy can also vary. So the SVM analysis were repeated with 500 different arbitrarysamples and calculated the average prediction accuracy. SVM, which has two model parameters gamma and cost parameters values can also affect prediction. We have experimented with various combination (not very rigorous) and chose the best cost = 100 and gamma = 0.01 for the analysis.

2.4.11 Pap staining

Papanicolaou stain is inclusive of both acidic and basic dyes and polychromatic Pap stain involving five dyes in three independent solutions. Haematoxylin is the nuclear stain that stains cell nuclei blue. Orange Green 6 (OG 6) is the orange coloured acidic counterstain staining matured and keratinized cells. Eosin Azure -36 is the second counterstain which consists of a polychrome mixture of eosin Y rendering pink color to cytoplasm of mature squamous cells, nucleoli and RBCs, light green SF stains blue to cytoplasm of metabolically active cells including parabasal, intermediate and columnar cells, whereas Bismarck brown stains keratinised cells. Pap smears were collected from women attending the early cancer detection clinic and camps of the department of Community oncology of RCC. Cervical scrapes were smeared in labelled glass slide. The slide was then fixed in 95 % ethanol for 15 min, followed by hydration in graded alcohol (70 % and 50 %). Further the slide was rinsed in distilled water. The smears were stained in modified Harris Hematoxylin for 2 min followed by washing

in distilled water. The differentiation was done in 0.05 % HCl. The slide was then blued in running tap water for 10 min. Again the dehydration step was continued in 50 % and 70 % alcohol. 95 % ethanol incubation for 2 min continued by OG-6 staining for 2 min. Then two times wash with 95 % ethanol for 2 min followed by EA-36 staining for 2.5 min. Again 2 times ethanol wash for 2 min each followed by absolute alcohol 2 min treatment with three changes. The slide was then cleared with 3 changes of xylene for 2 min each and was mounted with permanent mounting medium. Pap test as a differential staining technique renders red to pink colour to the keratinized mature cells with blue nucleus and blue to green colour to the immature or intermediate cells that are metabolically active with vesicular nucleus.

2.4.12 HPV analysis

HPV identification of all the samples selected for the study were performed in residual liquid based cytology samples by a multiplex PCR method using a HPV DNA analysis kit. Genomic DNA was extracted from cervical scrape cells and PCR reactions were carried out as per the protocol provided in the kit. The quality of DNA was checked in agarose gel electrophoresis. PCR was performed by using the reagents (amplification mix, Taq DNA polymerase and positive control DNA). Amplification reactions were performed in a reaction volume of 25 µl containing 21.6 µl amplification mix, 0.4 µl Taq polymerase and 3 µl genomic DNA. Positive and negative controls were also included in each reaction set. The reaction was carried out initially for 10 cycles with denaturation at 94 °C for 1 min, further annealing at 62 °C for 1 min, extension at 72 °C for 1 min, then 30-35 cycles of 94 °C for 45 sec, annealing at 58 °C for 45 sec, extension at 72 °C for 45 sec, 1 cycle of final extension at 72°C for 5 min and 4°C for infinity. The amplified product was visualized in 1.5 % gel.

2.5 Conclusion

In summary, a label free ultrasensitive Raman fingerprint has been benchmarked to generate a differential mapping for the identification of major three grades of cervical exfoliated cells i.e. normal (NRML), intermediate (HSIL) and squamous cell carcinoma (CSCC) of the cervix by employing a strategic platform based on SERS. A clear identification of SERS fingerprint of the well resolved biomolecular

variations ranging from nucleic acid, amino acids and protein backbone were established between NRML, HSIL and CSCC of clinical samples. Nucleic acids variations were further confirmed by SERS analysis of extracted DNA while amino acid metabolites were validated by UFLC analysis. The results indicated the prevalence of nucleobases adenine, guanine, cytosine, phosphate backbone and amino acids tryptophan, phenyl alanine and proline which are the major metabolites evolved during tumorigenesis. Further, spectral differentiation was validated by statistical analysis which included chemometric interpretations mainly by PCA, LDA and SVM. This is the first representation of SERS spectroscopic analysis in exfoliated cell samples. Moreover, the SERS based spectro-cytology was found to be minimally invasive and more sensitive than those employing serum or plasma as exfoliated cells represents a better source of sample for analyzing progression of cervical cancer. Taken together, the present strategy represents an accurate, simple and reliable method for the differential diagnosis of cervical cancer which might serve as a clinical detection technique in the near future. Also we envision to store the reference data in a chip model (**Scheme 2.2**) within a futuristic hand held Raman spectrometer for the screening of cervical cancer in large population.
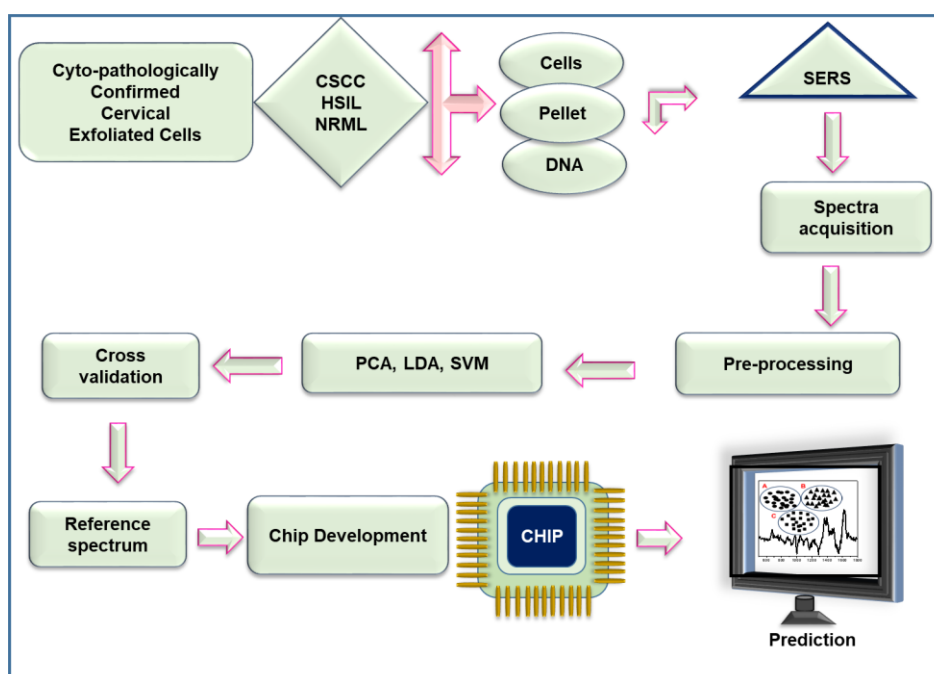
Scheme 2.2: Schematic representation of reference data in a chip model within a futuristic hand held Raman spectrometer for the screening of cervical cancer.

2.6 References

(1)   Cohen, P. A.; Jhingran, A.; Oaknin, A.; Denny, L. Cervical Cancer. *Lancet***2019**, *393*, 169–182.

(2)   Bray, F.; Ferlay, J.; Soerjomataram, I.; Siegel, R. L.; Torre, L. A.; Jemal, A. Global Cancer Statistics 2018: GLOBOCAN Estimates of Incidence and Mortality Worldwide for 36 Cancers in 185 Countries. *CA. Cancer J. Clin.***2018**, *68*, 394–424.

(3)   Jess, P. R. T.; Smith, D. D. W.; Mazilu, M.; Dholakia, K.; Riches, A. C.; Herrington, C. S. Early Detection of Cervical Neoplasia by Raman Spectroscopy. *Int. J. Cancer***2007**, *121* (12), 2723–2728.

(4)   Fahey, M. T.; Irwig, L.; Macaskill, P. Meta-Analysis of Pap Test Accuracy. *Am. J. Epidemiol.***1995**, *141*, 680–689.

(5)   Solomon, D.; Davey, D.; Kurman, R.; Moriarty, A.; O'Connor, D.; Prey, M.; Raab, S.; Sherman, M.; Wilbur, D.; Wright, T.; et al. The 2001 Bethesda System: Terminology for Reporting Results of Cervical Cytology. *JAMA***2002**, *287*, 2114–2119.

(6)   Boone, J. D.; Erickson, B. K.; Huh, W. K. New Insights into Cervical Cancer Screening. *J. Gynecol. Oncol.***2012**, *23* (4), 282–287.

(7)   Sørbye, S. W.; Suhrke, P.; Revå, B. W.; Berland, J.; Maurseth, R. J.; Al-Shibli, K. Accuracy of Cervical Cytology: Comparison of Diagnoses of 100 Pap Smears Read by Four Pathologists at Three Hospitals in Norway. *BMC Clin. Pathol.***2017**, *17* (1), 1–6.

(8)   Deepak, RU and Kumar, RR and Byju, NB and Sharathkumar, PN and Pournami, C. and others. Computer Assisted Pap Smear Analyser for Cervical Cancer Screening Using Quantitative Microscopy. *J. Cytol. Histol.***2015**, *S3*.

(9)   Cheng, J. X.; Xie, X. S. Vibrational Spectroscopic Imaging of Living Systems: An Emerging Platform for Biology and Medicine. *Science (80-.).***2015**, *350*, aaa88701-aa88709.

(10)   Krishna, C. M.; Sockalingum, G. D.; Bhat, R. a.; Venteo, L.; Kushtagi, P.; Pluot, M.; Manfait, M. FTIR and Raman Microspectroscopy of Normal, Benign, and Malignant Formalin-Fixed Ovarian Tissues. *Anal. Bioanal. Chem.***2007**, *387*,

1649–1656.

(11) Paidi, S. K.; Diaz, P. M.; Dadgar, S.; Jenkins, S. V.; Quick, C. M.; Griffin, R. J.; Dings, R. P. M.; Rajaram, N.; Barman, I. Label-Free Raman Spectroscopy Reveals Signatures of Radiation Resistance in the Tumor Microenvironment. *Cancer Res.***2019**, *79*, 2054–2064.

(12) Saranya, G.; Joseph, M. M.; Karunakaran, V.; Nair, J. B.; Saritha, V. N.; Veena, V. S.; Sujathan, K.; Ajayaghosh, A.; Maiti, K. K. Enzyme-Driven Switchable Fluorescence-SERS Diagnostic Nanococktail for the Multiplex Detection of Lung Cancer Biomarkers. *ACS Appl. Mater. Interfaces***2018**, *10*, 38807–38818.

(13) Movasaghi, Z.; Rehman, S.; Rehman, I. U. Raman Spectroscopy of Biological Tissues. *Appl. Spectrosc. Rev.***2007**, *42*, 493–541.

(14) Chen, P. H.; Shimada, R.; Yabumoto, S.; Okajima, H.; Ando, M.; Chang, C. T.; Lee, L. T.; Wong, Y. K.; Chiou, A.; Hamaguchi, H. O. Automatic and Objective Oral Cancer Diagnosis by Raman Spectroscopic Detection of Keratin with Multivariate Curve Resolution Analysis. *Sci. Rep.***2016**, *6*, 1–9.

(15) Vargis, E.; Kanter, E. M.; Majumder, S. K.; Keller, M. D.; Beaven, R. B.; Rao, G. G.; Mahadevan-Jansen, A. Effect of Normal Variations on Disease Classification of Raman Spectra from Cervical Tissue. *Analyst***2011**, *136*, 2981–2987.

(16) Duraipandian, S.; Mo, J.; Zheng, W.; Huang, Z. Near-Infrared Raman Spectroscopy for Assessing Biochemical Changes of Cervical Tissue Associated with Precarcinogenic Transformation. *Analyst.***2014**, *139*, 5379–5386.

(17) Jenkins, C. A.; Jenkins, R. A.; Pryse, M. M.; Welsby, K. A.; Jitsumura, M.; Thornton, C. A.; Dunstan, P. R.; Harris, D. A. A High-Throughput Serum Raman Spectroscopy Platform and Methodology for Colorectal Cancer Diagnostics. *Analyst.***2018**, *143*, 6014–6024.

(18) Kumar, S.; Rizwan, A.; Zheng, C.; Cheng, M.; Glunde, K.; Barman, I. Label-Free Raman Spectroscopy Detects Stromal Adaptations in Premetastatic Lungs Primed by Breast Cancer. *Cancer Res.***2017**, *77* (2), 247–256.

(19) Duraipandian, S.; Bergholt, M. S.; Zheng, W.; Ho, K. Y.; Teh, M.; Yeoh, K. G.; So, J. B. Y.; Shabbir, A.; Huang, Z. Real-Time Raman Spectroscopy for in Vivo, Online Gastric Cancer Diagnosis during Clinical Endoscopic Examination. *J. Biomed. Opt.***2012**, *17*, 081418.

(20) Meksiarun, P.; Ishigaki, M.; Huck-Pezzei, V. A. C.; Huck, C. W.; Wongravee, K.; Sato, H.; Ozaki, Y. Comparison of Multivariate Analysis Methods for Extracting the Paraffin Component from the Paraffin-Embedded Cancer Tissue Spectra for Raman Imaging. *Sci. Rep.***2017**, *7*, 1–10.

(21) Chan, J. W.; Taylor, D. S.; Zwerdling, T.; Lane, S. M.; Ihara, K.; Huser, T. Micro-Raman Spectroscopy Detects Individual Neoplastic and Normal Hematopoietic Cells. *Biophys. J.***2006**, *90*, 648–656.

(22) Brozek-Pluska, B.; Kopec, M.; Surmacki, J.; Abramczyk, H. Raman Microspectroscopy of Noncancerous and Cancerous Human Breast Tissues. Identification and Phase Transitions of Linoleic and Oleic Acids by Raman Low-Temperature Studies. *Analyst***2015**, *140*, 2134–2143.

(23) McLaughlin, G.; Fikiet, M. A.; Ando, M.; Hamaguchi, H. o.; Lednev, I. K. Universal Detection of Body Fluid Traces in Situ with Raman Hyperspectroscopy for Forensic Purposes: Evaluation of a New Detection Algorithm (HAMAND) Using Semen Samples. *J. Raman Spectrosc.***2019**, *50*, 1147–1153.

(24) Yan, Z.; Dutta, S.; Liu, Z.; Yu, X.; Mesgarzadeh, N.; Ji, F.; Bitan, G.; Xie, Y.-H. A Label-Free Platform for Identification of Exosomes from Different Sources. *ACS Sensors***2019**, *4*, 488–497.

(25) Lee, W.; Nanou, A.; Rikkert, L.; Coumans, F. A. W.; Otto, C.; Terstappen, L. W. M. M.; Offerhaus, H. L. Label-Free Prostate Cancer Detection by Characterization of Extracellular Vesicles Using Raman Spectroscopy. *Anal. Chem.***2018**, *90*, 11290–11296.

(26) Huefner, A.; Kuan, W. L.; Müller, K. H.; Skepper, J. N.; Barker, R. A.; Mahajan, S. Characterization and Visualization of Vesicles in the Endo-Lysosomal Pathway with Surface-Enhanced Raman Spectroscopy and Chemometrics. *ACS Nano***2016**, *10*, 307–316.

(27) Shin, H.; Jeong, H.; Park, J.; Hong, S.; Choi, Y. Correlation between Cancerous Exosomes and Protein Markers Based on Surface-Enhanced Raman Spectroscopy (SERS) and Principal Component Analysis (PCA). *ACS Sensors***2018**, *3*, 2637–2643.

(28) Hutchings, J.; Kendall, C.; Shepherd, N.; Barr, H.; Stone, N. Evaluation of Linear Discriminant Analysis for Automated Raman Histological Mapping of

Esophageal High-Grade Dysplasia. *J. Biomed. Opt.***2010**, *15*, 066015.

(29) Sattlecker, M.; Bessant, C.; Smith, J.; Stone, N. Investigation of Support Vector Machines and Raman Spectroscopy for Lymph Node Diagnostics. *Analyst***2010**, *135*, 895–901.

(30) Langer, J.; Jimenez de Aberasturi, D.; Aizpurua, J.; Alvarez-Puebla, R. A.; Auguié, B.; Baumberg, J. J.; Bazan, G. C.; Bell, S. E. J.; Boisen, A.; Brolo, A. G.; et al. Present and Future of Surface-Enhanced Raman Scattering. *ACS Nano***2020**, *14* (1), 28–117.

(31) Jimenez De Aberasturi, D.; Serrano-Montes, A. B.; Langer, J.; Henriksen-Lacey, M.; Parak, W. J.; Liz-Marzán, L. M. Surface Enhanced Raman Scattering Encoded Gold Nanostars for Multiplexed Cell Discrimination. *Chem. Mater.***2016**, *28*, 6779–6790.

(32) Cheng, J.; and Xie, X. S. Coherent Anti-Stokes Raman Scattering Microscopy: Instrumentation, Theory, and Applications. *J. Phys. Chem. B***2004**, *108*, 827–840.

(33) Wang, X.; Huang, S. C.; Huang, T. X.; Su, H. S.; Zhong, J. H.; Zeng, Z. C.; Li, M. H.; Ren, B. Tip-Enhanced Raman Spectroscopy for Surfaces and Interfaces. *Chem. Soc. Rev.***2017**, *46*, 4020–4041.

(34) Suzuki, Y.; Kobayashi, K.; Wakisaka, Y.; Deng, D.; Tanaka, S.; Huang, C.-J.; Lei, C.; Sun, C.-W.; Liu, H.; Fujiwaki, Y.; et al. Label-Free Chemical Imaging Flow Cytometry by High-Speed Multicolor Stimulated Raman Scattering. *PNAS***2019**, *116*, 15842–15848.

(35) Liu, Y.; Zhou, H.; Hu, Z.; Yu, G.; Yang, D.; Zhao, J. Label and Label-Free Based Surface-Enhanced Raman Scattering for Pathogen Bacteria Detection: A Review. *Biosens. Bioelectron.***2017**, *94*, 131–140.

(36) Narayanan, N.; Karunakaran, V.; Paul, W.; Venugopal, K.; Sujathan, K.; Kumar Maiti, K. Aggregation Induced Raman Scattering of Squaraine Dye: Implementation in Diagnosis of Cervical Cancer Dysplasia by SERS Imaging. *Biosens. Bioelectron.***2015**, *70*, 145–152.

(37) Kneipp, J.; Kneipp, H.; McLaughlin, M.; Brown, D.; Kneipp, K. In Vivo Molecular Probing of Cellular Compartments with Gold Nanoparticles and Nanoaggregates. *Nano Lett.***2006**, *6*, 2225–2231.

(38) Panikkanvalappil, S. R.; Hira, S. M.; Mahmoud, M. A.; El-Sayed, M. A. Unraveling

the Biomolecular Snapshots of Mitosis in Healthy and Cancer Cells Using Plasmonically-Enhanced Raman Spectroscopy. *J. Am. Chem. Soc.***2014**, *136* (45), 15961–15968.

(39)   Kang, B.; Austin, L. a; El-Sayed, M. a. Observing Molecular Events in Real-Time of Apoptosis Dynamics in Living Cancer Cells Using Nuclear Targeted Plasmonically Enhanced Raman Nanoprobes. *ACS Nano***2014**, *8* (5), 4883–4892.

(40)   Gonzalez-Solias, J.L.;Luevano-Colmenero, G.H.; Vargas-Mancilla, J. Surface Enhanced Raman Spectroscopy in Breast Cancer Cells. *LASER Ther.***2013**, 22(1): 37–42.

(41)   Chen, Y.; Zhang, Y.; Pan, F.; Liu, J.; Wang, K.; Zhang, C.; Cheng, S.; Lu, L.; Zhang, W.; Zhang, Z.; et al. Breath Analysis Based on Surface-Enhanced Raman Scattering Sensors Distinguishes Early and Advanced Gastric Cancer Patients from Healthy Persons. *ACS Nano***2016**, *10* (9), 8169–8179.

(42)   Li, S.; Li, L.; Zeng, Q.; Zhang, Y.; Guo, Z.; Liu, Z.; Jin, M.; Su, C.; Lin, L.; Xu, J.; et al. Characterization and Noninvasive Diagnosis of Bladder Cancer with Serum Surface Enhanced Raman Spectroscopy and Genetic Algorithms. *Sci Rep***2015**, *5*, 9582.

(43)   Mert, S.; Özbek, E.; Ötünçtemur, A.; Çulha, M. Kidney Tumor Staging Using Surface-Enhanced Raman Scattering. *J. Biomed. Opt.***2015**, *20* (4), 047002.

(44)   Feng, S.; Wang, W.; Tai, I. T.; Chen, G.; Chen, R.; Zeng, H. Label-Free Surface-Enhanced Raman Spectroscopy for Detection of Colorectal Cancer and Precursor Lesions Using Blood Plasma. *Biomed. Opt. Express***2015**, *6* (9), 3494.

(45)   Yan, B.; Li, B.; Wen, Z.; Luo, X.; Xue, L.; Li, L. Label-Free Blood Serum Detection by Using Surface-Enhanced Raman Spectroscopy and Support Vector Machine for the Preoperative Diagnosis of Parotid Gland Tumors. *BMC Cancer***2015**, *15* (1), 650.

(46)   Rubina, S.; Amita, M.; Kedar K., D.; Bharat, R.; Krishna, C. M. Raman Spectroscopic Study on Classification of Cervical Cell Specimens. *Vib. Spectrosc.***2013**, *68*, 115–121.

(47)   González-Solís, J. L.; Martínez-Espinosa, J. C.; Torres-González, L. A.; Aguilar-Lemarroy, A.; Jave-Suárez, L. F.; Palomares-Anda, P. Cervical Cancer Detection

Based on Serum Sample Raman Spectroscopy. *Lasers Med. Sci.***2014**, *29* (3), 979–985.

(48)   Low, J. J. H.; Ilancheran, A.; Ng, J.; Zheng, W.; Huang, Z.; Duraipandian, S. Simultaneous Fingerprint and High-Wavenumber Confocal Raman Spectroscopy Enhances Early Detection of Cervical Precancer In Vivo. *Anal. Chem.***2012**, *84* (14), 5913–5919.

(49)   Lyng, F. M.; O'Leary, J. J.; Traynor, D.; Martin, C. M.; Kearney, P.; Bonnier, F. Raman Spectral Signatures of Cervical Exfoliated Cells from Liquid-Based Cytology Samples. *J. Biomed. Opt.***2017**, *22* (10), 1.

(50)   Traynor, D.; Kearney, P.; O'Leary, J. J.; Lyng, F. M.; Martin, C.; Duraipandian, S. Raman Spectroscopic Detection of High-Grade Cervical Cytology: Using Morphologically Normal Appearing Cells. *Sci. Rep.***2018**, *8*, 1–8.

(51)   Feng, S.; Lin, D.; Lin, J.; Li, B.; Huang, Z.; Chen, G.; Zhang, W.; Wang, L.; Pan, J.; Chen, R.; et al. Blood Plasma Surface-Enhanced Raman Spectroscopy for Non-Invasive Optical Detection of Cervical Cancer. *Analyst***2013**, *138*, 3967–3974.

(52)   S.A. Sanchez-Rojo ´ a, B.E. Mart´ınez-Zeregaa, E.F. Velazquez-Pedroza ´ a, J.C. Mart´ınez-Espinosab, L. A. T.-G. ´ c; A. Aguilar-Lemarroyd, L.F. Jave-Suarez´d, P. P.-A. and J. L. G.-S. ´ ´ıs. Cervical Cancer Detection Based on Serum Sample Surface Enhanced Raman Spectroscopy. *Rev. Mex. F´ısica***2016**, *62*, 213–218.

(53)   Kim, E. S.; Samanta, A.; Cheng, H. S.; Ding, Z.; Han, W.; Toschi, L.; Chang, Y. T. Effect of Oncogene Activating Mutations and Kinase Inhibitors on Amino Acid Metabolism of Human Isogenic Breast Cancer Cells. *Mol. Biosyst.***2015**, *11*, 3378–3386.

(54)   Njoki, P. N.; Lim, I. I. S.; Mott, D.; Park, H. Y.; Khan, B.; Mishra, S.; Sujakumar, R.; Luo, J.; Zhong, C. J. Size Correlation of Optical and Spectroscopic Properties for Gold Nanoparticles. *J. Phys. Chem. C***2007**, *111*, 14664–14669.

(55)   Stamplecoskie, K. G.; Scaiano, J. C.; Tiwari, V. S.; Anis, H. Optimal Size of Silver Nanoparticles for Surface-Enhanced Raman Spectroscopy. *J. Phys. Chem. C***2011**, *115*, 1403–1409.

(56)   Polte, J.; Ahner, T. T.; Delissen, F.; Sokolov, S. Mechanism of Gold Nanoparticle Formation in the Classical Citrate Synthesis Method Derived from Coupled In Situ XANES and SAXS Evaluation. *J. Am. Chem. Soc.***2010**, *132*, 1296–1301.

(57)   David C. Wilbur, M. B. *Comprehensive Cytopathology*, III.; 2008.

(58)   Kuku, G.; Altunbek, M.; Culha, M. Surface-Enhanced Raman Scattering for Label-Free Living Single Cell Analysis. *Anal. Chem.***2017**, *89* (21), 11160–11166.

(59)   Sujai, P. T.; Joseph, M. M.; Saranya, G.; Nair, J. B.; Murali, V. P.; Maiti, K. K. Surface Charge Modulates the Internalization: Vs. Penetration of Gold Nanoparticles: Comprehensive Scrutiny on Monolayer Cancer Cells, Multicellular Spheroids and Solid Tumors by SERS Modality. *Nanoscale***2020**, *12* (13), 6971–6975.

(60)   Yooa, K. M.; Zhub, H. R.; Akinsb, D. L.; Prudented, R.; Celmerd, E.; Carond, A.; Gynecology, G.; Division, N. Raman, Fluorescence, and Time-Resolved Light Scattering as Optical Diagnostic Techniques to Separate Diseased and Normal Biomedical Media. *J. Photochem. Photobiol. B Biol.***1992**, *16*, 187–209.

(61)   Shen, T.; Guo, Q. Role of Pyk2 in Human Cancers. *Med. Sci. Monit.***2018**, *24*, 8172–8182.

(62)   Kuang, B. H.; Zhang, M. Q.; Xu, L. H.; Hu, L. J.; Wang, H. B.; Zhao, W. F.; Du, Y.; Zhang, X. Proline-Rich Tyrosine Kinase 2 and Its Phosphorylated Form PY881 Are Novel Prognostic Markers for Non-Small-Cell Lung Cancer Progression and Patients' Overall Survival. *Br. J. Cancer***2013**, *109*, 1252–1263.

(63)   Fendt, S.; Verfaillie, C.; Gru, T. G. P. Proline Metabolism Supports Metastasis Formation and Could Be Inhibited to Selectively Target Metastasizing Cancer Cells. *Nat. Commun.***2017**, *8*, 15267.

(64)   Liu, W.; Hancock, C. N.; Fischer, J. W.; Harman, M.; Phang, J. M. Proline Biosynthesis Augments Tumor Cell Growth and Aerobic Glycolysis : Involvement of Pyridine Nucleotides. *Sci Rep***2015**, *5*, 17206.

(65)   Kübler, K.; Heinenberg, S.; Rudlowski, C.; Keyver-Paik, M. D.; Abramian, A.; Merkelbach-Bruse, S.; Büttner, R.; Kuhn, W.; Schildhaus, H. U. C-Myc Copy Number Gain Is a Powerful Prognosticator of Disease Outcome in Cervical Dysplasia. *Oncotarget.***2015**, *6*, 825–835.

(66)   Gottschalk, E. Y.; Meneses, P. I. A Dual Role for the Nonreceptor Tyrosine Kinase Pyk2 during the Intracellular Trafficking of Human Papillomavirus 16. *J.Virol.***2015**, *89*, 9103–9114.

(67)   Chen, Y.; Dai, J.; Zhou, X.; Liu, Y.; Zhang, W.; Peng, G. Raman Spectroscopy Analysis of the Biochemical Characteristics of Molecules Associated with the

Malignant Transformation of Gastric Mucosa. *PLoS One***2014**, *9*, e93906.

(68) Ayre, W. B.; Ayre, J. E. Cytochemical Study of Glycogen in the Diagnosis of Cervical Cancer. *Am J Clin Pathol.***1950**, *20*, 644–650.

(69) Gregoire, A. T.; Ledger, W. D.; Moran, M. J. The Glycogen Content Of The Human Female Genital Tract In Cycling, Menopausal, And Women With Encometrial And Cervical Carcinoma. *Fertil. Steril.***2016**, *24*, 198–201.

(70) Su, P. F.; Wu, F. Y. H. Differential Suppression of the Tumorigenicity of HeLa and SiHa Cells by Adeno-Associated Virus. *Br J Cancer.***1996**, *73*, 1533–1537.

SERS Nanotag based Single Cell Imaging for the Recognition of
Dual Biomarker during progression of
Cervical Cancer
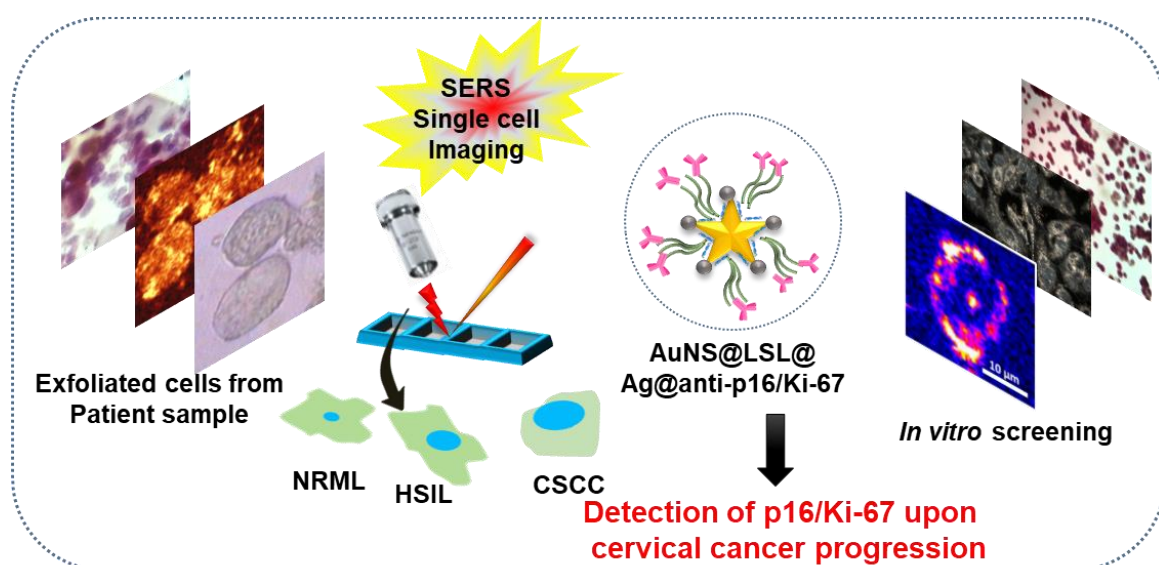
3.1 Abstract: *Among the type of cancers which enables the possibility of early diagnosis, monitoring the progression via single cell analysis is an attractive strategy. Cervical cancer is one such type which can be monitored throughout the long window period towards the progression to an invasive type. Herein, a surface enhanced Raman scattering (SERS) nanotag has been designed for the simultaneous detection of p16/Ki-67, a dual biomarker remarkable in the progression of squamous cell carcinoma in human cervix. SERS-tag fabricated with a hybrid gold nanostar having silver tips in order to achieve maximum Raman signature enhancement from the incorporated reporter molecule which is further tethered with the monoclonal antibodies against p16/K-i67. The SERS-tag was first validated in a cervical squamous cell line model, SiHa and subsequently extended to different grades of pathologically confirmed exfoliated cells from normal (NRML), high-grade intraepithelial lesion (HSIL) and cervical squamous cell carcinoma (CSCC) samples. Precise Raman mapped images constituted*

based on the intensity gradient of the signature peaks of the SERS-tags. A distinct gradation in the dysplastic HSIL and CSCC cells was observed which justify the prevalence of p16/Ki-67 whereas very feeble signals were obtained from the normal cell samples. Further validation of Raman imaging modality with gold standard immunocytochemistry dual staining analysis was performed. Thus the Raman image guided diagnosis in this study emphasizes the immense potential as a complementary platform for using cytology samples for cervical cancer diagnosis.

3.2 Introduction

Early detection of cancer is an effective strategy for eradicating this deadly disease. Precision medicine can get maximum benefit for specific treatment or therapies. The existing cancer detection techniques can only monitor the abnormal proliferation, if it turns out as a significantly detectable mass. Invasive techniques are required to assess whether it is benign or malignant for which healthy tissues need to be removed. Cytological, histological, molecular biology based techniques are conventionally employed to examine tumor samples obtained by biopsy or surgical procedures. Hence, in such a scenario, single cell based exfoliated cytology[1,2] has importance for early cancer detection. Cancers like cervical,[3] colon[4] and oral[5] shows precancerous lesions if detected, can be treated completely in early stage. Exfoliated cells detached from the cellular lining near the cancer site may be valuable non-invasive samples for the early detection of such type of cancers. Single cell analysis is promising in case of exfoliated cells which is reflected as a golden standard in the event of cervical cytology. In developed countries, the incidence of cervical cancer[6] has been much reduced by the introduction of proper screening programmes. Pap staining[7] has been established for identifying the abnormal cells in the cervical smears which evaluates the morphological changes in a grade dependent manner. HPV[8] , considered as the main causative factor behind cervical cancer, can be examined by HPV DNA polymerase chain reaction method for the amplification of viral gene. But as the HPV virus is short-lived in nature, HPV PCR cannot be fully relied cervical cancer diagnosis. Thus a combinatorial strategy including the Pap staining, HPV DNA analysis and vaccination is the ultimate diagnostic measure so far adopted by developed countries. But Pap test suffers some disadvantages like subjective nature, inter observer inconsistency, low sensitivity with high false negative rates etc.

Moreover, lack of skilled cytotechnologists, is also another vital factor which resulted in the quest for alternative techniques.[9] Recently detection of p16/Ki-67 dual marker in cytological specimens emerged as a precise indicator and highly objective technique for cervical precancerous lesions. CINtec® PLUS Cytology developed by Roche is one of the recent test to be used as an aid for the identification of transforming HPV infections which employs dual biomarker to detect p16[INK4a] and Ki-67 simultaneously.[10] It helps in recognising women with high-grade cervical dysplasia with positive HPV test results. p16/Ki-67 shows improved sensitivity[11], specificity[12] and inter-observer reproducibility[13] suggesting its implementation in routine cytology practice with limited training. A longitudinal study also showed the triage with p16/Ki-67 dual staining providing better long term risk stratification than cytology.[14,15] Even though the dual staining immunocytology is highly objective compared to Pap staining, the former is still highly time consuming.

Thus, the requirement of alternative methods which can supplement the present techniques is of great demand in the current scenario. Countless applications in multidisciplinary areas for understanding, analysing and modifying the inherent properties of a particular matter in nano scale has been presented by nanotechnology.[16] It possess huge potential for overcoming several bottle necks related to the diagnosis and treatment of various deadly diseases including cancer.[17] A large variety of nanomaterials including metallic nanoparticles, carbon nanotubes, quantum dots, dendrimers, polymeric nanoparticles etc. of different shape and size have been developed for cancer theranostics along with different imaging modalities.[16] Applications including biomarker detection based on cells,[18] circulating tumor cells,[19] DNA,[20] proteins,[21] and exosomes[22] has been evaluated with nanomaterial-assisted sensors rendering high sensitivity with specificity in a multiplexed pattern. Design of a nano-diagnostic platform with targeting moiety like peptides,[23] antibodies,[24] aptamers[25] and small molecules[26] renders its specificity precisely to a desired site. Raman spectroscopy recently emerged as an excellent optical imaging modality which can be employed for the ultrasensitive detection including single cell analysis.[27] With the incorporation of nanomaterial unit, SERS[28] overcame the major challenges faced by conventional Raman scattering in terms of enhancement. When the analyte molecules exists in a close proximity within the nano-

roughened surface , the signal intensity get enhanced upto 10^4 to 10^{10} folds making capable to detect even single molecule[29] unlike other imaging modalities like MRI, photo acoustic imaging etc. A few studies has recently shown the merits of SERS-tags for cervical cancer detection using EGFR, human protein tyrosine kinase-7 and cervical squamous cell carcinoma antigen.[30–32] Thus further exploration is essential to uplift the SERS technique for the clinical translation of cervical cancer detection.
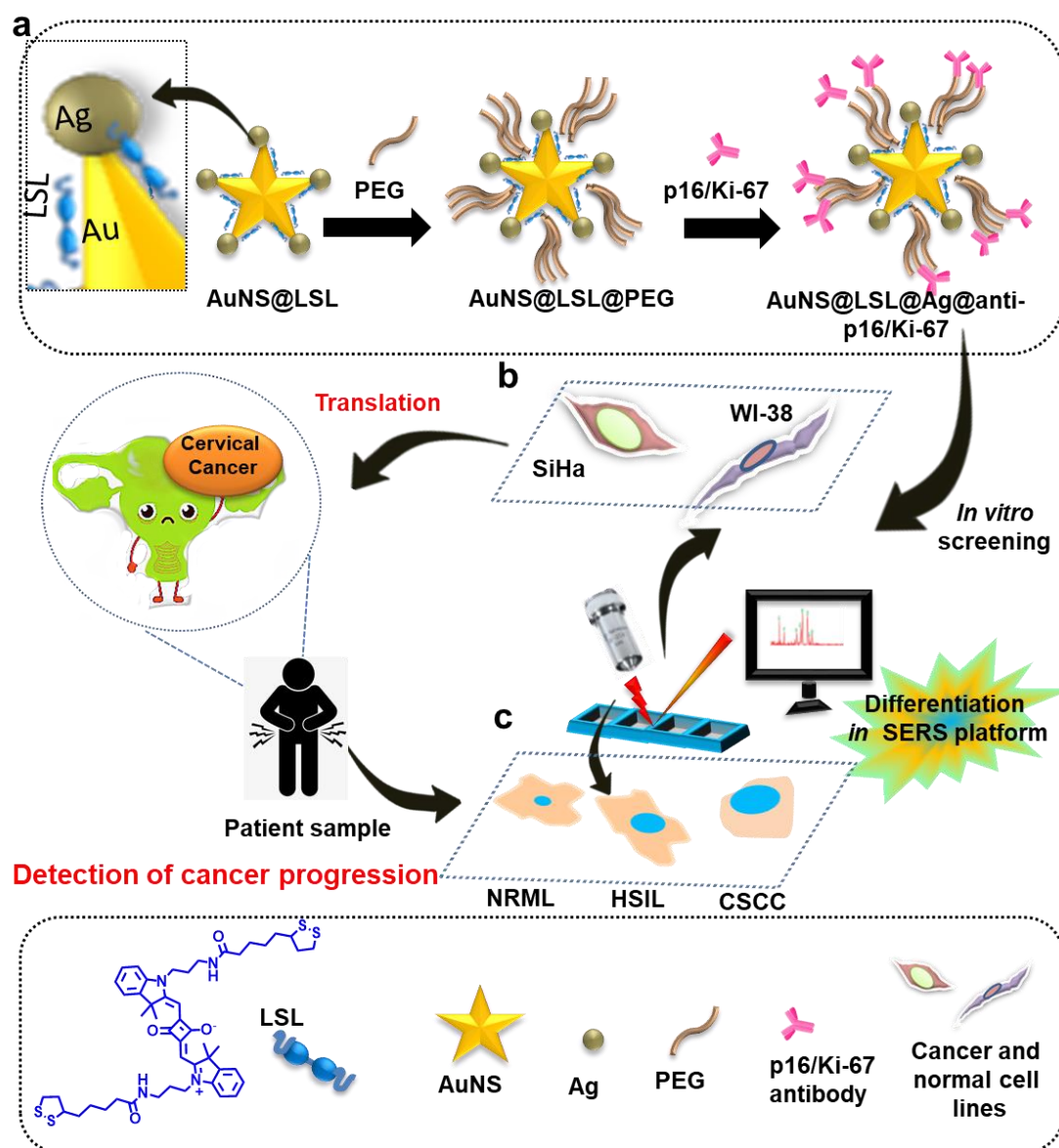
Scheme 3.1: Schematic illustration for experimental design for differentiating three grades viz. NRML, HSIL, CSCC using SERS-tags, a) synthetic scheme of AuNS@LSL@Ag@PEG@anti-p16/Ki-67, b) SERS analysis in SiHa and WI-38 and c) SERS analysis in clinical samples, NRML, HSIL and CSCC.

Herein, an ultrasensitive SERS substrate AuNS@Ag nanoflower were employed as an efficient SERS substrate for the detection of p16/Ki-67 biomarker through differential Raman imaging modality during cervical cancer progression. Previously reported lipoic acid appended squaraine molecule named "LSL" was incorporated into gold nanostar which is comprehended to act as a capping agent as well as Raman reporter. Further, a silver tip on the edges of gold nanostar, produces hotspots due to the tiny gaps formed by the silver, LSL and gold nanostar complex. The targeting unit, p16/Ki-67 dual antibody was tethered to form the SERS-tag. In the first stage, the recognition of p16/Ki-67 abundance in *in vitro* level through Raman mapping using cervical squamous cell line, SiHa has been demonstrated and complemented with immunocytochemistry analysis. The profiling of the cervical cancer progression using Raman imaging modality in major three stages has been executed starting from normal cell to invasive carcinoma cells (**Scheme 3.1**). The differential Raman image provides a clear profiling between NRML, HSIL and CSCC samples which was perfectly complemented with the immunohistochemistry staining providing a new insight for clinical diagnosis of cervical cancer patients.

3.3 Results and Discussion

3.3.1 Fabrication of nanoflower SERS-tag: AuNS@LSL@Ag@anti-p16/Ki-67

3.3.1.1 Synthesis and characterization of nanoflower core AuNS@LSL@Ag

Gold nanostar (AuNS) as SERS substrate was utilized for the ultrasensitive image guided detection of dual biomarker p16/Ki-67 in cervical cancer using an intrinsic Raman reporter dye molecule. The in-house di-lipoic acid appended squaraine Raman reporter (LSL) was synthesized[33] and incorporated in the AuNS for Raman mapping (**Scheme 3.1 a**). AuNS of size around 70-80 nm was synthesized to which the silver tip was fabricated on the top as spikes on AuNS (AuNS@LSL@Ag) by a straightforward protocol.[34] The core size of the nanostar exhibited around 50 nm with average branch number seven spikes. After the formation of silver tips, the AuNS changed its morphology drastically to flower shape whose tip thickness was well tuned by adjusting the concentration of silver nitrate. Colour of the colloidal solution changed from dark blue to green while silver tips occupied on top of the AuNS spikes (**Figure 3.1 a**). The double side lipoic acid containing LSL dye got unevenly covered

over the AuNS. Further, the reduced silver got deposited and grew at AuNS tips where it has not been covered by the LSL molecules generating nanogaps for Raman signal enhancement.
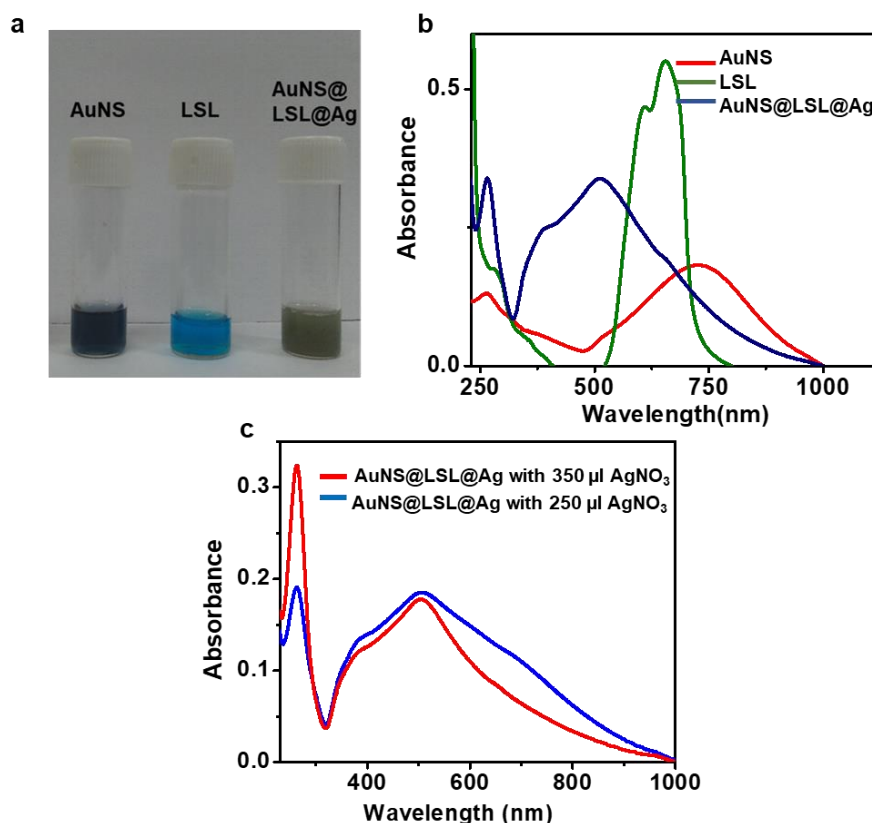
Figure 3.1: Photophysical evaluation of the synthesized SERS substrate, AuNS, LSL and AuNS@LSL@Ag a) color change, b) UV-vis absorbance and c) absorbance spectra showing increase in 260 nm peak with respect to addition of increased amount of silver nitrate during preparation of AuNS@LSL@Ag particles.

Furthermore, the UV-vis spectroscopic characterization of AuNS, LSL and AuNS @LSL@Ag were carried out, which showed an absorption peak around 726 nm, 650 nm and 510 nm respectively (**Figure 3.1 b**). Also a 260 nm peak was evident in the AuNS @LSL@Ag particle which attributed to increase with the amount of silver nitrate added in the construct for tip selective growth (**Figure 3.1 c**). The nano-constructs AuNS and AuNS@LSL@Ag was assessed by transmission electron microscopy which showed highly monodispersed nanoparticles (**Figure 3.2 a and b**).
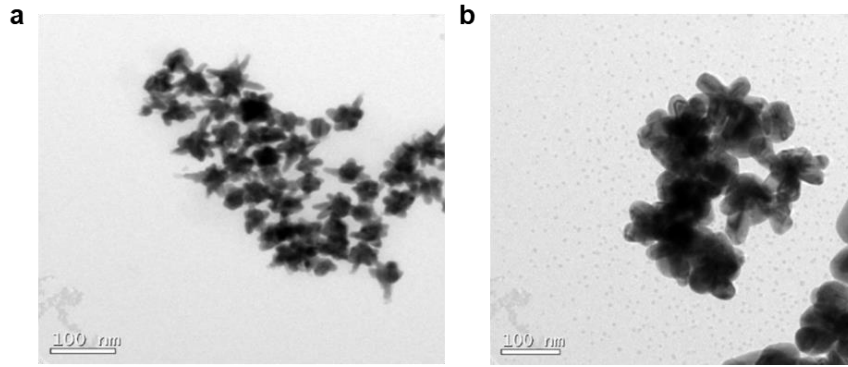
Figure 3.2: HR-TEM analysis (scale bar: 100 nm) of a) AuNS and b) AuNS@LSL@Ag.

Next, the SERS intensity of LSL *w.r.t.* 580 nm peak was compared between AuNS @LSL@Ag, AuNS@LSL and AgNP@LSL (bare silver nanoparticles). A gradual increase in SERS intensity was observed from AgNP@LSL to AuNS@LSL to AuNS@LSL@Ag in terms of the fold change ratio 1: 7: 12 respectively (**Figure 3.3 a and b**).
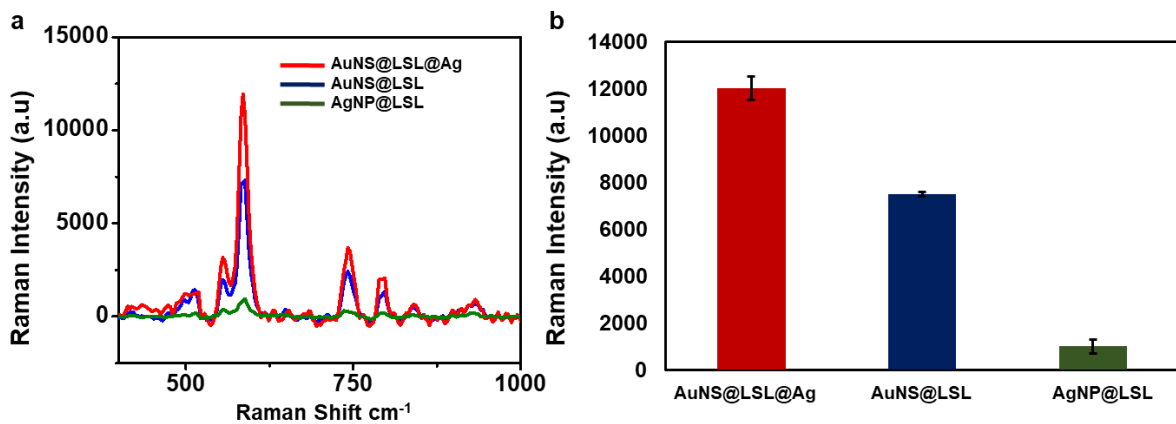
Figure 3.3: Characterization of substrate by SERS analysis, a) Comparison of SERS spectral intensity of LSL dye from AuNS@LSL, AuNS@LSL@Ag, AgNP@LSL and b) the corresponding intensity chart.

It is very much predicted that the AuNS enable to create more hot spots compared to spherical AgNPs, therefore higher plasmonic effect must be existed in AuNS which in turn generate greater electromagnetic field that causes enhanced Raman signal. In case of anisotropic gold-silver bimetallic nanostructures, the surface plasmon resonance (SPR) peak can be modulated to the optimal position due to the oriented nanogaps (termed as "hot spots") which enabled to generate an ultra-strong localized electromagnetic field yielding a strong SERS enhancement.[34] The synthesized nano-construct AuNS@LSL@Ag, transformed into a nanoflower, in which

the interior nanogaps oriented in a confined manner with the two arms of di-lipoic acid. Importantly, LSL functions as a selective capping agent as well as a SERS reporter. Therefore, around 12 fold changes in Raman signal intensity was observed from the desired SERS-tag which is further utilized for dual p16/Ki-67 antibody conjugation.

3.3.1.2 Preparation of pegylated nanoconstruct, AuNS@LSL@Ag@PEG

SERS-tags were subjected to perform the detection of biomarker with the differential progression of exfoliated cells of the cervix through a gradient Raman imaging technique. Raman image based investigation will be correlated directly with the occurrence of the overexpressed protein. AuNS@LSL@Ag was first pegylated using the hetero functional linker SH-PEG-COOH to generate the terminal free carboxyl functionality for covalent conjugation with the available amine moiety of monoclonal antibody which imparted the biocompatibility and uptake efficiency. Moreover, pegylation prevents the toxicity of the organic dye based Raman reporter and preserves the SERS-tags against aggregation in physiological condition.[35] UV-vis spectroscopic analysis of pegylated construct exhibited a red shift of nearly 8 nm in the absorption peak from 510 nm to 518 nm which stands as a confirmative indicator of the effective PEG encapsulation (**Figure 3.4 a and b**). Also a 260 nm peak was evident in the AuNS@LSL@Ag particle which attributed to increase with the amount of silver nitrate was found to be diminished. Further, dynamic light scattering (DLS) analysis also complemented the same effect by showing a shift from 98 nm to 106 nm (**Figure 3.4 c and d**).

3.3.1.3. Preparation of antibody conjugated nanoconstruct, AuNS@LSL@Ag@ PEG @anti-p16/Ki-67

An ultrasensitive SERS-tag was envisaged for the diagnosis of clinically appropriate biomarker in cervical cancer. Hence for achieving this objective, clinically relevant dual biomarker p16/Ki-67 was chosen which is prevalent in cervical cancer. Therefore, the corresponding antibody of p16/Ki-67 was conjugated using N-(3-(dimethylamino)-propyl)-N'-ethylcarbodiimide (EDC) and N-hydroxysuccinimide (NHS) coupling chemistry with the carboxyl functionalized PEG encapsulated SERS-tag using well established protocol.[36]
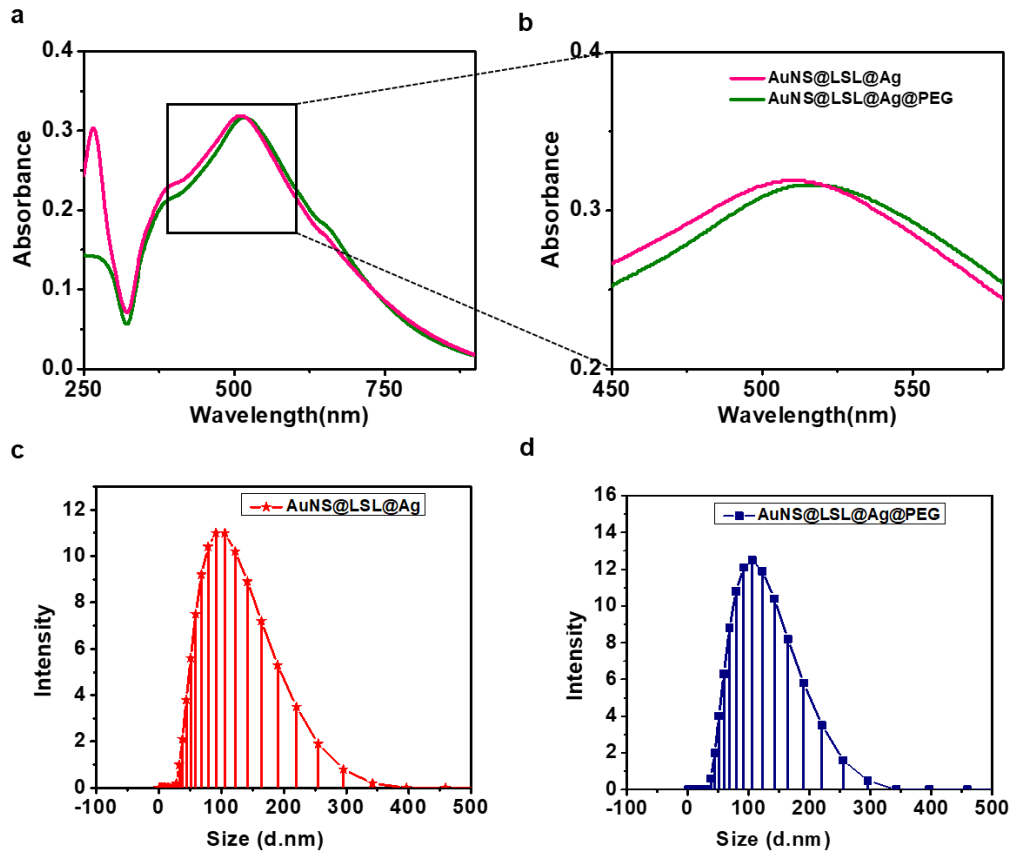
Figure 3.4: Characterization of PEG encapsulation, a) UV-vis absorbance of AuNS@LSL@Ag and AuNS@LSL@Ag@PEG, b) its zoomed image of the shift and DLS (c, d) of AuNS@LSL@Ag and AuNS@LSL@Ag@PEG nanoconstruct.

The UV-vis spectroscopic analysis of antibody conjugated SERS-tags exhibited an occurrence of a 275 nm protein absorption peak along with a 1-2 nm shift from the 518 nm plasmon peak which confirmed the effective binding of the antibody (**Figure 3.5 a**). As already a 260 nm peak was evident earlier in the AuNS@LSL@Ag particle absorbance spectrum, the 275 nm peak emerged may be due to antibody conjugation. Further confirmation of the antibody conjugated nanotag was also corroborated by the sodium dodecyl sulphate poly acrylamide gel electrophoresis (SDS-PAGE) analysis where the conjugated nanotag along with pure antibody was run in a 12 % polyacrylamide gel. Silver staining aided the visualization of the protein bands indicating the respective position of the pure antibody along with a slight upshift in nanotag added well showing successful conjugation (**Figure 3.5 b**). Dual antibody used for the study was utilized from a dual immunocytochemistry detection kit of p16/Ki-67 from Roche antibody which consisted of mouse monoclonal antibody for

p16 and rabbit monoclonal antibody for Ki-67. The kit serves to identify the twin biomarker co-expressed using two stains namely 3,3′-Diaminobenzidine (DAB) and Fast red respectively for p16 and Ki-67. In this study, Raman reporter was employed to construct the single SERS-tags which enabled to monitor the progression of p16/Ki-67biomarker by SERS technique.
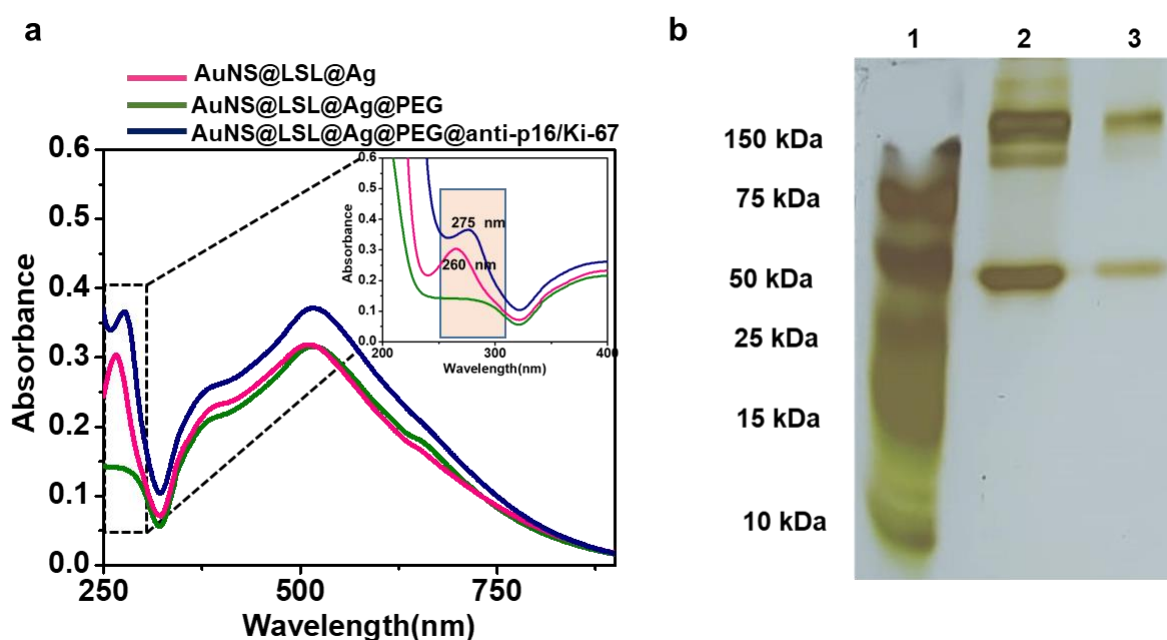
Figure 3.5: Characterization of antibody conjugated nanoconstructs, a) UV-vis absorbance of AuNS@LSL@Ag, AuNS@LSL@Ag@PEG and AuNS@LSL@Ag@PEG@anti-p16/Ki-67 [inset: evidence of shift from 260 nm to 275 nm due to antibody conjugation], b) PAGE analysis of the nanoconstruct, 1) Ladder, 2) pure p16/Ki-67, 3) AuNS@LSL@Ag@PEG@anti-p16/Ki-67.

3.3.2 *In vitro* analysis

3.3.2.1 Cell viability analysis of the nanotags

Subsequently, the cytotoxicity of the pegylated SERS-tag was assessed in a cervical squamous cell carcinoma cell line, SiHa and a normal lung fibroblast cell line, WI-38 by MTT assay. The Raman reporter alone showed a dose dependent toxicity (**Figure 3.6**) even from 0.1 upto 50 µM concentration.
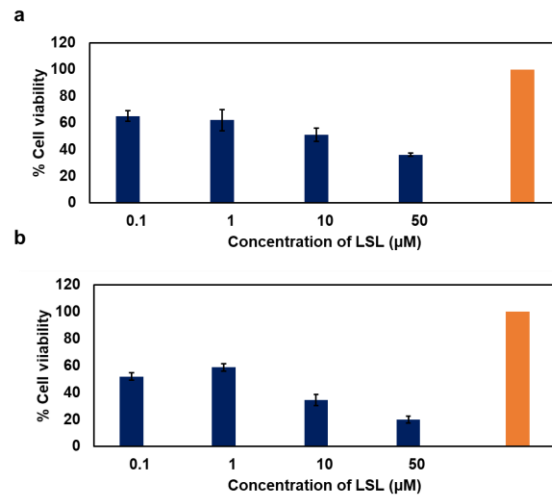
Figure 3.6: Cell viability analysis of the LSL dye in a) SiHa and b) WI-38 cell line.

The AuNS@LSL@Ag incorporated with 2.5 µM of the dye per ml of the pegylated tag showed a safe concentration for Raman mapping in cell lines. The PEG encapsulated SERS-tag AuNS@LSL@Ag@PEG exhibited an improved cell viability over 80 % which imparted better biocompatibility when compared with bare AuNS@LSL@Ag (**Figure 3.7**).
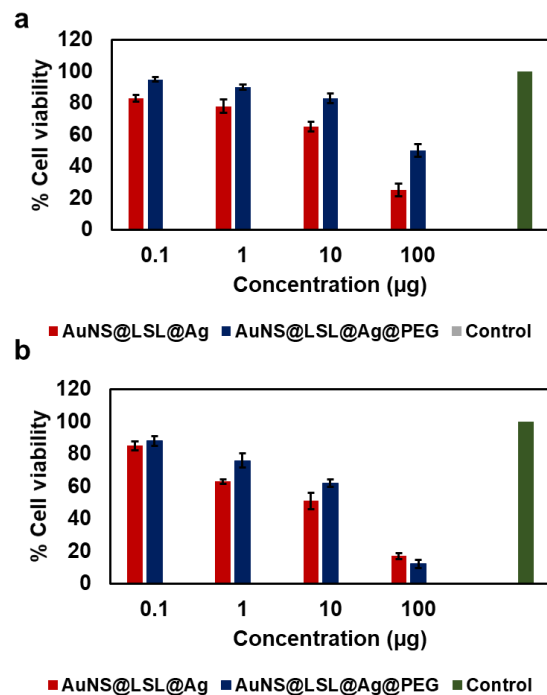
Figure 3.7: Cell viability analysis of the SERS-tag AuNS@LSL@Ag and AuNS@LSL@Ag@PEG in a) SiHa and b) WI-38 cell line.

3.3.2.2 Western blot

Evaluation of expression level of the biomarkers in both cell lines were carried out by western blot analysis employing respective antibodies using the beta actin as the control (**Figure 3.8**). As the dual antibody consists of mouse monoclonal antibody for p16 and rabbit monoclonal antibody for Ki-67, secondary antibodies of respective origin were utilized for this specific detection. High expression of p16 and Ki-67 was found in SiHa cell line whereas minimal expression was observed in WI-38. Therefore, the both the cell line were fully justified for nanotag based detection strategy.
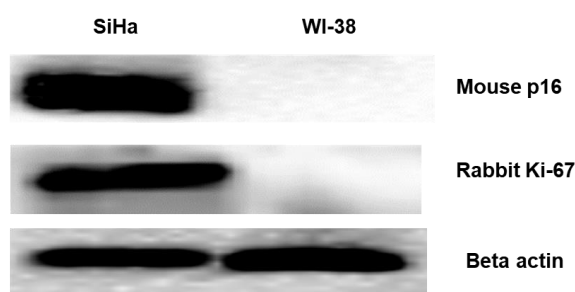
Figure 3.8: Western blot analysis of the expression level of p16/Ki-67 in SiHa and WI-38 cell line.

3.3.2.3 Recognition by Raman imaging

Next, p16/Ki-67 conjugated SERS-tags were utilized in order to investigate the recognition profile of the dual biomarker in cervical cancer cell, SiHa along with a negative control normal lung fibroblast cells WI-38. The SERS mapping profile was executed using confocal Raman system with 633 nm laser after incubation of the nanotags in both cells. In SiHa, a prominent SERS fingerprint was observed from cytoplasm as well as nuclear region indicating the abundance of p16/Ki-67 receptors, while the WI-38 cells under the same protocol revealed very feeble expression. A distinct bright field image of the SiHa cell and corresponding Raman mapped image, colour coded cluster image and 3D Raman image are depicted in **Figure 3.9 a-d** respectively. The corresponding average spectra based on signature peak at 580 cm^{-1} of the SERS-mapped images presented in **Figure 3.9 e**.
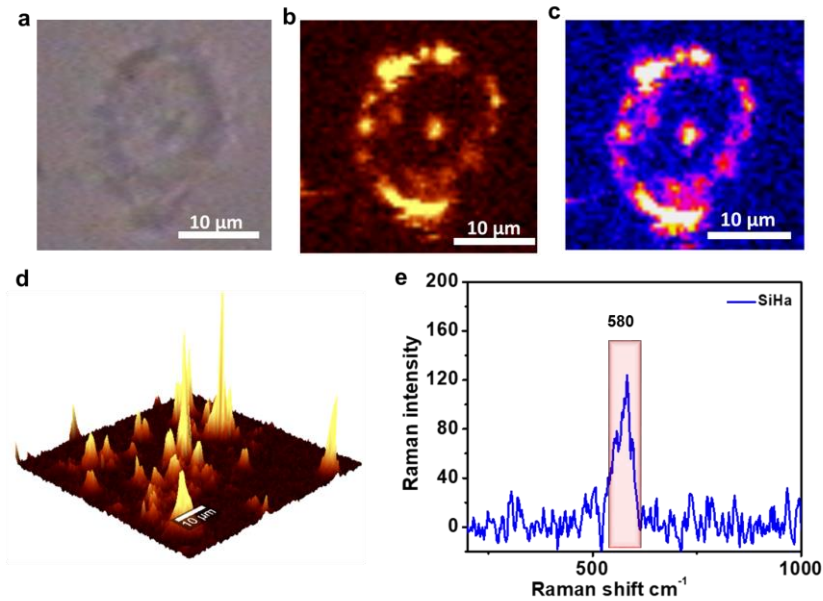
Figure 3.9: SERS imaging of p16/Ki-67 in SiHa cell line; a) bright field, b) Raman image, c) cluster image, d) 3D Raman image and e) SERS spectrum acquired from the cell.

Similarly, the bright field, SERS mapped image and corresponding average spectrum of WI-38 cell line also represented in **Figure 3.10 a-c** which indicated the absence of the expression of dual p16/Ki-67.
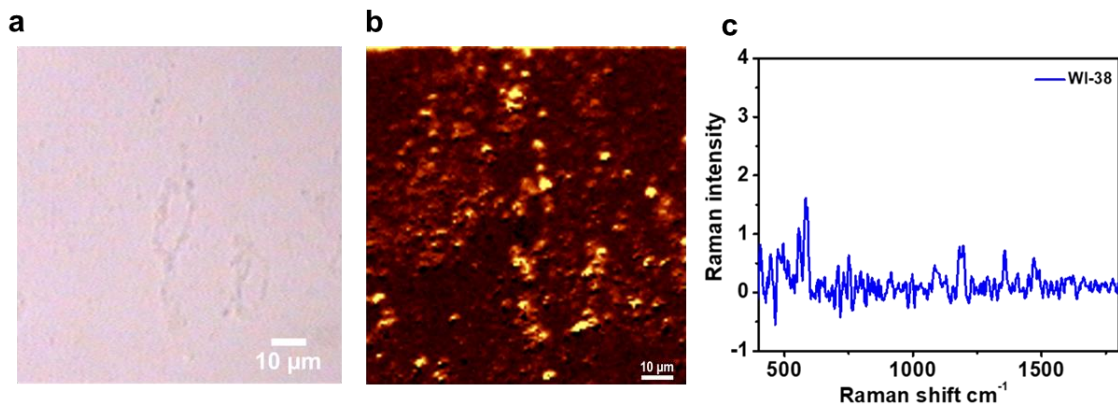
Figure 3.10: SERS imaging of p16/Ki-67 in WI-38 cell line, a) Bright field, b) Raman image and c) SERS spectrum acquired from the cell.

3.3.2.4 Recognition by dark field imaging

The SERS-tag based recognition of the dual biomarkers was further confirmed by dark field microscopic analysis. In dark field microscopy, localization of the metallic nanoparticles are visualized by bright and dark background images as it hits the specimen which exclude the un-scattered beam from the image.[37] The analysis was performed in SiHa and WI-38 cell lines which exhibited excellent

internalization of antibody conjugated SERS-tags agreeing well with the SERS imaging. A significant uptake of nanotags exhibited in cytoplasm in SiHa cells where as a negligible uptake of nanoparticles observed in the WI-38 cells (**Figure 3.11**). Therefore, a proof-of concept was evident in both SERS and dark field image based modality which assured the excellent specificity of the SERS-tags towards the squamous cell carcinoma cells from the cervix.
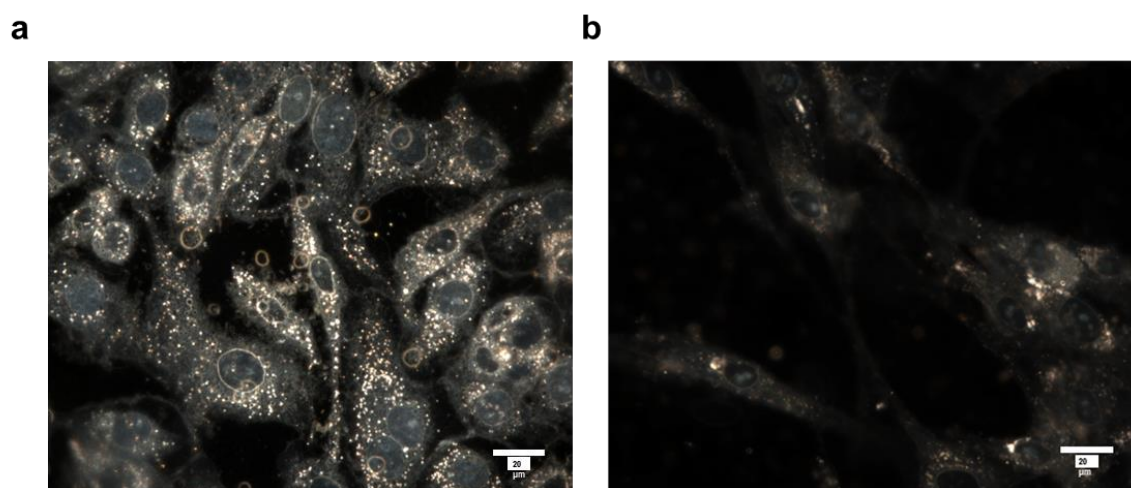
Figure 3.11: Dark field microscopic image performed in SiHa cell line and WI-38 cell line showing the internalization of the nanoparticles (scale bar: 20 μm).

3.3.2.5 Recognition by immunocytochemistry in cell lines

Furthermore, a comparative analysis was performed by dual immuno-cytochemistry kit for p16/Ki-67 protein in the cell lines. The positive SiHa cells were stained brown color in the cytoplasm by DAB and red color stained in the nucleus by the fast red dye which confirmed the overexpression of p16/Ki-67 biomarker (**Figure 3.12**). WI-38 cells responded negative with respective to both dyes. As the p16 and Ki-67 are mutually exclusive, their overexpression simultaneously is an excellent biomarker for cervical dysplasia. Even though the dual immunostaining is more sensitive than Pap staining, its time consuming analysis process hinders in practical clinical diagnosis of cervical cancer patients.
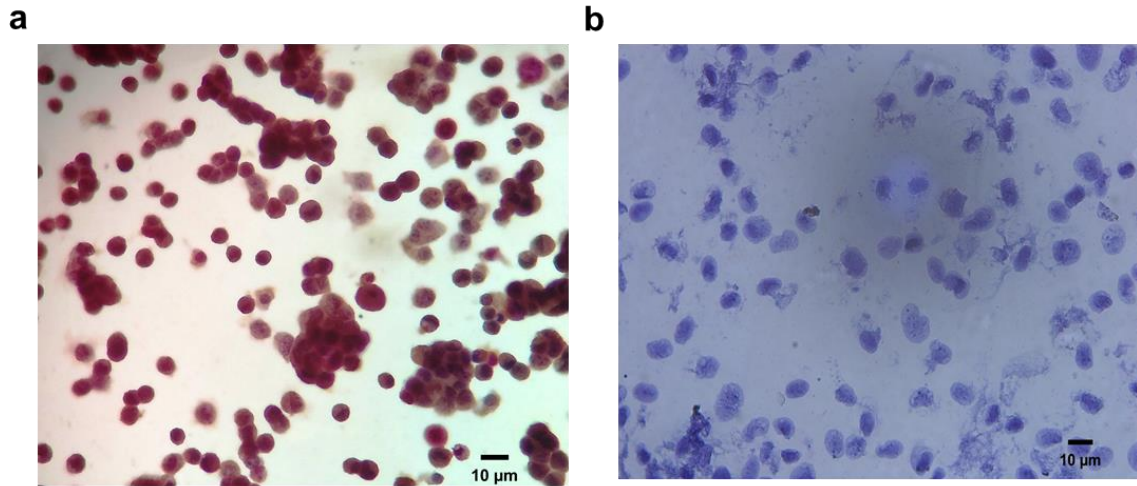
Figure 3.12: Dual immunostaining of p16/K-i67 biomarker in a) SiHa and b) WI-38 cell lines.

3.3.3 Evaluation of SERS-tag in clinical samples: Raman image guided differential recognition of the grades of cervical exfoliated cells

The Raman image guided recognition was implemented by precise modulation of the dual antibody conjugated SERS-tags in clinically confirmed cervical exfoliated cell samples by detecting the expression status of p16/Ki-67. The three major grades of exfoliated cells from cervical cancer patients along with healthy controls were utilized for Raman mapping. The Bethesda system introduced for reporting Pap smear results classifies cervical cancer into low grade squamous intraepithelial lesion (mild dysplasia/CIN1/LSIL), high grade squamous intraepithelial lesion (moderate dysplasia/ CIN II & III / HSIL) and invasive carcinoma (in situ carcinoma /severe dysplasia).[38] To evaluate the p16/Ki-67 biomarker in three major grades during the progression of cervical cancer, i.e. NRML, HSIL and CSCC samples were carried out. Such stage wise classification in Pap test aids clinicians to adopt proper treatment approaches. Prior to the SERS-tags based differentiation, the enrichment of exfoliated epithelial cells in the form of cell smear button was processed for SERS analysis. After incubation with the SERS-tag, the cells were selected for the analysis after morphological evaluation in terms of nucleus to cytoplasm ratio which turned out much higher in abnormal cells. The SERS-image based analysis implied notably higher level of expression of p16/Ki-67 protein in CSCC grade as reflected from the intense Raman signature peak at 580 cm^{-1} located in the nucleus as well as cytoplasm. Similarly, HSIL grades were selected based on the

ratio of nucleus to cytoplasm by the morphological characteristic of the single cell. The corresponding single spectrum and the SERS-mapping showed significant signals but to a lesser extent than from the CSCC grade. On the other hand, the nanotag produced only feeble signals from the NRML grade, thereby exhibiting the excellent specificity of the SERS-tags as capable to discriminate the grades or stages of cervical cancer progression (**Figure 3.13**).
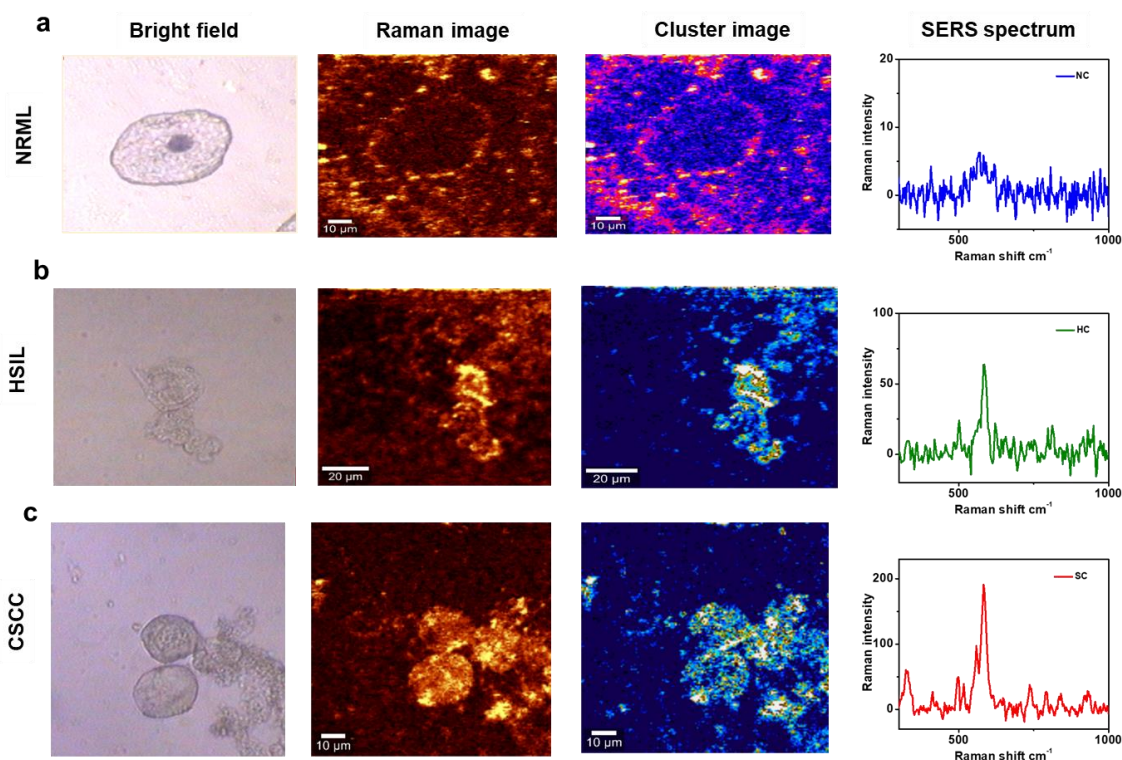
Figure 3.13: SERS imaging and spectral analysis of p16/Ki-67 biomarker in a) NRML, b) HSIL and c) CSCC clinical samples.

Finally, the Raman mapping of the three grades were complemented using the dual immunocytochemical analysis of NRML, HSIL and CSCC cells (**Figure 3.14**). The dysplastic cells were stained brown color in the cytoplasm by DAB and red color in nucleus by fast red dye which confirmed the overexpression of p16/Ki-67 biomarker in CSCC and HSIL cells. The NRML cells responded negative with respective to both the dyes. A distinct Raman imaged guided gradation was observed which enabled to profile semi-quantatively in terms of Raman intensity of the signature peak using dual antibody tagged SERS-tag as a new insight for staging of cervical cancer using the exfoliated single cell samples. The investigation harbours vast possibilities

in generating complementary or parallel clinical practices using SERS based platform in near future.
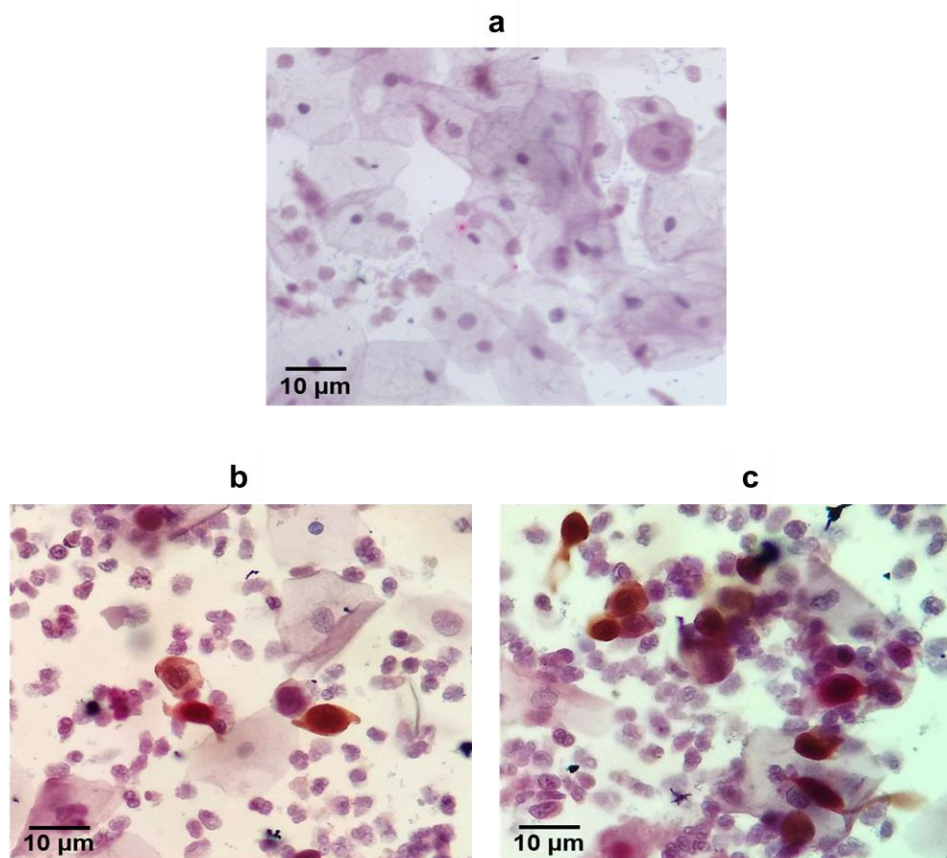
Figure 3.14: Dual immunocytochemistry of p16/Ki-67 biomarker in a) NRML, b) HSIL and c) CSCC clinical samples.

3.4 Experimental Section

3.4.1 Materials and reagents.

All chemicals were purchased from Sigma-Aldrich unless otherwise mentioned. The p16/Ki-67 antibody was utilized from dual staining CINtec® PLUS kit, purchased from Roche. The solvents employed were of reagent grade and procured from local companies. UV/vis absorbance analysis was performed using a UV-Vis spectrophotometer (Shimadzu UV- 2600). SERS experiments were achieved employing a WITec Raman microscope (WITec, Inc., Germany) comprising 600 g/mm grating with Peltier cooled charge-coupled device detector unit. 633 nm laser and 10 mW power were used for exciting the samples, and the spectra were collected in 400-1800 cm^{-1} region with 1 cm^{-1} resolution and 10 s and 3 accumulations. Calibration

was performed with a silicon standard having a 520 cm^{-1} Raman peak prior to each measurement. Data processing was performed using WITec Project 5.2 Plus (v2.1) software pack.

3.4.2 Synthesis of Raman reporter incorporated SERS substrate

Gold nanostars (AuNSs~ 100 nm) were synthesized by a seed-mediated growth method.[39] 15 nm Au seeds were prepared by heating 50 ml ultrapure water until boiling to which 1 mM trisodium citrate solution was added. After 10 min 3.4 mM gold chloride solution was supplemented resulting in a color change from dark purple to red which takes about 5 min. The solution was allowed to cool for 90 min with constant stirring. The synthesized nanoparticles characterization were done using UV-Vis Spectroscopy, DLS and TEM. For Au nanostars synthesis, 1 ml of the gold seed solution was added to 100 mL of 0.25 mM auric chloride solution. Further, 1 ml of 2 mM silver nitrate solution and 0.5 ml of 0.1 M ascorbic acid solution were dropped together. To upsurge the dispersity of the achieved Au nanostars, 1ml of 0.1 M Cetyl trimethylammonium bromide (CTAB) solution was supplemented. The 50 ml solution was centrifuged at 4000 rpm for 30 min and redispersed in 10 ml Milli Q water for future use. To incorporate silver on the gold nanostar, 1 mL of concentrated AuNS in hexadecyltrimethylammonium bromide 1 mM was transferred into a 1 ml microcentrifuge tube. LSL dye solution (25 µL, 100 µM) was dropped to the AuNS solution, which was kept at 40 °C in a thermostat for 3 h. Further, various amounts of 10 mM silver nitrate, 100 mM L-(+)-ascorbic acid, and 28 % ammonia solution were added at 50:5:1 ratio. The solution was well mixed and left undisturbed for 10 min to form a green colour solution.

3.4.3 Polymer encapsulation and preparation of antibody conjugated nanotags for p16-Ki67 detection in cervical cancer exfoliated cells

The as-obtained nanoprobes were encapsulated with polyethylene glycol and functionalized with the dual antibody to deliver the conjugated complex. 10 µM of SH-C$_2$H$_4$-CONHPEG-C$_3$H$_6$-COOH (RAPP Polymer GmbH, PEG MW: 3000 Dalton) solution was added to maintain 1:9 ratio of gold-dye (Au-LSL) solution in a microcentrifuge tube with vigorous mixing. After 15 min, the Au-colloid was added with 10 µM of CH$_3$-PEG-SH (RAPP Polymer GmbH, PEG MW: 5000 Dalton) to maximize surface coverage

and stabilization. After 3 h, Excess PEG was removed by three rounds of centrifugation at 4000 rpm, 15 min and resuspended in milli-Q water. Water was replaced by MES buffer pH 6.1 for covalent conjugation of antibodies at the carboxyl terminus of PEG. The antibodies were purified by filtration system (Amicon Ultra 3K centrifuge filters, Millipore) to remove the preservative, sodium azide. The PEG encapsulated nanotags were activated by 25 mM of N-(3-(dimethylamino)-propyl)-N'-ethylcarbodiimide (EDC) and 25 mM of N-hydroxysuccinimide (NHS). Excess EDC and NHS were removed by 3 rounds of centrifugation (8000 rpm, 15 mins) after 30 min and re-suspended in PBS. The nanotags were then added with p16/Ki-67 antibody (15μL) and incubated at 25 °C for 2 h followed by incubation at 4°C overnight. Further unbound antibodies were removed by a three round of centrifugation at 10000 rpm 5 mins. The pellet containing the antibody conjugated nanotags were then again resuspended in MES buffer and stored at 4°C. Conjugation of antibody conjugation was further confirmed by UV-Vis Spectroscopy analysis and 12 % SDS-PAGE gel analysis.

3.4.4 Cell culture

SiHa, the human cervical squamous cell carcinoma cell line was obtained from NCCS, Pune. The human lung fibroblast cell line WI-38 was procured from Regional Cancer Centre (Thiruvananthapuram, India). Cells were cultured in Dulbecco's modified Eagle's medium (DMEM) along with 10 % fetal bovine serum and antibiotics (100 U ml^{-1} penicillin/100 μg ml^{-1} streptomycin mixture) under 5% CO_2 atmosphere at 37 °C. Glass-bottom 4-well chamber slides were used to seed the cells two days prior for carrying out the imaging experiments.

3.4.5 Western blot in cell line lysates

Proteins were extracted from SiHa and WI-38 cells (2×10^6) employing RIPA buffer (Sigma Aldrich) and was then estimated using BCA assay (Thermo Pierce). Proteins were separated by 12% SDS-PAGE gel and further transferred to polyvinylidene difluoride membranes (PVDF), Millipore blocked with 5% skim milk and incubated with the primary antibodies. Horseradish peroxidase (HRP)-conjugated secondary antibody was used which was identified by the

chemiluminescent ECL substrate (Takara Clontech). The resultant bands were further quantified using Image J software normalized with β-actin.

3.4.6 Cytotoxicity analysis

The cytotoxicity analysis of the nanotag were measured against SiHa and WI-38 cell line using the 3-[4, 5-dimethylthiazol-2-yl]-2, 5-diphenyltetrazolium bromide (MTT) assay, which depends on the reduction of tetrazolium salt by dehydrogenase enzyme present in viable cells. Cell suspension 100 μl containing ∼10^4 cells/well were seeded in 96-well plate. Various concentrations of the constructs were added in each wells in triplicates. The plate was then incubated in a CO_2 incubator at 37 °C for 24 h. After incubation, 100 μl of MTT (0.5 mg/ ml) solution was added to each well and incubation was continued for 3 h. The insoluble formazan crystals developed were solubilized by the addition of DMSO solution. The plate was then incubated for 30 min in shaking. Further, the absorbance was measured at 570 nm using a microplate spectrophotometer (BioTek Synergy H1 multimode plate reader). The viability percentage for each construct relative to control were measured according to the following formulae Viability (%) = Abs of treated /Abs of Control X 100.

3.4.7 SERS imaging in cell lines

SERS detection in SiHa and WI-38 cells were done using confocal Raman microscope. The cells were cultured in 4 well chamber culture slides by seeding 10^4 cells/well which were incubated with the nanoconstructs containing 2.5 μM of the dye molecule for 4 h. Washing was done with PBS (pH 7.4) twice for removing the excess probes. The images were acquired on a X and Y direction, 100 × 100 μm mapping area with 150 × 150 points per line and an integration time of 0.01 s. The sample was excited with a 10 mW power using 633 nm laser excitation source with spectrograph grating 600 g/mm. The raw spectral data were pre-processed by Project FOUR 4.0 software before the statistical analysis to remove the interference noises, cosmic rays and oversaturated spectra. The background was removed by 4th polynomial function and smoothening of the SERS spectra was done by the Savitzky- Golay smoothing which in turn normalized in the region of 200–1800 cm^{-1}. Then the pre-processed data were put into the Origin Pro 8.0 software (Origin Lab, USA) to calculate and

create the mean spectrum of each group. The imaged-data was evaluated utilizing WITec Project Plus software.

3.4.8 Dual immunocytochemistry staining in cell lines

Immunocytochemistry were performed on SiHa and Wi-38 cells using p16/Ki-67 dual antibody using CINtec Plus Kit as per the instructions from the manufacturer. Initially, the cells were pre-fixed in absolute alcohol followed by wash with TBS buffer and antigen retrieval buffer were performed for exposing the antigenic sites. Further a ready to use primary antibody mix containing mouse monoclonal (E6H4™ clone) targeted against targeted against human p16INK4a (p16) protein and rabbit monoclonal antibody (274-11 AC3 clone) targeted against Ki-67 protein respectively were added. After 45 min incubation, followed by a TBS wash, a polymer reagent conjugated with HRP and goat anti-Mouse Fab' antibody fragments were used for p16 detection. Polymer reagent conjugated with alkaline phosphatase and goat anti-rabbit Fab' antibody fragments were employed for Ki-67 detection. The counter stain alcohol free hematoxylin was used followed by wet mounting and permanent DPX mounting.

3.4.9 Dark field imaging

Dark field imaging of SiHa and WI-38 cells were performed using CytoViva Enhanced Dark field illumination System 2.0. (BX 43F) with a 60X oil immersion objective. For imaging, cells were cultured in four well chamber slide seeded with a density of 10^4, cells/well which were incubated with the nanoconstructs for 4 h and PBS wash was done with pH 7.4 twice to discard the excess probes.

3.4.10 Cervical exfoliated cell sample collection and processing

The cervical smear samples were collected from the department of Community Oncology, RCC, Thiruvananthapuram, Kerala after getting prior approval from human ethical committee [HEC No.19/2014]. Informed consents were obtained from all the study subjects. A total of 3 CSCC samples and 3 HSIL samples were obtained from patients having clinically confirmed case of CSCC and HSIL respectively. Around 3 healthy female individuals were selected as the NRML group. The average age selected was 50 years. The cervical exfoliated cells were collected using sterile cytobrush and kept in liquid based cytology preservative fluid. The cells were density

gradient centrifuged and cervical exfoliated epithelial cells were monolayered on a glass slide for further SERS analysis.

3.5 Conclusion

An ultrasensitive strategy to target dual biomarker by SERS-tag was constituted to monitor the progression of clinically confirmed three major grades of cervical exfoliated cells and profiled first time through Raman mapping technique. In this strategy, single exfoliated cells collected from the cervical smear appeared to be an excellent candidate facilitating accurate detection of dual biomarker through SERS-tag. The facile preparation of the SERS-tag resulted in a ready to use detection kit for the overexpressed biomarkers in single cells in accord with the stage wise expression status by Raman imaging. The intrinsic incorporation of Raman reporter during the preparation of SERS substrate itself paved the way for its strong and reproducible signals. The highly efficient strategy rendered the detection of the dual biomarkers p16/Ki-67 in cell line level as well as in clinically confirmed patient samples which was well complemented with the comparative analysis of dark field imaging and finally dual immunocytochemistry. Further, taking into account of the influence of Raman image based diagnosis using well optimized SERS-tag exhibited as a promising approach towards clinical diagnosis of cancer.

3.6 References

(1)   Ayre, J. E. Selective Cytology Smear for Diagnosis of Cancer. *Am. J. Obstet. Gynecol.* **1947**, *53* (4), 609–617.

(2)   Maurice Fremont-Smith, Ruth M. Graham, J. V. M. Early Diagnosis of Cancer by Study of Exfolaited Cells. *J. Am. Med. Assoc.* **1948**, *138* (7), 469–474.

(3)   Tian, Q.; Li, Y.; Wang, F.; Li, Y.; Xu, J.; Shen, Y.; Ye, F.; Wang, X.; Cheng, X.; Chen, Y. MicroRNA Detection in Cervical Exfoliated Cells as a Triage for Human Papillomavirus – Positive Women. **2014**, *106* (9), dju241.

(4)   Hasegawa, J.; Nishimura, J. Exfoliated Malignant Cells at the Anastomosis Site in Colon Cancer Surgery : The Impact of Surgical Bowel Occlusion and Intraluminal Cleaning. **2011**, 875–880.

(5)   Sekine, J.; Nakatani, E.; Hideshima, K.; Iwahashi, T.; Sasaki, H. Diagnostic

Accuracy of Oral Cancer Cytology in a Pilot Study. **2017**, *12* (27).

(6)   Kamemoto, L. E.; Misra, A. K.; Sharma, S. K.; Goodman, M. T.; Hugh, L. U. K.; Dykes, A. C.; Acosta, T. Near-Infrared Micro-Raman Spectroscopy for in Vitro Detection of Cervical Cancer. *Appl. Spectrosc.* **2010**, *64*(3):255-61.

(7)   Tan, S. Y.; Tatsumura, Y. George Papanicolaou (1883-1962): Discoverer of the Pap Smear. *Singapore Med. J.* **2015**, *56* (10), 586–587.

(8)   Cohen, P. A.; Jhingran, A.; Oaknin, A.; Denny, L. Cervical Cancer. *Lancet* **2019**, *393*, 169–182.

(9)   Deepak, RU and Kumar, RR and Byju, NB and Sharathkumar, PN and Pournami, C. and others. Computer Assisted Pap Smear Analyser for Cervical Cancer Screening Using Quantitative Microscopy. *J. Cytol. Histol.* **2015**, *S3*.

(10)   Ravarino, A.; Nemolato, S.; Macciocu, E.; Fraschini, M.; Senes, G.; Faa, G.; Negri, G. CINtec PLUS Immunocytochemistry as a Tool for the Cytologic Diagnosis of Glandular Lesions of the Cervix Uteri. *Am. J. Clin. Pathol.* **2012**, *138* (5), 652–656.

(11)   Wentzensen, N.; Schwartz, L.; Zuna, R. E.; Smith, K.; Mathews, C.; Gold, M. A.; Allen, R. A.; Zhang, R.; Dunn, S. T.; Walker, J. L.; et al. Performance of P16/Ki-67 Immunostaining to Detect Cervical Cancer Precursors in a Colposcopy Referral Population. *Clin. Cancer Res.* **2012**, *18* (15), 4154–4162.

(12)   Pirtea, L.; Secosan, C.; Margan, M.; Moleriu, L.; Balint, O.; Grigoras, D.; Sas, I.; Horhat, F.; Jianu, A.; Ilina, R. P16/Ki-67 Dual Staining Has a Better Accuracy than Human Papillomavirus (HPV) Testing in Women with Abnormal Cytology under 30 Years Old. *Bosn. J. basic Med. Sci.* **2019**, *19* (4), 336–341.

(13)   Wentzensen, N.; Fetterman, B.; Tokugawa, D.; Schiffman, M.; Castle, P. E.; Wood, S. N.; Stiemerling, E.; Poitras, N.; Lorey, T.; Kinney, W. Interobserver Reproducibility and Accuracy of P16/Ki-67 Dual-Stain Cytology in Cervical Cancer Screening. *Cancer Cytopathol.* **2014**, *122* (12), 914–920.

(14)   Wentzensen, N.; Clarke, M. A.; Bremer, R.; Poitras, N.; Tokugawa, D.; Goldhoff, P. E.; Castle, P. E.; Schiffman, M.; Kingery, J. D.; Grewal, K. K.; et al. Clinical Evaluation of Human Papillomavirus Screening with P16/Ki-67 Dual Stain Triage in a Large Organized Cervical Cancer Screening Program. *JAMA Intern. Med.* **2019**, *179* (7), 881–888.

(15) Clarke, M. A.; Cheung, L. C.; Castle, P. E.; Schiffman, M.; Tokugawa, D.; Poitras, N.; Lorey, T.; Kinney, W.; Wentzensen, N. Five-Year Risk of Cervical Precancer Following P16/Ki-67 Dual-Stain Triage of HPV-Positive Women. *JAMA Oncol.* **2019**, *5* (2), 181–186.

(16) Choi, Y.-E.; Kwak, J.-W.; Park, J. W. Nanotechnology for Early Cancer Detection. *Sensors* **2010**, *10* (1), 428–455.

(17) Grodzinski, P.; Kircher, M.; Goldberg, M.; Gabizon, A. Integrating Nanotechnology into Cancer Care. *ACS Nano* **2019**, *13* (7), 7370–7376.

(18) Kneipp, J.; Kneipp, H.; McLaughlin, M.; Brown, D.; Kneipp, K. In Vivo Molecular Probing of Cellular Compartments with Gold Nanoparticles and Nanoaggregates. *Nano Lett.* **2006**, *6*, 2225–2231.

(19) Xiao, Y.; Lin, L.; Shen, M.; Shi, X. Design of DNA Aptamer-Functionalized Magnetic Short Nanofibers for Efficient Capture and Release of Circulating Tumor Cells. *Bioconjug. Chem.* **2020**, *31* (1), 130–138.

(20) Cai, C.; Guo, Z.; Cao, Y.; Zhang, W.; Chen, Y. A Dual Biomarker Detection Platform for Quantitating Circulating Tumor Dna (Ctdna). *Nanotheranostics* **2018**, *2* (1), 12–20.

(21) Dykman, L. A.; Bogatyrev, V. A.; Khlebtsov, B. N.; Khlebtsov, N. G. A Protein Assay Based on Colloidal Gold Conjugates with Trypsin. **2005**, *341*, 16–21.

(22) Shen, L.; Quan, L.; Liu, J. Tracking Exosomes in Vitro and in Vivo to Elucidate Their Physiological Functions : Implications for Diagnostic and Therapeutic Nanocarriers. *ACS Appl. Nano Mater.* **2018**, *1* (6), 2438–2448.

(23) Cui, Y.; Kim, S. N.; Naik, R. R.; McAlpine, M. C. Biomimetic Peptide Nanosensors. *Acc. Chem. Res.* **2012**, *45* (5), 696–704.

(24) Kumar, S.; Aaron, J.; Sokolov, K. Directional Conjugation of Antibodies to Nanoparticles for Synthesis of Multiplexed Optical Contrast Agents with Both Delivery and Targeting Moieties. *Nat. Protoc.* **2008**, *3*, 314–320.

(25) Cha, T. G.; Baker, B. A.; Sauffer, M. D.; Salgado, J.; Jaroch, D.; Rickus, J. L.; Porterfield, D. M.; Choi, J. H. Optical Nanosensor Architecture for Cell-Signaling Molecules Using DNA Aptamer-Coated Carbon Nanotubes. *ACS Nano* **2011**, *5* (5), 4236–4244.

(26) Wang, W. U.; Chen, C.; Lin, K. H.; Fang, Y.; Lieber, C. M. Label-Free Detection of Small-Molecule-Protein Interactions by Using Nanowire Nanosensors. *Proc.*

Natl. Acad. Sci. U. S. A. **2005**, *102* (9), 3208–3212.

(27) Kneipp, K.; Haka, A. S.; Kneipp, H.; Yoshizawa, N.; Boone, C.; Shafer-Peltier, K. E.; Otz, J. T. M.; Dasari, R. R.; Ichael, M.; Feld, S. Surface-Enhanced Raman Spectroscopy in Single Living Cells Using Gold Nanoparticles. *Appl. Spectrosc.* **2002**, *56* (2), 150–154.

(28) Henry, A. I.; Sharma, B.; Cardinal, M. F.; Kurouski, D.; Van Duyne, R. P. Surface-Enhanced Raman Spectroscopy Biosensing: In Vivo Diagnostics and Multimodal Imaging. *Anal. Chem.* **2016**, *88* (13), 6638–6647.

(29) Le Ru, E. C.; Etchegoin, P. G. Single-Molecule Surface-Enhanced Raman Spectroscopy. *Annu. Rev. Phys. Chem.* **2012**, *63* (1), 65–87.

(30) Narayanan, N.; Karunakaran, V.; Paul, W.; Venugopal, K.; Sujathan, K.; Kumar Maiti, K. Aggregation Induced Raman Scattering of Squaraine Dye: Implementation in Diagnosis of Cervical Cancer Dysplasia by SERS Imaging. *Biosens. Bioelectron.* **2015**, *70*, 145–152.

(31) Lu, D.; Xia, J.; Deng, Z.; Cao, X. Detection of Squamous Cell Carcinoma Antigen in Cervical Cancer by Surface-Enhanced Raman Scattering-Based Immunoassay. *Anal. Methods* **2019**, *11* (21), 2809–2818.

(32) Bamrungsap, S.; Treetong, A.; Apiwat, C.; Wuttikhun, T.; Dharakul, T. SERS-Fluorescence Dual Mode Nanotags for Cervical Cancer Detection Using Aptamers Conjugated to Gold-Silver Nanorods. *Microchim. Acta* **2016**, *183* (1), 249–256.

(33) Ramya, A. N.; Samanta, A.; Nisha, N.; Chang, Y. T.; Maiti, K. K. New Insight of Squaraine-Based Biocompatible Surface-Enhanced Raman Scattering Nanotag for Cancer-Cell Imaging. *Nanomedicine* **2015**, *10* (4), 561–571.

(34) Zhang, W.; Liu, J.; Niu, W.; Yan, H.; Lu, X.; Liu, B. Tip-Selective Growth of Silver on Gold Nanostars for Surface-Enhanced Raman Scattering. *ACS Appl. Mater. Interfaces* **2018**, *10* (17), 14850–14856.

(35) Suk, J. S.; Xu, Q.; Kim, N.; Hanes, J.; Ensign, L. M.; Sciences, H.; Sciences, M. PEGylation as a Strategy for Improving Nanoparticle-Based Drug and Gene Delivery. *Adv Drug Deliv Rev.* **2016**, *99*, 28–51.

(36) Maiti, K. K.; Dinish, U. S.; Samanta, A.; Vendrell, M.; Soh, K. S.; Park, S. J.; Olivo, M.; Chang, Y. T. Multiplex Targeted in Vivo Cancer Detection Using Sensitive

Near-Infrared SERS Nanotags. *Nano Today* **2012**, *7* (2), 85–93.

(37) Chaudhari, K.; Pradeep, T. Spatiotemporal Mapping of Three Dimensional Rotational Dynamics of Single Ultrasmall Gold Nanorods. *Sci. Rep.* **2014**, *4*, 27–29.

(38) Solomon, D.; Davey, D.; Kurman, R.; Moriarty, A.; O'Connor, D.; Prey, M.; Raab, S.; Sherman, M.; Wilbur, D.; Wright, T.; et al. The 2001 Bethesda System: Terminology for Reporting Results of Cervical Cytology. *JAMA* **2002**, *287*, 2114–2119.

(39) Hsiangkuo Yuan, Christopher G Khoury, Hanjun Hwang, Christy M Wilson, G. A.; Grant, and T. V.-D. Gold Nanostars: Surfactant-Free Synthesis, 3D Modelling, and Two-Photon Photoluminescence Imaging. *Nanotechnology* **2012**, *23* (7), 075102.

Development of Multiplexing Detection Platform for Breast Cancer Biomarkers by Non-invasive Surface Enhanced Raman Scattering Nanoprobe
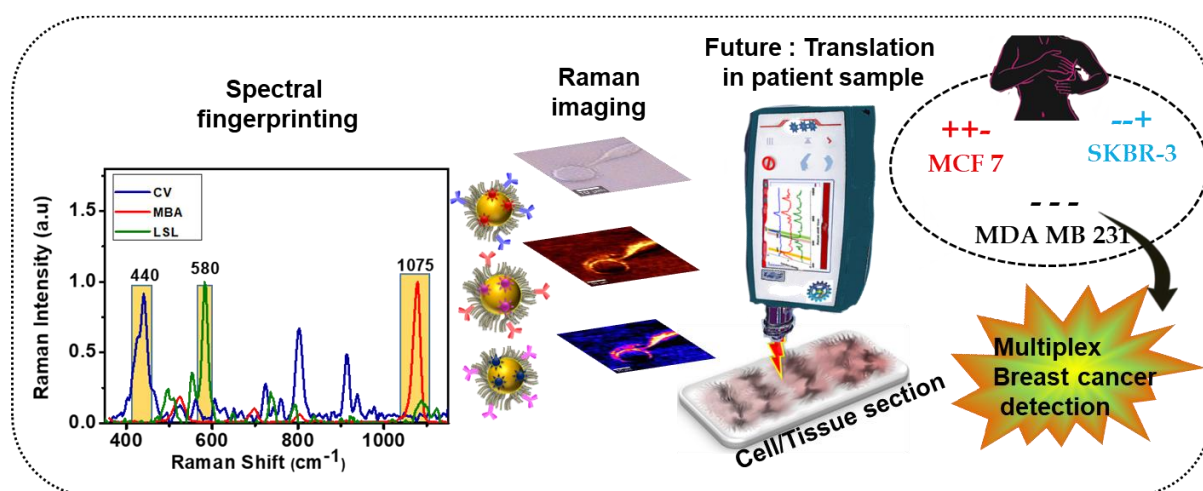
4.1 Abstract: *Identification of relevant biomarkers in breast cancer enables clinicians to improve the treatment strategies. Current gold standard immunohistochemistry is a time consuming technique with no possibility of multiplexing detection. Thus there is an urgent need of alternate technologies for the simultaneous detection of breast cancer biomarkers. Diagnostic SERS nanoprobes with Raman reporters having multiplexing capability for the ultrasensitive and rapid detection of biomarkers in breast cancer were elucidated. Initially a cocktail of monoclonal antibody conjugated SERS-tags with signature Raman peaks from incorporated Raman reporter were employed to detect the expression of triple biomarkers ER, PR and HER2 which are overexpressed in breast cancer cells lines. Later, the same strategy was followed for differential diagnosis in paraffin embedded retrospective breast cancer tissue samples. Immunohistochemistry was performed for the comparative analysis. SERS-tags based*

detection of biomarkers turned out to be an accurate, inexpensive, reliable and facile technique which can detect the biomarkers variations in different breast cancer subtypes. It is envisaged that the technique can be used as a screening method for breast cancer which can be translated to fresh tissue samples too.

4.2 Introduction

Breast cancer is the most common and leading type of cancer in women worldwide causing 2 million new cases with 6,27,000 deaths as of 2018.[1] In general, the survival rates are better for women with early stage cancers. Around the world, a significant variation exists in survival rates of breast cancer with 5-year survival of 80% in developed countries to below 40% for low resource countries.[2] The current diagnostic measures for breast cancer includes breast exam, mammogram, ultrasound scanning, magnetic resonance imaging, fine needle aspiration cytology (FNAC), biopsied material histopathology staining, FISH analysis etc.[3,4] A challenging feature of breast cancer is its heterogenous nature with differential expression of biomarkers. Biomarkers play a crucial part in breast cancer patient management, particularly in determining the kind of systemic therapy to be directed.[5] The three main biomarkers in the diagnosis of breast cancer include estrogen[6] (ER), progesterone[7] (PR) and human epidermal growth factor type 2 (HER2).[8] ER and PR, the key nuclear hormone receptors and HER2/neu gene overexpression are associated with breast cancer patient's prognosis and therapy.[9] The gene expression analysis also classifies breast cancer into four types named luminal A, luminal B, HER2 enriched and basal like.[10] These biomarkers are crucial in the estimation of breast cancer prognosis which plays a noteworthy role in treatment choice for breast cancer worldwide. Both ER and PR levels should be evaluated in newly diagnosed breast cancer patients who are expected to respond to hormone therapy and HER2 gene expression is mandatory for patients responding to antiHER2 therapy. Overall, the three biomarkers should be tested on determining the primary invasive tumor and monitoring the recurrent lesions. ER receptor is expressed around 80%, PR with 60-70% and HER2 overexpression with 15-20% in breast carcinoma. ER and PR usually show co-expression at about 70-80%. HER2 staining intensity is often evaluated by a grading system including 3+, 2+, 1+ and 0 grades correlating the staining intensity according to HER2 testing guidelines and recommendations.[11] Likewise several

combinations of subtypes of biomarkers come about in different origin of breast cancer. In addition, breast cancer that does not express ER, PR and HER2 are often denoted as triple negative breast cancer.

Study of ER/PR/HER2 overexpression is most commonly performed in formalin fixed paraffin embedded tissue samples by employing the golden standard immunohistochemistry technique to characterize tumor subtypes and post treatment residual tumor as commended by American Society of Clinical Oncology and College of American Pathologists.[12] IHC is relatively an easy, inexpensive technique, but the results will be influenced by a range of analytical factors like the type of antibody used, fixation methods, interobserver variability and is also time consuming. In addition, multiplexing is also not possible for evaluating the biomarker at the same time. Fluorescence in situ hybridization (FISH) analysis is a cytogenic analysis specifically used for detecting specific sequences in the HER2 gene using fluorescent probes. For HER2 detection, 95% concordance is required with IHC and FISH analysis. Eventhough FISH is a robust technique, it requires expensive reagents and laboratory equipment setup. [13-15] Thus, an alternative diagnostic system development is essential for the evaluation of the three biomarkers simultaneously in multiplexed manner.

Recently Raman spectroscopy emerged as a sensitive platform for the detection of a variety of diseases including cancer in a non-invasive manner. It is based on inelastic scattering of incident radiation which enables to capture unique fingerprint signatures corresponding to vibrations of target molecules with minute chemical changes. [16] The disadvantages faced by Raman spectroscopy in terms of weak signal was complemented by the emergence of SERS[17] which renders around 10^8 to 10^{14} fold signal enhancement. SERS is a highly promising ultrasensitive technique for the detection of biological and chemical molecules when adsorbed on roughened nano-metallic surfaces like gold or silver. Development of SERS based multifunctional diagnostic nanoprobes has been well exploited for the early and accurate detection of diseases in biomedical research. Novel high-tech tactics towards SERS substrates and its advanced applications in bio-medical diagnostics and therapy were the most noteworthy recent developments in SERS. Sensitive and multiplexed

detection of a variety of biomarkers in cancer diagnosis utilizing SERS has shown very promising in the current scenario. Functionalization of SERS-nanoprobes with targeting peptides, antibodies, aptamers etc towards cancer are investigated in vitro, in vivo and ex vivo experiments. The effective optical properties of SERS reporters with its narrow Raman signals enhances its capability for spectral multiplexing in contrast to quantum dots (Qds) and fluorescent dyes.

Multiplexing techniques are in demand for the detection of multiplex biomarkers at a time in terms of disease diagnosis which will improve diagnostic accuracy, minimize the use of expensive resources as well as time.[18] The detection of protein biomarkers plays a crucial role in cancer screening, diagnosis and therapy. Several investigations of biomarkers show the advantages of multiplexing studies *in vitro* as wells as *in vivo*. Three different biomarkers were targeted for EGF1R, ErbB2 and IGF1R in different breast cancer cell lines using perfluorocarbon/Qd nanoemulsions using *in vitro* fluorescence and functional magnetic resonance (f-MR) imaging showing the capability of a multiplexing platform.[19] An upconversion strategy employed for multiplexing technique for the evaluation of ER, PR and HER2 biomarkers in breast cancer using different colours from upconversion nanoparticles with studies extending from cell lines to tissue specimens.[20]Like wise different Raman reporters with non-overlapping multiplexing peaks can be engineered for making SERS-tags to probe multiple biomarkers at a time using single laser excitation wavelength. A SERS-tag possessing three main components, a metal nanoparticle for the signal enhancement, Raman reporter for labelling, a biocompatible layer and a targeting moiety for directing it towards the overexpressed biomarker, signatures it as ideal candidates for several biomedical multiplexing applications.[21] A multiplexed genotyping analysis was demonstrated for understanding the mutational status in cystic fibrosis using SERS which showed its benefits over fluorescence as a detection technique.[22] Self- assembly of branched DNA aptamer based SERS imaging method for simultaneous detection of mucin and nucelolin biomarkers on the surface of a breast cancer cell line also showed the potential of SERS spectral multiplexing.[23] Like-wise several studies emerged including joint SERS and computed tomography (CT) analysis[24], dual modal fluorescence-Raman endomicroscopic[25], multiplexed detection of breast cancer markers, CA 15-3, CA 27-29 and cancer embryonic antigen (CEA) in

liquid based biopsy samples[26] etc. Intraoperative identification of malignancy related biomarkers at surgical margin minimizes the re-excision rates in breast cancer. A clinical study quantified the simultaneous expression of HER2, ER, EGFR and CD44, biomarkers in fresh breast cancer tissue specimens using a cocktail of SERS-tags.[27–30] A potential SERS based multiplexed platform was evaluated for oral and breast cancer cell lines using cyanine and triphenylmethine dyes,[31] probing biomarkers in a teratoma model differentiated mouse embryonic stem cells comprising ectoderm, mesoderm and endoderm, cervical[32] and lung cancer.[33] Routine analysis of ER, PR, HER2 biomarker combination performed in immunohistochemistry is not capable of multi-plexing and is time consuming.
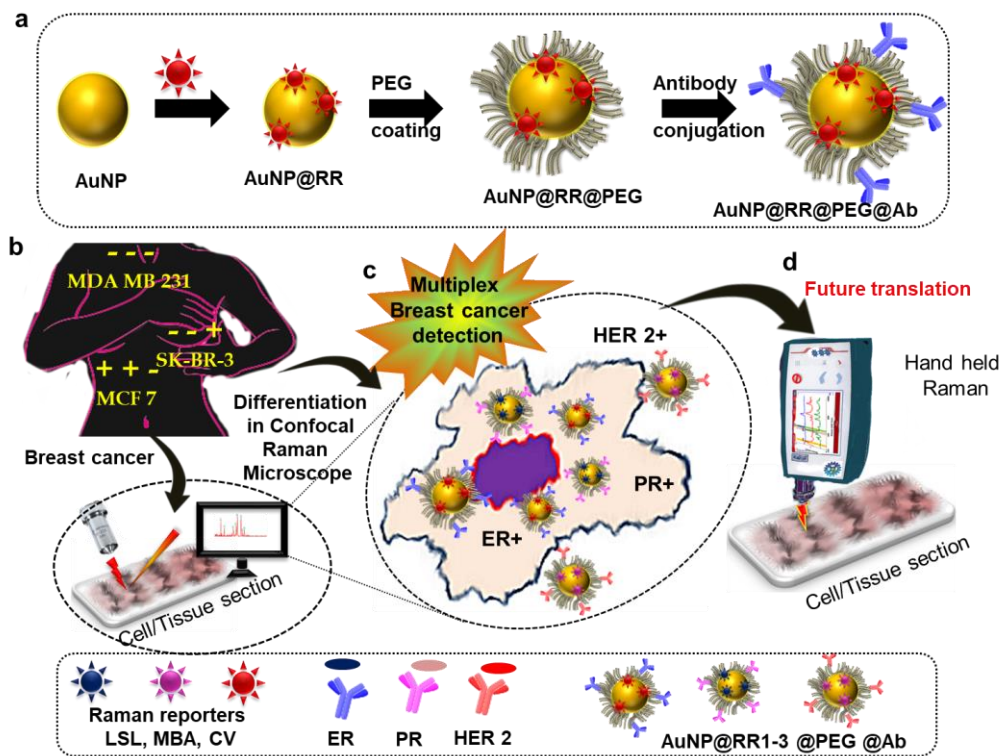
Scheme 4.1: Schematic illustration for experimental design for differentiating the clinically relevant triple biomarkers, ER, PR and HER2. a) Preparation strategy for the multiplexed SERS-tags by using AuNPs based substrate, b) biomarker detection of ER, PR and HER2 biomarker in three cell lines (MCF7, MDA-MB-231and SK-BR-3) having differential expression using confocal Raman microscope c) representative design for detection of biomarkers in cells/tissues by SERS-tags, d) SERS analysis in retrospective paraffin embedded breast tissue samples after antigen retrieval using a futuristic hand held Raman system.

Herein, SERS-tags were fabricated for the simultaneous detection of ER, PR and HER2 overexpression in a multiplex fashion in heterogenous breast cancer for developing better treatment strategies. Three different Raman reporters having non overlapping peaks were selected for preparing colloidal AuNPs based SERS-tags with respective targeting monoclonal antibodies. Expression status of ER, PR and HER2 biomarker proteins were monitored in three different cell line models having differential expression of the respective receptors. The study was extended to clinical samples as paraffin embedded breast cancer tissues. The tissue samples upon antigen retrieval step incubated with the nanotag cocktail provided SERS spectral pattern containing multiplexing peaks corresponding to each biomarker's expression status. Collectively, these findings turn out to be a facile, accurate and reliable technique to use it as a prognostic analysis for breast cancer.

4.3   Results and Discussion

4.3.1   Fabrication of SERS substrate

SERS substrate was chosen as AuNPs around 40-45 nm size for the development of multiplexed SERS-tags for the differential detection of breast cancer biomarkers, viz. ER, PR and HER2. Characterizations of the synthesized SERS substrate were confirmed by UV-vis Spectroscopy, HR-TEM and DLS. A 527 nm plasmonic peak was visualized by UV-vis spectroscopy which confirmed the size ranged of the AuNPs. Spherical shape and monodispersity of the particles were observed by HR-TEM analysis. Further, hydrodynamic diameter of about 60 nm was confirmed in the DLS analysis (**Figure 4.1**).
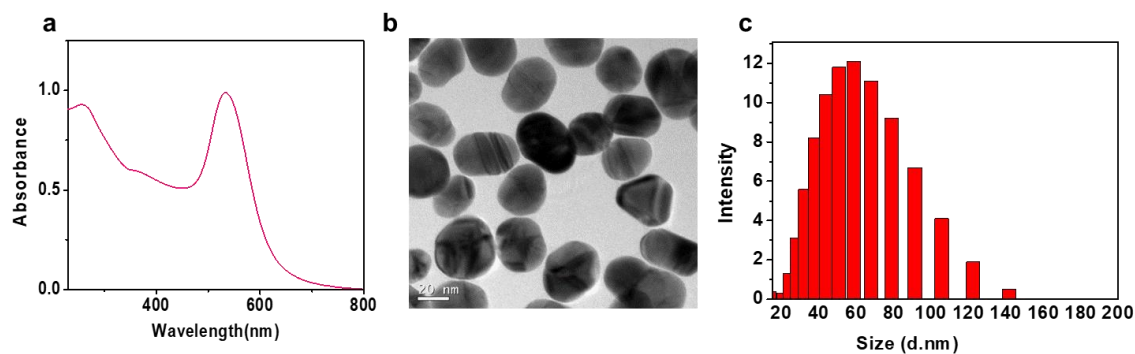
Figure 4.1: Characterization of AuNPs as the SERS substrate. a) UV-vis absorbance, b) HR-TEM, c) DLS analysis.

4.3.2   Multiplexing capability of Raman reporters

Multiplexing SERS nanotags for ER, PR and HER2 biomarkers were fabricated by the labelling three different Raman reporter dyes having specific non-overlapping signature peaks. The Raman reporters identified for multiplexing analysis were commercially purchased crystal violet (CV), 4-mercapto benzoic acid (MBA) and in-house synthesized squaraine based Raman reporter (LSL)[34] possessing unique non-overlapping multiplexing SERS peaks at 440, 1075 and 580 cm^{-1} respectively.
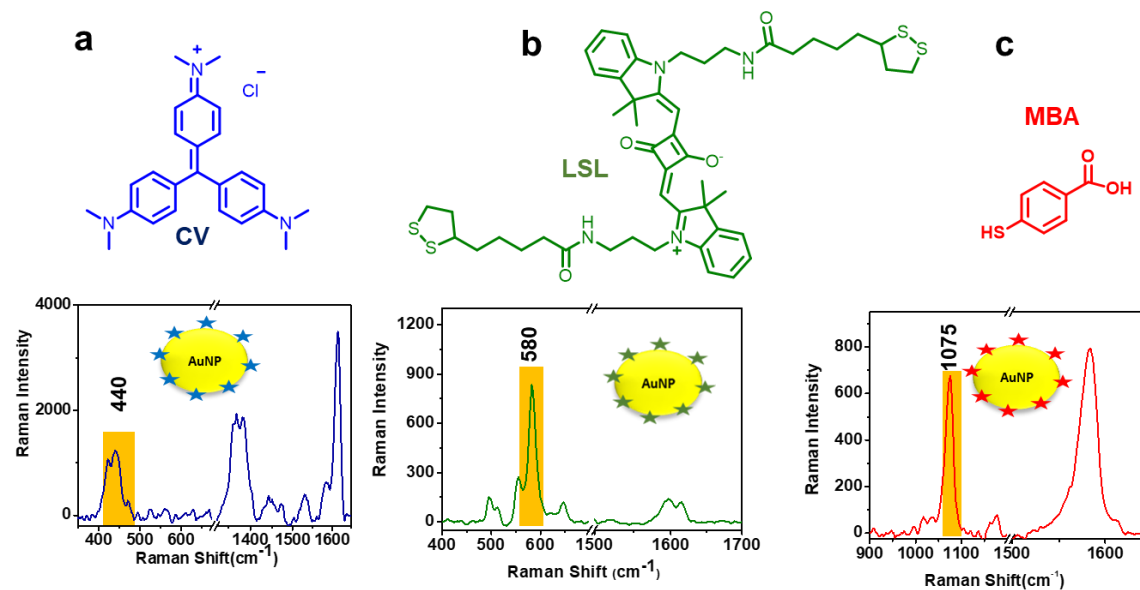
Figure 4.2: Structure and SERS fingerprint pattern of Raman reporters selected for the multiplexing study, **a**) Crystal Violet multiplexing peak at 440 cm^{-1}, b) Squaraine dye multiplexing peak at 580 cm^{-1}and c) Mercapto benzoic acid multiplexing peak at 1075 cm^{-1}.

The concentrations of the Raman reporters were selected based on its highest and stable SERS intensity using the AuNPs at 2 µM for CV, 20 µM for MBA and 0.5 µM for LSL per ml of the nanotag solution. The structure and fingerprint pattern of the selected Raman reporters were depicted in **Figure 4.2**. The stacked multiplexed pattern with specific multiplexing peak is shown in **Figure 4.3.**
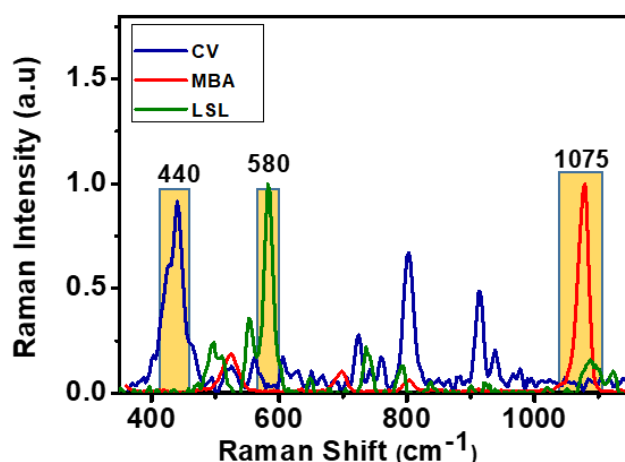
Figure 4.3: Non-overlapping multiplexing peaks of the Raman reporters CV, MBA and LSL by SERS analysis.

4.3.3 Pegylated and antibody conjugated biocompatible SERS-tags

For enabling biocompatibility and stability of the nanoprobe, PEG encapsulation was performed in the AuNPs incorporated Raman reporter. This reduces the toxicity of the Raman reporter and imparts functionalization for antibody conjugation as well. A slight plasmon shift of the AuNPs about 3 nm was visualized in UV-Vis spectroscopy from 527 nm to 530 nm and a 2-3 nm sized layer of PEG was identified in HR-TEM analysis. Furthermore, hydrodynamic diameter of the nanoparticle around 70 nm was observed in DLS which confirmed successful PEG encapsulation (**Figure 4.4**).
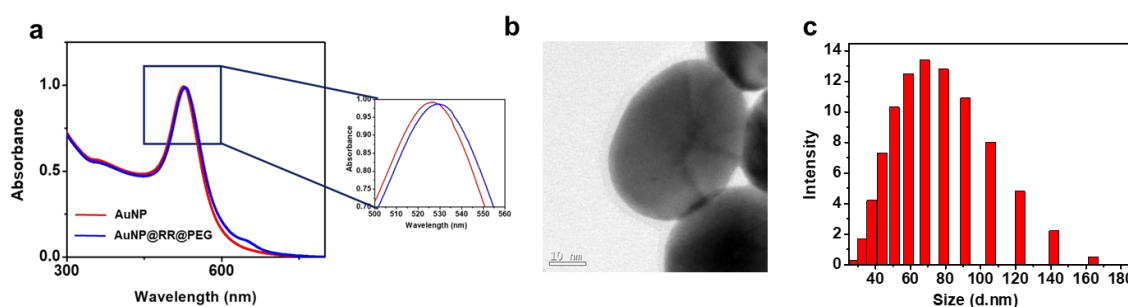
Figure 4.4: Characterization of pegylated nanoconstructs. a) UV-Vis absorbance of AuNPs and AuNP@RR@PEG, where "RR" is Raman Reporter, inset showing the shift after pegylation, b) HR-TEM and c) DLS analysis.

4.3.4 Conjugation of targeting antibodies to the pegylated SERS-tags

Three multiplexing SERS-tags were envisioned to develop for the detection of clinically applicable biomarkers in breast cancer. The detection of triple biomarkers ER, PR and HER2 are relevant for developing breast cancer treatment strategies. Hence these biomarkers were chosen which are prevalent in the subtypes of breast cancer. Thus, the corresponding antibodies of ER, PR and HER2 biomarkers were conjugated to the pegylated nanotags by the standard protocol for antibody conjugation.[32] The UV-Vis absorbance showed a 260 nm protein absorption peak with a slight 1-2 nm shift from the 530 nm plasmon peak confirming antibody conjugation (**Figure 4.5**).

Silver stained SDS-PAGE gel analysis also confirmed efficient antibody conjugation where the conjugated nanotag showed a slight upshift as indicated along with pure antibody (**Figure 4.6**).
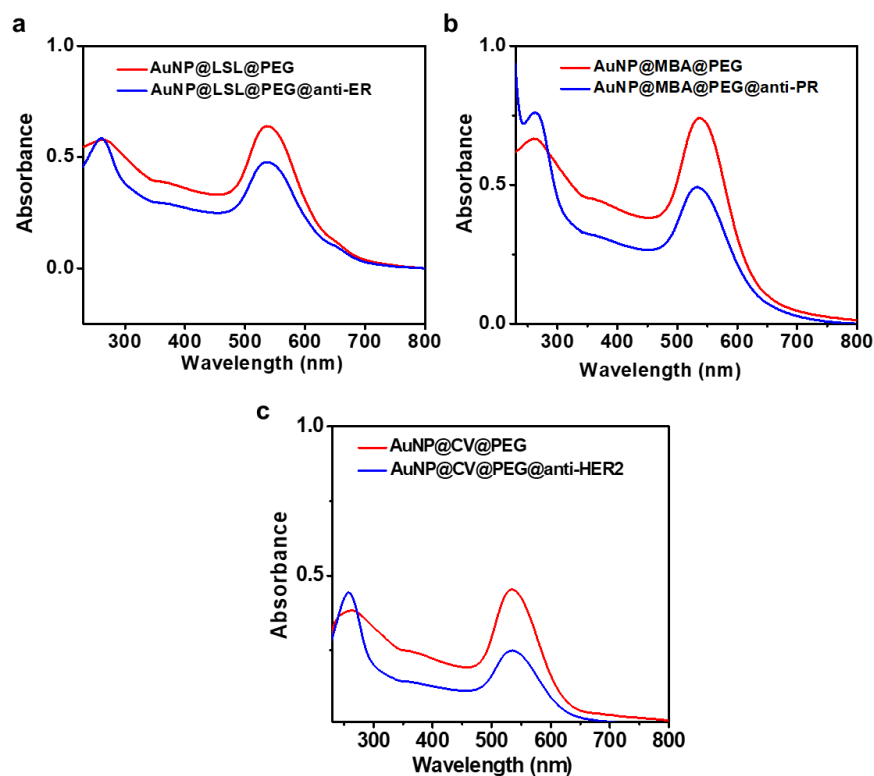
Figure 4.5: Characterization of antibody conjugated nanoconstructs by UV-vis spectroscopy comparing the Pegylated tags, a) AuNP@LSL@PEG@anti-ER, b) AuNP@MBA@PEG@anti-PR and c) AuNP@CV@PEG@anti-HER2.
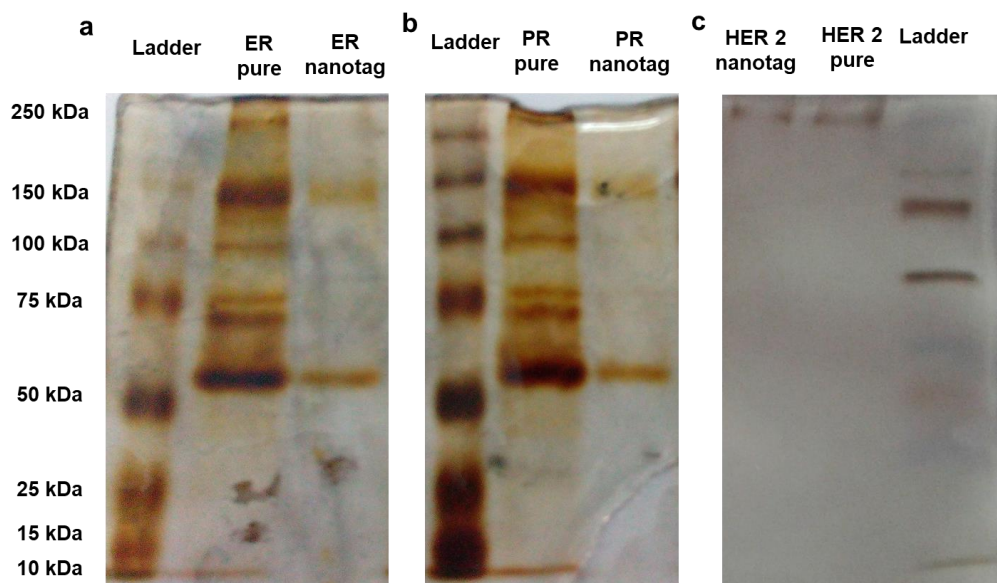
Figure 4.6: Characterization of antibody conjugated nanoconstructs by polyacrylamide gel electrophoretic technique, a) ladder, pure ER and ER nanotag, b) ladder, pure PR and PR nanotag and c) ladder, pure HER2 and HER2 nanotag.

Successful antibody conjugation was further confirmed by the 3, 3′, 5, 5′ Tetramethylbenzidine (TMB) assay. The formation of yellow colour formation indicated the presence of ER, PR and HER2 antibody bound to the NPs (**Figure 4.7**).
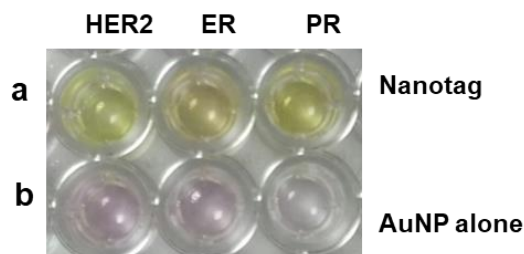
Figure 4.7: Characterization of antibody conjugated nanoconstructs by TMB assay, a) SERS-tags for HER2, ER and PR and b) AuNPs alone.

Furthermore, the SERS analysis of the antibody conjugated nanotags possessed excellent SERS intensity, even though a slight decrease was observed due to the particle loss during the process of antibody conjugation (**Figure 4.8**).
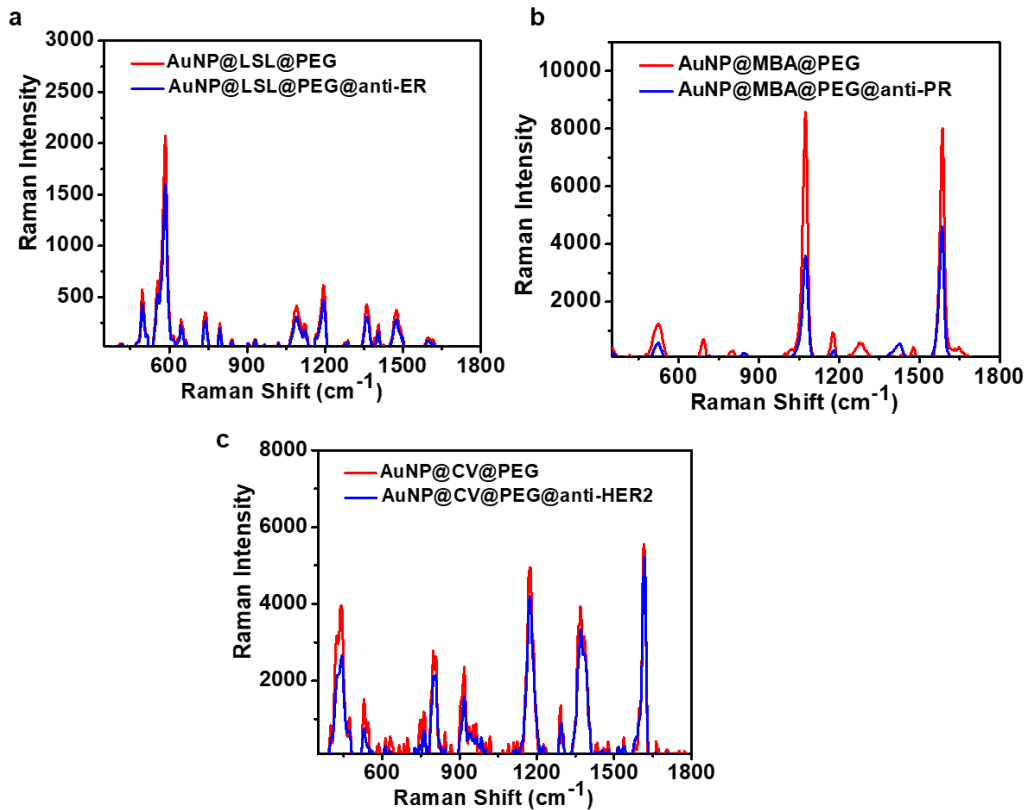
Figure 4.8: Characterization of antibody conjugated nanoconstructs by SERS analysis comparing the Pegylated tags, a) AuNP@LSL@PEG@anti-ER, b) AuNP@MBA@PEG@anti-PR and c) AuNP@CV@PEG@anti-HER2.

4.3.5 Western blot analysis

The expression level of the biomarkers in cell lines were performed by western blot analysis using respective antibodies with beta actin as the control (**Figure 4.9**). ER⁺ PR⁺ cell line, MCF7, ER⁻PR⁻ HER2⁻ cell line, MDA-MB-231 and HER⁺ cell line, SK-BR-3 were selected for the study as per the already reported expression status.[35] The ER and PR were found overexpressed in MCF7 cell line when compared with triple negative MDA-MB-231 cell line. HER2 overexpression was confirmed in SK-BR-3 cell line when matched with MDA-MB-231 cell line (**Figure 4.9**).
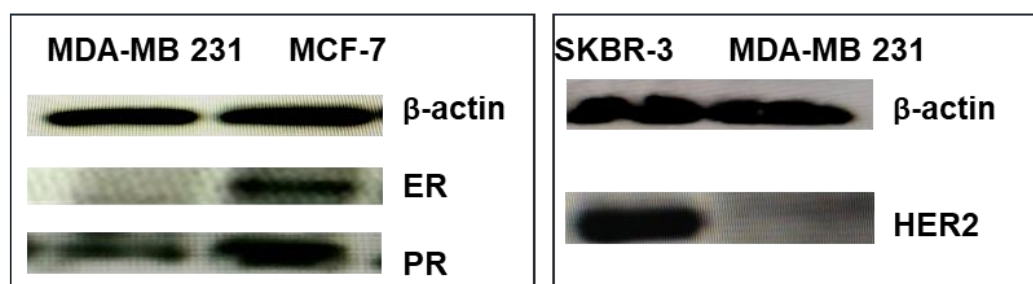
Figure 4.9: Evaluation of overexpression of ER, PR and HER2 in breast cancer cell lines by Western blot.

4.3.6 Immunophenotyping of cell lines by flow cytometry

Overexpression of the ER, PR and HER2 biomarkers were further confirmed by immunophenotyping analysis of the cells by flow cytometry. The expression status of ER was high in MCF7 cell line when compared with MDA-MB-231 and SK-BR-3 cells. Blank and isotype control were run along with the analysis. The shift in the FITC axis was evident from **Figure 4.10**. Thus, the cell lines were justified for SERS-tag based detection strategy.

The expression status of PR was also evaluated and from the **Figure 4.11**, it was clear that PR expression was high in MCF7 cell line when compared with MDA-MB-231 and SK-BR-3 cells. The shift in the fluorescein isothiocyanate (FITC) axis was significant for PR in MCF7when compared with other cells (**Figure 4.11**).
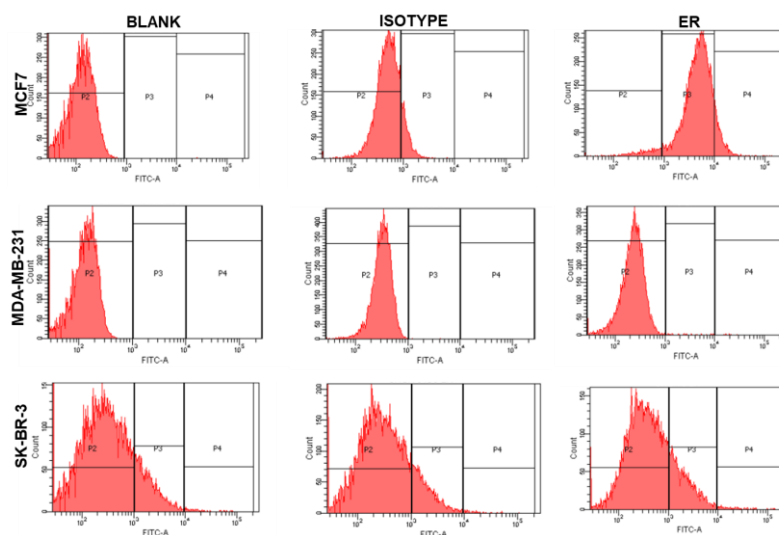
Figure 4.10: Evaluation of overexpression of ER along with blank and isotype control in breast cancer cell lines, MCF7, MDA-MB-231 and SK-BR-3 by immunophenotyping flow cytometry analysis.
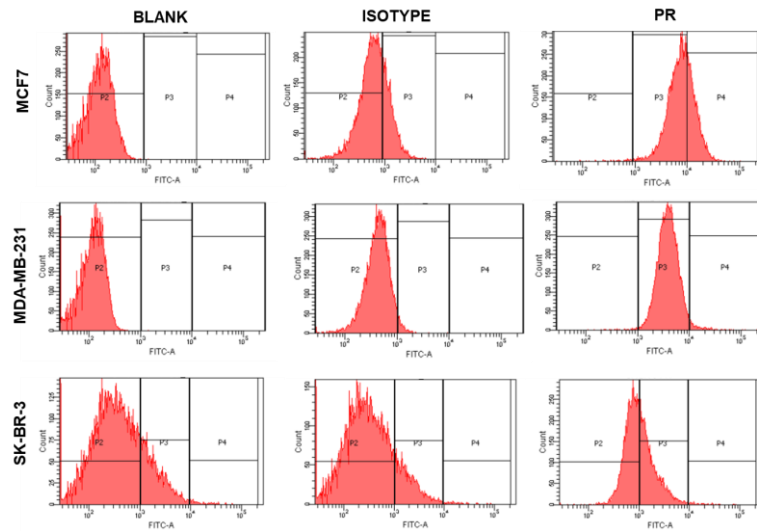
Figure 4.11: Evaluation of overexpression of PR along with blank and isotype control in breast cancer cell lines, MCF7, MDA-MB-231 and SK-BR-3 by immunophenotyping flow cytometry analysis.

Finally, the expression status of HER2 showed high expression in SK-BR-3 cell line when compared with MCF7 and SK-BR-3 cells. The shift in the FITC axis was significant compared with other cells (**Figure 4.12**).
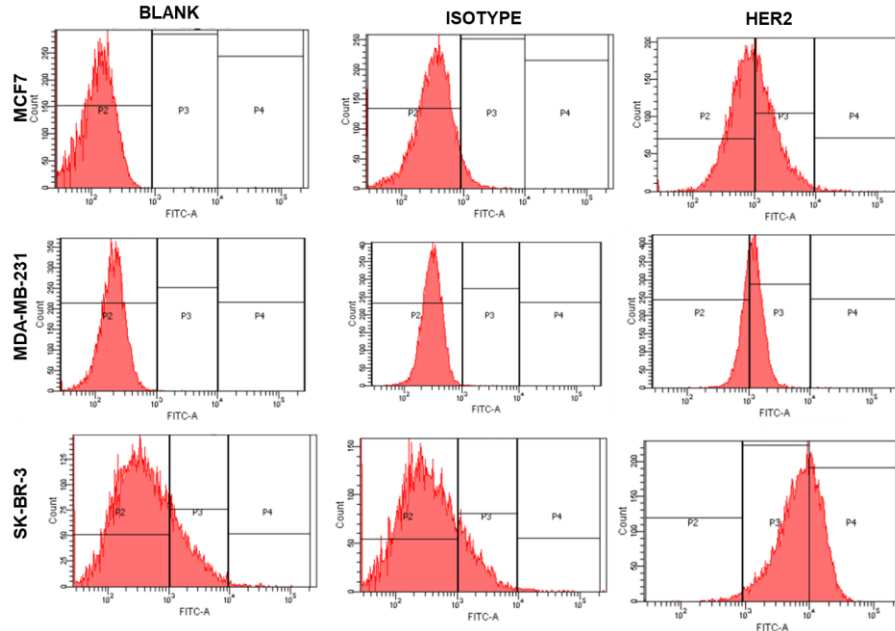
Figure 4.12: Evaluation of overexpression of HER2 along with blank and isotype control in breast cancer cell lines, MCF7, MDA-MB-231 and SK-BR-3 by immunophenotyping flow cytometry analysis.

4.3.7 Cell viability evaluation of SERS-tags

The cytotoxicity of the SERS-tags were performed prior to the cell line based SERS studies to find a optimal concentration for preventing cytotoxicity induced cell detachment during washing after nanotag treatment.
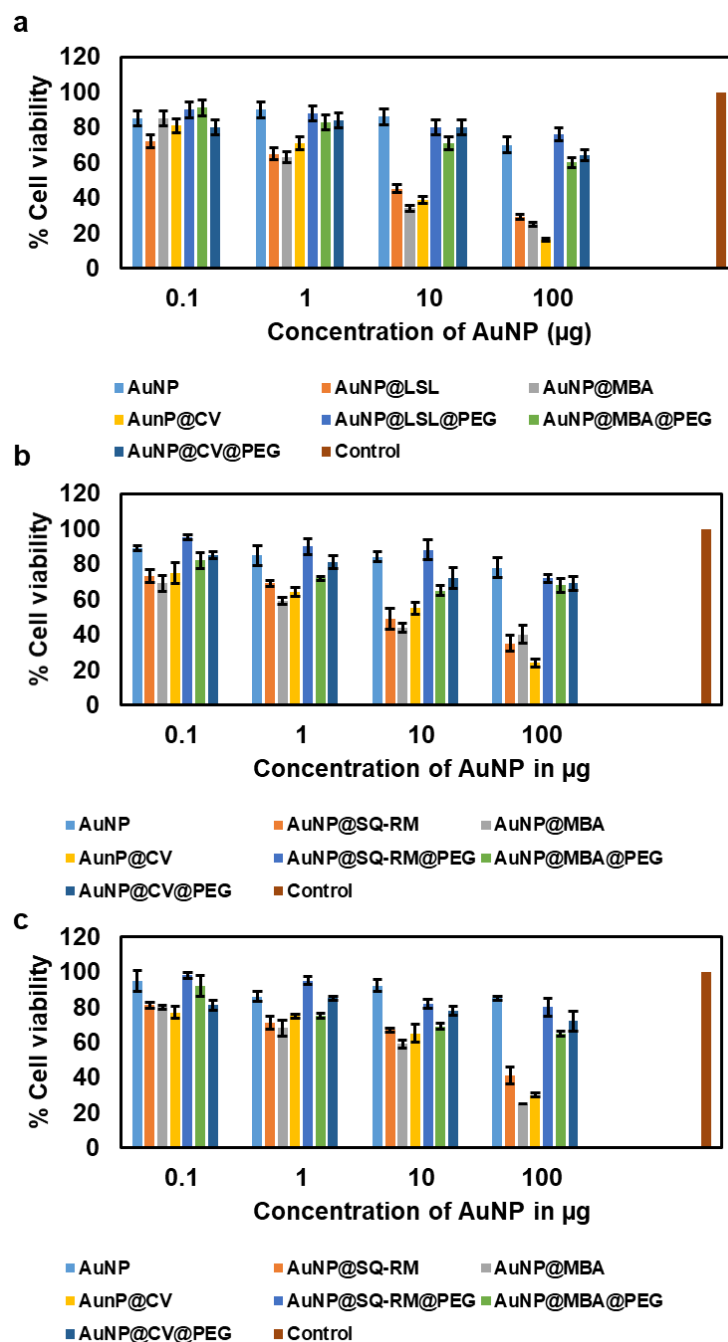
Figure 4.13: Cell viability assay after treatment with the SERS-tags, a) in MCF7, b) MDA-MB-231 and c) SK-BR-3 cell line. Average of three independent experiments.

The concentrations of Raman reporters selected based on the best SERS activity were 2 μM for CV, 20 μM for MBA and 0.5 μM for LSL per ml of the nanotag solution. Different concentrations in terms of the content of AuNPs were selected as 0.1, 1, 10 and 100 μg and the cell viability were performed using MTT assay in MCF7, MDA-MB-231 and SK-BR-3 cell line (**Figure 4.13**). Concentration related reduction in cell viability was observed in the MTT assay. It was found that around 80 % cell viability was observed for all the concentrations of AuNPs in all the three cell lines. The dye with AuNPs showed significant toxicity in all the three cell lines with increasing concentrations, but the PEG encapsulated construct of all the dyes increased the cell viability to around 70-80% assuring its utility in cell based SERS detection analysis.

4.3.8 SERS imaging analysis in cell lines

The ER, PR and HER2 conjugated SERS nanotags were employed to demonstrate the detection of the respective biomarkers in ER^+PR^+ cell line, MCF7, ER^- PR^- $HER2^-$ cell line, MDA-MB-231 and HER^+ cell line, SK-BR-3. The assessment was initiated upon incubation with AuNP@LSL@PEG@anti-ER tag and AuNP@MBA@PEG@anti-PR tag, in MCF7 cells. A prominent SERS fingerprint were observed at 580 and 1075 cm^{-1} from the nuclear region indicating the abundance of ER and PR receptors. The HER2 expression in SK-BR-3 was also visualized using AuNP@CV@PEG@anti-HER2 tag showing a prominent peak of CV at 440 cm^{-1} only in the cell surface area. A distinct bright field image of the cell, corresponding Raman image, cluster image are depicted in **Figure 4.14 a, b and c**. The corresponding average spectra based on signature peak of the SERS-mapped images are presented in **Figure 4.14 e**.
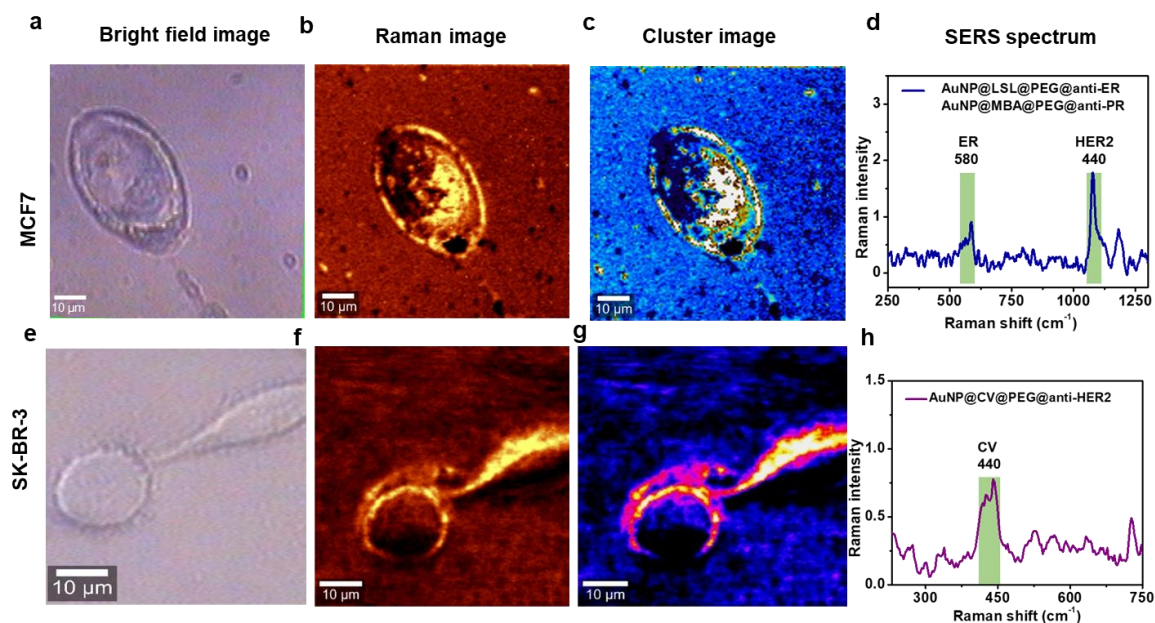
Figure 4.14: SERS analysis in ER⁺ PR⁺ cell line. MCF7; a) bright field image, b) Raman Image, c) cluster image, d) mean SERS spectrum after treatment with AuNP@LSL@PEG@anti-ER and AuNP@MBA@PEG@anti-PR , e) bright field image, f) Raman Image, g) cluster image and h) mean SERS spectrum after treatment with AuNP@CV@PEG@anti-HER2.

Similarly, the triple negative MDA-MB-231 cell lines revealed only minimal expression all the three tags. The bright field, Raman image and corresponding average spectrum of WI-38 cell line also represented in **Figure 4.15**.
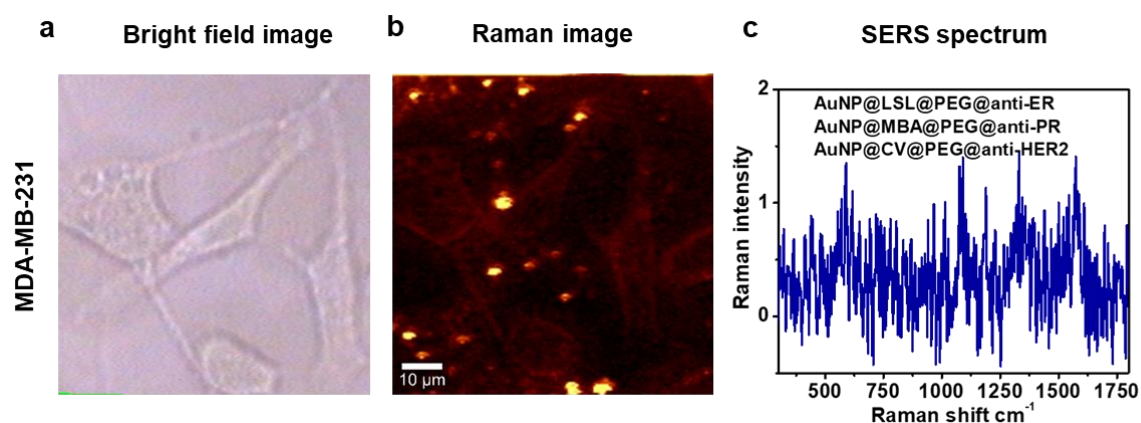
Figure 4.15: SERS analysis in ER⁻ PR⁻HER2⁻ cell line, MDA-MB-231, a) bright field image, b) Raman image and c) mean SERS spectrum after treatment with AuNP@LSL@PEG@anti-ER, AuNP@MBA@PEG@anti-PR and AuNP@CV@PEG@anti-HER2.

4.3.9 Dark field analysis in cell lines

The SERS nanotag based recognition of the biomarkers in breast cancer cell lines were further established by dark field microscopy. The localized metallic nanoparticles were visualized as bright spots in a dark background.[36] The analysis performed in MCF7, MDA-MB-231 and SK-BR-3 cell lines showed excellent internalization of the targeted SERS nanotags corroborating the results from SERS imaging. Accumulation of ER and PR nanotags were found in MCF7 cell line while HER2 nanotags were solely gathered in the cell surface area when compared with the untreated control. Negligible uptake of ER and PR nanotags were observed in MDA-MB-231 and SK-BR-3 cell lines. HER2 nanotag accumulation was less in MCF-7 and MDA-MB 231 cell lines (**Figure 4.16**). Thus a proof-of concept was revealed in both SERS modality and dark field microscopy assuring the excellent targetability of the SERS nanotags in real breast cancer paraffin embedded tissue samples.
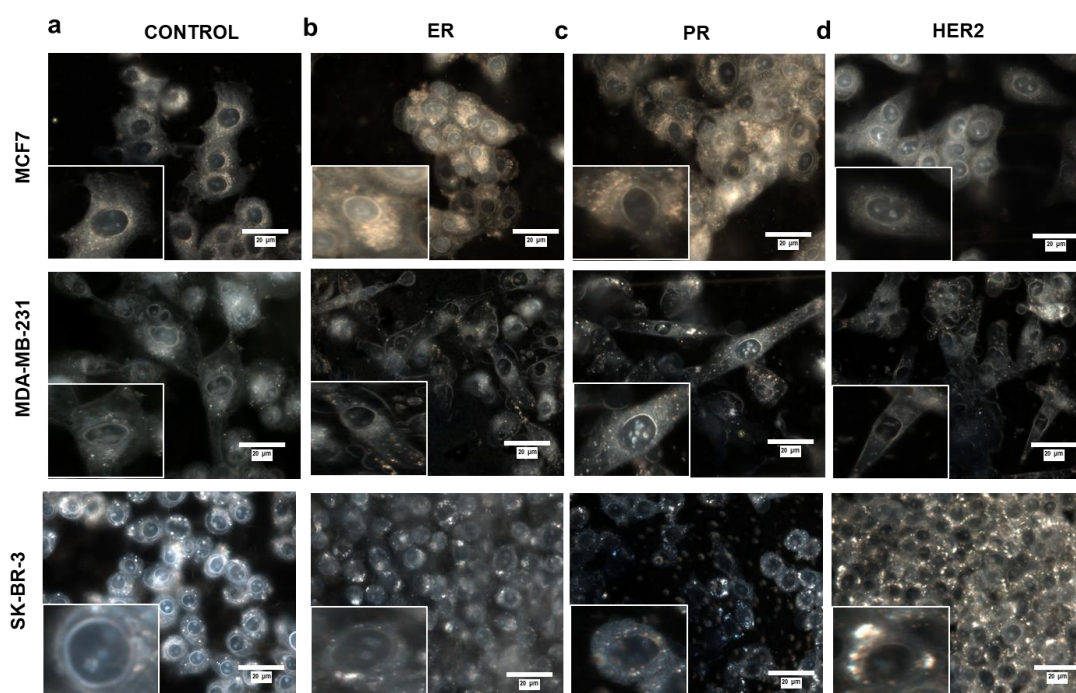
Figure 4.16: Uptake analysis of targeted SERS nanotags in MCF7, MDA-MB-231 and SK-BR-3 cell lines by dark field microscopy. a) untreated control, b) treated with AuNP@LSL@PEG@anti-ER, b) with AuNP@MBA@PEG@anti-PR and c) with AuNP@CV@PEG@anti-HER2.

4.3.10 Biomarker evaluation in breast tissue samples by SERS-tags

The SERS analysis guided recognition was implemented by the precise modulation of the three different biomarker targeted antibody conjugated SERS nanotags in clinically confirmed paraffin embedded breast cancer tissue samples. The SERS analysis in paraffin removed tissues was compared with the conventional immunohistochemical (IHC) analysis. In an IHC confirmed ER⁺ HER2⁻ tissue samples, incubation of SERS nanotag cocktail, AuNP@LSL@PEG@anti-ER and AuNP@CV@PEG@anti-HER2, resulted in the generation of 580 cm⁻¹ peak indicating the overexpression of ER biomarker (**Figure 4.17**). The absence of significant peak from 440 cm⁻¹ confirmed the less expression of HER2 in the tissue sample.

Likewise, in an IHC confirmed ER⁻ HER2⁺ tissue, incubation of SERS nanotag cocktail, AuNP@LSL@PEG@anti-ER and AuNP@CV@PEG@anti-HER2, resulted in the generation of 440 cm⁻¹ peak indicating the overexpression of HER2 biomarker (**Figure 4.18**). The absence of significant peak from 580 cm⁻¹ confirmed the less expression of ER in the tissue sample.
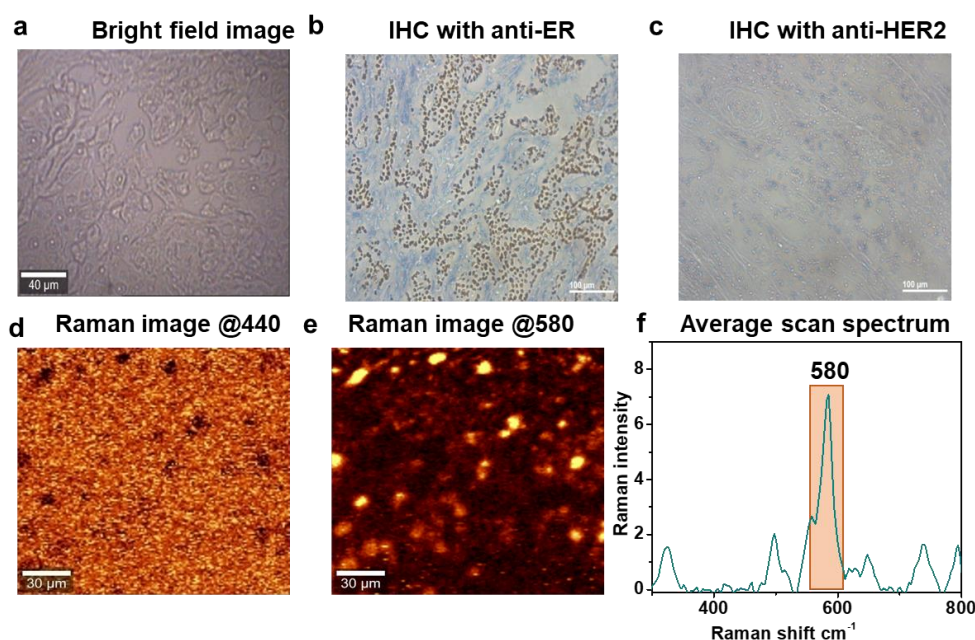
Figure 4.17: Immunohistochemistry analysis of ER⁺ HER2⁻ tissue. a) bright field image, b) IHC image with anti-ER, c) IHC image with anti-HER2 and SERS analysis of ER⁺ HER2⁻ tissue using AuNP@LSL@PEG@anti-ER and AuNP@CV@PEG@anti-HER2 nanotags, d) Raman image at 440 cm⁻¹ peak, e) Raman image at 580 cm⁻¹ peak and f) SERS average spectrum from the image scan of 580 cm⁻¹ peak.
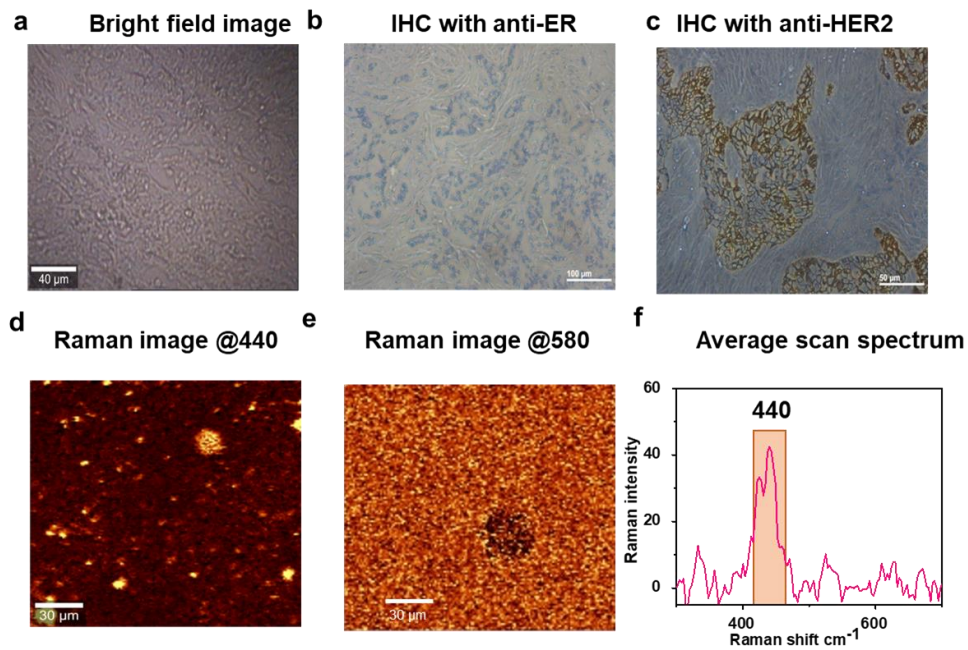
Figure 4.18: Immunohistochemistry analysis of ER⁻ HER2⁺ tissue. a) bright field image, b) IHC image with anti-ER, c) IHC image with anti-HER2 and SERS analysis of ER⁻ HER2⁺ tissue using AuNP@LSL@PEG@anti-ER and AuNP@CV@PEG@anti-HER2 nanotags, d) Raman image at 440 cm⁻¹ peak, e) Raman image at 580 cm⁻¹ peak and f) SERS average spectrum from the image scan of 440 cm⁻¹ peak.

Further, an ER⁺ HER2⁺ tissue was selected and upon incubation with SERS nanotag cocktail containing AuNP@LSL@PEG@anti-ER and AuNP@CV@PEG@anti-HER2, resu-lted in the generation of both 580 and 440 cm⁻¹ peak indicating the overexpression of both ER and HER2 biomarker (**Figure 4.19**).
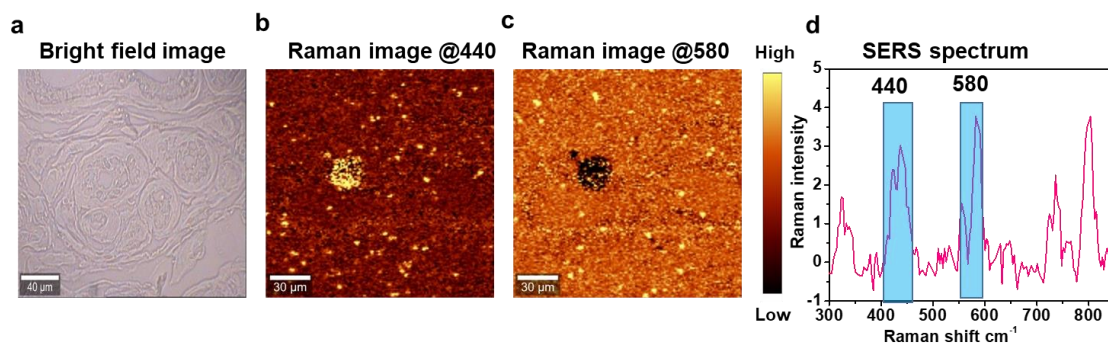
Figure 4.19: SERS analysis of ER⁺ HER2⁺ tissue using AuNP@LSL@PEG@anti-ER and AuNP@CV@PEG@anti-HER2 nanotag. a) Bright field image d) Raman image at 440 cm⁻¹ peak, e) Raman image at 580 cm⁻¹ peak and f) SERS average spectrum from the image scan of 440 cm⁻¹ and 580 cm⁻¹ peak.

When an ER⁻ HER2⁻ was incubated with SERS nanotag cocktail containing AuNP@LSL@PEG@anti-ER and AuNP@CV@PEG@anti-HER2, it resulted in the

generation of none of the 580 and 440 cm^{-1} peak indicating the less expression of both ER and HER2 biomarker (**Figure 4.20**).
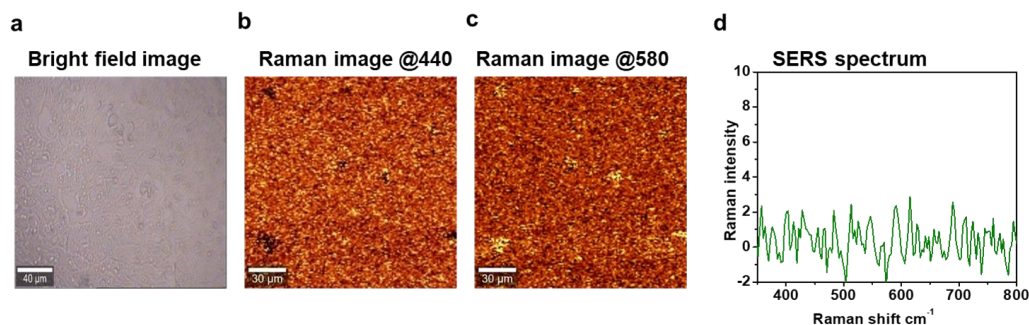
Figure 4.20: SERS analysis of ER$^-$ HER2$^-$ tissue using AuNP@CV@PEG@anti-HER2 and AuNP@LSL@PEG@anti-ER nanotags. a) Bright field image d) Raman image at 440 cm^{-1} peak, e) Raman image at 580 cm^{-1} peak and f) SERS average spectrum from the image scan of 440 cm^{-1} and 580 cm^{-1} peak.

Finally, the incubation of all the three SERS nanotag cocktail containing AuNP@LSL@PEG@anti-ER, AuNP@MBA@PEG@anti-PR and AuNP@CV@PEG@anti-HER2 in ER$^+$ PR$^+$ HER2$^+$ tissue resulted in the generation of all the multiplexing peaks, 580, 1075 and 440 cm^{-1} peak indicating the overexpression of ER, PR and HER2 biomarker (**Figure 4.21**).
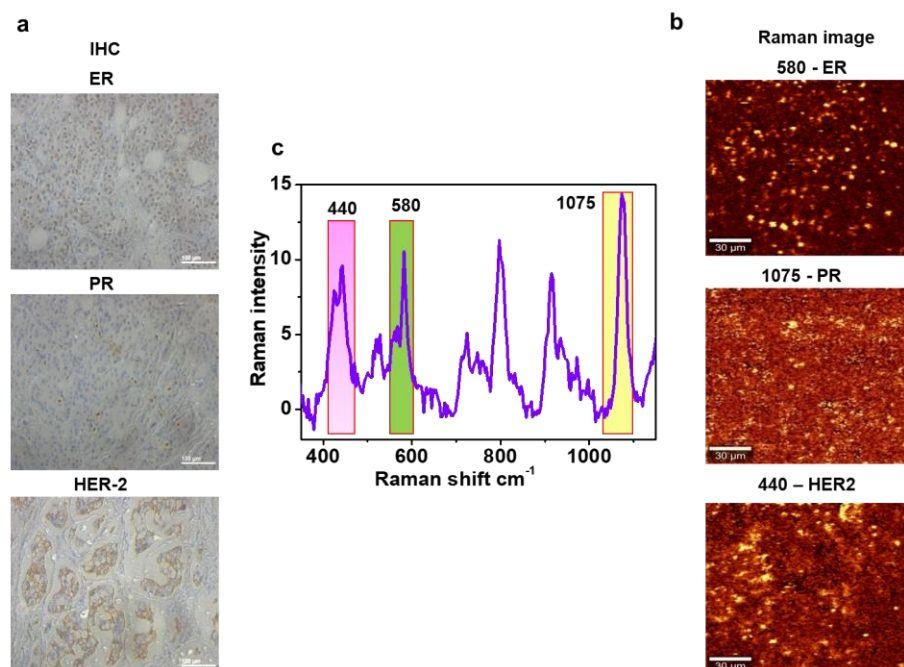
Figure 4.21: SERS analysis of ER$^+$ PR$^+$ HER2$^+$tissue using AuNP@LSL@PEG@anti-ER, AuNP@MBA@PEG@anti-PR and AuNP@CV@PEG@anti-HER2 nanotags. a) IHC image b) Raman image and c) SERS average spectrum from the image scan of 440 cm^{-1}, 580 cm^{-1} and 1075 cm^{-1} peak.

4.4 Experimental Section

4.4.1 Chemicals and reagents.

All chemicals were bought from Sigma-Aldrich unless otherwise mentioned. The ER, PR and HER2 antibodies were purchased from Abcam. Reagent grade solvents were used purchased from local companies. UV/vis spectroscopy analysis were performed using a UV-vis spectrophotometer (Shimadzu UV- 2600).

4.4.2 SERS substrate preparation

AuNPs of size around 40-45 nm were synthesized by the standard protocol for citrate reduction method. 50 ml ultrapure water was taken in a 100 ml round bottom flask with a magnetic bead. The solution was heated until boiling and 0.25 M gold chloride solution was added. After 10 min, 0.1 M of trisodium citrate solution was added with a resultant in a color change from dark purple to red taking about 5 min. Further, with constant stirring, the solution was permitted to cool for 1.5 hr. The as synthesized nanoparticles were characterized using UV-Vis Spectroscopy, TEM and DLS.

4.4.3 PEG encapsulation

The obtained nanoparticles were concentrated in 9:1 ratio with the Raman reporter. The NPs with the Raman reporter was incubated around 20 min in a tube rotator. Further the AuNP-dye mix was coated with a PEG layer for tethering the functional groups for antibody binding. The carboxyl terminal PEG (100 μM) was added in the AuNP-dye solution in a microcentrifuge tube along with rapid mixing in a rotator. After 15 min of incubation, the solution was exposed to excess of thiol PEG (100 μM) which enhances surface coverage and stability. Excess PEG was removed by two rounds of centrifugation (8000 rpm, 20 min) and was resuspended in ultra- pure Milli-Q water. The PEG encapsulated nanoprobe in Milli-Q was replaced with MES buffer for covalent conjugation of the NH_2 group of antibody with the carboxyl terminal of heterofunctional PEG. PEG encapsulation was confirmed successfully by UV-Vis spectroscopy and HR-TEM analysis.

4.4.4 Antibody conjugation

The antibodies purchased were purified by centrifuge filters (Millipore) in column filtration system to remove the sodium azide preservative. The carboxylic functional groups in the PEG coated nanotag were stimulated by EDC (25 mM) and NHS (25 mM) by incubating for 30 min. Excess of EDC and NHS were discarded by 2 rounds of centrifugation (8000 rpm, 10 min). The solution re-suspended in MES buffer and added with the respective antibody (ER/PR/HER2) [4 µg] incubated at 25 °C for 2 h. Later the nanotags were stored at 4°C overnight. The unbound antibodies were further removed by a centrifugation for 5 min at 10000 rpm thrice. The washed pellet containing the antibody conjugated probes were then re-suspended in fresh MES buffer and stored at 4°C. The confirmatory analysis for antibody conjugation was performed by UV-Vis spectroscopy and SDS-PAGE.

4.4.5 TMB assay

After conjugation with the antibody, nanotags were incubated with horse radish peroxidase (HRP)-labelled secondary antibody at room temperature (RT) for 1 h with gentle shaking. Further, the nanotags were washed with 1X PBS and centrifuged to remove the supernatant (3 times). Antibody conjugated nanotags were then incubated at RT for 1 h with blocking buffer. BSA (3%) in PBST was used as blocking buffer. After incubation, nanotags were washed with 1X PBS three times, with change of PBS every five minutes. SERS nanotag (25 µL) and PBS (25 µL) were added to the wells (1:1 ratio) of 96 well plate. TMB/H_2O_2 substrate was added to the nanotag followed by 30 min incubation in dark. The formation of yellow color indicates the presence of antibody bound to the NPs. After 30 min, stop solution (0.18M sulphuric acid) was added and the yellow colored product formed was measured at 450 nm.

4.4.6 Cell culture

The human breast cancer cell lines MCF7, MDA-MB-231, SK-BR-3 were obtained from American Type Culture Collection (ATCC). DMEM was used for the growth of the cell lines with 10 % fetal bovine serum and 1% antibiotics (penicillin/streptomycin mixture) at 37 °C under 5 % CO_2 atmosphere.

4.4.7 Western blot analysis

Proteins were extracted from cell lines MCF7, MDA-MB-231, SK-BR-3 using RIPA buffer (Sigma) and the yield was estimated using BCA assay (Thermo Pierce). Proteins were run using 12% SDS-PAGE gel and further transferred to PVDF membrane for blotting. The membrane was blocked with 5 % skim milk and was further incubated with primary antibodies. HRP conjugated secondary antibody was used for the hyper substrate (Takara Clontech) detection in gel documentation System (Biorad). The as obtained bands were quantified using Image J software normalizing with β-actin.

4.4.8 Cytotoxicity analysis

The cytotoxicity of the nanotag were measured in cell lines MCF7, MDA-MB-231, SK-BR-using MTT assay. The reduction of a tetrazolium salt by mitochondrial dehyd-rogenases in viable cells correlates with the extend of viability. Cell suspension containing approximately 10000 cells/well were seeded into a 96-well flat bottom glass plate and 100 μl of the nanoprobes at different concentrations were added to each wells in triplicates. The plate was further incubated in a CO_2 incubator at 37 °C for 24 h. After incubation, 0.5 mg/ml of MTT (100 μl) was added to each well incubating for 3 h. The formazan crystals developed which is insoluble were solubilized by DMSO solution incubated for 30 min. The absorbance was analysed using a microplate reader (BioTek Synergy H1 multimode plate reader) at 570 nm. The viability percentage for each construct relative to its control were measured based on the following formula, i.e. Viability (%) = Absorbance of treated /Absorbance of Control x 100.

4.4.9 SERS Imaging

SERS detection of breast cancer cell lines MCF7, MDA-MB-231, SK-BR-3 were implemented using confocal Raman microscopy. Cells were cultured in 4 well culture slides at a seeding density of 10^4 cells/well incubated with the nanoprobes and washed with PBS solution twice at pH 7.4 to remove the excess probes. SERS experiments were performed using a WITec Raman microscope (WITec, Inc., Germany) involving 600 g/mm grating and a detector unit, Peltier cooled charge-

coupled device. Excitation of the sample were done at 10 mW power and 633 nm laser. The spectra were acquired in the region of 400-1800 cm^{-1} with 3 cm^{-1} resolution and 10 s integration time with 3 accumulations. Prior to each experiment, silicon standard calibration was performed. The images were acquired on a 100 × 100 μm area along with 150 × 150 points per line having integration time of 0.01 s. The data processing was performed using software package, WITec Project 5.2 Plus (v2.1). The background noises was removed by a 4th polynomial function and smoothening of the spectra was performed by Savitzky- Golay.

4.4.10 Dark field imaging

Dark field imaging of cell lines, MCF7, MDA-MB-231, SK-BR-3 were achieved with a 60X oil immersion objective using CytoViva Enhanced Dark field illumination System 2.0. (BX 43F). The cells were cultured in four chambered culture slide at a seeding density of 10^4 cells/well incubated with the nanoconstructs for about 4 h and subsequent PBS washing twice with a pH 7.4 to clear the excess probes.

4.4.11 Paraffin embedded tissue sample collection and processing

Breast cancer tissue samples having differential biomarker expression status were obtained from Regional Cancer Centre, Thiruvananthapuram for SERS analysis. Ethical approval for the same was obtained from the respective authorities prior to the experiments. Preceding spectral analysis, tissue processing was performed by standardized steps specifically for the paraffin embedded formalin fixed tissue blocks. The deparaffinization in xylene was performed by repeated xylene wash thrice for 10-30 min each followed by hydration in different alcohol grades (absolute ethanol for 5-10 min each, 95 % ethanol for 5-10 min, 70 % ethanol for 5-10 min, 50 % ethanol for 5-10 min), then wash with distilled water for 5-10 min. For antigen retrieval, the specimens were treated with 10 mM citrate buffer (pH 6) at 500-700 W for 10 min in microwave oven and then kept for 1- 5 min rest. Then more volume of citrate buffer was added and again heated for 5-10 min at 500-700 W. The slides were allowed to cool at RT for 15-20 min and immersed in de-ionized water for 15-20 min at RT. Further, the slides were incubated with 3% BSA in PBS at RT followed by three times wash using PBS. The slides with the tissue were then incubated with antibody conjugated gold nanotags for 1-2 h in a humid chamber followed by 3-5 times PBS

wash. Raman spectral analysis and Raman imaging was performed under 633 / 785 nm laser.

4.4.12 Immunohistochemistry staining

The breast tissue sample were cut employing a microtome (Leica TP 1020) serially at 4 μm thickness and was transferred to APES coated slide incubating overnight at 60 °C. The staining involves a two day procedure. 1st day, before starting the protocol, the tissues were de-paraffinised by xylene (3 changes) for 10 min each. Further, the sections were hydrated in 95 %, 75 % to 50 % descending grade of alcohol from for 5 min each. The slides were then washed in water for 5 min. The next step was antigen retrieval, for which the slides were immersed in citrate buffer (10 mM) and microwaved in an oven at 700 W for 10 min. The slides were cooled for 1 min and added with distilled water. Again the slides were microwaved at 600 W for 5 min followed by cooling for 15 min and washing with distilled water for 10 min. Blockage of endogenous peroxidase activity was performed by peroxidase blocking buffer for 5 min followed TBS wash twice for 5 min. The slides were further incubated with protein block for 5 min followed by two times TBS was for 5 min. Then the slides were incubated with primary monoclonal antibody (ER/PR/HER2) with 1:100 dilution overnight at 4° C. Next day, washing of the slides were done twice in Tris buffered saline with Tween 20 (TBST) for 5 min. Post primary block was incubated in each slide for 30 min followed by two times TBST wash for 5 min. Then novolink polymer was incubated in the slides for 30 min followed by two times TBST wash for 5 min. Further, the slides were added with a visualizing agent, DAB, a chromogen. The slides were then rinsed with water for 1 min and immersed in counter stain haematoxylin for staining the nucleus. After that the slides were washed in running tap water. Further, the slides were dehydrated using 50 % and 95 % ascending grade of alcohol for 5 min and subsequently in absolute alcohol twice for 5 min. The slides were then rinsed twice for 10 min each in xylene. Finally, the slides were mounted using DPX with coverslip. The slides were then ready for observing through a microscope.

4.5   Conclusion

In summary, a SERS nanotags based multiplexing platform has been established for the accurate detection of clinically relevant biomarkers in breast cancer. A distinct sharp non-overlapping peaks from the Raman reporters enabled the detection of ER, PR and HER2 biomarkers in a specific and selective manner using antibody conjugated SERS nanotags. The analysis successfully exhibited multiplexed pattern in *in vitro* level as well as paraffin embedded retrospective clinically confirmed tissue samples from breast cancer patients. The study thus reveals a new diagnostic modality for the detection of tumors exhibiting differential biomarkers associated with patient to patient heterogeneity.

4.6   References

(1)   Bray, F.; Ferlay, J.; Soerjomataram, I.; Siegel, R. L.; Torre, L. A.; Jemal, A. Global Cancer Statistics 2018: GLOBOCAN Estimates of Incidence and Mortality Worldwide for 36 Cancers in 185 Countries. *CA. Cancer J. Clin.* **2018**, *68* (6), 394–424.

(2)   Coleman, M. P.; Quaresma, M.; Berrino, F.; Lutz, J. M.; De Angelis, R.; Capocaccia, R.; Baili, P.; Rachet, B.; Gatta, G.; Hakulinen, T.; et al. Cancer Survival in Five Continents: A Worldwide Population-Based Study (CONCORD). *Lancet Oncol.* **2008**, *9* (8), 730–756.

(3)   Weledji, E. P.; Tambe, J. Breast Cancer Detection and Screening. *Med. Clin. Rev.* **2018**, *04* (02), 1–12.

(4)   Shah, R.; Rosso, K.; David Nathanson, S. Pathogenesis, Prevention, Diagnosis and Treatment of Breast Cancer. *World J. Clin. Oncol.* **2014**, *5* (3), 283–298.

(5)   Goossens, N.; Nakagawa, S.; Sun, X.; Hoshida, Y. Cancer Biomarker Discovery and Validation. *Transl. Cancer Res.* **2015**, *4* (3), 256–269.

(6)   Russo, J.; Russo, I. H. The Role of Estrogen in the Initiation of Breast Cancer. *J. Steroid Biochem. Mol. Biol.* **2006**, *102* (1-5 SPEC. ISS.), 89–96.

(7)   Lange, C. A.; Yee, D. Progesterone and Breast Cancer. *Women's Heal.* **2008**, *4* (2), 151–162.

(8)   Costa, R. L. B.; Czerniecki, B. J. Clinical Development of Immunotherapies for HER2+ Breast Cancer: A Review of HER2-Directed Monoclonal Antibodies and

Beyond. *npj Breast Cancer* **2020**, *6* (10).

(9)   Duffy, M. J.; Harbeck, N.; Nap, M.; Molina, R.; Nicolini, A.; Senkus, E.; Cardoso, F. Clinical Use of Biomarkers in Breast Cancer: Updated Guidelines from the European Group on Tumor Markers (EGTM). *Eur. J. Cancer* **2017**, *75*, 284–298.

(10) Turashvili, G.; Brogi, E. Tumor Heterogeneity in Breast Cancer. *Front. Med.* **2017**, *4*, 227.

(11) Cornejo, K. M.; Kandil, D.; Khan, A.; Cosar, E. F. Theranostic and Molecular Classification of Breast Cancer. *Arch. Pathol. Lab. Med.* **2014**, *138* (1), 44–56.

(12) Hammond, M. E. H.; Hayes, D. F.; Dowsett, M.; Allred, D. C.; Hagerty, K. L.; Badve, S.; Fitzgibbons, P. L.; Francis, G.; Goldstein, N. S.; Hayes, M.; et al. American Society of Clinical Oncology/College of American Pathologists Guideline Recommendations for Immunohistochemical Testing of Estrogen and Progesterone Receptors in Breast Cancer. *J. Clin. Oncol.* **2010**, *28* (16), 2784–2795.

(13) Bogdanovska-Todorovska, M.; Kostadinova-Kunovska, S.; Jovanovik, R.; Krsteska, B.; Kondov, G.; Kondov, B.; Petrushevska, G. Correlation of Immunohistochemistry and Fluorescence in Situ Hybridization for HER-2 Assessment in Breast Cancer Patients: Single Centre Experience. *Open Access Maced. J. Med. Sci.* **2018**, *6* (4), 593–599.

(14) Wesoła, M.; Jeleń, M. A Comparison of IHC and FISH Cytogenetic Methods in the Evaluation of HER2 Status in Breast Cancer. *Adv. Clin. Exp. Med.* **2015**, *24* (5), 899–904.

(15) Furrer, D.; Sanschagrin, F.; Jacob, S.; Diorio, C. Advantages and Disadvantages of Technologies for HER2 Testing in Breast Cancer Specimens. *Am. J. Clin. Pathol.* **2015**, *144* (5), 686–703.

(16) Auner, G. W.; Koya, S. K.; Huang, C.; Broadbent, B.; Trexler, M.; Auner, Z.; Elias, A.; Mehne, K. C.; Brusatori, M. A. Applications of Raman Spectroscopy in Cancer Diagnosis. *Cancer Metastasis Rev.* **2018**, *37* (4), 691–717.

(17) Spring, H.; Cem, M. S. U. SERS Surface Enhanced Raman Spectroscopy. *Spring* **2001**.

(18) Guerrini, L.; Perez, N. P.; Rico, E. G.; Puebla, R. A. Cancer Characterization and Diagnosis with SERS - Encoded Particles. *Cancer Nanotechnol.* **2017**, *8* (5).

(19) Bae, P. K.; Chung, B. H. *Multiplexed Detection of Various Breast Cancer Cells by Perfluorocarbon/Quantum Dot Nanoemulsions Conjugated with Antibodies*; 2014.

(20) Zhou, L.; Wang, R.; Yao, C.; Li, X.; Wang, C.; Zhang, X.; Xu, C.; Zeng, A.; Zhao, D.; Zhang, F. Single-Band Upconversion Nanoprobes for Multiplexed Simultaneous in Situ Molecular Mapping of Cancer Biomarkers. *Nat. Commun.* **2015**, *6*, 1–10.

(21) Narayanan, N.; Karunakaran, V.; Paul, W.; Venugopal, K.; Sujathan, K.; Kumar Maiti, K. Aggregation Induced Raman Scattering of Squaraine Dye: Implementation in Diagnosis of Cervical Cancer Dysplasia by SERS Imaging. *Biosens. Bioelectron.* **2015**, *70*, 145–152.

(22) Graham, D.; Mallinder, B. J.; Whitcombe, D.; Watson, N. D.; Smith, W. E. Simple Multiplex Genotyping by Surface-Enhanced Resonance Raman Scattering. *Anal. Chem.* **2002**, *74* (5), 1069–1074.

(23) Li, Y.; Qi, X.; Lei, C.; Yue, Q.; Zhang, S. Simultaneous SERS Detection and Imaging of Two Biomarkers on the Cancer Cell Surface by Self-Assembly of Branched DNA-Gold Nanoaggregates. *Chem. Commun.* **2014**, *50* (69), 9907–9909.

(24) Xiao, M.; Nyagilo, J.; Arora, V.; Kulkarni, P.; Xu, D.; Sun, X.; Davé, D. P. Gold Nanotags for Combined Multi-Colored Raman Spectroscopy and x-Ray Computed Tomography. *Nanotechnology* **2009**, *21* (3).

(25) Jeong, S.; Kim, Y. Il; Kang, H.; Kim, G.; Cha, M. G.; Chang, H.; Jung, K. O.; Kim, Y. H.; Jun, B. H.; Hwang, D. W.; et al. Fluorescence-Raman Dual Modal Endoscopic System for Multiplexed Molecular Diagnostics. *Sci. Rep.* **2015**, *5*, 9455.

(26) Li, M.; Kang, J. W.; Sukumar, S.; Dasari, R. R.; Barman, I. Multiplexed Detection of Serological Cancer Markers with Plasmon-Enhanced Raman Spectro-Immunoassay. *Chem. Sci.* **2015**, *6* (7), 3906–3914.

(27) Wang, Y.; Reder, N. P.; Kang, S.; Glaser, A. K.; Yang, Q.; Wall, M. A.; Javid, S. H.; Dintzis, S. M.; Liu, J. T. C. Raman-Encoded Molecular Imaging with Topically Applied SERS Nanoparticles for Intraoperative Guidance of Lumpectomy. *Cancer Res.* **2017**, *77* (16), 4506–4516.

(28) Wang, Y. "Winston"; Khan, A.; Som, M.; Wang, D.; Chen, Y.; Leigh, S. Y.; Meza, D.; McVeigh, P. Z.; Wilson, B. C.; Liu, J. T. C. Rapid Ratiometric Biomarker Detection with Topically Applied SERS Nanoparticles. *Technology* **2014**, *02* (02), 118–132.

(29) Wang, Y.; Kang, S.; Khan, A.; Ruttner, G.; Leigh, S. Y.; Murray, M.; Abeytunge, S.; Peterson, G.; Rajadhyaksha, M.; Dintzis, S.; et al. Quantitative Molecular Phenotyping with Topically Applied SERS Nanoparticles for Intraoperative Guidance of Breast Cancer Lumpectomy. *Nat. Publ. Gr.* **2016**, 6:21242.

(30) Wang, Y. W.; Doerksen, J. D.; Kang, S.; Walsh, D.; Yang, Q.; Hong, D.; Liu, J. T. C. Multiplexed Molecular Imaging of Fresh Tissue Surfaces Enabled by Convection-Enhanced Topical Staining with SERS-Coded Nanoparticles. *Small* **2016**, *12* (40), 5612–5621.

(31) Maiti, K. K.; Samanta, A.; Vendrell, M.; Soh, K. S.; Olivo, M.; Chang, Y. T. Multiplex Cancer Cell Detection by SERS Nanotags with Cyanine and Triphenylmethine Raman Reporters. *Chem. Commun.* **2011**, *47*, 3514–3516.

(32) Narayanan, N.; Karunakaran, V.; Paul, W.; Venugopal, K.; Sujathan, K.; Kumar Maiti, K. Aggregation Induced Raman Scattering of Squaraine Dye: Implementation in Diagnosis of Cervical Cancer Dysplasia by SERS Imaging. *Biosens. Bioelectron.* **2015**, *70*, 145–152.

(33) Saranya, G.; Joseph, M. M.; Karunakaran, V.; Nair, J. B.; Saritha, V. N.; Veena, V. S.; Sujathan, K.; Ajayaghosh, A.; Maiti, K. K. Enzyme-Driven Switchable Fluorescence-SERS Diagnostic Nanococktail for the Multiplex Detection of Lung Cancer Biomarkers. *ACS Appl. Mater. Interfaces* **2018**, *10*, 38807–38818.

(34) Ramya, A. N.; Samanta, A.; Nisha, N.; Chang, Y. T.; Maiti, K. K. New Insight of Squaraine-Based Biocompatible Surface-Enhanced Raman Scattering Nanotag for Cancer-Cell Imaging. *Nanomedicine* **2015**, *10* (4), 561–571.

(35) Deborah L Holliday and Valerie Speirs. Choosing the Right Cell Line for Breast Cancer Research. *Breast Cancer Res.* **2011**, *13*, 215.

(36) Chaudhari, K.; Pradeep, T. Spatiotemporal Mapping of Three Dimensional Rotational Dynamics of Single Ultrasmall Gold Nanorods. *Sci. Rep.* **2014**, *4*, 27–29.

Effective Diagnostic Nanoprobe for the Detection of Alzheimer Biomarker based on SERS and MRI Dual Modalities
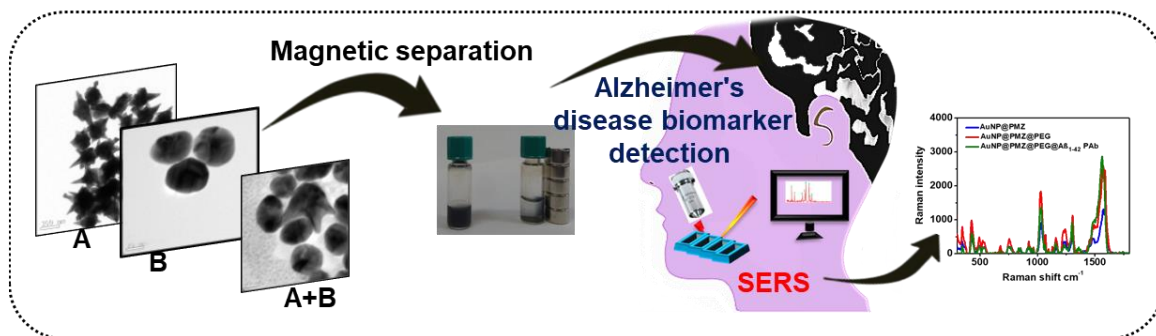
5.1 Abstract: *Development of facile techniques enabling low level detection of relevant biomarkers is a challenging area in the early diagnosis of diseases. Early detection is critical for improving the cognitive health in Alzheimer's disease (AD). Current practices do not evaluate the cognitive health leading to delayed diagnostic care. Aβ$_{1-42}$ is considered as a vital biomarker in this neurodegenerative disorder. Monitoring and tracking the level of Aβ$_{1-42}$ may be appropriate for developing early diagnostic measures for AD. An ultrasensitive SERS based sandwich immuno assay has been successfully demonstrated for a simple and selective detection of Aβ$_{1-42}$ protein relevant in AD. The current approach is based on a nanoprobe system consisting of two probes; an iron oxide based probe with strong magnetic properties enabling magnetic purification and possessing MRI contrast constitutes the first while a gold nanoparticle based probe which aids in SERS based detection using Promethazine, an amyloid binding molecule as the Raman reporter serves as the second. The iron oxide probe is conjugated with monoclonal antibody and gold nanoparticle probe is conjugated with polyclonal antibody against Aβ$_{1-42}$. The resultant sandwich complex formed with these nanoprobes*

was used for in vitro level and artificial cerebrospinal fluid spiked Aβ₁₋₄₂ detection. The detection limit was found to be 10 fM. Moreover, the sandwich immuno assay was also assessed for probing the Aβ₁₋₄₂ specificity against tau protein, bovine serum albumin and human serum albumin. Thus the study holds promise to detect the Aβ₁₋₄₂ protein in real clinical blood plasma samples from healthy, Mild Cognitive Impairment (MCI) and AD subjects.

5.2 Introduction

Alzheimer's disease is the most common form of dementia which is an overwhelming neurodegenerative disorder featured by progressive cognitive failure in elderly people.[1] Around 50 million people worldwide suffers dementia, a figure set to increase to 152 million by 2050 as reported by Alzheimer's Disease International, World Alzheimer Report 2019.[2] Dementia has a social, psychological, physical and economic impact on patients as well as care-givers, families and society. AD is characterized by an enormous loss of neurons and synapses in the brain with massive formation of both senile neuritic plaques and neurofibrillary tangles. Neuritic plaques are composed of a peptide termed beta amyloid (Aβ)[3] and neurofibrillary tangles made up of phosphorylated tau proteins.[4] The 40 or 42 amino acid containing Aβ₁₋₄₀ and Aβ₁₋₄₂, an amyloid precursor protein (APP) metabolism products accumulates in the AD brain causing the senile plaques.[5]

Despite the great trouble, there is no definite diagnosis for AD, than post-mortem analysis of brain senile plaques and neurofibrillary tangles. However, the current prognosis of AD is based on clinical symptoms including the neuropsychological test and neuroimaging which may be only useful several years after the initiation of pathological changes. Aβ deposits, the earliest pathological stage of AD in the brain can be identified by PET scanning or quantification in cerebrospinal fluid (CSF), which are considered as the so far best tools for diagnosis at the early stage. However as these methods are expensive and invasive, development of a cost-effective and non-invasive substitute tool is immediately necessary for the early recognition process. Reports suggest the Aβ pool in blood provides a clear measurement for early detection of AD.[6] An investigative report suggests that even though the blood based biomarker in AD is challenging, it seems feasible which

summarizes cross sectional studies showing less clinical utility of Aβ peptides as diagnostic biomarkers whereas longitudinal studies suggesting it as useful biomarkers for early onset of AD. Overall, studies conclude that a decrease in plasma $A\beta_{1-42}$ is a close event to disease onset reflecting sequestration in the brain.[7,8] A digital enzyme-linked immunosorbent assay has been successfully developed for the ultrasensitive detection of $A\beta_{1-42}$ peptide in human plasma with an LOD of 0.3 pg/ml. [9] Investigation in plasma Aβ peptide and tau protein using magnetic immuno reduction assays has also been developed for the sensitive detection in human plasma.[10-12] A recent report suggest that blood Aβ peptides can give information about early onset of AD.[13,14]

Nowadays, NPs are evolving as potential tools in biomedicine for novel diagnostic and drug delivery approaches for neurodegenerative disorders.[15] Among numerous bio-analyte such as proteins, nucleic acids, even single small molecule detection methods, SERS[16] has emerged as an area for intense research as a highly sensitive detection tool for low level detection of biomolecules since single molecule detection demonstration.[17] SERS is a Raman spectroscopic technique which provides enhanced Raman signal from Raman-active molecules which have been adsorbed onto specially prepared metal surfaces. Increase in the Raman signal intensity have been observed in the order of 10^8 to 10^{14} making SERS both highly sensitive and surface selective. The design and optimization of the substrate on which the SERS activity becomes significant is the most crucial aspect of a sensitive probe. Several studies has been performed using Raman spectroscopy as well as SERS for the detection of biomarkers in AD including label free detection of ADP3 peptoid[18], nanofluidic detection of Aβ,[19] surface plasmon resonance biosensor[20], detection of brain injury biomarkers[21] etc.

Moreover, the use of magnetic NPs together with SERS aids in efficient sample concentration and separation called magnet assisted SERS. A few studies established the sandwich type method for the detection of human Immunoglobulin G[22], tau protein[23], cancer antigen[24] etc. Metallic NPs like gold or silver NPs serves as few of the best SERS substrates[25] reported. Iron oxide NPs[26] has been extensively exploited for

a variety of biological applications including nanosensors,[27] cancer cell purification,[28] MRI[29–31] applications etc. Nanocomposites with iron core and gold/silver shell[32–34] are also fabricated for specialized applications in different sizes and shapes. A sandwich assay was established for detection of the tau protein which performed a complex method for the preparation of the magnetic nanoparticles.[23] Recently a sandwich SERS immunoassay have successfully performed for the multiplexed detection of A$\beta_{1\text{-}40}$ and A$\beta_{1\text{-}42}$ in blood using a magnetic bead conjugated with capture antibody and detection antibody immobilized with labelled silver nanoparticles.[35]

Herein, an effective and facile approach have been presented for A$\beta_{1\text{-}42}$ biomarker detection in AD based on a sandwich SERS immunoassay using two types of nanoprobes, *viz.* iron core- gold star NPs probe, designated as "IONP" and gold nanoparticle probe designated as "GNP". IONP consists of monoclonal antibody, Fe@AuNS@PEG@A$\beta_{1\text{-}42}$ MAb and GNP includes polyclonal antibody AuNP@PMZ@PEG@A$\beta_{1\text{-}42}$ PAb specific to A$\beta_{1\text{-}42}$ protein for the execution of the sandwich immuno assay. The presence of A$\beta_{1\text{-}42}$ was correlated with the key spectral features from a labelling Raman reporter molecule "Promethazine" (PMZ) incorporated to the GNP. In vitro level detection of overexpressed A$\beta_{1\text{-}42}$ protein in neuro cell lines also has been evaluated. Finally magnetic purification of the sandwich complex after spiking A$\beta_{1\text{-}42}$ protein has been investigated for the quantitative and sensitive detection in spiked artificial CSF. Selectivity of the probe towards A$\beta_{1\text{-}42}$ protein has also been carried out which shows its potential to emerge as an ultrasensitive assay for blood plasma based AD biomarker detection.
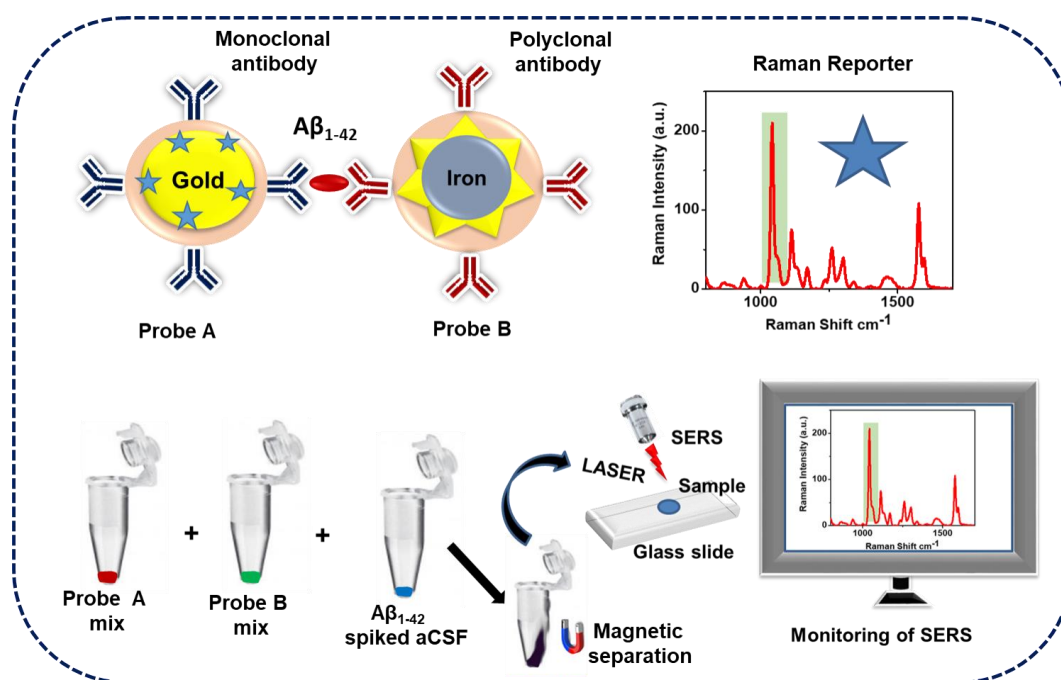
Scheme 5.1: Schematic representation for the detection of Aβ$_{1-42}$ biomarker in AD. The Aβ$_{1-42}$ in sample will get complexed with probe A (gold nanoparticle with Raman reporter and polyclonal antibody) and probe B (iron oxide nanoparticle with monoclonal antibody). After magnetic purification, the Raman reporter signal from the SERS analysis reveals the presence of the Aβ$_{1-42}$ biomarker.

5.3 Results and Discussion

5.3.1 Design and construction of nanoprobes Fe@AuNS@PEG@Aβ$_{1-42}$ MAb (IONP) and AuNP@PMZ@PEG@ Aβ$_{1-42}$ PAb (GNP).

The probe components required for the sandwich assay were fabricated based on iron oxide and gold nanoparticles. For IONP fabrication, initially iron oxide nanoparticle seeds around 10 nm in size were synthesized over which the decoration of spiky gold stars was performed. Both iron oxide nanoparticle seeds and iron oxide core gold star particles (Fe@AuNS) were characterized by Vibrating Sample Magnetometic analysis (VSM), UV-Vis Spectroscopy, HR-TEM and Energy Dispersive X-Ray Analysis (EDX) analysis (**Figure 5.1**). The gold star over iron seeds provides increased hotspots as well as functional groups for the coating of carboxyl functionalized PEG to tether the Aβ$_{1-42}$ specific monoclonal antibody. PEG encapsulation was performed to increase
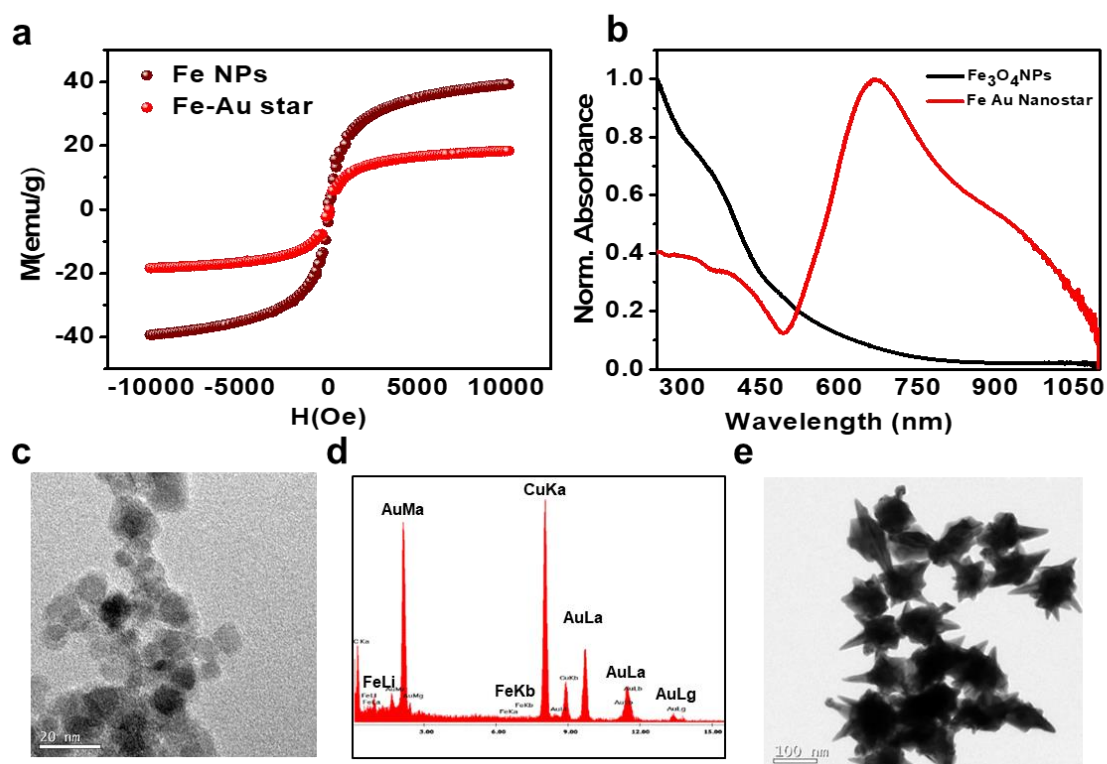
Figure 5.1: Characterization of iron oxide (Fe_3O_4) NPs a) VSM analysis and b) UV-Vis spectroscopy Fe_3O_4 NPs and Fe@AuNS. c) TEM analysis of Fe_3O_4 NP seeds, scale bar: 20 nm d) EDX analysis and e) TEM analysis of Fe_3O_4 NPs, scale bar: 20 nm.

Increase the biocompatibility and preserves the SERS nanoprobes against aggregation. UV-vis spectroscopic analysis of the pegylated construct exhibited a blue shift of nearly 11 nm in the absorption peak from 591 nm to 580 nm which confirms effective PEG encapsulation. TEM analysis also confirmed a thin layer of PEG surrounding the NP (**Figure 5.2**).
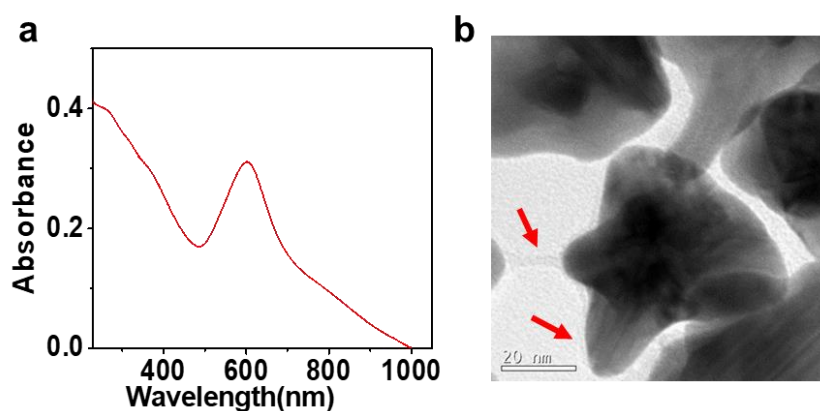
Figure 5.2: Characterization of pegylated Fe@AuNS, a) UV-Vis Spectroscopic analysis and b) HR-TEM analysis, scale bar: 20 nm.

For GNP synthesis, AuNP of size around (40-45 nm) were synthesized as the SERS substrate. Characterization of AuNPs was confirmed by UV-vis spectroscopy, HR-TEM and DLS. The Raman reporter used was PMZ which showed strong affinity to the surface of gold as it contains sulphur. An additional advantage of PMZ as Raman reporter is its well reported affinity towards $A\beta_{1-42}$ protein.[36] A 3 nm shift was observed in UV-vis Spectroscopy from 531 nm to 534 nm, a 2-3 nm PEG layer was visualized in TEM and the hydrodynamic diameter in DLS was found to be 73 nm confirming successful PEG encapsulation (**Figure 5.3**).

The monoclonal antibody of $A\beta_{1-42}$ conjugated to Fe@AuNS@PEG was characterized by UV-Vis spectroscopy. The 2 nm shift in the plasmon peak from 580 nm to 582 nm and the 280 nm protein peak was appeared which confirmed successful antibody conjugation process (**Figure 5.4 a).** The polyclonal antibody $A\beta_{1-42}$ conjugated to AuNP@PMZ@PEG was characterized by UV-Vis absorbance which showed a shift of 1 nm from 534 nm to 535 nm along with the appearance of a 280 nm peak confirming the antibody conjugation **(Figure 5.4 b).**
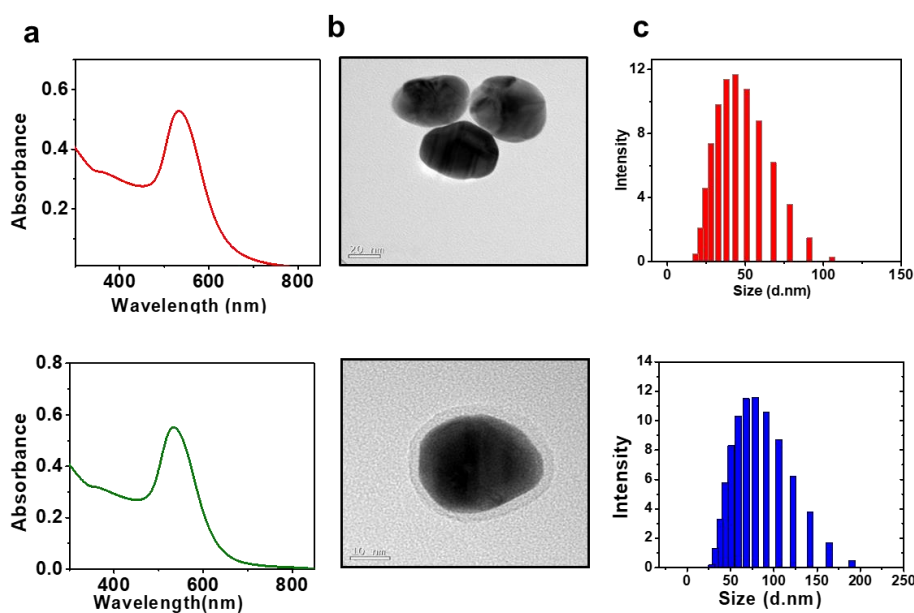
Figure 5.3: Characterization of AuNPs a) UV-Vis absorption spectra, b) HR-TEM (Scale bar: 20 nm) and c) DLS of AuNPs (size: 40 nm) (upper panel) and AuNP@PMZ@PEG (lower panel).
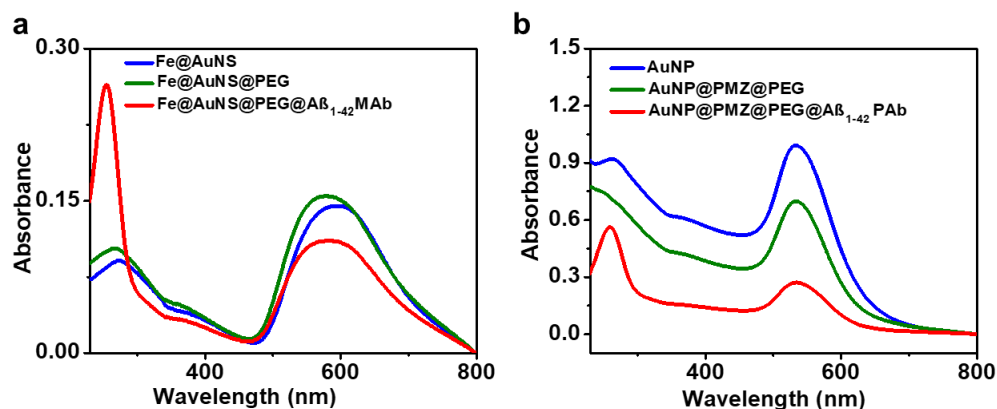
Figure 5.4: UV-Vis absorption spectra of the nanoprobes. a) Fe@AuNS (blue), Fe@AuNS@PEG (green), Fe@AuNS@PEG@Aβ_{1-42}MAb (red) b) AuNPs (blue), AuNP@PMZ@PEG (green), AuNP@PMZ@PEG@ Aβ_{1-42} PAb (red).

5.3.2 SERS studies based on AuNP@PMZ@PEG@Aβ_{1-42} PAb (GNP) and sandwich model study

The SERS analysis of the GNP incorporated with the PMZ Raman reporter was analyzed at different stages of its preparation towards polyclonal antibody conjugation and identified the Raman fingerprint (**Figure 5.5**). Incremental increase of SERS intensity was obtained with the PEG encapsulated AuNPs attached Raman reporter. After antibody conjugation, the intensity was slightly reduced because of some particle loss which has been re-suspended in PBS buffer from MilliQ water.
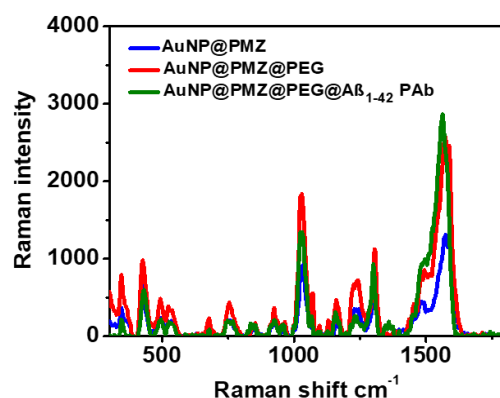
Figure 5.5: SERS signature evaluation of GNP at different stages of its preparation towards antibody conjugation.

Finally, to evaluate the performance of the prepared nanoprobes, commercially available Aβ_{1-42} peptide (Hyl flour TH 488 labelled) was employed to

form the sandwich complex. The SERS analysis of the sandwiched nanocomplex was magnetically   purified (**Figure 5.6 a-d**) and analyzed by SERS which indicated the Raman fingerprint of PMZ (**Figure 5.6 e**). The spectrum showed excellent enhancement of the PMZ signal due to the hotspots generation during the formation of sandwich complex by IONP and GNP.
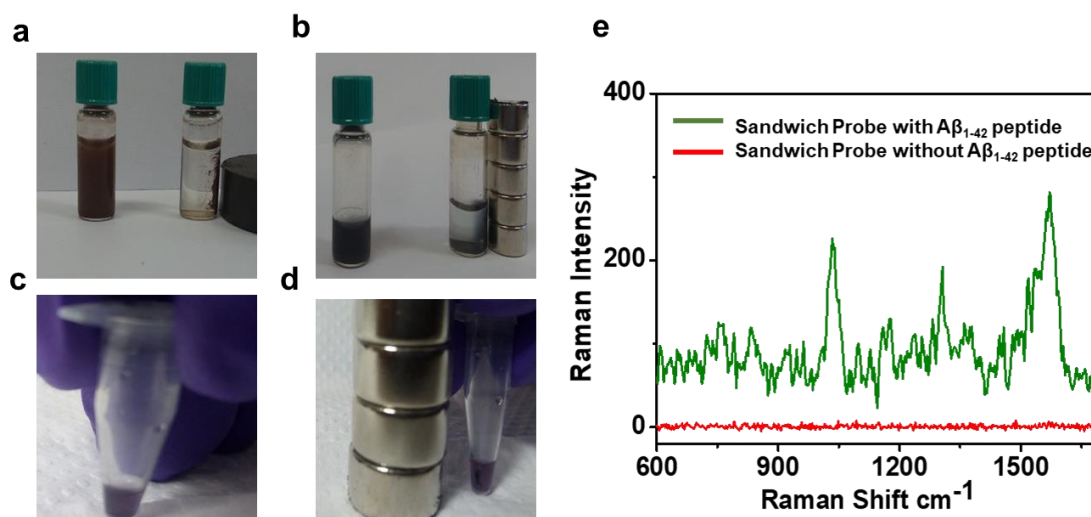
Figure 5.6: Magnetic purification of a) iron oxide seeds, b) Fe@AuNS, c) mixture both probes with Aβ$_{1-42}$ peptide, d) purification of sandwich complex and e) SERS analysis of magnetically purified sandwich complex, IONP and GNP along with externally added Aβ$_{1-42}$ peptide.

The EDX analysis in HR-TEM analysis also established the presence of both iron and gold in the complex (**Figure 5.7 a**). The HR-TEM morphologic analysis of the sandwiched nanoprobe also showed clear conjugation of monoclonal Aβ$_{1-42}$ antibody attached IONP and polyclonal antibody attached GNP to the externally added Aβ$_{1-42}$ peptide (**Figure 5.7 b**).
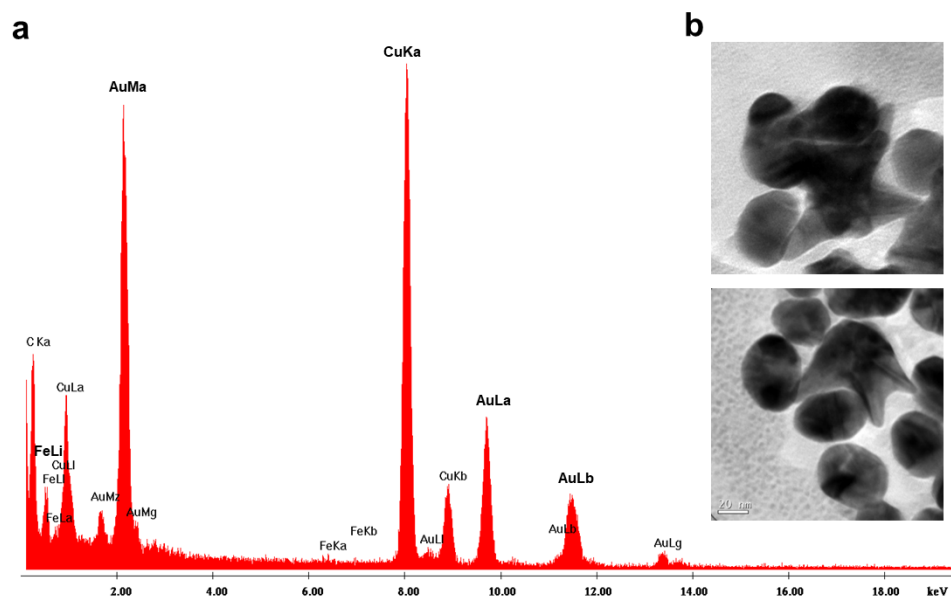
Figure 5.7: TEM analysis of the magnetically purified sandwich complex a) EDX analysis of sandwich complex, IONP and GNP along with externally added $A\beta_{1-42}$ peptide with externally added peptide, b) HR-TEM analysis, scale bar., 20 nm.

5.3.3 Evaluation of $A\beta_{1-42}$ protein in cell line models

Assessment of the nanoprobe was attempted in cell line level where two neuronal cell lines were selected based on its expression level of $A\beta_{1-42}$ protein. SH-SY5Y, a neuroblastoma cell line and C8-D30 astrocytes type III clone were compared for its expression level for $A\beta_{1-42}$ protein. The western blot analysis by using antibodies directed against $A\beta_{1-42}$ protein showed significant overexpression **(Figure 5.8**) in the SH-SY5Y compared with astrocytes keeping β-actin as the control protein.

The Congo red birefringence assay for the detection of amyloid fibrils was performed in both the cell lines to confirm the expression level of the $A\beta_{1-42}$ protein. The detection of yellow/green birefringence in optical polarized light microscopy is considered a positive signal for the presence of amyloid.
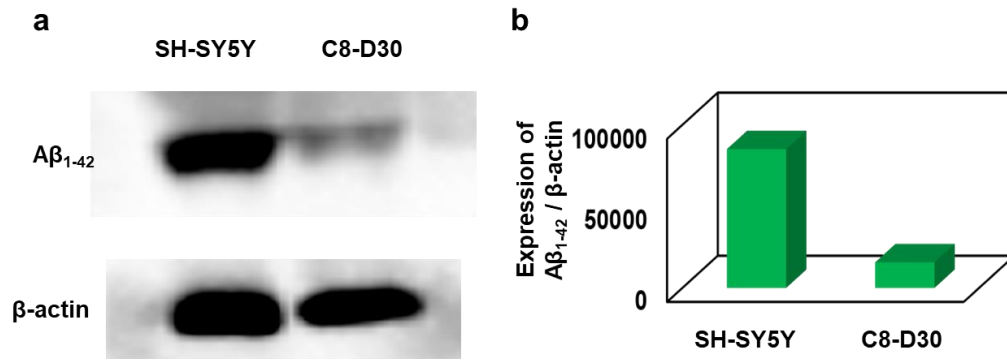
Figure 5.8: Protein level expression analysis of $A\beta_{1-42}$ in a) SH-SY5Y and C8-D30 by western blot, b) the bands normalized to β-actin and quantified using Image J software.

Congo red birefringence exists as a primary approach for identification of amyloid fibril both *in vivo* and *in vitro* conditions. The presence of apple green birefringence was confirmed in SH-SY5Y cell line and found minimal in C8-D30 astrocyte cells (**Figure 5.9**).
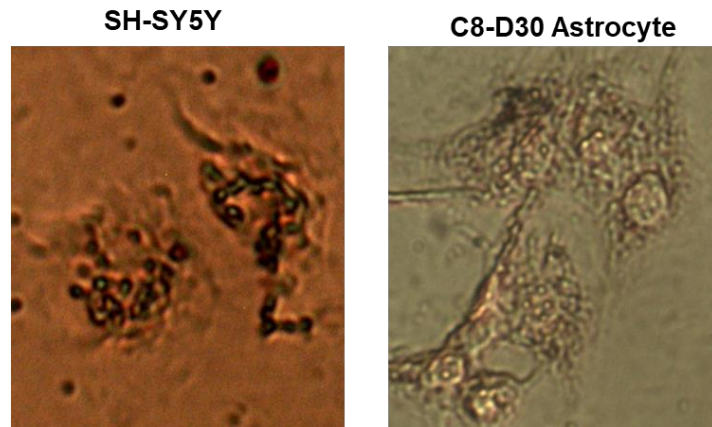
Figure 5.9: The Congo red birefringence assay to detect the expression of Aβ protein in SH-SY5Y cell line and C8-D30 astrocytes.

There are a few evidences supporting the fact that, lysosome is associated with Aβ accumulation and associated neurotoxicity. Abnormally enlarge endosomes, autophagosomes and lysosomes are found in AD and experimental AD models.[37–40] To analyse this probability, co-localization of Hyl flour TH 488 labelled $A\beta_{1-42}$ peptide in lysosome were performed in SH-SY5Y cell line and C8-D30 astrocytes. Incubated Hyl

flour TH 488 labelled Aβ$_{1\text{-}42}$ peptide with the SH-SY5Y cell line observed very well co-localized with the lysotracker red. Counter staining with Hoechst staining clearly showed the cytoplasmic staining of Hyl flour TH 488 labelled Aβ$_{1\text{-}42}$ peptide around the nucleus (**Figure 5.10 a and c**). The extend of co-localization was studied by the Pearson coefficient (r) correlation and Mander's overlap coefficient (R) (**Figure 5.10 b and d**). The SH-SY5Y neuroblastoma cell line was thus selected for investigating the synthesized diagnostic nanoprobe for Aβ$_{1\text{-}42}$ peptide relevant in AD. C8-D30 astrocyte type III clone showed no co-localization of Hyl flour TH 488 labelled Aβ$_{1\text{-}42}$ peptide (**Figure 5.11**).
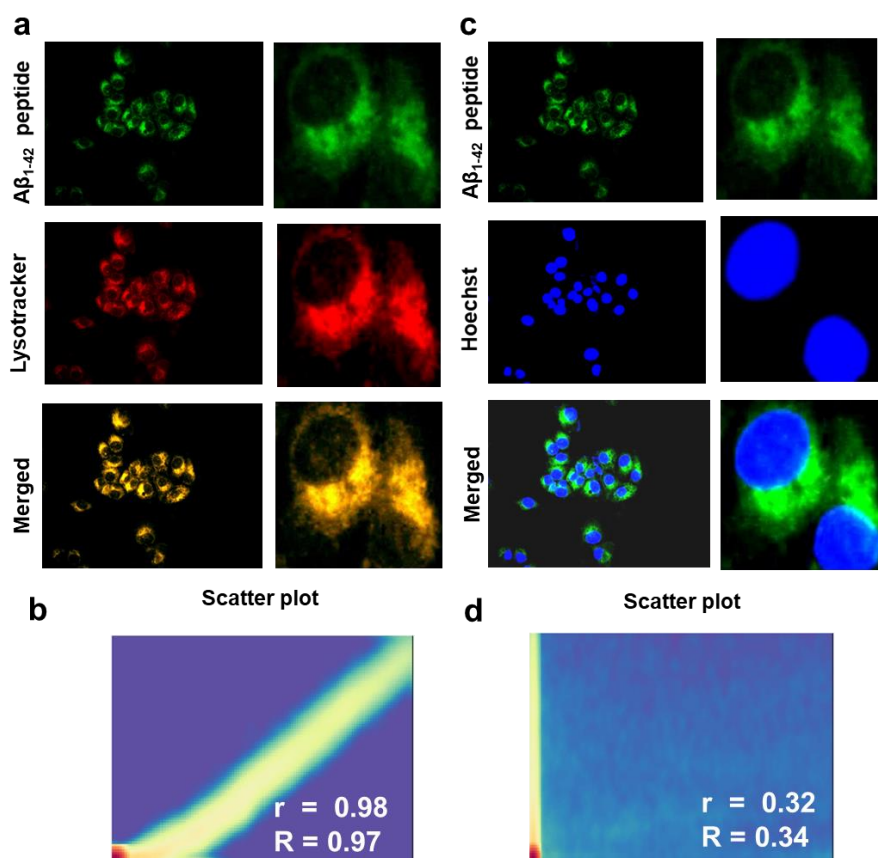
Figure 5.10: Co-localization of Aβ$_{1\text{-}42}$ peptide in SH-SY5Y cells. a) co-localization with lysotracker b) scatter plot, r and R represent Pearson's correlation coefficient and Mander's overlap coefficient, respectively.
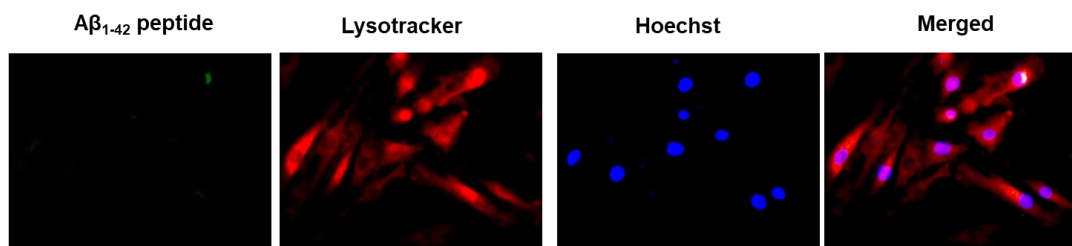
5.3.5 Uptake analysis of iron oxide nanoparticles

Perls' Prussian blue staining assay was performed to confirm the uptake of iron oxide nanoparticles in SH-SY5Y and C8-D30 astrocyte cell line. The uptake of sandwiched nanocomplex (IONP and GNP cocktail) was revealed in SH-SY5Y cell line by its significant blue color deposits. Only minimal uptake was observed in C8-D30 astrocyte cell line **(Figure 5.14 a).**
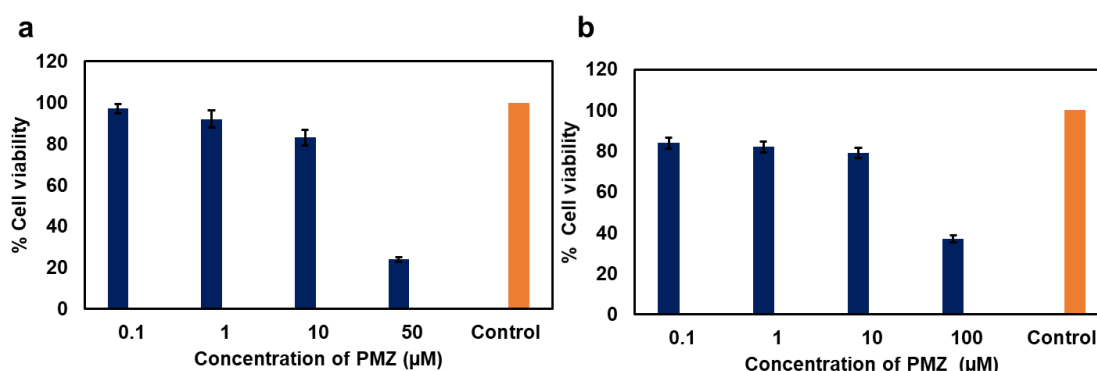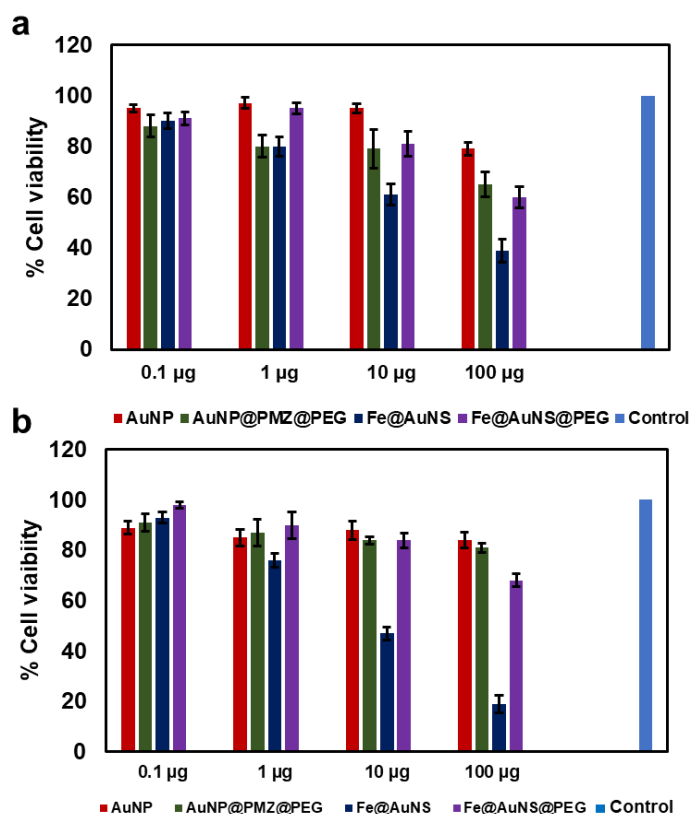
Figure 5.13: Percentage cell viability analysis AuNP, AuNP@PMZ@PEG, Fe@AuNS and Fe@AuNS@PEG by MTT assay in a) SH-SY5Y and b) C8-D30 astrocyte cell lines. Average of three independent experiments.

Further assessment through dark field microscopy confirmed the uptake of nanoparticles inside the cells (**Figure 5.14 b**). In dark field microscopy,[41] the metallic nanoparticles are localized in the cells which can be visualized by the bright spots of nanoparticles in the dark background as the light hits the specimen excluding the image's un-scattered beam. Therefore, a proof-of concept was confirmed from both Prussian blue staining and dark field which assured the excellent uptake of the iron oxide component in the sandwich complex towards $A\beta_{1-42}$ peptide.

Moreover, inductively coupled plasma mass spectrometry (ICP-MS) analysis was performed to confirm the uptake efficiency in SH-SY5Y cell line. The analysis[42] showed that SH-SY5Y cells administered with the antibody cocktail demonstrated significantly higher gold content of 857 ppb against the very low concentration of 38 ppb in cells without treatment, indicating the target specific buildup of our nanoprobe in $A\beta_{1-42}$ rich SH-SY5Y cells (**Figure 5.15**).
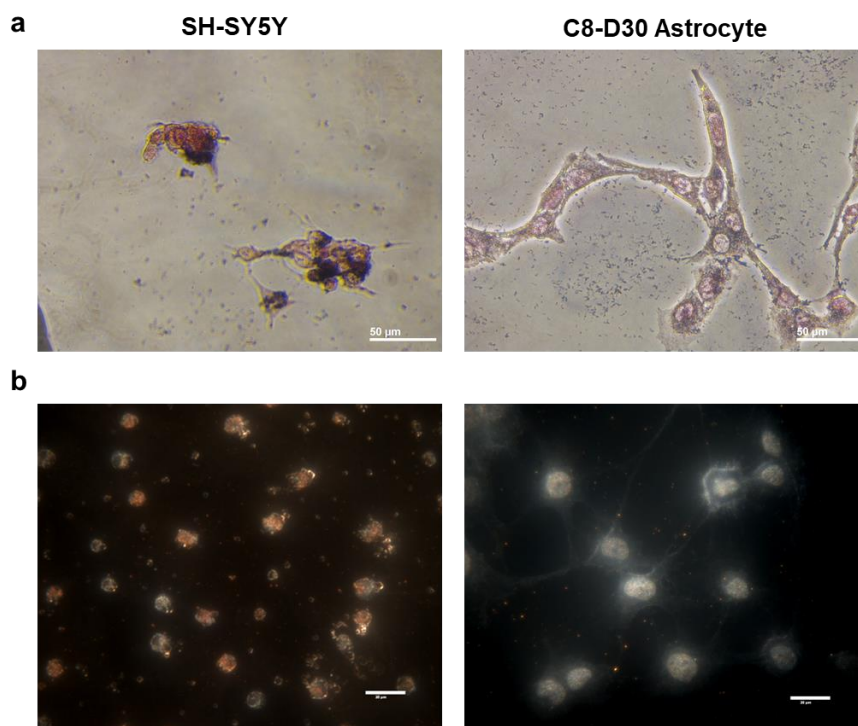
Figure 5.14: Uptake analysis. a) Perls' Prussian blue staining for iron oxide nanoparticles and b) dark field microscopy for uptake of gold nanoparticles in IONP and GNP sandwich complex in SH-SY5Y and C8-D30 astrocyte cell lines.
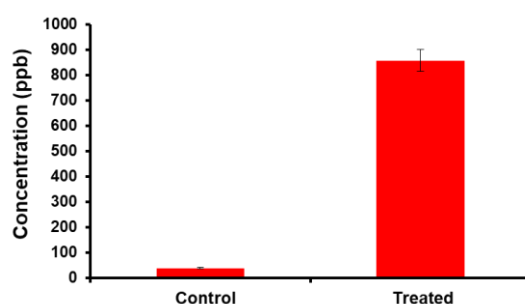
Figure 5.15: ICP-MS analysis of uptake of GNP in SH-SY5Y cell line.

5.3.6 SERS analysis

SERS based diagnostic immunoassay for the detection of $A\beta_{1-42}$ peptide was performed in beta amyloid expressing SH-SY5Y cell line. The signature peak of PMZ was acquired as the diagnostic signals from $A\beta_{1-42}$ peptide arising from the cells most probably from the lysosomes. The GNP component and the gold star coated over iron oxide core were designed in such a way to act as the substrates for SERS analysis. SH-SY5Y cells expressing $A\beta_{1-42}$ peptide selectively accumulated the antibody conjugated sandwich nanoprobe (**Figure 5.16**).
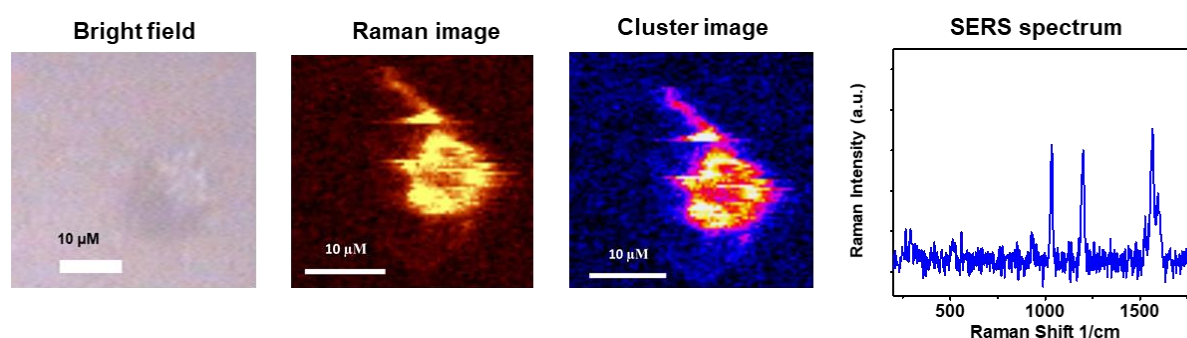
Figure 5.16: SERS imaging of $A\beta_{1-42}$ complexed with IONP and GNP to form a sandwich complex in SH-SY5Y cell line.

5.3.7 MRI analysis

The iron oxide based nano probe was designed in such a way that the core contained iron oxide nanoparticle acted as a contrast agent in MRI. Initially the iron oxide spions and Au-spions were subjected to serial dilution for evaluating the contrast. Spions gave contrast approximately with concentration 25 μg/ml and Au-spions showed contrast approximately with 50 μg/ml (**Figure 5.17 a**). Corresponding visual effect based on dilutions prepared in micro centrifuge tubes are also depicted in **Figure 5.17 b**.
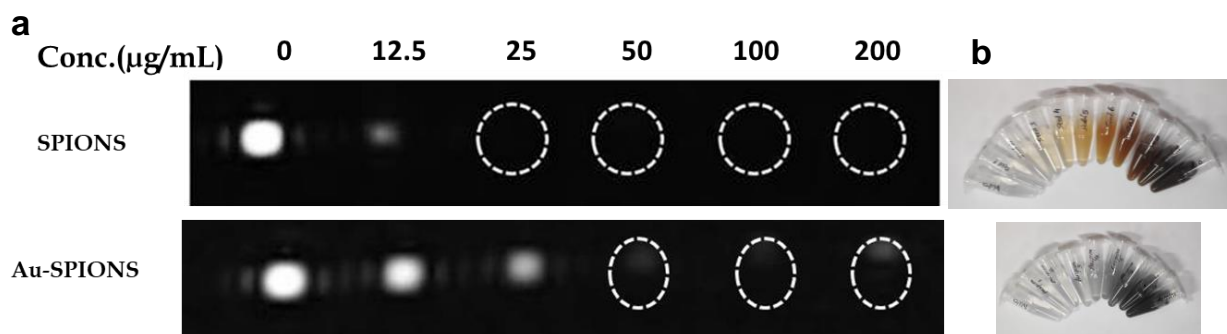
Figure 5.17: Characterization of a) magnetic property by MRI analysis for a series of concentration, b) visual gradation of serial diluted spions and Au-spions.

Cell line uptake study also demonstrated the excellent MRI contrast of the synthesized nanoprobes. Iron oxide generates T2 weighted image which becomes darker when the contrast increases. In SH-SY5Y cell line, the contrast image was obtained starting from concentration 60 μg/ml (**Figure 5.18**) whereas C8-D30 did not produced a contrast till 96 μg/ml. LOD in case of MRI analysis was not performed as it will not show any contrast beyond 50 μg/ml.
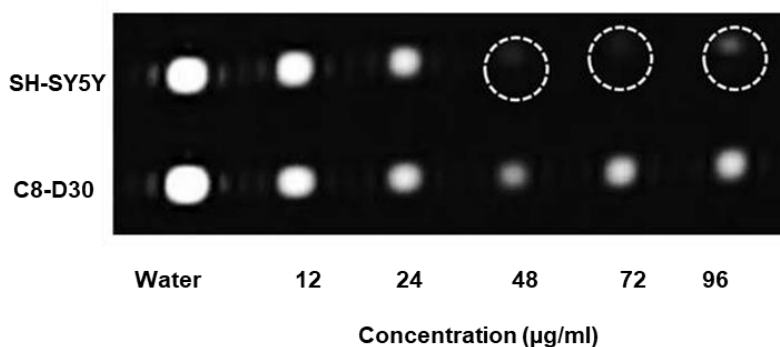
Figure 5.18: MRI contrast of $A\beta_{1-42}$ inside cells complexed with IONP and GNP to form a sandwich complex in SH-SY5Y and C8-D30 astrocyte cell line using series of Fe@AuNS@PEG@$A\beta_{1-42}$ MAb concentration.

5.3.8 Selectivity of nanoprobe toward $A\beta_{1-42}$ peptide along with other analytes

The selectivity of the constructed nanoprobes towards $A\beta_{1-42}$ peptide was analyzed along with other analytes like tau protein, BSA and Human Serum Albumin (HSA). 50 nM of $A\beta_{1-42}$ peptide was analyzed along with 250 nM of tau, BSA and HSA. A precise selectivity of the nanoconstruct towards $A\beta_{1-42}$ peptide was observed

whereas no significant spectrum is obtained from the other analytes having five times high concentration than the Aβ1-42 peptide (**Figure 5.19).**
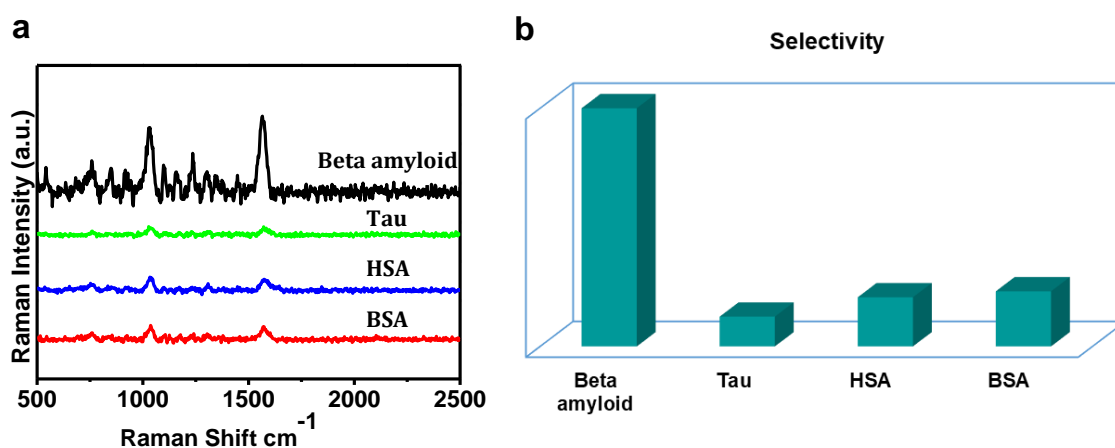
Figure 5.19: Selectivity study. a) SERS Selectivity analysis of the IONP and GNP to form a sandwich complex towards Aβ1-42 and other analytes like tau protein, HSA and BSA, b) its intensity variations represented as bar diagram.

5.3.9 Limit of detection of Aβ1-42 peptide in artificial cerebrospinal fluid

Artificial cerebrospinal fluid (aCSF) is considered as a vehicle for administering agents to the central nervous system (CNS). Here using aCSF which thoroughly matches the concentrations of electrolyte and physiological compatibility in the case of endogenous CSF, enabling to differentiate Aβ1-42 spiked samples in a concentration dependent manner by SERS spectral evaluation. The sensitivity studies showed that the aCSF[43] spiked Aβ1-42 showed a LOD of about 10 fM after which no detection was possible (**Figure 5.20**).
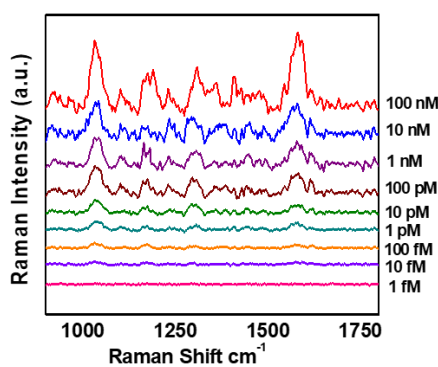
Figure 5.20: LOD analysis of spiked Aβ1-42 complexed with IONP and GNP to form a sandwich complex in artificial cerebrospinal fluid ranging from 1 nM to 1 fM.

5.4 Experimental Section

5.4.1 Materials and reagents.

All chemicals and reagents were purchased from Sigma-Aldrich unless otherwise mentioned. The $A\beta_{1-42}$ peptide Hyl flour TH 488 labelled and monoclonal antibody were purchased from AnaSpec. The polyclonal antibody against $A\beta_{1-42}$ was obtained from Cell Signaling Technology. UV/vis absorbance analysis was performed employing Shimadzu UV- 2600 UV-vis spectrophotometer. SERS analysis were performed using WITec Raman microscope (WITec, Inc., Germany) comprising 600 g/mm grating with Peltier cooled charge-coupled device (CCD) detector unit. Excitation of the samples was done using a 633 nm laser with laser power 10 mW. The spectra were collected in the range of 400-1800 cm^{-1} with 1 cm^{-1} resolution and 10 s integration time with 3 accumulations. Silicon standard calibration was performed with a 520 cm^{-1} Raman peak prior to each measu- rement. WITec Project 5.2 Plus (v2.1) software were used for data processing.

5.4.2 Synthesis of gold nanoparticles

Citrate reduction method was used for the preparation of gold nanoparticles. For the synthesis of 40 nm gold nanoparticles, water was first boiled to 100° C with constant stirring using a magnetic stir bar at 500 rpm and added 250 mM chloroauric acid solution in to it and again boiled for 10 min. After 10 min, 100 mM tri sodium citrate solution was added, resulting in the color change from pale yellow to dark purple to red. The color change to red will take around 5 min and heating was stopped to let the solution to cool to RT.

5.4.3 Incorporation of PMZ, an amyloid binding molecule as the Raman reporter

The Raman reporter PMZ of concentration 100 μM were mixed with AuNPs in 1:9 ratio (v/v). The solution was incubated for 10 min so that the reporter gets chemisorbed to the gold colloid. The reporter concentration in the final tag was maintained as 10 μM.

5.4.4 PEG encapsulation of gold nanoparticles (AuNP@PMZ@PEG)

PEG encapsulation using PEG-SH (100 μM) and SH-PEG-CO$_2$H (100 μM) was done for the biocompatibility, stabilization of the dye and attachment of targeting antibody. First PMZ incorporated construct was added with the 20 μL of SH-PEG-CO$_2$H followed by incubation for 15 min. Further 300 μL of PEG-SH was added followed by incubation for 3 h. Finally the solution was centrifuged for 8000 rpm for 20 min twice and re-suspended in MilliQ water.

5.4.5 Preparation and characterization of iron oxide core- gold nanostar (Fe@AuNS)

Iron core- gold nanostars is prepared in a three step continuous procedures.

5.4.6 Iron oxide synthesis (spions)

75 ml each of Iron (II) salt (0.01 M) and Iron (III) salt (0.05 M) were heated for 2 h in a 3 neck flask at nitrogen atmosphere at 80°C. After that 30 ml of Sodium hydroxide (1.5 M) and 10 ml of Tri sodium citrate (0.03 M) were added for condensation for 2 h at 80°C. The resultant product was further purified and centrifuged several times till neutral attained pH. Then followed by air-drying at 70°C to obtain the powdered form.

5.4.7 Synthesis of seed decorated iron oxide nanoparticles

200 μL of 0.5% of solution of spion was taken in a microcentrifuge. 10 μL of 2% ammonium hydroxide and 200 μL of 0.01 M silver nitrate added. The solution was kept for 30 min at RT, followed by addition of 1 ml of purified water to the solution and centrifuged at 12000 rpm for 30 min. Supernatant was decanted and repeated once more. 500 μL of water was added to the final precipitate. Finally an aqueous solution of sodium borohydride (0.01 M, 100 μL) was added and stirred vigorously to reduce the silver ion. The seed obtained were purified by centrifuging at 12000 rpm at 30 min. The solution was further aged for several hours before use for star shaped shell growth.

5.4.8 Preparation of spiky gold star over spions

The growth solution was equipped by mixing the aqueous solution of CTAB (0.1 M, 10 mL) auric chloride (0.01 M, 421 µL), silver nitrate (0.01 M, 64 µL), ascorbic acid (0.1 M, 67 µL). For the complete star shaped shell formation 100 µl of seed decorated bead solution was added into the growth solution. Color was developed after 5 min and the reaction was continued for 2 h.

5.4.9 Monoclonal antibody conjugation of iron core- gold nanostar (Fe@AuNS)

Iron oxide nanoparticles were synthesized initially followed by decoration of spiky gold stars over it. An encapsulation with PEG (PEG-SH & SH-PEG-CO$_2$H) was done to increase the biocompatibility, stabilization of the dye and attachment of targeting antibody. The Aβ_{1-42} monoclonal antibody was purified using Amicon Ultra 3K centrifuge filters, Millipore by centrifugal filtration to remove the preservative sodium azide. The carboxylic groups of the PEG encapsulated nano tag were activated by EDC (25 mM) and NHS (25 mM). The activated particles were mixed with the Aβ_{1-42} monoclonal antibody and incubated for 2 h followed by storing in 4°C overnight. Further unbound antibodies were removed by centrifugation. The pellet containing the antibody conjugated nanotags (Fe@AuNS@PEG@Aβ_{1-42} MAb) were then again resuspended in PBS and stored at 4 °C.

5.4.10 Polyclonal antibody conjugation of AuNPs

The polyclonal antibody Aβ_{1-42} was purified using Amicon Ultra 3K centrifuge filters (Millipore) by centrifugal filtration to remove sodium azide. The carboxylic groups in the PEG encapsulated nano tag were activated by EDC (25 mM) and NHS (25 mM). The activated particles were mixed with antibody and incubated for 2 hours followed by storing in 4°C overnight. The unbound antibodies were washed out by centrifugation. The pellet containing the antibody conjugated SERS nanotags (AuNP@PMZ@PEG@Aβ_{1-42} PAb) were resuspended in PBS and stored at 4 °C.

5.4.11 SERS analysis of GNPs and sandwiched monoclonal and polyclonal nanotags with the peptide

The SERS analysis of the gold nanoparticle with the Raman reporter was analyzed and for identifying the Raman fingerprint of PMZ. The monoclonal antibody conjugated IONP-Au star and polyclonal antibody conjugated gold nanoparticle complexed with $A\beta_{42}$ peptide were purified using an external magnet (Neodymium magnet). The SERS analysis of the sandwiched nanocomplex were performed using Promethazine Raman reporter in confocal Raman microscope (WI-Tec, Inc., Germany, alpha 300R) with a 633 nm laser beam directed through 20X objective with 600g/mm grating and a Peltier cooled CCD detector.

5.4.12 HR-TEM and EDX analysis of sandwiched monoclonal and polyclonal nanoconstruct with the externally added peptide (Beta Amyloid Protein Hyl flour TH 488 labelled)

The $A\beta_{1-42}$ polyclonal antibody conjugated AuNPs and $A\beta_{1-42}$ monoclonal antibody conjugated Fe@AuNS was incubated for 2 h with externally added $A\beta_{1-42}$ peptide. The complex was purified using an external magnet. The TEM and EDX analysis of the sandwiched nanoprobe complex was performed.

5.4.13 Western blot analysis.

Proteins were extracted from SH-SY5Y and C8-D30 cells (2×10^6) using RIPA buffer. The protein concentration was then estimated using BCA assay using BSA standards. Proteins were separated according to the molecular weight by 12 % SDS-PAGE and blotted to PVDF membranes. The membrane was further blocked with 5 % skim milk and incubated with corresponding primary antibodies. HRP conjugated secondary antibody was employed for all primary antibodies which were recognized by the chemiluminescent western blot hyper substrate (Takara, Japan). The resulting bands were further quantified using Image J software. Beta-actin was used as the control.

5.4.14 Congo red birefringence assay

Congo red assay is established for the scrutiny of in situ and ex vivo amyloid and was later applied for the *in vitro* sample examination also. A combination of alkaline sodium chloride solution with alkaline congo red solution was applied in SH-SY5Y and astrocyte cells. After washing, the stained sample was examined using polarized light microscopy.

5.4.15 Co-localization assay

$A\beta_{1-42}$, the main constituent of AD senile plaques, has been found to accumulate within the lysosomal compartment in neurons. So to confirm the presence of expression of beta amyloid peptide in SH-SY5Y Neuroblastoma, a $A\beta_{1-42}$ peptide Hyl flour TH 488 (500 nM) labelled was incubated with the cell line seeded in 96 well plate. C8-D30 astrocyte type III clone was also incubated with the same peptide for a comparative analysis.

5.4.16 Cell viability assay

The cytotoxicity of the nanoconstruct was analyzed using MTT assay. Initially the different concentrations of PMZ was screened from 1 μM to 50 μM. After optimizing the concentration of the Raman reporter, the assay variables control, AuNP, AuNP@ PMZ@ PEG, Fe@AuNS and Fe@AuNS@PEG. The stock concentration of AuNP and Fe@AuNS was 1 mg/ml and 1.6 mg/ml respectively and AuNPs contains 10 μM final concentration of Promethazine. 0.1, 1, 10 and 100 μg/ml concentrations were performed for each construct. The cells were seeded at a density of 10000 cells/ well in 100 μL complete medium (DMEM, Himedia) supplemented with 10% FBS (Himedia) and antibiotics (Antibiotics Antimycotic 100x diluted to 1X, Himedia). A 96-multiwell flat bottom microtiter plate was used for seeding and incubation was done for 24 h at 37°C with 5 % CO_2 for cells to adhere. Cells were then treated with 100 μL compounds (diluted in DMEM medium) followed by further incubation for 24 h. 100 μL MTT solution (0.5 mg/ml in HBSS, Sigma) was added and incubated for 3 h. The solution was further removed and resulting formazan crystals solubilised in DMSO. Culture plates were shaken gently for 20 min to solubilise the crytals and the

optical density was measured spectro-photometrically using a microplate reader (BioTek) at 570 nm. The relative cell viability in percentage was calculated as: Absorbance of treated/Absorbance of control x 100.

5.4.17 Perls' Prussian blue staining for uptake of iron oxide nanoparticles

Prussian blue uses separate solutions of potassium ferrocyanide and acid to stain tissue to identify iron uptake. Ferric iron deposits in cells then react with the soluble ferrocyanide in the stain, to form insoluble Prussian blue dye in situ. They are visualizable microscopically as blue or purple deposits, within cells counter stained by neutral red. Thus the uptake analysis using sandwiched nanocomplex (nanoprobe solution conta-ining Fe@AuNS@PEG@Aβ_{1-42} MAb and AuNP@PMZ@PEG@Aβ_{1-42} PAb) were performed in SH-SY5Y neuro cell line and C8-D30 astrocytes.

5.4.18 Dark field microscopy

Dark field imaging of SH-SY5Y and C8-D30 cells were performed using CytoViva Enhanced Dark field illumination System 2.0. (BX 43F). 60 X oil immersion objective was used for the imaging. Cells were cultured at a seeding density of 10^4 cells/well in a four well chamber slide. Cells were further incubated with the nanoconstructs for 4 h and were washed with PBS (pH 7.4) twice to remove the excess nanoprobes from the cells.

5.4.19 ICP-MS analysis

ICP-MS analysis in SH-SY5Y cells was performed in which the cells were first seeded in 12-well plates at seeding density around 1 x 10^5 cells/well, which was further incubated with the probe for 24 h duration. Prior to the analysis, cells were washed off with PBS three times to wash the unbound molecules. Cells were later trypsinized and lysed with RIPA buffer with rapid vortexing. The cell lysate 0.5 ml was then taken in digestion vessel in a microwave reactor (MARS 5 194A07) by mixing the sample with aquaregia in 1:10 v/v ratio. Microwave-assisted digestion was implemented using (1) 15 min ramp till 130^0 C from ambient and held for 2 minutes at 800 W applied power (2). Further the temperature (T) was increased to 185^0 C in a 10 min ramp time and kept the samples at 185^0 C at 30 min at 800 W applied power.

After digestion the samples were diluted to 25 ml and were finally subjected to ICP-MS analysis (Thermo Fisher scientific, Model; iCAP RQ 00472).

5.4.20 SERS analysis of Aβ$_{1\text{-}42}$ in SH-SY5Y cell line

The SERS based diagnostic platform for the detection of Aβ$_{1\text{-}42}$ was done in beta amyloid expressing SH-SY5Y cell line. The SERS nanoprobe solution containing Fe@AuNS@PEG@Aβ$_{1\text{-}42}$MAb and AuNP@PMZ@PEG@Aβ$_{1\text{-}42}$ PAb cocktail were incubated in SH-SY5Y cell line. After 2 h incubation, washing of the unbound nanoprobe was done and then continuing with the SERS analysis and imaging. The analysis was performed in confocal Raman microscope (WI-Tec, Inc., Germany, alpha 300R) with a laser beam of 633 nm wavelength using 20X objective with 600g/mm grating and a Peltier cooled CCD detector.

5.4.21 Utilization of MRI detection platform

Magnetic relaxivity calculations were conducted in a 1.5 T whole body MRI scanner (MAGNETOM Avento Tim, Siemens, Munich, Germany). A twelve channel head coil was used. Scanning parameters were as follow, T = 22°C, FOV = 20 cm × 40 cm, slice thickness = 10 mm. For the measurement of longitudinal relaxation time T1, an inversion recovery sequence was employed. The echo time (TE) and repetition time (TR) were set at 11 and 4000 ms respectively. By changing the inversion time (TI) from 50 to 3000 ms, the MR signal was analysed. A modified T2 relaxometry spin echo sequence was done for T2 relaxometry measurements at three different planes of the phantoms. Signals from MR were measured for varying TE values of 15–120 ms for a fixed TR of 2000 ms. From the resultant MRI pixel intensity maps, T1 and T2 relaxation times were measured with respect to each concentration. To determine the optimal concentration, 5 x 10^4 cells were labeled with different nanoprobe concentration ranging from 12- 96 μg along with cells without treatment as the control. The cells were washed and re-dispersed in fresh PBS which was then MR-imaged within the microcentrifuge tubes.

5.4.22 Selectivity of nanoprobe toward Aβ$_{1-42}$ peptide along with other analytes

The selectivity of the nanoprobe towards Aβ$_{1-42}$ peptide was analysed along with other analytes like tau protein, BSA and HSA. 50 nM of Aβ$_{1-42}$ peptide was analysed along with 5 times concentration i.e. 250 nM of tau, BSA and HSA.

5.4. 23 Limit of detection of Aβ$_{1-42}$ peptide in artificial cerebrospinal fluid

The a CSF was prepared according to well-accepted protocols and contained following concentration of salts and sugars: 2.5 mM KCl, 124 mM NaCl, 2.0 mM MgSO$_4$, 26 mM NaHCO$_3$, 1.25 mM KH$_2$PO$_4$, 4 mM sucrose, 10 mM glucose, and 2.5 mM CaCl$_2$.[43] The aCSF was then used for a preparation of model spiked samples. The aCSF was spiked with concentrations ranging from 100 nM to 1 fM of Aβ$_{1-42}$ to find the LOD in the case of SERS. The probes Fe@AuNS@PEG@Aβ$_{1-42}$ MAb were initially added to the peptide in aCSF fluid magnetically purified the complex which was further added with the second probe AuNP@PMZ@PEG@Aβ$_{1-42}$ PAb. After incubation, the final complex was magnetically separated and washed and dispersed in aCSF fluid for SERS analysis.

5.5 Conclusion

Diagnosis of neurodegenerative diseases is a major challenging area with unmet medical requirements where intervention of nanotechnology plays an exceptional role for the development of highly sensitive diagnostic modalities. In this context, SERS-nanoprobes has been well explored utilizing sandwich SERS immuno assay for the rapid and sensitive detection of Aβ$_{1-42}$ protein. The nanoprobes have been constructed employing monoclonal antibody functionalized iron oxide nanoparticle and polyclonal antibody conjugated gold nanoparticle with an amyloid binding molecule as the Raman reporter. This strategy exhibited advantages over conventional methods like ELISA and other imaging techniques which are time consuming and expensive. The approach rendered sensitive, precise and specific detection of Aβ$_{1-42}$ with a LOD of 10 fM using a simple magnetic purification method. The method can be modified to analyze multiple targets and as an alternative strategy to fluorescent probes for detection of biomarkers relevant in several diseases. Hence,

the proof-of concept study based on SERS-nano-probes reflected its potentiality for early detection of Aβ$_{1-42}$ in healthy, MCI and AD clinical samples.

5.6 References

(1)   Huynh, R. A.; Mohan, C. Alzheimer's Disease: Biomarkers in the Genome, Blood, and Cerebrospinal Fluid. *Front. Neurol.* **2017**, *8*:102.

(2)   International, A. D. *World Alzheimer Report 2019, Attitudes to Dementia*; 2019.

(3)   Friedrich, R. P.; Tepper, K.; Rönicke, R.; Soom, M.; Westermann, M.; Reymann, K.; Kaether, C.; Fändrich, M. Mechanism of Amyloid Plaque Formation Suggests an Intracellular Basis of Aβ Pathogenicity. *Proc. Natl. Acad. Sci. U. S. A.* **2010**, *107* (5), 1942–1947.

(4)   Lue, L. F.; Guerra, A.; Walker, D. G. Amyloid Beta and Tau as Alzheimer's Disease Blood Biomarkers: Promise From New Technologies. *Neurol. Ther.* **2017**, *6* (s1), 25–36.

(5)   Matsui, T.; Ingelsson, M.; Fukumoto, H.; Ramasamy, K.; Kowa, H.; Frosch, M. P.; Irizarry, M. C.; Hyman, B. T. Expression of APP Pathway MRNAs and Proteins in Alzheimer's Disease. *Brain Res.* **2007**, *1161* (1), 116–123.

(6)   Pesini, P.; Pérez-Grijalba, V.; Monleón, I.; Boada, M.; Tárraga, L.; Martínez-Lage, P.; San-José, I.; Sarasa, M. Reliable Measurements of the β -Amyloid Pool in Blood Could Help in the Early Diagnosis of AD. *Int. J. Alzheimers. Dis.* **2012**, No. 604141.

(7)   Thambisetty, M.; Lovestone, S. Blood-Based Biomarkers of Alzheimers Disease: Challenging but Feasible. *Biomark. Med.* **2010**, *4* (1), 65–79.

(8)   Seppälä, T. T.; Herukka, S. K.; Hänninen, T.; Tervo, S.; Hallikainen, M.; Soininen, H.; Pirttilä, T. Plasma Aβ42 and Aβ40 as Markers of Cognitive Change in Follow-up: A Prospective, Longitudinal, Population-Based Cohort Study. *J. Neurol. Neurosurg. Psychiatry* **2010**, *81* (10), 1123–1127.

(9)   Song, L.; Lachno, D. R.; Hanlon, D.; Shepro, A.; Jeromin, A.; Gemani, D.; Talbot, J. A.; Racke, M. M.; Dage, J. L.; Dean, R. A. A Digital Enzyme-Linked Immunosorbent Assay for Ultrasensitive Measurement of Amyloid-β 1-42 Peptide in Human Plasma with Utility for Studies of Alzheimer's Disease Therapeutics. *Alzheimer's Res. Ther.* **2016**, *8* (1), 1–15.

(10)   Lue, L. F.; Sabbagh, M. N.; Chiu, M. J.; Jing, N.; Snyder, N. L.; Schmitz, C.; Guerra, A.; Belden, C. M.; Chen, T. F.; Yang, C. C.; et al. Plasma Levels of Aβ42 and Tau Identified Probable Alzheimer's Dementia: Findings in Two Cohorts. *Front. Aging Neurosci.* **2017**, *9* :226.

(11)   Yang, C. C.; Yang, S. Y.; Chieh, J. J.; Horng, H. E.; Hong, C. Y.; Yang, H. C.; Chen, K. H.; Shih, B. Y.; Chen, T. F.; Chiu, M. J. Biofunctionalized Magnetic Nanoparticles for Specifically Detecting Biomarkers of Alzheimer's Disease in Vitro. *ACS Chem. Neurosci.* **2011**, *2* (9), 500–505.

(12)   Chiu, M.-J.; Chen, T.-F.; Hu, C.-J.; Yan, S.-H.; Sun, Y.; Liu, B.-H.; Chang, Y.-T.; Yang, C.-C.; Yang, S.-Y. Nannoparticle-Based Immunomagnetic Assay of Plasma Biomarkers for Differentiating Dementia and Prodromal States of Alzheimer's Disease – A Cross-Validation Study. *Nanomed-Nanotechnol. Biol. Med.* **2020**, 102182.

(13)   Nakamura, A.; Kaneko, N.; Villemagne, V. L.; Kato, T.; Doecke, J.; Doré, V.; Fowler, C.; Li, Q. X.; Martins, R.; Rowe, C.; et al. High Performance Plasma Amyloid-β Biomarkers for Alzheimer's Disease. *Nature* **2018**, *554* (7691), 249–254.

(14)   Polanco, J. C.; Li, C.; Bodea, L. G.; Martinez-Marmol, R.; Meunier, F. A.; Götz, J. Amyloid-β and Tau Complexity - Towards Improved Biomarkers and Targeted Therapies. *Nat. Rev. Neurol.* **2018**, *14* (1), 22–40.

(15)   Nazem, A.; Mansoori, G. A. Nanotechnology Solutions for Alzheimer's Disease: Advances in Research Tools, Diagnostic Methods and Therapeutic Agents. *J. Alzheimer's Dis.* **2008**, *13* (2), 199–223.

(16)   Langer, J.; Jimenez de Aberasturi, D.; Aizpurua, J.; Alvarez-Puebla, R. A.; Auguié, B.; Baumberg, J. J.; Bazan, G. C.; Bell, S. E. J.; Boisen, A.; Brolo, A. G.; et al. Present

and Future of Surface-Enhanced Raman Scattering. *ACS Nano* **2020**, *14* (1), 28–117.

(17)   Kneipp, K.; Haka, A. S.; Kneipp, H.; Badizadegan, K.; Yoshizawa, N.; Boone, C.; Shafer-Peltier, K. E.; Motz, J. T.; Dasari, R. R.; Feld, M. S. Surface-Enhanced Raman Spectroscopy in Single Living Cells Using Gold Nanoparticles. *Appl Spectrosc* **2002**, *56* (2), 150–154.

(18)   Zhao, Z.; Zhu, L.; Bu, X.; Ma, H.; Yang, S.; Yang, Y.; Hu, Z. Label-Free Detection of Alzheimer's Disease through the ADP3 Peptoid Recognizing the Serum Amyloid-Beta42 Peptide. *Chem. Commun.* **2015**, *51* (4), 718–721.

(19)   Chou, I. H.; Benford, M.; Beier, H. T.; Coté, G. L.; Wang, M.; Jing, N.; Kameoka, J.; Good, T. A. Nanofluidic Biosensing for β-Amyloid Detection Using Surface Enhanced Raman Spectroscopy. *Nano Lett.* **2008**, *8* (6), 1729–1735.

(20)   Haes, A. J.; Hall, W. P.; Chang, L.; Klein, W. L.; Van Duyne, R. P. A Localized Surface Plasmon Resonance Biosensor: First Steps toward an Assay for Alzheimer's Disease. *Nano Lett.* **2004**, *4* (6), 1029–1034.

(21)   Wang, Y.; Zhao, P.; Mao, L.; Hou, Y.; Li, D. Determination of Brain Injury Biomarkers by Surface-Enhanced Raman Scattering Using Hollow Gold Nanospheres. *RSC Adv.* **2018**, *8* (6), 3143–3150.

(22)   Balzerova, A.; Fargasova, A.; Markova, Z.; Ranc, V.; Zboril, R. Magnetically-Assisted Surface Enhanced Raman Spectroscopy (MA-SERS) for Label-Free Determination of Human Immunoglobulin g (IgG) in Blood Using Fe3O4@Ag Nanocomposite. *Anal. Chem.* **2014**, *86* (22), 11107–11114.

(23)   Zengin, A.; Tamer, U.; Caykara, T. A SERS-Based Sandwich Assay for Ultrasensitive and Selective Detection of Alzheimer's Tau Protein. *Biomacromolecules* **2013**, *14* (9), 3001–3009.

(24)   Lu, D.; Xia, J.; Deng, Z.; Cao, X. Detection of Squamous Cell Carcinoma Antigen in Cervical Cancer by Surface-Enhanced Raman Scattering-Based Immunoassay.

Anal. Methods **2019**, *11* (21), 2809–2818.

(25) Sharma, B.; Frontiera, R. R.; Henry, A.-I.; Ringe, E.; Van Duyne, R. P. SERS: Materials, Applications, and the Future. *Mater. Today* **2012**, *15* (1–2), 16–25.

(26) Schlorf, T.; Meincke, M.; Kossel, E.; Glüer, C. C.; Jansen, O.; Mentlein, R. Biological Properties of Iron Oxide Nanoparticles for Cellular and Molecular Magnetic Resonance Imaging. *Int. J. Mol. Sci.* **2011**, *12* (1), 12–23.

(27) Peng, X.-H.; Chen, Z. G.; Shin, D. M.; Qian, X.; Nie, S.; Mao, H.; Wang, A. Y. Targeted Magnetic Iron Oxide Nanoparticles for Tumor Imaging and Therapy. *Int. J. Nanomedicine* **2008**, *3* (3), 311–321.

(28) Wei, H.; Wang, A. Antibody Iron Oxide NPs for Cancer Cell Separation in Blood. *Biomaterials* **2012**, *32* (36), 9758–9765.

(29) Oghabian, M. A.; Guiti, M.; Haddad, P.; Gharehaghaji, N.; Saber, R.; Alam, N. R.; Malekpour, M.; Rafie, B. Detection Sensitivity of MRI Using Ultra-Small Super Paramagnetic Iron Oxide Nano-Particles (USPIO) in Biological Tissues. *Annu. Int. Conf. IEEE Eng. Med. Biol. - Proc.* **2006**, 5625–5626.

(30) Saraswathy, A.; Nazeer, S. S.; Jeevan, M.; Nimi, N.; Arumugam, S.; Harikrishnan, V. S.; Varma, P. R. H.; Jayasree, R. S. Citrate Coated Iron Oxide Nanoparticles with Enhanced Relaxivity for in Vivo Magnetic Resonance Imaging of Liver Fibrosis. *Colloids Surfaces B Biointerfaces* **2014**, *117*, 216–224.

(31) Huang, J.; Zhong, X.; Wang, L.; Yang, L.; Mao, H. Improving the Magnetic Resonance Imaging Contrast and Detection Methods with Engineered Magnetic Nanoparticles. *Theranostics* **2012**, *2* (1), 86–102.

(32) Menichetti, L.; Manzoni, L.; Paduano, L.; Flori, A.; Kusmic, C.; De Marchi, D.; Casciaro, S.; Conversano, F.; Lombardi, M.; Positano, V.; et al. Iron Oxide-Gold Core-Shell Nanoparticles as Multimodal Imaging Contrast Agent. *IEEE Sens. J.* **2013**, *13* (6), 2341–2347.

(33) Zeleňáková, A.; Zeleňák, V.; Degmová, J.; Kováč, J.; Sedláčková, K.; Kusý, M.; Sitek, J. The Iron-Gold Magnetic Nanoparticles: Preparation, Characterization and

Magnetic Properties. *Rev. Adv. Mater. Sci.* **2008**, *18* (6), 501–504.

(34)   Liang, C. H.; Wang, C. C.; Lin, Y. C.; Chen, C. H.; Wong, C. H.; Wu, C. Y. Iron Oxide/Gold Core/Shell Nanoparticles for Ultrasensitive Detection of Carbohydrate-Protein Interactions. *Anal. Chem.* **2009**, *81* (18), 7750–7756.

(35)   Yang, J. K.; Hwang, I. J.; Cha, M. G.; Kim, H. I.; Yim, D. Bin; Jeong, D. H.; Lee, Y. S.; Kim, J. H. Reaction Kinetics-Mediated Control over Silver Nanogap Shells as Surface-Enhanced Raman Scattering Nanoprobes for Detection of Alzheimer's Disease Biomarkers. *Small* **2019**, *15* (19), 1–12.

(36)   McClure, R. A.; Chumbley, C. W.; Reyzer, M. L.; Wilson, K.; Caprioli, R. M.; Gore, J. C.; Pham, W. Identification of Promethazine as an Amyloid-Binding Molecule Using a Fluorescence High-Throughput Assay and MALDI Imaging Mass Spectrometry. *NeuroImage Clin.* **2013**, *2* (1), 620–629.

(37)   Zheng, L.; Cedazo-Minguez, A.; Hallbeck, M.; Jerhammar, F.; Marcusson, J.; Terman, A. Intracellular Distribution of Amyloid Beta Peptide and Its Relationship to the Lysosomal System. *Transl. Neurodegener.* **2012**, *1*, 1–7.

(38)   Hu, X.; Crick, S. L.; Bu, G.; Frieden, C.; Pappu, R. V.; Lee, J. M. Amyloid Seeds Formed by Cellular Uptake, Concentration, and Aggregation of the Amyloid-Beta Peptide. *Proc. Natl. Acad. Sci. U. S. A.* **2009**, *106* (48), 20324–20329.

(39)   Nixon, R. A. Amyloid Precursor Protein & Endosomal-Lysosomal Dysfunction in Alzheimer's Disease: Inseparable Partners in a Multifactorial Disease. *FASEB J.* **2017**, *31* (7), 2729–2743.

(40)   Colacurcio, D. J.; Pensalfini, A.; Jiang, Y.; Nixon, R. A. Dysfunction of Autophagy and Endosomal-Lysosomal Pathways: Roles in Pathogenesis of Down Syndrome and Alzheimer's Disease. *Free Radic. Biol. Med.* **2018**, *114*, 40–51.

(41)   Chaudhari, K.; Pradeep, T. Spatiotemporal Mapping of Three Dimensional Rotational Dynamics of Single Ultrasmall Gold Nanorods. *Sci. Rep.* **2014**, *4*, 27–29.

(42) Sujai, P. T.; Joseph, M. M.; Saranya, G.; Nair, J. B.; Murali, V. P.; Maiti, K. K. Surface Charge Modulates the Internalization: Vs. Penetration of Gold Nanoparticles: Comprehensive Scrutiny on Monolayer Cancer Cells, Multicellular Spheroids and Solid Tumors by SERS Modality. *Nanoscale* **2020**, *12* (13), 6971–6975.

(43) Ahmadov, T. O.; Joshi, P.; Zhang, J.; Nahan, K.; Caruso, J. A.; Zhang, P. Paramagnetic Relaxation Based Biosensor for Selective Dopamine Detection. *Chem. Commun.* **2015**, *51* (57), 11425–11428.

List of Patents and Publications

Related to Thesis

Patents

1. Kaustabh Kumar Maiti,K. Sujathan,**Varsha Karunakaran**;Screening Kit for Detection of Grades of Cervical Cancer and Process for the Thereof Preparation; **PCT Int. Appl. (2020), WO2020021568A120200130. Language: English, Database: CAPLUS, Date: 30th January, 2020**.

2. Maiti Kaustabh Kumar; Kunjuraman Sujathan; Murali Vishnu Priya; **Varsha Karunakaran**; S Deepika; M Madhukrishnan; Valliamma Neelakantapillai Saritha; Asha Lekshmi; A Diagnostic Screening Kit for Simultaneous Detection of Clinically Relevant Biomarkers from Breast Cancer Tissue Samples using Surface Enhanced Raman Scattering Platform and Process for the Preparation Thereof; **Indian Patent Application no. 202011034768, dated 11.08.2020.**

Publications

3. **Varsha Karunakaran**; Valliamma N. Saritha; Manu M. Joseph; Jyothi B Nair; Giridharan Saranya; Kozhiparambil G. Raghu; Kunjuraman Sujathan*; Krishnannair S. Kumar*; Kaustabh K. Maiti* Diagnostic Spectro-Cytology Revealing Differential Recognition of Cervical Cancer Lesions by Label-free Surface Enhanced Raman Fingerprints and Chemometrics.; **Nanomedicine: Nanotechnology, Biology, and Medicine**, 29(**2020**)102276.

4. **Varsha Karunakaran**; Deepika S, Valliamma N. Saritha.; Ramya A.N.; Vishnu Priya Murali.; P.T. Sujai; K.G. Raghu; K. Sujathan*; Kaustabh Kumar Maiti*; New Insight of Raman Image Guided Detection of Clinically Confirmed Grades of Cervical Exfoliated Cells by Dual Biomarker Appended SERS-Tag; *Manuscript under review.*

5. **<u>Varsha Karunakaran;</u>** Vishnu Priya Murali; Valliamma Neelakantapillai Saritha; Asha Lekshmi; Deepika S; Madhukrishnan M; Shamna K; Exploring the multiplexing SERS platform for the differential detection of clinically relevent breast cancer biomarkers using surface enhanced scattering nanoprobes; *Manuscript under preparation.*

6. **<u>Varsha Karunakaran;</u>** Saranya Giridharan; Manu M Joseph; Vishnu Priya Murali; Deepika S; Kaustabh Kumar Maiti*; An insight into a dual modal detection platform for the early diagnosis of Alzheimer's Disease biomarker $A\beta_{1-42}$ using SERS and MRI; *Manuscript under preparation.*

Not Related to Thesis

7. Rakesh K. Mishra, Samiyappan Vijayakumar, Arindam Mal, **<u>Varsha Karunakaran</u>**, Jith C. Janardhanan, Kaustabh Kumar Maiti, Vakayil K. Praveen and Ayyappanpillai Ajayaghosh*; Bimodal Detection of Carbon Dioxide Using Fluorescent Molecular Aggregates; ***Chem. Commun***., **2019**, 55, 6046-6049.

8. Palasseri T. Sujai, Manu M. Joseph, **<u>Varsha Karunakaran</u>**, Giridharan Saranya, Ramya N. Adukkadan, Shanmughan Shamjith, Reshmi Thomas, Jyothi B. Nair, Rotti Srinivasamurthy Swathi, and Kaustabh Kumar Maiti*; Biogenic Cluster-Encased Gold Nanorods as a Targeted Three-in-One Theranostic Nanoenvelope for SERS-Guided Photochemotherapy against Metastatic Melanoma; ***ACS Appl. Bio Mater***. **2019**, 2, 1, 588-600

9. Manu. M. Joseph, Nisha. Narayanan, Jyothi. B. Nair, **<u>Varsha Karunakaran</u>**, A. N. Ramya, P. T. Sujai, G. Saranya , Jayadev. S. Arya, Vineeth. M. Vijayan, Kaustabh. Kumar Maiti; Exploring the margins of SERS in practical domain: An emerging diagnostic modality for modern biomedical applications ***Biomaterials.,*** **2018,** *181*, 140-181.

10. Giridharan Saranya, Manu M. Joseph, **<u>Varsha Karunakaran</u>**, Jyothi B. Nair, Valliamma N. Saritha, Vamadevan S. Veena, Kunjuraman Sujathan*, Ayyappanpillai Ajayaghosh*, and Kaustabh K. Maiti*; Enzyme-Driven Switchable

Fluorescence-SERS Diagnostic Nanococktail for the Multiplex Detection of Lung Cancer Biomarkers; ***ACS Appl. Mater. Interfaces*** **2018,** 10, 45, 38807-38818

11. Magnetic properties of biocompatible CoFe2O4 nanoparticles using a facile synthesis; Annrose Sunny, Aneesh Kumar K.S., **<u>Varsha Karunakaran</u>**, Aathira M., Geeta R. Mutta, Kaustabh K. Maiti, V. Raghavendra Reddy, M. Vasundhara*, ***Nano-Structures & Nano-Objects***, **2018**, 69–76.

12. Adukkadan N. Ramya, Manu M. Joseph,* Santhi Maniganda, **<u>Varsha Karunakaran</u>**, Sreelekha T.T,* and Kaustabh Kumar Maiti*; Emergence of Gold-Mesoporous Silica Hybrid Nano-Theranostic: Dox-Encoded, Folate Targeted Chemotherapy with Modulation of SERS Fingerprinting for Apoptosis Toward Tumor Eradication; ***Small***, **2017**, 13, 1700819

13. Bincy Mariyam Mathai, Manu M. Joseph, Santhi Maniganda, Jyothi B. Nair, J. S. Arya, **<u>Varsha Karunakaran</u>**, K. V. Radhakrishnan* and Kaustabh Kumar Maiti *; Guanidinium rich dendron-appended hydnocarpin exhibits superior anti-neoplastic effects through caspase mediated apoptosis; ***RSC Adv.***, **2016**, 6, 52772-52780

14. Nisha Narayanan, Lakshmi V. Nair, **<u>Varsha Karunakaran</u>**, Manu M. Joseph, Jyothi B. Nair, Ramya A. N, Ramapurath S. Jayasree* and Kaustabh Kumar Maiti*; Investigation of apoptotic events at molecular level induced by SERS guided targeted theranostic nanoprobe; ***Nanoscale.***, **2016**, 8, 11392-1139

15. Adukkadan N. Ramya, Manu M. Joseph, Jyothi B. Nair, **<u>Varsha Karunakaran</u>**, Nisha Narayanan, and Kaustabh Kumar Maiti*; New Insight of Tetraphenylethylene-based Raman Signatures for Targeted SERS Nanoprobe Construction Toward Prostate Cancer Cell Detection; ***ACS Appl. Mater. Interfaces***., **2016**, 8, 10220-10225

16. Nisha Narayanan, **<u>Varsha Karunakaran</u>**, Willi Paul, Karunakaran Venugopal, K. Sujathan, Kaustabh Kumar Maiti*; Aggregation induced Raman scattering of squaraine dye: Implementation in diagnosis of cervical cancer dysplasia by SERS imaging *; **Biosensors and Bioelectronics.**, **2015**, 70, 145-152

17. Sajitha Syed; Vidya Jalaja ; **<u>Varsha Karunakaran</u>** and Parameswaran Binod*, Ashok Pandey; Cloning and expression of L-asparaginase from E.coli in

eukaryotic expression system; *Biochemical Engineering Journal.*, **2015**, 102, 14–17

List of Posters & Conferences

1. **Presented a poster** in the **8th Annual Meeting of Indian Academy of Biomedical Sciences (IABS) and conference on "Deliberation on Translation of Basic Scientific Insights into Affordable Healthcare Products"** conducted on 25th -27th February **2019** hosted by CSIR-National Institute for Interdisciplinary Science and Technology (NIIST),Thiruvananthapuram, Kerala; An Effective Diagnostic Nano-Probe for Detection of Alzheimer Biomarker Based on SERS and MRI Dual Modalities; Poster presentation; **Varsha Karunakaran**, Saranya Giridharan Vishnu Priya Murali, Madhukrishnan M and Kaustabh Kumar Maiti*

2. **Presented a poster** in **31st Kerala Science Congress** held on 27-28th January **2019** organized by Kerala State Council for Science Technology & Environment, Jawaharlal Nehru Tropical Botanic Garden & Research Institute at Fatima Mata National College, Kollam, Kerala; A New Insight on Early Diagnosis of Alzheimer's Disease Biomarkers by Label Based SERS Immunosensor; Poster presentation; **Varsha Karunakaran**, Saranya Giridharan and Kaustabh Kumar Maiti*.

3. **Best Poster Award** in **3rd Annual Conference of Indian Society of Nanomedicine**, **NANOBIOTECK-2018** held and organized by All India Institute of Medical Sciences (AIIMS) and Indian Institute of Technology (IIT), Delhi in partner with Department of Biotechnology, Govt. of India from 24th -27th October 2018; An ultrasensitive SERS based non-invasive label free diagnosis of exfoliated cells from cervical pre- cancerous lesions by Raman fingerprinting;

Poster presentation; **Varsha Karunakaran**, Saritha V.N.,. Satheesh Kumar, K.Sujathan, Kaustabh Kumar Maiti*.

4. **Best Paper Award (Oral presentation)** in Health Sciences on the **30th Kerala Science Congress** (Jan 28-30th **2018**) on '**Viruses** and infectious diseases', organized by KSCSTE at Government Brennen College, Thalassery; New insight on non-invasive label free diagnosis of the cervical pre- cancers by metabolomics and genomics profiling using differential SERS fingerprinting; Oral presentation; **Varsha Karunakaran**, Saritha V.N.,. Satheesh Kumar, K.Sujathan, Kaustabh Kumar Maiti*.

5. **Best Poster Award** in **The International Symposium on Photonics Applications and Nanomaterials**; Organized by Sree Chitra Tirunal Institute for Medical Sciences & Technology , Thiruvananthapuram (Oct, 28-30th, **2015**); A New Insight of Squaraine Based Raman Reporters for Construction of Diagnostic SERS Nano-Probe in Cancer Screening, Poster presentation : Nisha Narayanan, Ramya A N, **Varsha Karunakaran** and, Kaustabh K. Maiti*.

6. Participated in **The Ramanbhai Foundation 7th International Symposium on Current Trends in Pharmaceutical Sciences**" Advances in New Drug Discovery & Development"; Organized by Zydus Research Centre, Ahmedabad, India (Feb, 2- 4th, **2015**); An Efficient Approach on Guanidium Appended Molecular Transporter For Targeted Delivery of Doxorubicin Towards Malignant Cells: A Future Prospect in Cancer Therapy; Poster presentation: Jyothi B Nair, Santhi Maniganda, **Varsha Karunakaran**, Kaustabh Kumar Maiti*.